Theoretical determination of NMR parameters of metabolites and proteins

Zeinab Atieh Harb

N° of order 185-2011 Year 2011

THESIS OF THE UNIVERSITE OF LYON

Delivered by

L'UNIVERSITE CLAUDE BERNARD LYON 1

ECOLE DOCTORALE

PHYSIQUE ET ASTROPHYSIQUE DE LYON

to obtain

PHD DEGREE

(Decree of 7 August 2006)

PHD defense on 17 October 2011

by

Zeinab ATIEH

TITLE :

Theoretical Determination of NMR Parameters of Metabolites and Proteins

JURY : M. Dirk VAN ORMONDT, reporter
M. Claude LESECH, reporter
M. Dominique SUGNY
M. Abdul-Rahman ALLOUCHE, director of thesis
Mme Monique Frecon, co-director of thesis
Mme Danielle GRAVERON-DEMILLY

UNIVERSITE CLAUDE BERNARD - LYON 1

Président de l'Université	**M. A. Bonmartin**
Vice-président du Conseil d'Administration	M. le Professeur G. Annat
Vice-président du Conseil des Etudes et de la Vie Universitaire	M. le Professeur D. Simon
Vice-président du Conseil Scientifique	M. le Professeur J-F. Mornex
Secrétaire Général	M. G. Gay

COMPOSANTES SANTE

Faculté de Médecine Lyon Est – Claude Bernard	Directeur : M. le Professeur J. Etienne
Faculté de Médecine et de Maïeutique Lyon Sud – Charles Mérieux	Directeur : M. le Professeur F-N. Gilly
UFR d'Odontologie	Directeur : M. le Professeur D. Bourgeois
Institut des Sciences Pharmaceutiques et Biologiques	Directeur : M. le Professeur F. Locher
Institut des Sciences et Techniques de la Réadaptation	Directeur : M. le Professeur Y. Matillon
Département de formation et Centre de Recherche en Biologie Humaine	Directeur : M. le Professeur P. Farge

COMPOSANTES ET DEPARTEMENTS DE SCIENCES ET TECHNOLOGIE

Faculté des Sciences et Technologies	Directeur : M. le Professeur F. Gieres
Département Biologie	Directeur : M. le Professeur F. Fleury
Département Chimie Biochimie	Directeur : Mme le Professeur H. Parrot
Département GEP	Directeur : M. N. Siauve
Département Informatique	Directeur : M. le Professeur S. Akkouche
Département Mathématiques	Directeur : M. le Professeur A. Goldman
Département Mécanique	Directeur : M. le Professeur H. Ben Hadid
Département Physique	Directeur : Mme S. Fleck
Département Sciences de la Terre	Directeur : Mme le Professeur I. Daniel
UFR Sciences et Techniques des Activités Physiques et Sportives	Directeur : M. C. Collignon
Observatoire de Lyon	Directeur : M. B. Guiderdoni
Ecole Polytechnique Universitaire de Lyon 1	Directeur : M. P. Fournier
Ecole Supérieure de Chimie Physique Electronique	Directeur : M. G. Pignault
Institut Universitaire de Technologie de Lyon 1	Directeur : M. le Professeur C. Coulet
Institut de Science Financière et d'Assurances	Directeur : M. le Professeur J-C. Augros
Institut Universitaire de Formation des Maîtres	Directeur : M. R. Bernard

Table of contents

Dedications

I would like to acknowledge that during this work, I was directed by Dr. Abdul-Rahman ALLOUCHE. I thank him deeply for his guidance and patience.

I would also like to thank Dr. Monique AUBERT-FRÉCON for her support and assistance. Dr. AUBERT-FRÉCON helped me, with patience, through her very contribution to the field of theoretical study.

I thank the members of the jury because they have agreed to read my work and criticize it. Besides, I thank all the members of our team.

I would like to dedicate this Doctoral dissertation to my parents who always encouraged and supported me.

Finally, I would like to thank my husband, Dr. Mahdi, for his support and encouragement. I couldn't have completed this effort without his assistance, tolerance, and enthusiasm.

Introduction

Nuclear magnetic resonance NMR was first described and measured in molecular beams by Isidor Rabi in 1938, and in 1944 Rabi was awarded the Nobel Prize in physics for his invention of the atomic and molecular beam magnetic resonance method of observing atomic spectra.

Later, Felix Bloch and Edward Purcell noticed that magnetic nuclei, like ^{1}H, could absorb radio frequency (RF) energy when placed in a magnetic field of a strength specific to the identity of the nuclei. When this absorption occurs, the nucleus is described as being in resonance. Different atomic nuclei within a molecule resonate at different frequencies for the same magnetic field strength. With this discovery, NMR was born and soon became an important analytical method in the study of the composition of chemical compounds. For this discovery, Bloch and Purcell were awarded the Nobel Prize in physics in 1952.

In 1991, Richard Ernst got the Nobel Prize in Chemistry for his contributions to the development of the methodology of high resolution nuclear magnetic resonance (NMR) spectroscopy. Later, Kurt Wüthrich was awarded the Nobel Prize in Chemistry in 2002 for his development of nuclear magnetic resonance spectroscopy for determining the three-dimensional structure of biological macromolecules in solution. One year later, in 2003, Paul C. Lauterbur and Peter Mansfield got the Nobel Prize in Medicine for their discoveries concerning magnetic resonance imaging (MRI).

After these discoveries, NMR became the premier organic spectroscopy available to chemists to determine the detailed chemical structure of the chemicals they were synthesizing. Besides, a well-known technique of NMR technology has been the Magnetic Resonance Imaging (MRI), which is utilized extensively in the medical radiology field to obtain image slices of soft tissues in the human body, offering by that a powerful new probe of the body's internal anatomy and function. Magnetic resonance spectroscopy (MRS) complements MRI as a non-invasive means for the characterization of tissue. While MRI uses the signal from hydrogen protons from water to form anatomic images, MRS uses the signals from nuclei of chemical molecules to determine the concentration of metabolites which are bio-markers of diseases in the tissue examined. Usually, in vivo MRS is used for detecting and quantifying metabolites.

In MRS, the analysis of signals obtained from patients and based on a database of prior knowledge about MRS-signals of metabolites is now very popular. The NMR related database contains either the signals or the spectra of metabolites. The latter can be measured *in vitro* or simulated from quantum mechanics. In the case of simulated database one needs two types of spin-Hamiltonian parameters: chemical shifts δ and indirect spin-spin coupling constants J, which characterize an MRS-signal. The parameters δ and J may be obtained from two ways: (1) in vitro measurements of metabolite in solution, from which the determination of chemical shifts is easy however the determination of spin-spin coupling constants is hard and becomes impossible in the cases of complex multiplets, and (2) computer simulations which are based on quantum chemistry calculations for the spin-Hamiltonian parameters and are feasible for not too large molecules.

The present work aims to calculate, using the density functional theory, reliable ^{1}H NMR parameters of seven metabolites (putrescine, spermidine, spermine, acetate, sarcosine, alanine, and serine). The three polyamines (putrescine, spermidine, spermine) and sarcosine are considered as biomarkers of prostate cancer. While the concentrations of polyamines have been shown to decrease in the presence of prostate cancer, the concentration of sarcosine has been revealed to highly increase during prostate cancer progression and it can be detected in urine. On the other hand, the three metabolites acetate, serine and alanine are biomarkers of brain illnesses. The increased concentration of acetate allows the primary identification of brain cancer.

Usually, NMR spectrum obtained for a tissue in the human body is very complex since it corresponds to a large number of metabolites with overlapping NMR spectra. Thus, in order to distinguish the presence or absence of a specific metabolite, its resonance peaks are determined through simulation from NMR parameters and then they are used within quantitation processes. One aim of this work is to simulate, for several metabolites of interest, reliable theoretical NMR spectra.

In order to obtain NMR spectra in agreement with experiment, the present work tends to study the effects of inclusion of isomer contributions from conformers of higher energy, in the calculation of NMR parameters for metabolites. Besides, it aims to understand molecular vibration and its effects on the calculated NMR parameters. Moreover, solvent effects are planned to be studied explicitly with water molecules around the metabolite and implicitly using a continuum model.

The calculation of NMR parameters using quantum chemistry methods is feasible for relatively small molecules, especially if the effects of solvent, isomers, and vibration are taken into account. Unfortunately, high accuracy calculations are limited by the high computational costs for many systems of interest (proteins, DNA, RNA ...) making large size molecules out of reach of traditional quantum chemistry approaches. An alternative would be a model that allows the predictions of parameters.

The second part of this work shall be devoted to put forward a model that allows the prediction of chemical shifts of biological molecules. It must be general in the sense that it is able to predict the chemical shifts for many types of nuclei (H, C, N) and for any biological molecule (metabolites, proteins, DNA, RNA, ...) being small or large.

The present work is divided into four chapters, two of which present the theoretical methods used in this work while the other two show the obtained results. The first chapter is devoted to present the quantum chemical methods used in the calculation of NMR parameters for motionless molecules while the second chapter presents the methods used to calculate the dynamical effects on NMR parameters. The third chapter shows the results obtained for metabolites, and the fourth chapter presents the model that allows the prediction of chemical shifts for any biological molecule, including proteins.

In the first chapter, we shall present the concept of NMR parameters: chemical shifts and indirect spin-spin coupling constants, derive their theoretical expressions, and show how to simulate an NMR spectrum starting from its parameters. Then, we will shortly describe the Density Functional Theory (DFT) chosen for the calculation of NMR parameters of metabolites. After that, we will present the general basis sets and shed the light on those used in the present work. This shall be followed by a rapid presentation of semi-empirical methods that served in the calculation of some effects on the NMR parameters. The first chapter will terminate by the two methods used for adding solvent, which are the Polarizable Continuum Model (PCM) and Our own N-layered Integrated molecular Orbital and molecular Mechanics (ONIOM) method.

The second chapter will differ from the first one in the sense that it will treat the methods used to calculate the dynamical effects on NMR parameters. First, we shall present Born-Oppenheimer molecular dynamics method used in the determination of conformers for a certain molecular geometry. A description of Berendsen thermostat, used in conserving a constant temperature during molecular dynamics, will be given. This shall be followed by the two methods used to study the molecular vibration which are Atom-centered density matrix propagation dynamics method (ADMP), and the perturbative method.

The third chapter, divided into three parts A, B, and C, will display the results related to metabolites. Part A will allow the choice of reliable methods to be used in the calculation of NMR parameters for metabolites: theoretical method with DFT approach (functional/basis set), and methods of calculation of different effects on NMR parameters (isomers, vibration, and solvent). Part B will present the full results in a selection of our published papers. In part C, a synthesis of all the results obtained for metabolites will be presented. It must be noted that results given in part B will be complementary to results of part A, where in part A the strategies of calculation shall be determined and in part B, results for metabolites using the chosen strategies shall be displayed.

The fourth chapter will present a new model that we have developed, BioShift, which can be used to predict chemical shifts for biological molecules (proteins, DNA, RNA, polyamines). It shall be tested for proteins and compared to well-known models especially designed for the prediction of chemical shifts of proteins. Bioshift will be also tested for small molecules.

The present work terminates by a general conclusion and some perspectives that open up new prospects in the calculation of NMR parameters.

Chapter 1

Quantum Chemical Calculations of Static NMR parameters

The calculation of NMR parameters, chemical shifts δ and indirect spin-spin coupling constants J, originating from magnetic perturbations has been implemented in a framework of many quantum chemical calculation methods. NMR calculations using the Density Functional Theory (DFT) [1; 2] are mainly done in our work; in fact, DFT is known to be a promising method for NMR calculations in complex molecules with a good accuracy [3; 4]. For the reliable calculation of chemical shifts δ and indirect spin-spin coupling constants J for biological molecules, the effect of a solvent on the calculated NMR parameters may be significant. In some cases, it may provide the leading correction to a calculated NMR parameter [5]. Two approaches based on different methodologies of the solvent model are used in our work. In the first way, we have used the Polarizable Continuum Model (PCM) [6] which relies on the effective mean polarization of a dielectric cavity constructed around the target molecule. In the second way, a hybrid method is examined through the "Our own N-layered Integrated molecular Orbital and molecular Mechanics" (ONIOM) [7] model where a complex of the target molecule with the explicit molecules of water is constructed.

The main goal of this chapter is to provide a basis for understanding the concept of NMR parameters, the basic connections between these parameters and the simulated NMR spectra, and the different theoretical methods used in our work needed to perform the calculation of the NMR parameters.

I NMR parameters: concept and theory

I.1 Parameters of NMR spectrum

Nuclear magnetic resonance spectroscopy provides detailed information on the structure and dynamics of molecules through NMR spectra. In general, a NMR spectrum is characterized by: i) a number of distinct signals, ii) hyperfine structure of individual signals, iii) a signal intensity and line-width. Here, we are going to discuss the first two properties while the third is out of our interest.

I.1.1 Signal position - chemical shift

A nucleus K of spin $\vec{I}_K$ and gyromagnetic ratio γ_K is characterized by a magnetic moment $\vec{m}_K$

$$\vec{m}_K = \gamma_K \hbar \, \vec{I}_K \tag{1.1}$$

where $\hbar$ is the reduced Plank's constant. In the presence of an external magnetic field $\vec{B}$, nucleus K possesses an energy given by

$$E = -\vec{m}_K.\vec{B} \tag{1.2}$$

In the case of a molecule placed in a magnetic field, electrons respond by creating their own magnetic field proportional to $\vec{B}$. In other words, the electronic cloud around nucleus K creates an induced magnetic field $\vec{B}_{ind}$ proportional to the electronic current (Biot et Savart law [8; 9]) which is, in turn, proportional to the external field.

$$\vec{B}_{ind} = -\boldsymbol{\sigma_K}.\vec{B} \tag{1.3}$$

where $\boldsymbol{\sigma_K}$ is the chemical shielding tensor of nucleus K. Note that $\vec{B}_{ind}$ is not necessarily parallel or anti-parallel to $\vec{B}$. The induced field of electrons deshields the external magnetic field and the effective magnetic field at the nucleus K differs from the applied field. The total magnetic field at the nucleus K is

$$\vec{B}_{total} = \vec{B} + \vec{B}_{ind} = (1 - \boldsymbol{\sigma_K}).\vec{B} \tag{1.4}$$

And hence the total energy becomes

$$E = -\vec{m}_K.\vec{B}_{total} = -\vec{m}_K.(1 - \boldsymbol{\sigma_K})\vec{B} \tag{1.5}$$

The same nuclei in the molecule can in principle experience different effective magnetic fields as a result of diverse chemical and structural environment.

The NMR spectrum is a record of the emission of electromagnetic radiation by a nucleus at a given frequency of radiation. The signal position due to the radiation of nucleus K with spin $\vec{I}_K$ is defined by the resonance frequency ω_K (called the Larmor frequency), which can be related to the magnetic field as

$$\omega_K = \frac{2E}{\hbar} = -2\,\gamma_K.\vec{I}_K.\vec{B}_{total} \tag{1.6}$$

In the present work, we have studied the isotropic chemical shieldings of spin ½ nuclei, where an isotropic chemical shielding is calculated by averaging the trace of the corresponding shielding tensor (equation (1.7)). Then, the Larmor frequency emitted by the nucleus K of spin $I_K = 1/2$ can be expressed in terms of the chemical shielding of the nucleus K as in equation (1.8).

$$\sigma_K = \frac{1}{3}Tr(\boldsymbol{\sigma_K}) \tag{1.7}$$

$$\omega_K = -\gamma_K\big(B(1 - \sigma_K)\big) \tag{1.8}$$

Equation (1.8) outlines the connection between chemical shieldings and experimental NMR spectra. However, from an experimental point of view, the frequency axis in NMR spectroscopy is a substantial problem because as can be seen from the above equation, the resonance frequency depends on the magnitude of the magnetic field. Not only the resonance frequencies acquired at different magnetic fields have to be scaled, but also the absolute frequency scale (~10^6 Hz) is not appropriate for reporting NMR spectra. To solve these problems at once, a relative scale was introduced and is called the chemical shift δ. The chemical shift can be calculated for any nucleus according to equation (1.9).

$$\delta_K = \frac{\nu_0 - \nu_K}{\nu_0} \tag{1.9}$$

In equation (1.9), $\nu_K = \omega_K/2\pi$ is the resonance frequency of nucleus K for which the chemical shift δ_K is to be calculated and ν_0 is the resonance frequency of a given nucleus in a standard substance. Usually, relative shifts for protons are calculated with respect to the reference compound tetramethylsilane TMS which is chosen for chemical shift calculations in the present work.

The chemical shift is usually expressed as the difference between chemical shieldings of the reference nucleus and nucleus K (equation (1.10))

$$\delta_K = \frac{\sigma_0 - \sigma_K}{1 - \sigma_0} \approx \sigma_0 - \sigma_K \tag{1.10}$$

In equation (1.10), the assumption $1 - \sigma_0 \approx 1$ has been made, σ_0 being ~10^{-5}. Chemical shieldings and shifts are usually scaled with ‘ppm’ (parts per million).

I.1.2 The hyper fine structure of the NMR signal - indirect spin-spin interaction

By the hyperfine structure of a NMR signal, it is meant the fine splitting of resonance peaks as a result of nuclear spin-spin interaction. There are two mechanisms: indirect and direct spin-spin interaction. However, in isotropic solutions, rotational Brownian diffusion averages the inter-nuclear direct spin-spin interactions to zero. In other words, in isotropic solutions, these interactions do not affect the hyperfine structure of NMR signals. Thus, we limit our study to indirect spin-spin interactions between nuclei.

The indirect spin-spin coupling (scalar coupling or J-coupling) is the effect of mutual interaction between two nuclear spins mediated by electrons polarized by the nuclear magnetic moments. Thus, indirect spin-spin couplings propagate along the chemical bonds; however, their magnitude reduces dramatically as the number of bonds separating the nuclei increases. The indirect spin-spin couplings depend on the local distribution of electrons in the vicinity of the coupled nuclei; specific change of the electronic environment is reflected by a change in J value. The J-coupling constant is a consequence of the nuclear magnetic moments and is, therefore, independent of the external magnetic field. J-couplings are exhibited in NMR spectra as the splitting of resonance lines of the coupled nuclei (see figure (1.1)). Besides, J-coupling constants are scaled in Hz and their values can be either positive or negative.

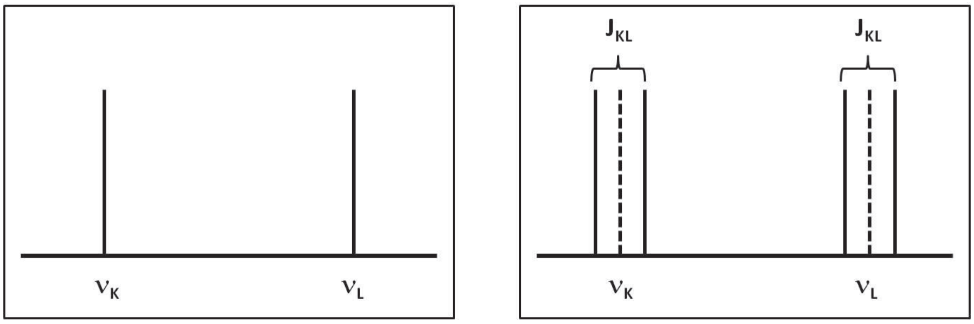

(i) (ii)

Figure 1.1: (i) resonance due to the emission of nuclei K & L with zero J-coupling, (ii) with non-zero J-coupling

Each NMR signal can be characterized, besides its position and hyperfine structure, by its intensity and half-width. Both intensity and half-width are related to the relaxation phenomena of nuclei; however, they were not studied here thoroughly.

I.2 Calculation of NMR parameters

As it was explained earlier, there are two types of NMR parameters that can be calculated by quantum chemical methods and can be correlated with the signal position and the hyperfine structure of a NMR spectrum: chemical shieldings and indirect spin-spin coupling constants. Both parameters are second order molecular properties i.e. second order partial derivatives of the energy.

NMR constants $\boldsymbol{\sigma}$ and $\boldsymbol{J}$ are tensors represented by 3×3 matrices. Calculations provide values for the six components of each tensor (six components instead of nine because of symmetry). Besides, in isotropic solutions, an isotropic NMR parameter is calculated from the trace of its corresponding tensor.

$$M = \frac{1}{3} Tr(\boldsymbol{M}) = \frac{1}{3}\left(M_{xx} + M_{yy} + M_{zz}\right) \qquad \boldsymbol{M} = \boldsymbol{\sigma}, \boldsymbol{J} \tag{1.11}$$

In the present work, we have considered isotropic values for $\boldsymbol{\sigma}$ and $\boldsymbol{J}$ represented by σ and J respectively.

I.2.1 Chemical shift $\boldsymbol{\sigma}$

I.2.1.1 GIAO method

It is known that when a system is placed in an external magnetic field, the canonical momentum $\vec{P}$ is replaced by the mechanical momentum $\vec{P} + \alpha\vec{A}$ in the quantum mechanical equations for electrons, where $\alpha \approx 1/137$ is the fine structure constant, and $\vec{A}$ is the vector potential. Thus, for a hydrogen atom placed in a magnetic field $\vec{B}$, the electronic Hamiltonian is given by

$$h = -\frac{\vec{\nabla}^2}{2} + V(\vec{r}) + \alpha\vec{A}.\vec{P} + \frac{\alpha^2}{2}\vec{A}^2 \tag{1.12}$$

where $V(\vec{r})$ is the electrostatic potential energy at position $\vec{r}$. The vector potential $\vec{A}$ consists of the external potential $\vec{A}_0$ due to $\vec{B}$ and the potential $\vec{A}_K$ due to the magnetic moment $\vec{m}_K$ of nucleus K placed at position.$\vec{R}_K$. Note that the Hamiltonian is expressed in atomic units, in which all the equations of section I.2.1.1 shall be given. Inserting $\vec{A} = \vec{A}_0 + \vec{A}_K$ in equation (1.12), we obtain the corresponding Hamiltonian.

$$\vec{A}_0 = \frac{1}{2}\vec{B} \times (\vec{r} - \overrightarrow{R_0}) \tag{1.13}$$

$$\vec{A}_K = \frac{\vec{m}_K \times (\vec{r} - \vec{R}_K)}{\left|\vec{r} - \vec{R}_K\right|^3} \tag{1.14}$$

The homogenous magnetic field $\vec{B}$ represented by the potential vector $\vec{A}_0$ is clearly independent of the gauge origin $\vec{R}_0$ since $\vec{\nabla}.\vec{A}_0 = 0$. Thus, there is no unique choice of $\vec{A}_0$ for a given magnetic field $\vec{B}$. However, we would expect that values of observable quantities (such as σ) do not depend on the chosen origin. This is true only in the limit case of exact wavefunction. For the approximate solution of the electronic problem, the calculated observable would be dependent on the choice of $\vec{A}_0$ [10]. This is a major problem for quantum chemistry. The origin of this problem is due to the finite basis set representation used for molecular orbitals. For atoms, there is no problem in using finite basis as long as the basis are eigenfunctions of the angular momentum $\vec{L}$.

The Gauge origin problem in a molecule can be surmounted by using more than one gauge origin for the external magnetic field. This is known as the local or distributed gauge origins, which ensures a good description of magnetic interactions. The idea of distributed origins can be achieved by introducing a gauge transformation of the wavefunction

$$\Psi \rightarrow \Psi' = \Psi \prod_{i=1}^{N} \sum_{A=1}^{N_F} \exp\,(\Lambda_A\,(r_i))P_A^i \tag{1.15}$$

where *N* is the number of electrons and N_F is the number of fragments in a given system. The gauge factor $\Lambda_A(r_i)$ which is given by

$$\Lambda_A(r_i) = \frac{i\alpha}{2}[(\vec{R}_A - \vec{R}) \times \vec{B}].\vec{r} \tag{1.16}$$

shifts the gauge origin of a one electron wave function from $\vec{R}$ to the gauge origin $\vec{R}_A$. P_A^i is the projector on the one electron subspace and on the local fragment *A*. Note that the above transformation $\Psi \rightarrow \Psi'$ indeed defines a valid gauge transformation leaving for the exact solution of the Schrödinger equation all physical observables invariant. This concept has first been applied in the so-called GIAO method (Gauge Including Atomic Orbitals) [11; 12] where to each atomic orbital an individual gauge origin is associated.

Thus, the GIAO approach is based on choosing local gauge origins for atomic orbitals $|\chi_\mu\rangle$. In addition, it is convenient to attach the additional phase factors to the atomic orbitals instead of attaching them to the Hamiltonian. That means, the new AO that are called gauge including atomic orbitals or London orbitals are field dependent, and they are given by

$$|\chi_\mu(\vec{B})\rangle = \exp(\frac{-i\alpha}{2}(\vec{B} \times \vec{R}_\mu).\vec{r})|\chi_\mu(0)\rangle \tag{1.17}$$

where $|\chi_\mu(0)\rangle$ denotes the usual field-independent atomic orbitals centered at $\vec{R}_\mu$ and $\vec{r}$ represents the electron coordinates.

I.2.1.2 Shielding tensor calculation

We recall that when a magnetic field $\vec{B}$ is applied to a molecule containing a magnetic nucleus K with magnetic moment $\vec{m}_K$, its ground state energy changes due to the interaction of the induced electronic currents with the nuclear magnetic moment and with the applied field. For weak static perturbations, the molecular electronic energy $E(\vec{m}_K, \vec{B})$ can be expanded in a Taylor series around the unperturbed energy value. In this expansion, the term bilinear in $\vec{B}$ and $\vec{m}_K$ will be exactly equal to the change in the nuclear Zeeman energy $-\vec{m}_K(1-\boldsymbol{\sigma_K})\vec{B}$ resulting from interaction with the surrounding electrons. Therefore, the Taylor coefficient given by a second derivative of the molecular electronic energy $E(\vec{m}_K,\vec{B})$ with respect to the field strength and the nuclear magnetic moment can be identified with the nuclear shielding tensor $\boldsymbol{\sigma_K}$.

$$\boldsymbol{\sigma_K} = \frac{\partial^2 E}{\partial \vec{B} \partial \vec{m}_K}$$
$$\sigma_K^{ij} = \frac{\partial^2 E}{\partial B^i \partial m_K^j} \quad i,j = x,y,z \tag{1.18}$$

Equation (1.18) represents the good starting point for the evaluation of the components of the chemical shielding tensor at the GIAO-DFT level which is mainly used in the present work. The molecular electronic energy E can be expressed as

$$E = \langle hP \rangle + \frac{1}{2}\langle PG_{2e}(P) \rangle + E_{xc} \tag{1.19}$$

$$F = \frac{\partial E}{\partial P} = h + G_{2e}(P) + G_{xc} = h + G \tag{1.20}$$

where P is the density matrix, h is the one-electron Hamiltonian given previously in equation (1.12), E_{xc} is the exchange-correlation energy in the framework of DFT method, F is the one-electron Kohn-Sham operator, and G_{xc} is the exchange-correlation piece of F (for more information about Kohn-Sham DFT see section II). The matrix elements of $G_{2e}(P)$ are given by

$$G_{2e}(P)_{\mu\nu} = \langle \chi_\mu | G_{2e}(P) | \chi_\nu \rangle = \sum_{rs} P_{rs} \langle \chi_\mu \chi_r | \chi_\nu \chi_s \rangle \tag{1.21}$$

where $\langle \chi_\mu \chi_r | \chi_\nu \chi_s \rangle$ is the antisymmetrized two-electron integral over the atomic orbitals χ_μ. For Pure DFT methods, $G_{2e}(P)$ represents the Coulomb electrostatic energy while for hybrid methods, it includes a coefficient for the Hartree-Fock exchange C_{HFx}.

$$\langle \chi_\mu \chi_r | \chi_\nu \chi_s \rangle = \int \chi_\mu^* \chi_r^* \frac{1}{r_{12}} [\chi_\nu \chi_s - C_{HFx} \chi_s \chi_\nu] d\tau_1 \tau_2 \tag{1.22}$$

The coefficient C_{HFx} is zero for pure DFT and non-zero for hybrid methods.

Now, using equation (1.18), the elements of the shielding tensor of nucleus K can be derived from equation (1.19) with the help of the interchange theorem of perturbation theory (13; 14).

$$\sigma_K^{ij} = \sum_{\mu,\nu} P_{\mu\nu} \frac{\partial^2 h_{\mu\nu}}{\partial B^i \partial m_K^j} + \sum_{\mu,\nu} \frac{\partial P_{\mu\nu}}{\partial B^i} \frac{\partial h_{\mu\nu}}{\partial m_K^j} \tag{1.23}$$

In equation (1.23), $h_{\mu\nu}$ are the elements of the one-electron Hamiltonian matrix and $P_{\mu\nu}$ are the elements of the density matrix in the atomic orbital representation. Then,

$$h_{\mu\nu} = \langle \chi_\mu | h | \chi_\nu \rangle \tag{1.24}$$

$$P_{\mu\nu} = \langle \chi_\mu | P | \chi_\nu \rangle \tag{1.25}$$

The density matrix of a closed shell molecule can be given in terms of the coefficients of the expansion of the molecular orbitals ϕ_l in terms of the atomic orbitals χ_μ.

$$\phi_l = \sum_l c_{\mu l}\, \chi_\mu \tag{1.26}$$

Then,
$$P_{\mu\nu} = 2\sum_l {c_{\mu l}}^{*} c_{\nu l} \tag{1.27}$$

To calculate the shielding tensor elements, the derivatives of the Hamiltonian h are needed. The Hamiltonian h of equation (1.12) can be reformulated by inserting the explicit form of the vector potential (equations (1.13) and (1.14)) and thus, the first and second derivatives of $h_{\mu\nu}$ ($\frac{\partial h_{\mu\nu}}{\partial m_K^j}$ and $\frac{\partial^2 h_{\mu\nu}}{\partial B^i \partial m_K^j}$) can be expressed in the atomic units as

$$\frac{\partial h_{\mu\nu}}{\partial m_K^j} = \left\langle \chi_\mu \middle| \frac{\partial h}{\partial m_K^j} \middle| \chi_\nu \right\rangle = -i\alpha \left\langle \chi_\mu \middle| \frac{\left[(\vec{r} - \vec{R}_K) \times \vec{\nabla}\right]^j}{\left|\vec{r} - \vec{R}_K\right|^3} \middle| \chi_\nu \right\rangle \tag{1.28}$$

$$\frac{\partial^2 h_{\mu\nu}}{\partial B^i \partial m_K^j} = \left\langle \chi_\mu \middle| \frac{\partial^2 h}{\partial B^i \partial m_K^j} \middle| \chi_\nu \right\rangle = \frac{\alpha^2}{2} \left\langle \chi_\mu \middle| \frac{\vec{r}.\left(\vec{r} - \vec{R}_K\right)\delta^{ij} - \vec{r}^j.\left(\vec{r} - \vec{R}_K\right)^i}{\left|\vec{r} - \vec{R}_K\right|^3} \middle| \chi_\nu \right\rangle \tag{1.29}$$

where $\vec{r}$ is the position of the electron, $\vec{R}_K$ is the position of nucleus K, $\alpha \approx 1/137$ is the fine structure constant, and δ^{ij} is the Dirac delta function.

Equation (1.29) is true for field-independent basis functions; however, in the GIAO approach, the basis functions are field dependent (see equation (1.17)) and thus, the derivation with respect to B^i includes additional terms.

$$\begin{aligned} \frac{\partial^2 h_{\mu\nu}}{\partial B^i \partial m_K^j} &= \frac{\partial^2 \langle \chi_\mu | h | \chi_\nu \rangle}{\partial B^i \partial m_K^j} = \left\langle \chi_\mu \middle| \frac{\partial^2 h}{\partial B^i \partial m_K^j} \middle| \chi_\nu \right\rangle + \left\langle \frac{\partial \chi_\mu}{\partial B^i} \middle| \frac{\partial h}{\partial m_K^j} \middle| \chi_\nu \right\rangle + \left\langle \chi_\mu \middle| \frac{\partial h}{\partial m_K^j} \middle| \frac{\partial \chi_\nu}{\partial B^i} \right\rangle \\ &= \left\langle \chi_\mu \middle| \frac{\partial^2 h}{\partial B^i \partial m_K^j} \middle| \chi_\nu \right\rangle + i\alpha \left\langle \chi_\mu \middle| \left(\frac{\vec{r}}{2} \times (\vec{R}_\nu - \vec{R}_\mu)\right) \frac{\partial h}{\partial m_K^j} \middle| \chi_\nu \right\rangle \end{aligned} \tag{1.30}$$

Now, inserting equations (1.28) and (1.29) in (1.30), the expression of $\frac{\partial^2 h_{\mu\nu}}{\partial B^i \partial m_K^j}$ can be obtained which, if multiplied by $P_{\mu\nu}$, generates the first term of the chemical shielding (see equation (1.23).

The second term of the nuclear magnetic shielding requires, in addition to the derivative of the one-electron Hamiltonian given in equation (1.28), the derivative of the density matrix with respect to the magnetic field.

$$\begin{aligned}\frac{\partial P_{\mu\nu}}{\partial B^i} = \frac{\partial\langle\chi_\mu|P|\chi_\nu\rangle}{\partial B^i} &= \left\langle\chi_\mu\middle|\frac{\partial P}{\partial B^i}\middle|\chi_\nu\right\rangle + \left\langle\frac{\partial\chi_\mu}{\partial B^i}\middle|P\middle|\chi_\nu\right\rangle + \left\langle\chi_\mu\middle|P\middle|\frac{\partial\chi_\nu}{\partial B^i}\right\rangle \\ &= \left\langle\chi_\mu\middle|\frac{\partial P}{\partial B^i}\middle|\chi_\nu\right\rangle + i\alpha\left\langle\chi_\mu\middle|\left(\frac{\vec{r}}{2}\times(\vec{R}_\nu - \vec{R}_\mu)\right)P\middle|\chi_\nu\right\rangle\end{aligned} \tag{1.31}$$

The two terms $\left\langle\frac{\partial\chi_\mu}{\partial B^i}\middle|P\middle|\chi_\nu\right\rangle$ and $\left\langle\frac{\partial\chi_\mu}{\partial B^i}\middle|P\middle|\chi_\nu\right\rangle$ are easily obtained through the explicit dependence of the atomic orbitals of the GIAO approach on the magnetic field (equation (1.17)); however, the term $\frac{\partial P}{\partial B^i}$ is obtained via the solution of the coupled-perturbed (CP) equations [15; 16] for which a brief description will be given in the part I.2.1.3.

I.2.1.3 Coupled perturbed equations

For a perturbed system, the expansion of the one-electron Hamiltonian h and the density matrix P can be expressed as

$$h = h_0 + \lambda h^{(1)} + \lambda^2 h^{(2)} + \cdots \tag{1.32}$$

$$P = P_0 + \lambda P^{(1)} + \lambda^2 P^{(2)} + \cdots \tag{1.33}$$

where h_0 and P_0 are the unperturbed Hamiltonian and density matrix respectively, and λ represents the external perturbation which is the magnetic field $\vec{B}$ in the present case. The perturbed density matrix P obeys the two conditions:

$$FP - PF = 0 \quad (1.34)$$

$$P^2 = P \quad (1.35)$$

where $F = h + G$ has been already defined in equation (1.20). In the first condition (equation (1.34)) the density matrix commutes with F, while in the second (equation (1.33)) it is considered to be idempotent [17]. These two conditions are sufficient and necessary to solve for the perturbed density matrix. The change in P cause a change in F which can be also expressed as a perturbation series.

$$F = F_0 + \lambda\Delta^{(1)} + \lambda^2\Delta^{(2)} + \cdots \quad (1.36)$$

where

$$\Delta^{(i)} = h^{(i)} + G(P^{(i)}) \quad (1.37)$$

Inserting equations (1.33) and (1.36) into (1.34) and separating the orders, one obtains the zeroth and first order equations.

$$F_0P_0 - P_0F_0 = 0 \quad (1.38)$$

$$F_0P^{(1)} - P^{(1)}F_0 + \Delta^{(1)}P_0 - P_0\Delta^{(1)} = 0 \quad (1.39)$$

Besides, inserting equation (1.33) in (1.35) and separating the orders, one finds by equating the zeroth and first orders

$$P_0^2 = P_0 \quad (1.40)$$

$$P_0P^{(1)} + P^{(1)}P_0 = P^{(1)} \quad (1.41)$$

Now, we define the projection operators P_1 and P_2 for the subspaces spanned by the n occupied orbitals and the $(m - n)$ empty orbitals respectively.

$$P_1 = P_0 \quad (1.42)$$

$$P_2 = 1 - P_0 \quad (1.43)$$

Using the projection operators, any $m \times m$ matrix M can be resolved into the sum of four projected parts $M_{ij} = P_i M P_j$ $(i, j = 1, 2)$. Then, an equation $A = B$ is equivalent to the four equations $A_{ij} = B_{ij}$.

Projecting equation (1.41) and taking into account the projection operator properties ($P_i^2 = P_i$ and $P_i P_j = 0$ for $i \neq j$), one finds that the (11) and (22) components of the first-order change must vanish while the (12) and (21) components are Hermitian conjugate. Then, $P^{(1)}$ can be expressed as

$$P^{(1)} = P_{12}^{(1)} + P_{21}^{(1)} = P_{12}^{(1)} + P_{12}^{(1)\dagger} \tag{1.44}$$

To determine $P_{12}^{(1)}$, we use the projection of equation (1.39).

$$F_0 P_{12}^{(1)} - P_{12}^{(1)} F_0 - \Delta_{12}^{(1)} = 0 \tag{1.45}$$

Equation (1.45) can be rewritten as

$$P_{12}^{(1)} = F_0^{-1}\left(P_{12}^{(1)} F_0 + \Delta_{12}^{(1)}\right) \tag{1.46}$$

Starting with $P_{12}^{(1)} = 0$ in the right hand side, the solution of $P_{12}^{(1)}$ can be calculated iteratively where its formal solution can be expressed as

$$P_{12}^{(1)} = \sum_{n=0}^{\infty} F_0^{-(n+1)} \Delta_{12}^{(1)} F_0^{n} \tag{1.47}$$

However, from equation (1.37), $\Delta_{12}^{(1)}$ depends on $P_{12}^{(1)}$ thus, the equation (1.47) has to be solved iteratively till convergence. $P_{12}^{(1)}$ may be determined more conveniently in terms of the eigenvectors of F_0; this may be done [17] by writing F_0 in terms of its eigenvalues ε_i and the projection operators of the eigenvectors.

$$F_0 = \sum_{i=1}^{m} \varepsilon_i \, \rho_i \tag{1.48}$$

where $\rho_i = C_i C_i^\dagger$ is the projection operator for the eigenvector C_i. In addition, the projection operators P_1 and P_2 can be expressed as $P_1 = \sum_{o(occ)} \rho_o$ and $P_2 = \sum_{u(unocc)} \rho_u$. Now, taking advantage of the fact that $f(F_0) = \sum_{i=1}^{m} f(\varepsilon_i)\, \rho_i$, equation (1.47) can be rewritten as

$$\begin{aligned} P_{12}^{(1)} &= \sum_{n=0}^{\infty} F_0^{-(n+1)} P_1 \Delta^{(1)} P_2 F_0^n = \sum_{n=0}^{\infty} \sum_{o(occ)} \sum_{u(unocc)} \varepsilon_o^{-(n+1)} \rho_o \Delta^{(1)} \rho_u \varepsilon_u^n \\ &= \sum_{n=0}^{\infty} \sum_{o(occ)} \sum_{u(unocc)} \left(\frac{\varepsilon_u^n}{\varepsilon_o^{n+1}}\right) \left(C_o^\dagger \Delta^{(1)} C_u\right) C_o C_u^\dagger \end{aligned} \tag{1.49}$$

This expression is a geometric series with respect to n; it converges to give the form

$$P_{12}^{(1)} = \sum_{\substack{o(occ)\\ u(unocc)}} \frac{C_o^\dagger \Delta^{(1)} C_u}{\varepsilon_o - \varepsilon_u} C_o C_u^\dagger \tag{1.50}$$

Once $P_{12}^{(1)}$ is obtained, $P^{(1)}$ can be easily calculated from equation (1.44).

$$P^{(1)} = \sum_{\substack{o(occ)\\ u(unocc)}} \frac{C_o^\dagger \Delta^{(1)} C_u}{\varepsilon_o - \varepsilon_u} \left(C_o C_u^\dagger - C_u C_o^\dagger\right) \tag{1.51}$$

In our calculations of chemical shielding tensor, we were in need for the derivative of the density matrix with respect to the magnetic field ($\frac{\partial P}{\partial B^i}$) which is represented by $P^{(1)}$ in the coupled perturbed equations while $\Delta^{(1)}$ stands for $\frac{\partial F}{\partial B^i}$.

Usually, the orthonormality of the molecular orbitals is considered as an additional constraint added directly to the electronic energy. Then, the equation (1.19) can be rewritten in a more convenient way as

$$E' = \langle hP \rangle + \frac{1}{2}\langle PG_{2e}(P) \rangle + E_{xc} - 2\sum_{rs}^{occ} \varepsilon_{rs}\left(\sum_{\mu\nu} c_{\mu r}^{*} c_{\nu s} S_{\mu\nu} - \delta_{rs}\right) \tag{1.52}$$

where ε_{rs} is demonstrated to be a diagonal matrix whose diagonal elements are the orbital energies [18], and $S_{\mu\nu}$ is the overlap matrix given by

$$S_{\mu\nu} = \langle \chi_\mu | \chi_\nu \rangle \tag{1.53}$$

As a result, the constraint term added in equation (1.52) gives a new expression for $\frac{\partial P}{\partial B^i}$.

$$\frac{\partial P}{\partial B^i} = \frac{1}{2} P_0 \frac{\partial S}{\partial B^i} P_0 + \sum_{\substack{o(occ) \\ u(unocc)}} \frac{C_o^{\dagger}\left(\frac{\partial F}{\partial B^i} - \varepsilon_o \frac{\partial S}{\partial B^i}\right) C_u}{\varepsilon_o - \varepsilon_u} \left(C_o C_u^{\dagger} - C_u C_o^{\dagger}\right) \tag{1.54}$$

$\frac{\partial S_{\mu\nu}}{\partial B^i}$ and $\frac{\partial F_{\mu\nu}}{\partial B^i}$ are given by

$$\frac{\partial S_{\mu\nu}}{\partial B^i} = i\alpha \left(\frac{\vec{r}}{2} \times (\vec{R}_\nu - \vec{R}_\mu)\right)^i \langle \chi_\mu | \chi_\nu \rangle \tag{1.55}$$

$$\frac{\partial F_{\mu\nu}}{\partial B^i} = \frac{\partial h_{\mu\nu}}{\partial B^i} + \frac{\partial G_{\mu\nu}}{\partial B^i} \tag{1.56}$$

$$\frac{\partial h_{\mu\nu}}{\partial B^i} = \left\langle \chi_\mu \middle| \frac{\partial h}{\partial B^i} \middle| \chi_\nu \right\rangle + \left\langle \frac{\partial \chi_\mu}{\partial B^i} \middle| h \middle| \chi_\nu \right\rangle + \left\langle \chi_\mu \middle| h \middle| \frac{\partial \chi_\nu}{\partial B^i} \right\rangle$$
$$= -i\alpha \left\langle \chi_\mu \middle| \left(\frac{\vec{r}}{2} \times \vec{\nabla}\right)^i \middle| \chi_\nu \right\rangle + i\alpha \left\langle \chi_\mu \middle| \left(\frac{\vec{r}}{2} \times (\vec{R}_\nu - \vec{R}_\mu)\right)^i h \middle| \chi_\nu \right\rangle \tag{1.57}$$

$$\frac{\partial G_{\mu\nu}}{\partial B^i} = \frac{\partial}{\partial B^i}\left[\sum_{rs} P_{rs}\langle \chi_\mu \chi_r | \chi_\nu \chi_s \rangle + G_{xc}\right] \tag{1.58}$$

Note that equation (1.54) must be solved iteratively because $\frac{\partial F}{\partial B^i}$ and $\frac{\partial P}{\partial B^i}$ depend on each other.

I.2.2 Indirect spin-spin coupling constant *J*

Consider a molecular system, where the nuclear magnetic moments are given by $\vec{m}_P$. It is evident that electrons will interact with the nuclear magnetic moments. These interactions are tiny relative to the electrostatic interactions between the electrons and nuclei and are therefore adequately described by perturbation theory. For closed-shell molecules, there is no first order change in the electronic energy. To second order, the change is described in terms of the reduced indirect spin-spin coupling tensor $\boldsymbol{K_{PQ}}$.

$$E(\vec{m}) = E(0) + \sum_{P>Q} \vec{m}_P \boldsymbol{K_{PQ}} \vec{m}_Q + O(\vec{m}^3) \tag{1.59}$$

where $\vec{m}$ denotes the collection of all magnetic moments $\vec{m}_P$ in the molecule. Therefore, the $\boldsymbol{K_{PQ}}$ tensor (describing the coupling between nuclei *P* and *Q*) is simply given by

$$\boldsymbol{K_{PQ}} = \frac{\partial^2 E}{\partial \vec{m}_P \partial \vec{m}_Q} \tag{1.60}$$

The spectroscopically observed indirect NMR spin-spin coupling tensor $\boldsymbol{J_{PQ}}$ is proportional to the reduced tensor $\boldsymbol{K_{PQ}}$. $\boldsymbol{J_{PQ}}$ is also calculated as the mixed second order partial derivative of the total electronic energy E with respect to the nuclear magnetic moments $\vec{m}_P$ and $\vec{m}_Q$ of the coupled nuclei P and Q.

$$\boldsymbol{J_{PQ}} = h\frac{\gamma_P}{2\pi}\frac{\gamma_Q}{2\pi}\frac{\partial^2 E}{\partial\vec{m}_P\partial\vec{m}_Q} = h\frac{\gamma_K}{2\pi}\frac{\gamma_L}{2\pi}\boldsymbol{K_{PQ}} \tag{1.61}$$

where h is plank's constant, γ_P and γ_Q are the gyromagnetic rations of P and Q. The corresponding scalar spin-spin coupling constant is one third of the trace of this tensor i.e. the average of the diagonal elements of $\boldsymbol{J_{PQ}}$.

As a result of the magnetic hyperfine coupling of the nuclear spin to the orbital motion of the electrons and to the spin of the electrons, four additional terms must be added to the Hamiltonian.

$$H_m = H^{DSO} + H^{PSO} + H^{FC} + H^{SD} \tag{1.62}$$

First, the spin-orbit SO coupling represents the interaction between the nuclear magnetic moments and the orbital magnetic moments of electrons. There are two spin-orbit operators: the diamagnetic SO (DSO) operator and the paramagnetic SO (PSO) operator.

Next, the interaction between nuclear and electronic spin magnetic moments leads to the Fermi contact (FC) term and the spin-dipole (SD) term. While the FC operator represents the interaction at the position of the nucleus, the SD operator represents the interaction at a distance.

The expression of H_m given in the equation (1.62) can be rewritten in such a way that the nuclear magnetic moments are shown explicitly.

$$H_m = \sum_{P<Q}\vec{m}_P\boldsymbol{H_{PQ}^{DSO}}\vec{m}_Q + \sum_P\vec{m}_P(iH_P^{PSO} + H_P^{FC} + H_P^{SD}) \tag{1.63}$$

The factor of i has been introduced to make the operator real. However, H_m can be expressed in terms of one-particle operators $\boldsymbol{h_{PQ}^{DSO}}$, h^{PSO}, h^{FC}, and h^{SD}.

$$H_m = \int d^3r\Psi^+(\vec{r})\left[\sum_{P<Q} \vec{m}_P \boldsymbol{h_{PQ}^{DSO}} \vec{m}_Q + \sum_P \vec{m}_P (ih_P^{PSO} + h_P^{FC} + h_P^{SD})\right]\Psi(\vec{r}) \qquad (1.64)$$

Note that $\boldsymbol{h_{PQ}^{DSO}}$ is a tensor while the three operators h^{PSO}, h^{FC}, and h^{SD} are vectors. These four operators are given, in the atomic units, by

$$\boldsymbol{h_{PQ}^{DSO}} = \alpha^4 \left(\frac{\vec{r}_P}{r_P^3}^T . \frac{\vec{r}_Q}{r_Q^3} I - \frac{\vec{r}_P}{r_P^3} . \frac{\vec{r}_Q}{r_Q^3}^T \right) \qquad (1.65)$$

$$h_P^{PSO} = \alpha^2 \frac{\vec{r}_P}{r_P^3} \times \vec{\nabla} \qquad (1.66)$$

$$h_P^{FC} = \frac{8\pi\alpha^2}{3} \delta(\vec{r}_P)\vec{s} \qquad (1.67)$$

$$h_P^{SD} = \alpha^2 \frac{3(\vec{s}.\vec{r}_{PK})\vec{r}_P - r_P^2 \vec{s}}{r_P^5} \qquad (1.68)$$

where I is 3×3 unit matrix, $\alpha \approx 1/137$ is the fine structure constant, $\vec{r}_P = \vec{r} - \vec{R}_P$ is the relative position with respect to the nucleus P, $\vec{s}$ is the electron spin, and $\delta(\vec{r}_P)$ is the Dirac delta function. Similarity, the isotropic reduced coupling constant can be decomposed into four components related to the four coupling mechanisms [19].

$$K_{PQ} = K_{PQ}^{DSO} + K_{PQ}^{PSO} + K_{PQ}^{FC} + K_{PQ}^{SD} \qquad (1.69)$$

$$K_{PQ}^{DSO} = \frac{1}{3} \int d^3r \rho^0(\vec{r}) Tr(\boldsymbol{h_{PQ}^{DSO}}) \qquad (1.70)$$

$$K_{PQ}^{PSO} = -\frac{2}{3} \langle \Psi^0 | H_P^{PSO} | \Psi^{Q,PSO} \rangle \qquad (1.71)$$

$$K_{PQ}^{FC} = \frac{2}{3} \langle \Psi^0 | H_P^{FC} | \Psi^{Q,FC} \rangle \qquad (1.72)$$

$$K_{PQ}^{SD} = \frac{2}{3}\langle\Psi^0|H_P^{SD}|\Psi^{Q,SD}\rangle \tag{1.73}$$

where Ψ^0 is the ground-state wavefunction for $\vec{m}_P = \vec{m}_Q = 0$ while $\Psi^{Q,X}$ is the perturbed wavefunction by the magnetic moment of nucleus Q (X stands for PSO, FC, or SD), and ρ^0 is the density of the unperturbed state.

For the calculation of K_{PQ} using the density functional theory (see part II), equation (1.60) is a good starting point. The magnetic field generating from the magnetic moments of nuclei leads to four additional terms in the DFT energy corresponding to the four additional terms in the Hamiltonian of equation (1.62), which can be expressed in terms of one-particle operators (equations (1.65) – (1.68)).

$$E_m = E^{DSO} + E^{PSO} + E^{FC} + E^{SD} \tag{1.74}$$

$$E^{DSO} = \sum_{P<Q}\vec{m}_P\sum_{ls}^{occ}\langle\phi_{ls}|\boldsymbol{h}_{\boldsymbol{PQ}}^{\boldsymbol{DSO}}|\phi_{ls}\rangle\vec{m}_Q \tag{1.75}$$

$$E^{PSO} = \sum_{P}\vec{m}_P\sum_{ls}^{occ}\langle\phi_{ls}|ih_P^{PSO}|\phi_{ls}\rangle \tag{1.76}$$

$$E^{FC} = \sum_{P}\vec{m}_P\sum_{ls}^{occ}\langle\phi_{ls}|h_P^{FC}|\phi_{ls}\rangle \tag{1.77}$$

$$E^{SD} = \sum_{P}\vec{m}_P\sum_{ls}^{occ}\langle\phi_{ls}|h_P^{SD}|\phi_{ls}\rangle \tag{1.78}$$

where ϕ_{ls} is the spin-orbital defined by $\phi_{ls} = \phi_l.\sigma(s)$ with ϕ_l denoting the space orbital and $\sigma(s)$ denoting the two dimensional spinor. Now, evaluating the energy derivative of equation (1.60) for the DFT energy, the contributions to the isotropic reduced coupling constant can be given by

$$K_{PQ}^{DSO} = \frac{2}{3}\sum_{l}^{occ}\langle\phi_l^0|Tr\boldsymbol{h}_{\boldsymbol{PQ}}^{\boldsymbol{DSO}}|\phi_l^0\rangle \tag{1.79}$$

$$K_{PQ}^{PSO} = -\frac{4}{3}\sum_{l}^{occ}\langle\phi_l^0|h_P^{PSO}|\phi_l^{Q,PSO}\rangle \quad (1.80)$$

$$K_{PQ}^{FC} = \frac{2}{3}\sum_{ls}^{occ}\langle\phi_{ls}^0|h_P^{FC}|\phi_{ls}^{Q,FC}\rangle \quad (1.81)$$

$$K_{PQ}^{SD} = \frac{2}{3}\sum_{ls}^{occ}\langle\phi_{ls}^0|h_P^{SD}|\phi_{ls}^{Q,SD}\rangle \quad (1.82)$$

where ϕ_{ls}^0 represents the ground-state spin-orbitals for $\vec{m}_P = \vec{m}_Q = 0$ while ϕ_{ls}^Q represents the perturbed spin-orbitals by the magnetic moment of nucleus Q. The first order spin-orbitals are given, using the standard perturbation theory, by

$$|\phi_{ls}^{Q,X}\rangle = \sum_{l's'}^{vir}\frac{\langle\phi_{l's'}^0|F_Q^X|\phi_{ls}^0\rangle}{e_l - e_{l'}}|\phi_{l's'}^0\rangle \quad (1.83)$$

where the sum runs over virtual orbitals, X stands for PSO, FC, or SD, e_l and $e_{l'}$ are the unperturbed energies corresponding to the spin-orbitals ϕ_{ls}^0 and $\phi_{l's'}^0$ respectively, and F_Q^X is the first-order-term of the perturbed Kohn-Sham (KS) (see part II.3) operator which is solved iteratively.

$$F_Q^X = h_Q^X + \tilde{F}_Q^X \;\; with \;\; \tilde{F}_Q^X = \sum_{ls}^{occ}\int d^3r\frac{\delta F}{\delta\phi_{ls}(\vec{r})}\,\phi_{ls}^{Q,X}(\vec{r}) \quad (1.84)$$

Indirect scalar spin-spin coupling constants are often dominated by the FC contributions. However, all four contributions to the spin-spin coupling constants should be considered in any attempt to have a quantitative accuracy; the PSO, DSO and SD contributions may often be small but can rarely be neglected.

I.3 Simulation of the NMR spectrum starting from its parameters σ and J

In all our work, we have studied proton NMR spectra, which is the application of nuclear magnetic resonance with respect to hydrogen. Here, we will discuss the simulation of proton NMR spectra starting from known parameters. Once σ and J are calculated for a given molecule, we can simulate the NMR spectrum. This allows the comparison with experimental spectrum as well as the analysis of the NMR spectra obtained from patients using a basis of metabolites.

A proton is a charged particle of spin $I = 1/2$; it generates a magnetic moment along its axis of rotation. The magnitude of the magnetic moment in any given direction has two equal, but opposite, observable values ($1/2$ and $-1/2$) that correspond to the spin quantum numbers. Thus, if a proton is found in a magnetic field along z-direction, it can be regarded as to line up with the field ($I_z = -1/2$) or against the field ($I_z = 1/2$). The magnetic moment of a proton cannot be detected experimentally unless the proton is placed in an external magnetic field; we recall that the energy of the nucleus in this case is given by

$$E = \pm\gamma\hbar\, B/2 \tag{1.85}$$

and the Hamiltonian can be written in the form [20]

$$H = \gamma\hbar B I_z \tag{1.86}$$

The notation $\pm$ represents the up and down spins and B is the strength of the field at the nucleus. It is good to introduce at this point suitable wave functions to describe the magnetic states of individual nuclei (protons). The spin wavefunction α is assigned to the nucleus with $I_z = 1/2$ and the wavefunction β to the nucleus with $I_z = -1/2$. Taking the shielding tensor σ into account would just require the replacement of the magnetic field by its new value $B = (1-\sigma)B_0$ where B_0 is the applied magnetic field; then, for example, the energy corresponding to the wavefunction α becomes $\gamma\hbar(1-\sigma)\, B_0/2$.

For a molecule having many protons, it is more convenient to analyze the over-all energy levels of the molecule. If we have *N* protons and each proton has two magnetic states, 2^N possible combinations of the spin quantum numbers are found. The Hamiltonian describing this system can be given by

$$H = \sum_{k=1}^{N} H_k + \sum_{i<j}^{N} \sum_{j=1}^{N} H_{ij} \tag{1.87}$$

where H_k is the hamiltonian due to the shielding at nucleus *k* (equation (1.86)) and H_{ij} is the spin-spin interaction operator between nuclei i and j. The spin-spin Hamiltonian has the form

$$\begin{aligned} H_{ij} &= h\,J_{ij}.I(i).I(j) = hJ_{ij}.\left(I_x(i).I_x(j) + I_y(i).I_y(j) + I_z(i).I_z(j)\right) \\ &= \frac{h\,J_{ij}}{4}(2\mathrm{p}_{12} - 1) \end{aligned} \tag{1.88}$$

where J_{ij} is the coupling spin-spin constant, and p_{12} is a permutation operator that interchanges possible pairs of the specified index numbers of the nuclei in product wave functions.

The total wave function, describing the group of *N* protons, cannot be expressed as the product of the individual wave functions of nuclei when these nuclei are identical. It is impossible to designate which members of equivalent nuclei have $I_z = -1/2$ and which members have $I_z = 1/2$. This problem is solved by forming wavefunctions as a combination of equivalent states.

For example, for a two nucleus molecule, four possible wavefunctions describing the nuclei *1 & 2* are possible

$$\begin{aligned} \psi_1 &= \alpha(1)\alpha(2) \\ \psi_2 &= \alpha(1)\beta(2) \\ \psi_3 &= \beta(1)\alpha(2) \\ \psi_4 &= \beta(1)\beta(2) \end{aligned} \tag{1.89}$$

The problem lies in states ψ_2 and ψ_3 which are equivalent. We cannot differentiate which nucleus has a spin up and which one has a spin down. This problem is solved by introducing the mixed total wavefunction

$$\psi = a\psi_2 + b\psi_3 \tag{1.90}$$

where a and b are the mixing coefficients. The energy of this state is given by

$$\begin{aligned} E = \frac{\langle\psi|H|\psi\rangle}{\langle\psi \mid \psi\rangle} &= \frac{\langle(a\psi_2 + b\psi_3)|H|(a\psi_2 + b\psi_3)\rangle}{\langle(a\psi_2 + b\psi_3) \mid (a\psi_2 + b\psi_3)\rangle} \\ &= \frac{a^2\langle\psi_2|H|\psi_2\rangle + b^2\langle\psi_3|H|\psi_3\rangle + 2\mathrm{ab}\langle\psi_3|H|\psi_2\rangle}{a^2 + b^2} \end{aligned} \tag{1.91}$$

Two mixed states must replace the equivalent states ψ_2 and ψ_3. These states are determined once the coefficients a and b are known. This is done using the variational method where the maximum and minimum values for E are calculated. In other words, a and b values are obtained by solving $\partial E/\partial a = 0$ and $\partial E/\partial b = 0$. This gives

$$\begin{bmatrix} \langle\psi_2|H|\psi_2\rangle - E & \langle\psi_2|H|\psi_3\rangle \\ \langle\psi_2|H|\psi_3\rangle & \langle\psi_3|H|\psi_3\rangle - E \end{bmatrix} \begin{bmatrix} a \\ b \end{bmatrix} = 0 \tag{1.92}$$

Non trivial solutions for a and b $\left(\begin{matrix} a \\ b \end{matrix} \neq \begin{matrix} 0 \\ 0 \end{matrix}\right)$ can be obtained by equating to zero the following determinant

$$\begin{vmatrix} \langle\psi_2|H|\psi_2\rangle - E & \langle\psi_2|H|\psi_3\rangle \\ \langle\psi_2|H|\psi_3\rangle & \langle\psi_3|H|\psi_3\rangle - E \end{vmatrix} = 0 \tag{1.93}$$

which leads to two values for E. Inserting these E values in equation (1.92) and taking in consideration the normalization condition which forces that $a^2 + b^2 = 1$, one obtains the eigenvector $\begin{bmatrix} a \\ b \end{bmatrix}$. Simplifying calculations, the energies of the four states can be all gathered in a single determinant.

$$\begin{vmatrix} \langle\psi_1|H|\psi_1\rangle - E & \langle\psi|H|\psi_2\rangle & \langle\psi_1|H|\psi_3\rangle & \langle\psi_2|H|\psi_4\rangle \\ \langle\psi_1|H|\psi_2\rangle & \langle\psi_2|H|\psi_2\rangle - E & \langle\psi_2|H|\psi_3\rangle & \langle\psi_2|H|\psi_4\rangle \\ \langle\psi_1|H|\psi_3\rangle & \langle\psi_2|H|\psi_3\rangle & \langle\psi_3|H|\psi_3\rangle - E & \langle\psi_3|H|\psi_4\rangle \\ \langle\psi_1|H|\psi_4\rangle & \langle\psi_2|H|\psi_4\rangle & \langle\psi_3|H|\psi_4\rangle & \langle\psi_4|H|\psi_4\rangle - E \end{vmatrix} = 0 \qquad (1.94)$$

This can be generalized to *N* proton molecule with

$$\begin{bmatrix} \langle\psi_1|H|\psi_1\rangle - E & \langle\psi_1|H|\psi_2\rangle & \cdots & \langle\psi_1|H|\psi_m\rangle \\ \langle\psi_1|H|\psi_2\rangle & \langle\psi_2|H|\psi_2\rangle - E & \cdots & \langle\psi_2|H|\psi_m\rangle \\ \cdots & \cdots & \cdots & \cdots \\ \langle\psi_1|H|\Psi_m\rangle & \langle\psi_2|H|\psi_m\rangle & \cdots & \langle\psi_m|H|\psi_m\rangle - E \end{bmatrix} \begin{bmatrix} a_1 \\ a_2 \\ \vdots \\ a_m \end{bmatrix} = 0 \qquad (1.95)$$

Note that the matrix is symmetric and that $m = 2^N =$ number of possible states. Diagonalizing this matrix leads to the energy values and eigenvectors. Once the energies are determined, we can calculate the energies of emission i.e. the difference in *E* between states where the transition is allowed. Let F_z be the sum of I_z of the *N* protons. An allowed transition between two states requires that F_z changes by one unit ($\Delta F_z = \pm 1$). Proceeding in that way, the NMR spectrum for the molecule under study can be obtained.

II Density functional theory DFT

In the present work, the theoretical calculation of NMR parameters, accomplished with the help of the equations given in section I, is done using the density functional theory that showed, in the last few years, a remarkable success in the calculation of NMR parameters [(4)].

Density Functional Theory (DFT) is a theoretical method that derives properties of the molecule based on a determination of the electron density of the molecule. There are roughly three categories of density functional methods: (i) Local density approximation (LDA) which assume that the density of the molecule is uniform throughout the molecule [(21; 22)], (ii) Gradient corrected (GC) methods which account on the non-uniformity of the electron density [(23)], (iii) Hybrid methods which attempt to incorporate some of the more useful features from ab initio methods (specifically exchange contributions from Hartree-Fock methods) as improvements of the functionals used in DFT, such as B3LYP [24; 25] which is the most commonly used functional in our computational work.

One advantage of DFT is that it is a general-purpose method, and can be applied to most systems. DFT methods are now implemented in most popular software packages, including Gaussian which we have used in our calculations.

On the other hand, one of the main disadvantages of DFT methods is the challenge in determining the most appropriate functional for a particular application. In our practice, we conclude that the B3LYP functional (together with the 6-311++G** basis set) can be considered to be a good choice for calculating NMR parameters (see chapters IV and V).

In this section, we will describe the remarkable theorems of DFT which allow us to find ground-state properties of a system without dealing directly with the many-electron wavefunction $|\Psi\rangle$.

In what follows, equations are given in atomic units ($\hbar = m = a_0 = e = 1$) such that m and e are the electron's mass and charge, and a_0 is Bohr's radius. We will deal with a system of N electrons moving in a static potential, and adopt a conventional normalization in which $\langle\Psi|\Psi\rangle = N$.

II.1 Theory of the density matrix

For a system of N electrons, the electronic wavefunction depends on $4N$ parameters; in fact, to each electron there correspond four parameters (three due to its position and one due to its spin). To simplify the notations, spin variable will not be explicitly indicated in this section and the electronic wavefunction will be written as $\Psi(\overrightarrow{r_1}, \overrightarrow{r_2}, \ldots, \overrightarrow{r_N})$.

The electronic Hamiltonian describing the system is given by

$$H = \sum_{i=1}^{N} \left[-\frac{1}{2}\nabla_i^2 - \sum_{A} \frac{Z_A}{r_{iA}}\right] + \sum_{i<j}^{N} \frac{1}{r_{ij}} = T + V_{ext} + V_{ee} \tag{1.96}$$

In equation (1.96), r_{iA} is the distance between *i-th* electron and A, r_{ij} is the distance between the *i-th* electron and the *j-th* electron, and Z_A is the mass of nucleus A. Thus, T represents the kinetic energy of electrons, V_{ext} denotes the external potential on electrons due to the nuclei, and V_{ee} represents the electron-electron interactions. Thus, the electronic energy E calculated from the Hamiltonian given in equation (1.96) depends on $4N$ parameters as a result of its relation with the wavefunction.

$$E = \frac{\langle \Psi | H | \Psi \rangle}{\langle \Psi \mid \Psi \rangle} \tag{1.97}$$

The theory of the density matrix [26] was elaborated to simplify the general expression of the energy through reducing the number of variables. The density matrix for a system of N particles is defined as the product of the wavefunction with its complex conjugate and it is given by

$$\gamma_N(\overrightarrow{r_1}, \overrightarrow{r_2}, \ldots, \overrightarrow{r_N}; \overrightarrow{r_1}', \overrightarrow{r_2}', \ldots, \overrightarrow{r_N}') = \Psi(\overrightarrow{r_1}, \overrightarrow{r_2}, \ldots, \overrightarrow{r_N}) \Psi^*(\overrightarrow{r_1}', \overrightarrow{r_2}', \ldots, \overrightarrow{r_N}') \tag{1.98}$$

Besides, the *reduced* density matrix of order p $(1 \leq p \leq N)$ which describes the density of the N particles taken in groups of p particles is defined as

$$\begin{aligned} &\gamma_p(\overrightarrow{r_1}, \overrightarrow{r_2}, \ldots, \overrightarrow{r_p}; \overrightarrow{r_1}', \overrightarrow{r_2}', \ldots, \overrightarrow{r_p}') \\ &\qquad = C_p^N \int .. \int \gamma_N(\overrightarrow{r_1}, \overrightarrow{r_2}, \ldots, \overrightarrow{r_N}; \overrightarrow{r_1}', \overrightarrow{r_2}', \ldots, \overrightarrow{r_N}') d\overrightarrow{r_{p+1}} \ldots d\overrightarrow{r_N} \end{aligned} \tag{1.99}$$

where the binomial coefficient C_p^N is the number of ways of choosing p particles from N, taking the indistinguishable arrangements into consideration. Thus, the density matrix reduced to one particle (1-RDM) is

$$\gamma_1(\overrightarrow{r_1}; \overrightarrow{r_1}') = N \int .. \int \gamma_N(\overrightarrow{r_1}, \overrightarrow{r_2}, \ldots, \overrightarrow{r_N}; \overrightarrow{r_1}', \overrightarrow{r_2}', \ldots, \overrightarrow{r_N}') d\overrightarrow{r_2} \ldots d\overrightarrow{r_N} \tag{1.100}$$

If 1-RDM is restricted to its diagonal, we obtain the electronic density of one particle in the element of volume $d\overrightarrow{r_1}$ (equation (1.100)).

$$\gamma_1(\vec{r_1};\vec{r_1}) = N\int \ldots \int |\Psi(\vec{r_1},\vec{r_2},\ldots,\vec{r_N})|^2 d\vec{r_2}\ldots d\vec{r_N} = \rho_1(\vec{r_1}) \tag{1.101}$$

The reduced density matrix to two particles (2-RDM) restricted to its diagonal gives the density of electron 1 in the element of volume $d\vec{r_1}$ and the density of electron 2 in the element of volume $d\vec{r_2}$.

$$\gamma_2(\vec{r_1},\vec{r_2};\vec{r_1},\vec{r_2}) = \rho_2(\vec{r_1};\vec{r_2}) = C_2^N\int \ldots \int |\Psi(\vec{r_1},\vec{r_2},\ldots,\vec{r_N})|^2 d\vec{r_3}\ldots d\vec{r_N} \tag{1.102}$$

Implementing 1-RDM and 2-RDM in the general definition of the electronic energy (equation (1.97)), Hohenberg and Kohn [27] were able to express the energy as a functional of the electronic density.

$$\begin{aligned} E = \int [-\frac{1}{2}\nabla^2\gamma_1(\vec{r_1};\vec{r_1}')]_{\vec{r_1}=\vec{r_1}'}d\vec{r_1} - \sum_A \int [\frac{Z_A}{r_{1A}}\gamma_1(\vec{r_1};\vec{r_1}')]_{\vec{r_1}=\vec{r_1}'}d\vec{r_1} \\ + \iint [\frac{\gamma_2(\vec{r_1},\vec{r_2};\vec{r_1}',\vec{r_2}')}{r_{12}}]_{\substack{\vec{r_1}=\vec{r_1}' \\ \vec{r_2}=\vec{r_2}'}} d\vec{r_1}d\vec{r_2} \end{aligned} \tag{1.103}$$

$$E = \underbrace{\int -\frac{1}{2}\nabla^2\rho_1(\vec{r_1})d\vec{r_1}}_{kinetic\ energy} - \underbrace{\sum_A \int \frac{Z_A}{r_{1A}}\rho_1(\vec{r_1})d\vec{r_1}}_{nuclear\ attraction} + \underbrace{\iint \frac{\rho_2(\vec{r_1},\vec{r_2})}{r_{12}}d\vec{r_1}d\vec{r_2}}_{electron-electron\ repulsion} \tag{1.104}$$

We conclude that the diagonal elements of the first and second order density matrices (1-RDM and 2-RDM) completely determine the total energy. This appears to vastly simplify the task in hand. Thus, the solution of the full Schrödinger equation for Ψ is not required to find the total energy, and it is sufficient to determine ρ_1 and ρ_2. By that, the problem in a space of 3*N* coordinates has been reduced to a problem in a 6 dimensional space.

Approaches based on the direct minimization of $E(\rho_1, \rho_2)$ suffer from the specific problem that the density matrices must be constructible from an antisymmetric wavefunction Ψ. This constraint is non-trivial and it is currently an unsolved problem [28]. In view of this, we conclude that equation (1.104) does not lead immediately to a reliable method for computing the total energy without calculating the many body wavefunction.

The observation which underpins density functional theory is that we do not even require ρ_2 to find E; the ground state energy is completely determined by the diagonal elements of the first order density matrix.

II.2 The Hohenberg-Kohn theorems

DFT was not put on a firm theoretical footing until the two theorems of Hohenberg-Kohn (H-K) [(27).]

The first theorem demonstrates the existence of one-to-one mapping between the ground state electronic density ρ_0 and the ground state wavefunction Ψ_0 of a many-particle system, and that all ground state properties can be expressed as a functional of this density. Besides, it can be shown that there exists one external potential V_{ext} which generates this electronic density.

$$E_0[\rho_0] = \int \rho_0(\vec{r})V_{ext}(\vec{r})d\vec{r} + T[\rho_0] + E_{ee}[\rho_0] = \int \rho_0(\vec{r})V_{ext}(\vec{r})d\vec{r} + F_{HK}[\rho_0] \tag{1.105}$$

In equation (1.105), we denote by E_0 the ground state energy, T the kinetic energy, and E_{ee} the interelectronic energy. The two terms T and E_{ee} form the functional of Hohenberg and Kohn F_{HK}. This functional is universal for all systems having N electrons although its analytical global expression is not known yet. While the kinetic energy expression T remains an unsolved problem, the electron-electron term E_{ee} is decomposed into two contributions: the classic term (Coulombic repulsion) and the quantum term (exchange-correlation interaction).

The second H-K theorem proves that the ground state density minimizes the total electronic energy of the system. In other words, the ground state energy can be calculated using the variational principle applied to the energy with respect to the electronic density.

$$E_0 = \min_{\rho} E[\rho(\vec{r})] \tag{1.106}$$

Traditional methods in electronic structure theory, in particular Hartree-Fock theory, are based on the complicated many-electron wave function. The main objective of the density functional theory is to replace the many-body electronic wave function by the electronic density as the basic quantity. DFT exploits the advantages of the density which is a simple quantity to deal with.

II.3 Theory of Kohn and Sham

To apply the DFT formalism one obviously needs good approximations for the functional $F_{HK} = T + E_{ee}$. For example, obtaining an expression for the kinetic energy of interacting electrons in terms of the charge density is a hard problem. This yields some difficulties in calculating the ground state energy. In 1965, Kohn and Sham (K-S) [29; 26] proposed a new method to calculate the ground state electronic energy. Within the framework of Kohn-Sham, the problem of interacting electrons situated in a static external potential V_{ext} is reduced to a problem of non-interacting electrons moving in an effective potential V_s. In other words, a fake system which is composed of N non-interacting fermions is constructed; in which its density and total energy are the same as the real system. One main advantage of this scheme is that it allows a straightforward determination of a large part of the kinetic energy in a simple way. Another advantage, from a more physical point of view, is that it provides an exact one-particle picture of interacting electronic systems. This then provides a rigorous basis for the one-particle arguments used in solid state physics and chemistry to explain and predict certain features of chemical bonding.

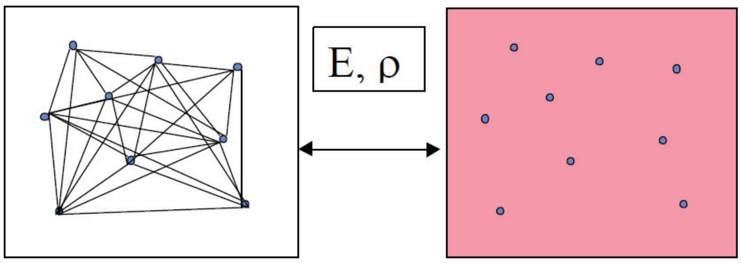

Figure 1.2: a cartoon representing the relationship between the real many body system (left hand side) and the non-interacting system of Kohn-Sham Density Functional Theory (right hand side)

We introduce a non-interacting N-particle system with ground state density ρ and external potential V_s. The ground state is a Slater determinant [30] of N orbitals ϕ_i satisfying the equation

$$F\phi_i = \left[-\frac{1}{2}\vec{\nabla}^2 + V_s(\vec{r})\right]\phi_i = \epsilon_i\phi_i \tag{1.107}$$

If we apply the first theorem of Hohenberg-Kohn to this non-interacting system, we find that there is, at most, one external potential V_s which generates ρ, and for a given ground state density ρ, all the properties of the system can be determined. This is in particular true for the kinetic energy $T_s[\rho]$ and the total energy $E[\rho]$ which are given by

$$T_s[\rho] = \sum_{i=1}^{N} -\frac{1}{2}\int \phi_i{}^*\vec{\nabla}^2\phi_i d\vec{r} \tag{1.108}$$

$$E[\rho] = T_s[\rho] + \int \rho(\vec{r})V_s(\vec{r})d\vec{r} \tag{1.109}$$

On the other hand, we recall that for the real system, the operators T and E_{ee} are universal for all systems, while the external potential V_{ext} is system dependent. V_{ext} is generated by the system's nuclei which are considered to be fixed according to the Born-Oppenheimer approximation [31], and the energy associated with the real system is

$$E[\rho] = T[\rho] + E_{ee}[\rho] + \int \rho(\vec{r})V_{ext}(\vec{r})d\vec{r} \tag{1.110}$$

Defining $J[\rho]$ as the classic Coulombic interaction between electrons, it can be written as

$$J[\rho] = E_{ee}[\rho] - E_{non-classical}[\rho] = \frac{1}{2}\iint \frac{\rho(\vec{r})\rho(\vec{r}')}{|\vec{r}-\vec{r}'|}d\vec{r}d\vec{r}' \tag{1.111}$$

where $E_{non-classical}$ is the non-classical energy composed of the exchange energy, the

Coulomb correlation, and correlation of self-interaction. Then, the energy of the real system (equation (1.110)) can be expressed as the sum of two terms: the analytically calculable part and the exchange correlation part.

$$E[\rho] = \underbrace{\int \rho(\vec{r})V_{ext}(\vec{r})d\vec{r} + T_s[\rho] + J[\rho]}_{analytically\ calculated\ part} + \underbrace{T[\rho] - T_s[\rho] + E_{ee}[\rho] - J[\rho]}_{exchange-correlation\ energy} \tag{1.112}$$

where the exchange correlation energy is given by

$$E_{xc}[\rho] = T[\rho] - T_s[\rho] + E_{ee}[\rho] - J[\rho] = \int V_{xc}(\vec{r})\rho(\vec{r})d\vec{r} \tag{1.113}$$

Thus, the exact energy of the real system can be finally written under the form

$$E[\rho] = T_s[\rho] + J[\rho] + \int \rho(\vec{r})V_{ext}(\vec{r})d\vec{r} + E_{xc}[\rho] \tag{1.114}$$

Since an analogue is considered between the fake and the real systems, their densities and energies are identical. Hence, the expression of the energy of the fake system (equation (1.109)) can be implemented in equation (1.114).

$$T_s[\rho] + \int \rho(\vec{r})V_s(\vec{r})d\vec{r} = T_s[\rho] + J[\rho] + \int \rho(\vec{r})V_{ext}(\vec{r})d\vec{r} + E_{xc}[\rho] \tag{1.115}$$

Applying, to equation (1.115), the variational principle with respect to the electronic density, one finds

$$\frac{\delta(T_s[\rho])}{\delta\rho(\vec{r})} + V_s(\vec{r}) = \frac{\delta(T_s[\rho])}{\delta\rho(\vec{r})} + \int \frac{\rho(\vec{r}')}{|\vec{r} - \vec{r}'|}d\vec{r}' + V_{ext}(\vec{r}) + \frac{\delta(E_{xc}[\rho])}{\delta\rho(\vec{r})} \tag{1.116}$$

$$V_s(\vec{r}) = V_{ext}(\vec{r}) + \int \frac{\rho(\vec{r}')}{|\vec{r} - \vec{r}'|}d\vec{r}' + V_{xc}(\vec{r}) \tag{1.117}$$

Once the expression of $V_s(\vec{r})$ is determined (equation (1.117)), Kohn-Sham equations (equation (1.107)) can be solved where their solutions, i.e. the different orbitals ϕ_i, satisfy the two conditions

$$\sum_{i}^{N} |\phi_i|^2 = \rho(\vec{r}) \quad and \quad \langle \phi_i | \phi_j \rangle = \delta_{ij} \tag{1.118}$$

The obtained orbitals, which are solutions to the KS operator *F,* can produce the electronic density of the system. However, the obtained value of ρ results in a new value of V_s (V_s depends on ρ). And, for a new V_s, Kohn-Sham equations need to be solved again giving new orbitals ϕ_i, which ends up with a new value of ρ.

The problem of solving Kohn-Sham equations has to be done in a Self-Consistent Field SCF i.e. iterative way. Usually, one starts with an initial guess for $\rho(\vec{r})$, then calculates the corresponding V_s and solves the Kohn-Sham equations for ϕ_i. From these, one calculates a new density and starts again. This procedure is then repeated until convergence is reached and the ground state density is calculated. From the calculated value of ρ, the ground state energy of the molecular system can be easily computed (equation (1.114)).

Kohn-Sham molecular orbitals are usually expanded as a linear combination of atomic orbitals (LCAO) [(32)].

$$\phi_i = \sum_{\mu} c_{\mu i} \chi_{\mu} \tag{1.119}$$

The coefficients $c_{\mu i}$ are the weights of the contributions of the atomic orbitals χ_μ to the orbitals ϕ_i. The atomic basis function χ_μ are one-electron functions centered on nuclei of the component atoms of the molecule. The atomic orbitals used are typically those of hydrogen-like atoms since these are known analytically i.e. Slater-type orbitals but other choices are possible like Gaussian functions from standard basis sets. Thus, we conclude that the appropriate choice of the basis sets is very important in solving Kohn-Sham equations and thus, in calculating the different molecular properties, the chemical shieldings and J-couplings in our case. Section III shall be devoted to describe the basis sets used in the present work.

II.4 Exchange correlation functionals

We recall that the exchange-correlation energy contains Fermi correlation between electrons of the same spin, the correlation of self-interaction, Coulomb correlation between electrons of opposite spin and the difference in the kinetic energy between the fake and the real system (equation (1.113)). However, the exchange-correlation energy is conventionally split into two parts: the exchange part and the correlation part.

$$E_{xc} = E_x + E_c \tag{1.120}$$

The major problem with DFT is that the exact functionals for exchange and correlation are not known. In fact, V_s cannot be calculated if V_{xc} is not known (equation (1.117)) which prevents solving the Kohn-Sham equations.

Over the years, many approximate exchange-correlation functionals have been developed and tested. In the absence of a single, universal function, some of these are better suited than others in calculating certain physical quantities. We shall here describe the main classes of exchange-correlation functionals, discussing briefly the functionals used in the present work (PBE, OPBE, B3LYP, and PBE0). Three approximations of the exchange-correlation energy are described: (i) the local density approximation, (ii) the generalized gradient approximation, and (iii) the hybrid approximation.

II.4.1 Local density approximation

The most famous approximation of E_{xc} is the local density approximation (LDA) [21; 22] which is the simplest approximation for the exchange-correlation energy. One advantage of this approximation is that it makes the system easier to solve (or more precisely, require less computation). In LDA, the exchange-correlation energy of an electronic system is constructed by assuming that the exchange-correlation energy per electron at a point $\vec{r}$ in the electron gas, $\varepsilon_{xc}[\rho(\vec{r})]$, is equal to the exchange-correlation energy per electron in a homogeneous electron gas that has the same electron density at the point $\vec{r}$. Then, LDA is local in the sense that the electron exchange-correlation energy at any point in space is a function of the electron density at that point only.

$$E_{xc}[\rho] = \int \varepsilon_{xc}[\rho(\vec{r})]\rho(\vec{r})d\vec{r} \tag{1.121}$$

LDA has been very successful in solid state physics but less so in chemistry, being less accurate than ab initio wavefunction theory. The LDA exchange-correlation functional is usually constructed by combining the Dirac-Slater exchange functional E_x^{DS} [33; 34] with the Vosko-Wilk-Nusair correlation functional E_c^{VWN} [35] (SVWN functional), a parameterization based on accurate simulations of the uniform electron gas [36].

The local spin-density approximation (LSDA) [37] is a generalization of the LDA to include the electron spin.

$$E_{xc}[\rho_\alpha, \rho_\beta] = \int \varepsilon_{xc}(\rho_\alpha, \rho_\beta)\rho(\vec{r})d\vec{r} \quad and \quad \rho = \rho_\alpha + \rho_\beta \tag{1.122}$$

II.4.2 Generalized gradient approximation

The LDA uses the exchange-correlation energy for the uniform electron gas at every point in the system regardless of the homogeneity of the real density. For nonuniform densities, the exchange-correlation energy can deviate significantly from the uniform result. This deviation can be expressed in terms of the gradient and higher spatial derivatives of the total density. The generalized gradient approximation (GGA) [23] uses the gradient of the density to correct for this deviation. Thus, GGA is local but it takes into account, in addition to the density, the gradient of this density at the same coordinate.

$$E_{xc}[\rho_\alpha, \rho_\beta] = \int \varepsilon_{xc}(\rho_\alpha, \rho_\beta, \vec{\nabla}\rho_\alpha, \vec{\nabla}\rho_\beta)\rho(\vec{r})d\vec{r} \tag{1.123}$$

With the emergence of GGA and the development of gradient-corrected exchange-correlation functionals, Kohn-Sham theory became competitive with the wavefunction theory. A commonly used GGA exchange correlation functional is the Perdew-Burke-Enzerhof

(PBE) functional [23; 38]. PBE is based on the properties of the slowly varying electron gas. Another known functional is the OPBE which is the result of combining the newly developed exchange functional OPTX [39; 40] with PBE.

II.4.3 Hybrid functionals

Hybrid functionals incorporate a portion of exact exchange from Hartree-Fock theory together with exchange and correlation from other sources (such as LDA or GGA). The Hartree-Fock exchange energy is calculated as, for a *N* electron molecule

$$E_x^{HF}[\{\Psi_i\}] = -\sum_{i=1}^{\frac{N}{2}}\sum_{j=1}^{\frac{N}{2}}\iint \frac{\phi_i^*(\vec{r})\phi_j(\vec{r})\phi_j^*(\vec{r}')\phi_i(\vec{r}')}{|\vec{r}-\vec{r}'|}\, d\vec{r}d\vec{r}' \qquad (1.124)$$

The popular B3LYP functional is mainly used in the present work for the calculation of NMR parameters for different metabolites and it is given by

$$E_{xc}^{B3LYP} = E_{xc}^{LDA} + a_0(E_x^{HF} - E_x^{LDA}) + a_x(E_x^{GGA} - E_x^{LDA}) + a_c(E_c^{GGA} - E_c^{LDA}) \qquad (1.125)$$

where $a_0 = 0.20$, $a_x = 0.72$, and $a_c = 0.81$ are three empirical parameters determined by fitting the predicted values to a set of atomization energies, ionization potentials, proton affinities, and total atomic energies; the local density approximation to the exchange-correlation energy is given by $E_{xc}^{LDA} = E_x^{LDA} + E_c^{LDA} = E_x^{DS} + E_c^{VWN}$; E_x^{GGA} is the Becke 88 [41] exchange functional and E_c^{GGA} is the LYP (Lee, Yang, Parr) [42; 43] correlation functional.

Another well-known hybrid functional is the PBE0 [44; 45] (sometimes called PBE1PBE) which is a non-empirical functional based on PBE with 25% of the exact exchange.

III Basis sets

From section II, we found that one important task in performing electronic structure calculations is the choice of the exchange-correlation functional. Another important task is the choice of a basis set for expanding the molecular orbitals (here Kohn-Sham orbitals). A large basis set is expected to provide accurate results but also requires a large computational cost. A small basis set, on the other hand, is computationally efficient but introduces inaccuracies in the results. It is therefore desirable to have a sequence of basis sets such that the accuracy can be controlled and at the same time being as compact as possible. In our study, we have tested three groups of basis sets in order to choose the most appropriate in calculating NMR parameters. In this part, we will present these types of basis sets having the notations X-YZG, pc-n, and pcJ-n.

Basis sets were first developed by Slater. The expression of Slater Type Orbitals (STO) [46] given in its Cartesian form is

$$\phi_i^{Slater} = STO = N x^m y^n z^o e^{-\zeta r} \tag{1.126}$$

where N is the normalization constant, ζ is the orbital exponent which accounts for how diffuse (large) the orbital is, and x, y, and z are the Cartesian coordinates.. The quantities m, n, and o are integers such that $m + n + o = l$, the atomic orbital quantum number. When $m + n + o = 0$, then STO is a s-type Gaussian function; when $m + n + o = 1$, then STO is a p-type orbital; and when $m + n + o = 2$, the STO is a d-type Orbital. Molecular calculations using STO's can be very tedious due to the evaluation of two-electron multicenter molecular integrals involving more than two atoms.

An alternative to STO is the Gaussian Type Orbital (GTO) given by

$$\phi_i^{Gaussian} = GTO = N x^m y^n z^o e^{-\alpha r^2} \tag{1.127}$$

where α is the orbital exponent and $m + n + o = l$, the atomic orbital quantum number. When $m + n + o = 0$, then GTO is said to be a s-type Gaussian function; when $m + n + o = 1$, then GTO is a p-type Gaussian; and when $m + n + o = 2$, then GTO is a d-type Gaussian.

Notice that the difference between the STO and GTO is in the exponential part. The product of two GTOs is another GTO and by that, calculations of the needed integrals become analytical, which represents a huge practical advantage as compared to STOs. However, some accuracy is lost by using GTOs so that a significantly larger number of GTOs than STOs is necessary to achieve a similar accuracy. Typically one STO should be replaced by at least three GTOs, this corresponds to a STO-3G basis set. To bypass this disadvantage i.e to reduce the number of primitive Gaussians to be fully treated, contracted Gaussian functions (that still approximate Slater-type orbitals) can be constructed as linear combinations of primitive Gaussian functions with different values of α.

$$\phi_i^{contracted} = \sum_{w=1}^{b} d_{wi}\phi_i^{Gaussian} \tag{1.128}$$

The values of the contraction coefficients d_{wi} and the orbital exponent α are obtained by fitting a contracted Gaussian function to a STO or by finding the contracted Gaussian functions that minimize the self-consistent-field energies of atoms.

III.1 Extended basis sets

The *minimal* basis set is the minimum number of basis functions needed to describe the ground state of atoms in a molecule ex: The minimal basis for C atom ($1s^2$, $2s^2$, $2p^2$) contains 5 basis functions:1s, 2s, $2p_x$, $2p_y$, $2p_z$.. Beyond the minimum number of basis functions required to describe each atom, extra basis functions, if added, introduce the *extended* basis sets. There are different types of extended basis sets: multiple-zeta (double, triple, etc), split-valence, including polarization and/or diffuse functions.

III.1.1 Double-zeta basis sets

Minimal basis sets are generally not sufficient to describe accurately atoms and molecules. This problem is solved by using the extended basis sets replacing each orbital in the minimal basis set with several basis functions that differ in size i.e. with different zeta values. For instance, in the double-zeta basis sets, each orbital in the minimal basis set is replaced by two basis functions. For the C atom, a double-zeta basis set contains 10 functions: 1s, 1s', 2s, 2s', $2p_{(x,y,z)}$ and $2p'_{(x,y,z)}$. The functions s and p differ from the functions s' and p' by their zeta value.

The triple and quadruple-zeta basis sets work in the same way, except the use of three and four orbitals instead of two.

III.1.2 Split valence basis sets

Often it takes too much computational effort to use a double-zeta form for every orbital in the minimal basis set. Instead, acceptable simplifications are made by using a double (or more)-zeta form only for the valence orbitals while the inner-shell electrons are described in the minimal basis assumption. Such a basis set is called a "split-valence basis set". For the C atom a split-valence basis set contains 9 functions: 1s, 2s, 2s', $2p_{(x,y,z)}$ and $2p'_{(x,y,z)}$.

III.1.3 Polarization functions

Extended basis set are also obtained by adding polarization functions characterized by an orbital quantum number l larger than the larger l in the minimal basis set approximation. As an example, for C: $1s^2$, $2s^2$, $2p^2$, "d, f ..." orbitals (l=2, 3…) are polarization functions while "p (l=1)" orbitals are polarization functions for H.

III.1.4 Diffuse functions

The loosely bond electrons in an atom are sometimes important in calculating some quantities. To treat correctly this long-range area, very important for instance for van der Waals systems or anions, computations can use added diffuse functions i.e. functions with very small exponents.

III.2 The basis sets used in the present work

III.2.1 Pople's basis sets

The notation for the split-valence basis sets arising from the group of John Pople [47] is typically X-YZG in which G indicates that Gaussian functions are used. In this case, the core orbitals are composed of X primitive Gaussian functions. Besides, the valence orbitals are composed of two basis functions; the first one is composed of a linear combination of Y primitive Gaussian functions, and the other is composed of a linear combination of Z primitive Gaussian functions. However, the valence orbitals can be represented by more than two basis functions, so that the notation becomes X-YZU…G.

For example, the 6-311G basis set has one contracted Gaussian function that is a linear combination of six primitive Gaussian functions for each inner-shell atomic orbital and three basis functions, one contracted Gaussian function that is a linear combination of three primitive Gaussians and two primitive Gaussian functions, for each valence orbital.

In standard notations of atomic basis sets, one asterisk (*) at the end of the name of a Pople's basis set denotes that polarization has been taken into account in the 'p' orbitals by adding a 'd' orbital. Two asterisks (**) means that polarization has been taken into account for the 's' orbitals too by adding a 'p'. Besides, diffuse basis sets are represented by the '+' signs. One '+' means that we are accounting for the diffuse 'p' orbitals, while '++' signals that we are accounting for both 'p' and 's' diffuse orbitals.

Several Pople's basis sets were used and tested in NMR calculations in the present work some of which are 6-311+G**, 6-311++G**, 6-311++G(2d,2p), and 6-311++G(3df,3pd). The notation (2d,2p) in the basis set 6-311++G(2d,2p) means that polarization has been taken into account for the 'p' orbitals by adding two 'd' orbitals, and for the 's' orbitals by adding two 'p' orbitals. Besides, the notation (3df,3pd) in the basis set 6-311++G(3df,3pd) means that polarization has been taken into account for the 'p' orbitals by adding three 'd' orbitals and one 'f' orbital, and for the 's' orbitals by adding three 'p' orbitals and one 'd' orbital.

III.2.2 Polarization consistent basis sets

Some of the most widely used basis sets are those developed by Dunning and coworkers [(48; 49)], since they are designed to converge systematically to the complete-basis-set (CBS) limit. However, these correlation-consistent polarized (cc-p) basis sets were developed for wavefunction based methods including electron correlation. These basis sets have the notation (cc-pVXZ) where X stands for D,T,Q,5,6,... (D=double, T=triples, etc.), Z means zeta, and V indicates valence basis sets. In analogy with cc-pVXZ basis sets and for independent particle models, such as DFT, the polarization consistent basis sets [(50; 51)] (pc-*n*) were developed to provide a fast and controlled convergence towards CBS. In pc-n basis sets, *n* indicates the level of polarization beyond the atomic system i.e. pc-0 is unpolarized, pc-1 is of double zeta quality with a single polarization function, pc-2 is of triple zeta quality with d- and f-type polarizations, etc.

Both (cc-pVXZ) and (pc-*n*) have been constructed using energetic criteria such that the functions contributing similar amounts of energy are included at the same stage. Besides, both are able to optimize polarization exponents for systems and augment with full set of diffuse functions and also with tight functions (pcJ-*n*) [(52)]. In our work, we have tested pc-*n* basis set for *n*=0, 1, 2, 3.

III.2.3 Polarization consistent basis sets for J-couplings

After developing the basis sets (pc-*n*), it was found that the basis set convergence for calculating nuclear spin-spin couplings can be improved by adding a single p-type function with a large exponent (tight function) and allowing for a slight decontraction of the p-functions. This resulted in the (pcJ-n) basis sets (polarization consistent basis sets for the calculation of J-couplings). In our work, we have tested pcJ-n basis set for n=0, 1, 2, 3.

IV Semi-empirical methods

Semi-empirical calculations are set up with the same general structure as Hartree-Fock HF calculations based on a wavefunction formulism. Within this framework, certain pieces of information are approximated or completely omitted in the semi-empirical approach. Usually, the core electrons are not included in the calculation and only a minimal basis set is used. Also, some of the two-electron integrals are omitted and a large number of multicenter integrals in the electronic repulsion term are neglected. In order to correct for the errors introduced by omitting part of the calculation, the method is parameterized. Often, these parameters replace some of integrals that are excluded. Parameters to estimate the omitted values are obtained by fitting the results to experimental data or ab initio calculations

The good side of semi-empirical calculations is that they are much faster than the ab initio calculations while the bad side lies in the results that can be sometimes erratic. If the molecule under study is similar to molecules in the data base used to parameterize the method, then the results may be very good; if not, the answers may be poor.

Modern semi-empirical models are based on the Neglect of Diatomic Differential Overlap (NDDO) [(53)] method in which the overlap matrix S is replaced by the unit matrix ($S_{jk} = \langle \chi_j | \chi_k \rangle$ with χ_j the j-th basis vector). This allows one to replace the Hartree-Fock equation $|H - ES| = 0$ with a simpler equation $|H - E| = 0$. Approximations are also made when evaluating one- and two-electron integrals. Semi-empirical models based on NDDO differ by these approximations and by the parametrization philosophy.

The Modified Neglect of Diatomic Overlap (MNDO [(54)]) method is the oldest NDDO-based model that parameterizes one-center two-electron integrals based on spectroscopic data for isolated atoms, and evaluates other two-electron integrals using the idea of multipole-multipole interactions from classical electrostatics. The main advantage of MNDO over earlier methods was that the values of the parameters were optimized to reproduce molecular rather than atomic properties. When it first appeared, MNDO was immediately popular because of its increased accuracy but afterwards, various limitations were found, such as the inability to describe the hydrogen bond.

In 1985, an attempt, AM1 (Austin Model 1 [55]) was made to improve MNDO by adding a stabilizing Gaussian function to the core-core interaction to represent the hydrogen bond. The modification resulted in non-physical attractive forces that mimic van der Waals interactions.

In the next years, improvements led to the PM3 (Parametric Method 3 [56]) method where various changes to the original set of approximations used in MNDO were proposed. PM3 uses a Hamiltonian that is very similar to the AM1 Hamiltonian, but the parameterization strategy is different. While AM1 is parameterized largely based on small number of atomic data, PM3 is parameterized to produce a large number of molecular properties.

The previous semi-empirical methods tried to improve NDDO through the modification of approximations and the extension to specific elements. Then came the PM6 (parametric method 6 [57]) method that was set for three reasons: (i) to investigate the incorporation of some of the reported modifications to the core-core approximations into the NDDO methodology, (ii) to carry out an optimization of all main group elements (with emphasis on compounds of interest in biochemistry), and (iii) to extend the methodology by performing a restricted optimization of parameters for transition metals. Because of its construction and parameterization for more than 80 elements, PM6 method was found to be superior to other similar methods; in particular, PM6 corrects major errors in AM1 and PM3 calculations.

Semi-empirical methods allow treating quantum systems with a relatively large size in a rather cheap way. Then, these methods can be used for studies requiring the repetition of many quantum computations.

V Polarizable continuum model PCM

In vitro experimental spectra are often taken for molecules in solution (D_2O), and then any comparison between experimental and theoretical spectra requires that solvent effects be taken into account in the theoretical study. For that, solvent effects on NMR parameters are studied in the present work using two methods: an explicit method and an implicit one. In the explicit method, solvent molecules surrounding the target molecule are considered during calculation while in the implicit model, solvent molecules are replaced by their charges and the interaction between the target molecule and these charges is considered. This section shall be devoted to discuss the implicit model.

Since the number of solvent molecules that needs to be considered to adequately represent the solvent is very large, this difficulty can be overcome by treating the surrounding medium (or solvent) as a continuum having an effective dielectric constant ϵ while the solute is treated quantum mechanically. One method that uses this technic is called the Polarizable Continuum Model (PCM) [58; 59; 60] that seems to be very effective in studying solvent effects.

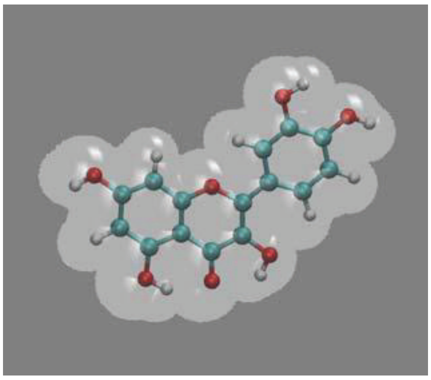

Figure 1.3: schematic representation of PCM model

A molecule M in a solution can be seen as if placed in a cavity surrounded by a polarizable dielectric medium. The electrostatic potential V of the whole system (molecule + medium) is the sum of electrostatic potential V_M generated by the charge distribution of the molecule ρ_M and the reaction potential V_m generated by the polarization $\vec{P}$ of the dielectric medium

$$V(\vec{r}) = V_M(\vec{r}) + V_m(\vec{r}) \tag{1.129}$$

where the molecular charge distribution ρ_M contains both the electronic density ρ_e (given as ρ in Kohn-Sham equations) and the nuclear distribution ρ_n.

$$\rho_M = \rho_e + \rho_n \tag{1.130}$$

The general equation of Poisson which is given by

$$-\vec{\nabla}\left[\epsilon\vec{\nabla}V(\vec{r})\right] = 4\pi\rho_{total}(\vec{r}) \tag{1.131}$$

can be divided into two parts corresponding to inside and outside the cavity.

$$-\vec{\nabla}^2 V(\vec{r}) = 4\pi\rho_M(\vec{r}) \quad inside\ the\ cavity \tag{1.132}$$

$$-\epsilon\vec{\nabla}^2 V(\vec{r}) = 0 \quad outside\ the\ cavity \tag{1.133}$$

Using boundary conditions on the cavity surface, one finds

$$V_{in} = V_{out} \tag{1.134}$$

$$\left(\frac{\partial V}{\partial \vec{n}}\right)_{in} = \epsilon\left(\frac{\partial V}{\partial \vec{n}}\right)_{out} \tag{1.135}$$

where $\vec{n}$ is the out-ward pointing vector perpendicular to the cavity surface. The first condition (equation (1.134)) expresses the continuity of the potential across the surface while the second condition (equation (1.135)) involves the discontinuity of the component of the field that is perpendicular to the cavity surface. Equation (1.135) can be rewritten as

$$\vec{E}_{in}.\vec{n} = \epsilon \vec{E}_{out}.\vec{n} \tag{1.136}$$

This difference between the normal components of electric fields at the boarder inside and outside the cavity, allows introducing an auxiliary quantity which is the surface charge distribution $\sigma(\vec{s})$ spread on the cavity surface (C). The symbol $\vec{s}$ denotes the position variable and it is used to emphasize that this charge distribution is limited to (C). This approach of solvation methods is called the Apparent Surface Charge method (ASC). In such method, the potential due to the solvent is defined as

$$V_\sigma(\vec{r}) = \int_C \frac{\sigma(\vec{s})}{|\vec{r} - \vec{s}|} d^2\vec{s} = V_m \tag{1.137}$$

In the ASC approach, the source of the solute potential is reduced to a charge distribution limited to a closed surface. This simplifies the electrostatic problem with respect to other formulations in which the whole dielectric medium is considered as the source of the reaction potential. Despite this remarkable simplification, the challenge remains in the integration of $\sigma(\vec{s})$ over a surface of complex shape. The solution lies in the discretization of the integral into a finite number of elements.

The cavity surface (C) is approximated in terms of a set of finite elements (called tesserae) small enough to consider $\sigma(\vec{s})$ almost constant within each tessera. With $\sigma(\vec{s})$ completely defined point by point, it is possible to define a point charge, q_k, at the position $\vec{s}_k$ in the area A_k such that $q_k = \sigma(\vec{s}_k)A_k$. Then, equation (1.137) becomes

$$V_\sigma(\vec{r}) = \sum_k \frac{\sigma(\vec{s}_k)A_k}{|\vec{r} - \vec{s}_k|} = \sum_k \frac{q_k}{|\vec{r} - \vec{s}_k|} \tag{1.138}$$

Once the point charges on the surface (C) are defined, the potential V_σ can be easily obtained. In what follows, we shall not make use of the point charges q_k but we will use instead the original ones in terms of $\sigma(\vec{s})$.

The electric medium is characterized by a polarization function proportional to the external field; however, it can be given by the gradient of the potential vector $V(\vec{r})$.

$$\vec{P} = \frac{\epsilon - 1}{4\pi}\vec{E} = -\frac{\epsilon - 1}{4\pi}\left(\vec{\nabla}V\right) \tag{1.139}$$

Besides, the charge density σ is related to the normal component of the electric polarization and it is given by

$$\sigma = -\vec{P}.\vec{n} = \frac{\epsilon - 1}{4\pi}\left[\vec{\nabla}V\right].\vec{n} = \frac{\epsilon - 1}{4\pi}\left(\frac{\partial V}{\partial \vec{n}}\right)_{out} \tag{1.140}$$

Now, substituting equation (1.135) in equation (1.140), one finds the expression of the surface charge density in terms of internal potential

$$\sigma(\vec{s}) = \frac{\epsilon - 1}{4\pi\epsilon}\left(\frac{\partial V}{\partial \vec{n}}\right)_{in} = \frac{\epsilon - 1}{4\pi\epsilon}\frac{\partial}{\partial \vec{n}}(V_M + V_\sigma)_{in} \tag{1.141}$$

with

$$V_M = \sum_A \frac{Z_A}{\left|\vec{R}_A - \vec{s}\right|} + \int_V \frac{\rho(\vec{r})}{|\vec{r} - \vec{s}|} d^3\vec{r} \tag{1.142}$$

The calculation of $\sigma(\vec{s})$ can be done in an iterative way. For a given electronic density $\rho(\vec{r})$, we start with a value of σ which gives a value of V_σ (equation (1.137)) which is in turn inserted in equation (1.141) to give another new value of σ. This is repeated until convergence for σ is obtained.

For the molecular system with electronic density $\rho(\vec{r})$, PCM model introduces the interaction between ρ and σ (noted $V_{\rho\sigma}$). This interaction energy is added to the unperturbed energy to form the total electronic energy of the molecule.

$$E = E^0[\rho] + E_{\rho\sigma} = E^0[\rho] + \frac{1}{2}\int_V \int_C \frac{\rho(\vec{r})\sigma(\vec{r}')}{|\vec{r} - \vec{r}'|} d\vec{r} d\vec{r}' \tag{1.143}$$

where E^0 is the unperturbed electronic energy given in equation (1.114). This introduces to the Kohn-Sham equations a new term added to the external potential V_s such that

$$V_s(\vec{r}) = V_s^0(\vec{r}) + \frac{\delta E_{\rho\sigma}}{\delta\rho} = V_s^0(\vec{r}) + \frac{1}{2}\int_C \frac{\sigma(\vec{r}')}{|\vec{r} - \vec{r}'|} d\vec{r}' \tag{1.144}$$

Note that the added term is σ dependent. The problem of solving the Kohn-Sham equation has now to be done in a self-consistent way taking into consideration the new perturbation resulting from the solvent effect. The converged σ obtained from the iteration of equation (1.141) is inserted into equation (1.144) which leads to a new electronic density ρ. The new value of ρ is reinserted in equation (1.141) and iterations continue until convergence is achieved.

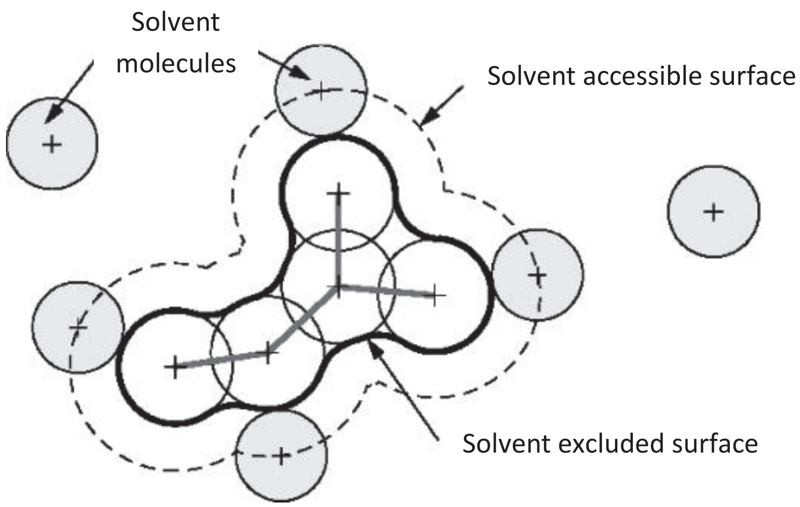

Figure 1.4: the solvent excluding surface used in the calculation of electrostatic energy $E_{\rho\sigma}$ using PCM model

Energy terms are calculated using the solute cavity obtained as a set of interlocking van der Waals spheres centered at the atomic positions. These spheres are located on the heavy (that is non-hydrogen) elements only. In our calculations, we have used the United Atomic Topology Model (UA0) [61] which is applied using the atomic radii of the Universal Force Field (UFF) [62]. In this model, the electrostatic energy $E_{\rho\sigma}$ is calculated using the solvent excluding surface which is an approximate surface found by multiplying the radii by a constant factor (in general 1.1). Basically, this leads to obtain proper radii for each non-hydrogen atom.

VI ONIOM model

In the explicit method of solvation, solvent molecules surrounding the target molecule are taken explicitly into account during calculations which means dealing with large-size systems. Unfortunately, for these large-size molecular systems, high accuracy calculation levels are limited by the high computational costs.

One way to overcome these limitations is hybrid methods which allow the combination of two or more computational techniques in one calculation making it possible to investigate large systems with high precision. The region of the system of interest is treated with an accurate method while the remainder of the system is treated at a lower level. The advantages of such methods is that they allow the combination of an accurate quantum-mechanical description with the low computational cost of classical mechanics, provide a realistic description for the site of interest, and permit a detailed analysis of the role of the environment.

Here, we are going to focus on Gaussian's hybrid method called ONIOM (Our own N-layered Integrated molecular Orbital and molecular Mechanics [(63; 64)]). It is a general method that can combine any number of molecular orbital methods (quantum mechanics QM [(65)]) as well as molecular mechanics (MM [(66)]) methods (MM will be discussed later).

In ONIOM calculations, the molecular system under investigation is usually divided into two or three regions that are treated at different levels of accuracy:

1. The higher layer is the smallest one, and it is treated with the most accurate method. This layer is also called Model System (MS).
2. The low layer consists of the entire molecule. This layer is usually treated with an inexpensive level of calculation (MM, semi-empirical method ..)
3. The Middle layer which is only present in a 3-layer ONIOM model. It is treated with a method that is intermediate in accuracy between the high level method and the low level method.

The entire molecule is referred to as the Real System (R). In the present work, the 2-layer ONIOM method is used.

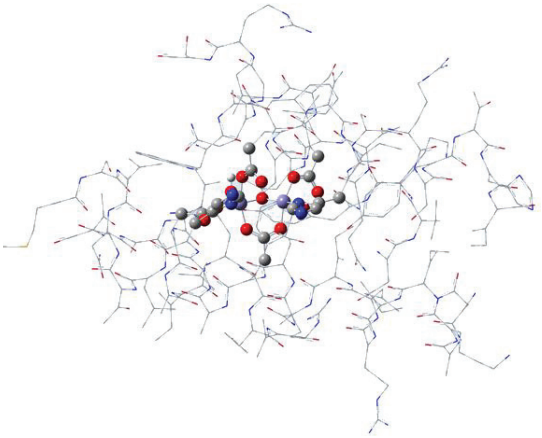

Figure 1.5: 2-layer assignment. The different visualizations (wire-frame and ball-stick) correspond to the low and high layers respectively.

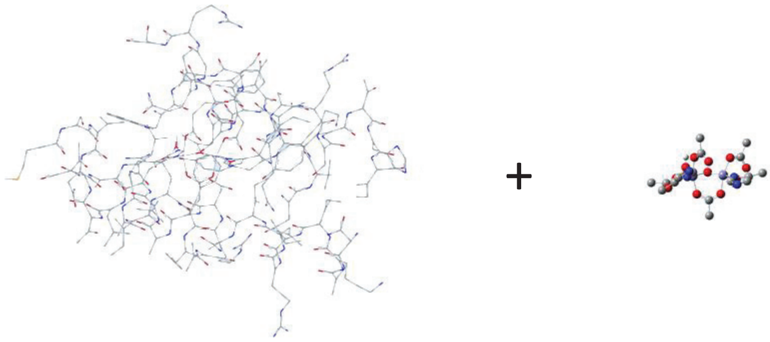

Figure 1.6: The Real and Model Systems

The ONIOM method works by approximating the energy of the Real System as a combination of the energies computed by less computationally expensive means. In a two-layer ONIOM calculation, the energy is computed as the energy of the Model System adding two types of corrections:

1. due to the size difference between the model system and the real system $[E^{low}(R) - E^{low}(MS)]$
2. due to the high accuracy method used for the model system $\left[E^{high}(MS) - E^{low}(MS)\right]$

$$\begin{aligned} E^{ONIOM} &= E^{low}(MS) + [E^{low}(R) - E^{low}(MS)] + \left[E^{high}(MS) - E^{low}(MS)\right] \\ &= E^{low}(R) + E^{high}(MS) - E^{low}(MS) \end{aligned} \tag{1.145}$$

The Real system contains all the atoms and is calculated only with the low accuracy method. The Model System contains the part of the system that is treated at the high accuracy method. Both low and high accuracy calculations need to be carried out for the Model system. Note that in the ONIOM expression, all three sub-calculations are on complete systems. Besides, when there is a bonded interaction between the two regions, the model system includes a hydrogen link atom to saturate the open valence.

If a Quantum Mechanics method is combined with Molecular Mechanics, calculations are referred to as QM:MM (64) calculations. When the ONIOM (QM:MM) scheme is applied using equation (1.145), the interaction between the two regions is included via MM calculations and therefore follows the mechanical or classical embedding formalism. This includes the electrostatic interaction which is evaluated as the interaction of the MM partial charges with partial (point) charges assigned to the atoms in the QM region.

However, ONIOM calculations can optionally take advantage of *electronic embedding* which enables both steric and electrostatic properties of the entire molecule to be taken into account. In this technique, the charge distribution of the MM region interacts with the actual charge distribution of the QM region; the partial charges from the MM region are included in the QM Hamiltonian, which provides a more accurate description of the electrostatic interaction and allows the wave function to respond to the charge distribution of the MM region.

The most important consideration when planning an ONIOM study is the selection of the various layers used in calculation. The general principle to keep in mind is that the model system contains the chemically active portion. Besides, bond breaking or formation should not take place within the MM region and atoms linked by double or triple bonds should be placed within the same ONIOM region. Moreover, to be completely safe, the model system must be extended three bonds from any connectivity change. This last advice ensures that ONIOM energy remains continuous despite the changes in the connectivity during the reaction.

In fact, standard MM methods cannot handle bond breaking and forming, and a discontinuity in the potential function is observed. Thus, in QM:MM calculations, for the ONIOM surface to be continuous during a chemical reaction, the MM contribution to the energy must be continuous. The MM contribution is defined as the S-value where the ONIOM energy can be written as

$$E^{ONIOM} = E^{high}(MS) + S^{MM} = E^{model,QM} + S^{MM} \tag{1.146}$$

$$S^{MM} = E^{low}(R) - E^{low}(MS) = E^{real,MM} - E^{model,MM} \tag{1.147}$$

The S-value describes the contribution from the MM region, which includes both the energy of the MM region as well as the interaction between the QM region and the MM region.

VI.1 Molecular mechanics

Molecular mechanics (MM [66]) allows the calculation of structural and thermodynamic properties of molecular systems composed of thousands of atoms. In MM calculations, electrons are not treated explicitly as in quantum mechanics; atoms are represented by charged masses related to each other by means of springs. Unlike in QM calculations where the energy is found by solving Schrodinger equation, in MM calculations the energy of molecular systems is described by empirical functions. The parameters of these empirical functions, which are usually derived from experiments or precise quantum-chemical calculations, form a force field. An example of a typical force field, Amber field [67], is of the form

$$\begin{aligned} E^{total} = &\sum_{bonds} K_r(r - r_{eq})^2 + \sum_{angles} K_\theta(\theta - \theta_{eq})^2 + \sum_{dihedrals} \frac{V_n}{2}[1 + \cos(n\varphi - \gamma)] \\ &+ \sum_{i<j} \left[s_{ij}{}^{VdW} \left(\frac{A_{ij}}{r_{ij}^{12}} - \frac{B_{ij}}{r_{ij}^{6}} \right) + s_{ij}^{q} \frac{q_i q_j}{\varepsilon r_{ij}} \right] \end{aligned} \tag{1.148}$$

The first three terms describe the bonded interactions, formed by all the bonds, angles, and dihedrals that are present in the system. The number of bonded terms scales linearly with the size of the system. The last term describes the non-bonded interaction between each pair of atoms in the system. The van der Waals interaction $\left(A_{ij}/r_{ij}^{12} - B_{ij}/r_{ij}^{6}\right)$ and the Coulomb interaction $q_i q_j/\varepsilon r_{ij}$ are scaled by the factors $s_{ij}{}^{VdW}$ and $s_{ij}{}^{q}$ respectively. The number of non-bonded terms scales quadratically with the size of the system.

References

1. *Density Functional Theory.* **R. Dreizler, and E. Gross.** 1995, Plenum Press, New York.

2. *A Chemist's Guide to Density Functional Theory.* **W. Koch, and M. C. Hothausen.** 2002, Wiley-VCH, Weinheim.

3. *Theoretical Chemistry Accounts.* **A. Bagno, and G. Saielli.** 2006, Theor. Chem. Acc., Vol. 117, p. 603.

4. *Calculation of NMR and EPR Parameters: Theory And Applications.* **M. Kaupp, M. Buhl, and V. G. Malkin.** 2004, Wiley-VCH.

5. *A theoretical study of the NMR spin-spin coupling constants.* **J. Autschbach, and B. Le Guennic.** 2003, J. Am. Chem. Soc., Vol. 125, p. 13585.

6. *Quantum mechanical continuum solvation models.* **J. Tomasi, B. Mennucci, and R. Cammi.** 2005, Chem. Rev., Vol. 105, p. 2999.

7. *Combining quantum mechanics methods with molecular mechanics methods in ONIOM.* **T. Vreven, K. S. Byun, I. Komaromi, S. Dapprich, J. A. Montgomery, K. Morokuma, and M. J. Frisch.** 2006, Chem. Theory and Comput., Vol. 2, p. 815.

8. *Classical electrodynamics.* **J.D.Jackson.** 1999, Wiley, New York. 0-471-30932-X.

9. *Lehrbuch der theoretischen physik.* **L.D. Landau, and E.M. Lifschitz.** 1981, Akademie-Verlag, Berlin, p. 120.

10. *Ab initio calculations of molecular properties.* **W.Kutzelnigg.** 1989, J. Mol. Struct.Theochem, Vol. 202, p. 11.

11. *Théorie quantique des courants interatomiques dans les combinaisons aromatiques.* **F.London.** 1937, J. Phys. Radium, Vol. 8, p. 397.

12. *Efficient Implementation of the Gauge-Independent Atomic Orbital Method for NMR Chemical Shift Calculations.* **K. Wolinski, J. F. Hinton, and P. Pulay.** 1990, J. Am. Chem. Soc., Vol. 112, p. 8251.

13. *Methods of molecular quantum mechanics.* **R.McWeeny.** 1989, Academic Press, New York.

14. *The variation method in quantum chemistry.* **S.T.Epstein.** 1974, Academic Press, New York.

15. *Advanced quantum chemistry.* **H.F.Hameka.** 1963, Addision-Wesley, New York, p. 162.

16. *Self-consistent Perturbation Theory of Diamagnetism. I. A Gauge-Invariant LCAO (Linear Combination of Atomic Orbitals) Method for NMR Chemical Shifts.* **R.Ditchfield.** 1974, R. Mol. Phys., Vol. 27, p. 789.

17. *Perturbation Theory for the Fock-Dirac Density Matrix.* **R.McWeeny.** 1962, Phys. Rev, Vol. 126, p. 1028.

18. *Modern Quantum Chemistry.* **A. Szabo, and N. S. Ostlund.** 1989, Mc Graw-Hill, New York.

19. *Electron Coupled Interactions between Nuclear Spins in Molecules.* **N.F.Ramsey.** 1953, Phys. Rev., Vol. 91, p. 303.

20. *Valence.* **C.A.Coulson.** 1952, Oxford University Press, London.

21. *Density functional theory of atoms and molecules.* **R. G. Parr, and W. Yang.** 1994, Oxford University Press. ISBN 978-0-19-509276-9.

22. *Note on exchange phenomena in the thomas-fermi atom.* **Dirac.** 1930, Proc. Cambridge Phil. Roy. Soc, Vol. 26, p. 376.

23. *Generalized gradient approximation made simple.* **J. P. Perdew, K. Burke, and M. Ernzerhof.** 1996, Phys. Rev. Lett., Vol. 77, p. 3865.

24. *Development of the Colle-Salvetti correlation-energy formula into a functional of the electron density.* **C. Lee, W. Yang, and R. G. Parr.** 1988, Phys. Rev. B, Vol. 37, p. 785.

25. *A new mixing of Hartree–Fock and local density-functional theories.* **A.D.Becke.** 1993, J. Chem. Phys., Vol. 98, p. 5648.

26. *Density functional theory of atoms and molecules.* **R. G. Parr, and W. Yang.** 1989, Oxford University Press, New York.

27. *Inhomogeneous Electron Gas.* **P. Hohenberg, and W. Kohn.** 1964, Phys. Rev., Vol. 136, p. B864.

28. *Density Matrices and Density Functionals.* **V. H. Smith, and E. Erdahl.** 1987, Reidel, Dordrecht.

29. *Self-Consistent Equations Including Exchange and Correlation Effects.* **W. Kohn, and L. J. Sham.** 1965, Phys.Rev. A, Vol. 101, p. A1133.

30. *The theory of complex spectra.* **Slater, J.** 1929, Physical Review, Vol. 34, p. 2.

31. **M. Born, and J. R. Oppenheimer.** 1927, Ann. Phys., Vol. 84, p. 457.

32. *Inorganic Chemistry: Principles of Structure and Reactivity.* **J.Huheey.** 1972, Harper & Row.

33. **P.A.Dirac.** 1930, Proc. Cambridge Philos. Soc., Vol. 26, p. 376.

34. *A Simplification of the Hartree-Fock Method.* **J.C.Slater.** 1951, Phys. Rev., Vol. 81, p. 385.

35. *Accurate spin-dependent electron liquid correlation energies for local spin density calculations: a critical analysis.* **S. H. Vosko, L.Wilk, and M. Nusair.** 1980, Can. J. Phys., Vol. 58, p. 1200.

36. *Ground State of the Electron Gas by a Stochastic Method.* **D. M. Ceperley, and B. J. Alder.** 1980, Phys. Rev. Lett., Vol. 45, p. 566.

37. *Spin-Density Gradient Expansion for the Kinetic Energy.* **G. L. Oliver, and J. P. Perdew.** 1982, Phys. Rev. A, Vol. 20, p. 397.

38. *Errata: Generalized gradient approximation made simple.* **J. P. Perdew, K. Burke, and M. Ernzerhof.** 1997, Phys. Rev. Lett., Vol. 78, p. 1396.

39. *Left-right correlation energy.* **N. C. Cohen, and A. J. Handy.** 2001, Mol. Phys., Vol. 99, p. 403.

40. *Assessment of a new local exchange functional OPTX.* **W. M. Hoe, A. Cohen, and N. C. Handy.** 2001, Chem. Phys. Lett., Vol. 341, p. 319.

41. *Density-functional exchange-energy approximation with correct asymptotic-behavior.* **A.D.Becke.** 1988, Phys. Rev. A, Vol. 38, p. 3098.

42. *Development of the Colle-Salvetti correlation-energy formula into a functional of the electron density.* **C. Lee, W. Yang, and R. G. Parr.** 1988, Phys. Rev. B, Vol. 37, p. 785.

43. *Results obtained with the correlation-energy density functionals of Becke and Lee, Yang and Parr.* **B. Miehlich, A. Savin, H. Stoll, and H. Preuss.** 1989, Chem. Phys. Lett., Vol. 157, p. 200.

44. *Toward reliable density functional methods without adjustable parameters: The PBE0 model.* **C. Barone, and V. Adamo.** 1999, J. Chem. Phys., Vol. 110, p. 6158.

45. *Atoms, molecules, solids, and surfaces: Applications of the generalized gradient approximation for exchange and correlation.* **J. P. Perdew, J. A. Chevary, S. H. Vosko, K. A. Jackson, M. R. Pederson, D. J. Singh, and C. Fiolhais.** 1992, Phys. Rev. B, Vol. 46, p. 6671.

46. *Atomic Shielding Constants.* **J.C.Slater.** 1930, Phys. Rev., Vol. 36, p. 57.

47. *The performance of the Becke—Lee—Yang—Parr (B—LYP) density functional theory with various basis sets.* **Peter M. W. Gill, Benny G. Johnson, and John A. Pople.** 1992, Chem. Phys. Lett., Vol. 197, p. 499.

48. *Gaussian basis sets for use in correlated molecular calculations. I. The atoms boron through neon and hydrogen.* **T.H.Dunning.** 1989, J. Chem. Phys., Vol. 90, p. 1007.

49. *Gaussian basis sets for use in correlated molecular calculations. V. Core-valence basis sets for boron through neon.* **D. E. Woon, and T. H. Dunning.** 1995, J. Chem. Phys., Vol. 103, p. 4572.

50. *Polarization consistent basis sets: principles.* **F.Jensen.** 2001, J. Chem. Phys., Vol. 115, p. 9113.

51. *Erratum: "Polarization consistent basis sets: Principles".* **F.Jensen.** 2002, J. Chem. Phys., Vol. 116, p. 3502.

52. *The basis set convergence of spin−spin coupling constants calculated by density functional methods.* **F.Jensen.** 2006, J. Chem. Theo. Comp., Vol. 2, p. 1360.

53. *Approximate Molecular Orbital Theory.* **J. Pople, and D. Beveridge.** 1970, McGraw-Hill.

54. *Ground states of molecules. 38. The MNDO method. Approximations and parameters.* **M. J. S. Dewar, and W. Thiel.** 1977, Journal of the American Chemical Society, Vol. 99, p. 4899.

55. *Development and use of quantum mechanical molecular models. 76. AM1: a new general purpose quantum mechanical molecular model.* **M. J. S. Dewar, E. G. Zoebisch, E. F. Healy, and J. J. P. Stewart.** 1985, Journal of the American Chemical Society, Vol. 107, p. 3902.

56. *Optimization of Parameters for Semi-Empirical Methods I-Method.* **J.J.P.Stewart.** 1989, J. Comput. Chem., Vol. 10, p. 209.

57. *Optimization of parameters for semiempirical methods V: Modification of NDDO approximations and application to 70 elements.* **J.J.P.Stewart.** 2007, J. Mol. Model., Vol. 13, p. 1173.

58. *Quantum mechanical continuum solvation models.* **J. Tomasi, B. Mennucci, and R. Cammi.** 2005, Chem. Rev., Vol. 105, p. 2999.

59. *Electrostatic interaction of a solute with a continuum. A direct utilizaion of AB initio molecular potentials for the prevision of solvent effects.* **S. Miertus, E. Scrocco, and J. Tomasi.** 1981, Chem. Phys., Vol. 55, p. 117.

60. *Analytical Second Derivatives of the Free Energy in Solution by Polarizable Continuum models.* **M. Cossi, and V. Barone.** 1998, J. Chem. Phys., Vol. 109, p. 6246.

61. *A new definition of cavities for the computation of solvation free energies by the polarizable continuum model.* **V. Barone, M. Cossi, and J. Tomasi.** 1997, J. Chem. Phys., Vol. 107, p. 3210.

62. *Excited states and solvatochromic shifts within a nonequilibrium solvation approach: A new formulation of the integral equation formalism method at the self-consistent field, configuration interaction, and multiconfiguration self-consistent field level.* **B. Mennucci, R. Cammi, and J. Tomasi.** 1998, J. Chem. Phys., Vol. 109, p. 2798.

63. *A new ONIOM implementation in Gaussian98. Part I. The calculation of energies, gradients, vibrational frequencies and electric field derivatives.* **S. Dapprich, I. Komaromi, K.S. Byun, K. Morokuma, and M.J. Frisch.** 1999, Journal of Molecular Structure THEOCHEM, Vol. 461, p. 1.

64. *Hybrid Methods: ONIOM(QM:MM) and QM/MM.* **T. Vreven, and K. Morokuma.** 2006, Annual Reports in Computational Chemistry, Vol. 2, p. 35.

65. *Introduction to Quantum Mechanics.* **Griffiths, and J. David.** 2004, Prentice Hall. ISBN 0-13-111892-7.

66. *Molecular Mechanics.* **N. L. Allinger, and U. Burkert.** 1982, An American Chemical Society Publication. ISBN 0-8412-0885-9.

67. *A Second Generation Force Field for the Simulation of Proteins, Nucleic Acids, and Organic Molecules.* **W. D. Cornell, P. Cieplak, C. I. Bayly, I. R. Gould, K. M. Jr. Merz, D. M. Ferguson, D. C. Spellmeyer, T. Fox, J. W. Caldwell, and P. A. Kollman.** 1995, J. Am. Chem. Soc., Vol. 117, p. 5179.

Chapter 2

Dynamical Effects on NMR Parameters

For the reliable calculation of NMR parameters, we have taken into account, in addition to solvent effects, the effects of isomers and vibration.

The effect of isomers originates from the fact that at ambient temperature, not only ground-state molecules may be present but also excited molecules of higher energy. Here, we are interested in the stable spatial isomers. The presence of isomers at ambient temperature affects the experimental NMR spectra. Thus, isomer effects must be taken into account in the theoretical calculation of NMR parameters to ensure a fair comparison between experimental and simulated spectra. The conformation research for isomers is done using Born-Oppenheimer molecular dynamics [(1)] (MD) simulations where the potential energy of atoms is calculated semi-empirically based on the PM6 method. Isomer effects are calculated in the present work assuming a Boltzmann distribution. The averaged NMR parameter (δ or J) is calculated as an average of the NMR parameter of the various isomers weighted by Boltzmann factor.

The vibrational effects on the NMR parameters are the result of the molecular vibration which is available even at a temperature of zero absolute. NMR parameters often show a strong dependence on the molecular geometry, and studies have demonstrated that the effects of molecular motion may change NMR properties by more than 10% [(2)]. In the present work, vibrational effects are calculated using two approaches based on different methodologies. In the first way, the atom-centered density matrix propagation (ADMP [(3; 4; 5)]) method is used. In the second way, vibrational effects are calculated quantum-mechanically through a perturbative method [(6)] that we have implemented in Gaussian [(7)].

This chapter is devoted to describe the three main methods: MD, ADMP, and the perturbative method for vibrational corrections to NMR parameters.

I Molecular dynamics

One of the principle tools in the theoretical study of biological molecules is the method of molecular dynamics (MD) simulation. This computational method calculates the time dependent behavior of a molecular system. MD simulations provide detailed information on the conformational changes of many molecules of interest, and thus, they have been used in the present work to search for isomers.

I.1 Born-Oppenheimer molecular dynamics

The Schrödinger equation is usually so complex that it can be solved only for a few simple cases. Therefore, to describe the dynamics of molecular systems, approximation procedures are used to simplify the problem; one of these approximations is that of Born-Oppenheimer. The idea is to split the Schrödinger equation, which describes the state of both the electrons and nuclei, into two coupled equations. The influence of the electrons on the motion of nuclei is then described by an effective potential which results from the solution of the electronic Schrödinger equation. As a further approximation, the nuclei move according to the classical Newton's equations using effective potentials which result from quantum mechanical computations or empirical potentials.

Starting from the non-relativistic time-dependent Schrödinger equation of a molecular system,

$$i\hbar \frac{\partial}{\partial t} \Phi(\{\vec{r}_i\}, \{\vec{R}_I\};\ t) = \mathcal{H}(\{\vec{r}_i\}, \{\vec{R}_I\})\, \Phi(\{\vec{r}_i\}, \{\vec{R}_I\};\ t) \qquad (2.1)$$

we express the total wavefunction Φ as a function of electronic degrees of freedom $\{\vec{r}_i\}$, nuclear degrees of freedom $\{\vec{R}_I\}$, and time t. The total molecular Hamiltonian $\mathcal{H}$ is the sum of kinetic energy of the atomic nuclei, kinetic energy of the electrons, interelectronic repulsion, electronic – nuclear attraction, and internuclear repulsion

$$\begin{aligned}\mathcal{H} &= -\sum_I \frac{\hbar^2}{2M_I}\vec{\nabla}_I^2 - \sum_i \frac{\hbar^2}{2m_e}\vec{\nabla}_i^2 + \sum_{i<j}\frac{e^2}{|\vec{r}_i - \vec{r}_j|} - \sum_{I,i}\frac{e^2 Z_I}{|\vec{R}_I - \vec{r}_j|} + \sum_{I<J}\frac{e^2 Z_I Z_J}{|\vec{R}_I - \vec{R}_J|} \\ &= -\sum_I \frac{\hbar^2}{2M_I}\vec{\nabla}_I^2 + \mathcal{H}_e(\{\vec{r}_i\},\{\vec{R}_I\})\end{aligned} \tag{2.2}$$

where $\mathcal{H}_e$ is the electronic Hamiltonian. Clearly, an exact solution of equation (2.1) is not possible and approximations must be made.

To derive the Born-Oppenheimer approximation, one uses the fact that the difference in masses between electrons and atomic nuclei is large. Due to this difference, the ratio of the velocity v_K of a nucleus to the velocity of an electron v_e is in general smaller than 10^{-2}. Therefore, one assumes that the electrons adapt instantaneously to the changed nuclear configuration and always occupy the ground-state of that nuclear configuration. This can be exploited by assuming

$$\Phi(\{\vec{r}_i\},\{\vec{R}_I\};\, t) = \sum_{j=0}^{\infty} \Psi_j(\{\vec{r}_i\},\{\vec{R}_I\})\, \varphi_j(\{\vec{R}_I\};\, t) \tag{2.3}$$

where $\varphi_j(\{\vec{R}_I\};\, t)$ represents the nuclear wavefunctions, and $\Psi_j(\{\vec{r}_i\},\{\vec{R}_I\})$ denotes the electronic wavefunctions which are solutions to the electronic Schrodinger equation (2.4) with the orthonormality condition satisfying $\int \Psi_j^*(\{\vec{r}_i\},\{\vec{R}_I\})\Psi_l(\{\vec{r}_i\},\{\vec{R}_I\})\, d\vec{r} = \delta_{jl}$.

$$\mathcal{H}_e(\{\vec{r}_i\},\{\vec{R}_I\})\Psi_j(\{\vec{r}_i\},\{\vec{R}_I\}) = E_j\Psi_j(\{\vec{r}_i\},\{\vec{R}_I\}) \tag{2.4}$$

Now, inserting equation (2.3) into the time-dependent Schrödinger equation (2.1) with the Hamiltonian operator (2.2), followed by multiplication from the left by $\Psi_j^*(\{\vec{r}_i\},\{\vec{R}_I\})$ and integration over the electronic coordinates, this leads to a set of coupled differential equations.

$$i\hbar\frac{\partial}{\partial t}\varphi_j = -\sum_I \frac{\hbar^2}{2M_I}\vec{\nabla}_I^2\varphi_j + \left\{\int d\vec{r}\,\Psi_j^*(\{\vec{r}_i\},\{\vec{R}_I\})\,\mathcal{H}_e(\{\vec{r}_i\},\{\vec{R}_I\})\Psi_j(\{\vec{r}_i\},\{\vec{R}_I\})\right\}\varphi_j$$
$$+\sum_l C_{jl}\varphi_{jl} = -\sum_I \frac{\hbar^2}{2M_I}\vec{\nabla}_I^2\varphi_j + E_j(\{\vec{R}_I\})\varphi_j + \sum_l C_{jl}\varphi_{jl} \tag{2.5}$$

with

$$C_{jl} = -\left\langle \Psi_j \middle| \sum_I \frac{\hbar^2}{M_I}\vec{\nabla}_I \middle| \Psi_l \right\rangle \vec{\nabla}_I - \left\langle \Psi_j \middle| \sum_I \frac{\hbar^2}{2M_I}\vec{\nabla}_I^2 \middle| \Psi_l \right\rangle \tag{2.6}$$

The non-adiabatic coupling terms C_{jl} contribute very little to the energy, which can be demonstrated using the time-independent perturbation theory [8]. In the case that all coupling operators C_{jl} are negligible, the set of differential equations (2.5) becomes uncoupled

$$i\hbar\frac{\partial}{\partial t}\varphi_j = -\sum_I \frac{\hbar^2}{2M_I}\vec{\nabla}_I^2\varphi_j + E_j(\{\vec{R}_I\})\varphi_j \tag{2.7}$$

where each electronic eigenvalue E_j will give rise to an electronic surface, and these surfaces are known as Born-Oppenheimer surfaces. On each Born-Oppenheimer surface, the nuclear eigenvalue problem can be solved, which yields a set of levels (rotational and vibrational) in the nuclear motion.

However, as a next step, the nuclear wave function φ_j will be approximated by classical point particles. For this, we first write the wave function φ_j in terms of an amplitude factor $A > 0$ and a phase S which are both considered to be real.

$$\varphi_j(\{\vec{R}_I\};\, t) = A(\{\vec{R}_I\};\, t)exp\left[iS(\{\vec{R}_I\};\, t)/\hbar\right] \tag{2.8}$$

We can substitute (2.8) into the equation of nuclei (2.7) and then, separate the real and imaginary parts. This leads to the coupled system of equations

$$\frac{\partial S}{\partial t}+\sum_{I}\frac{1}{2M_I}\left(\vec{\nabla}_I S\right)^2+E_j\left(\{\vec{R}_I\}\right)=\hbar^2\sum_{I}\frac{1}{2M_I}\frac{\vec{\nabla}_I^2 A}{A} \tag{2.9}$$

$$\frac{\partial A}{\partial t}+\sum_{I}\frac{1}{M_I}\left(\vec{\nabla}_I A\right).\left(\vec{\nabla}_I S\right)+\sum_{I}\frac{1}{2M_I}A\left(\vec{\nabla}_I^2 S\right)=0 \tag{2.10}$$

The equation of S (2.9) contains one term that depends on $\hbar$, a contribution that vanishes if the classical limit is taken as $\hbar \to 0$.

$$\frac{\partial S}{\partial t}+\sum_{I}\frac{1}{2M_I}\left(\vec{\nabla}_I S\right)^2+E_j\left(\{\vec{R}_I\}\right)=0 \tag{2.11}$$

The resulting equation (2.11) is now isomorphic to equations of motion in the Hamilton-Jacobi formulation of classical mechanics

$$\frac{\partial S}{\partial t}+\mathcal{H}\left(\{\vec{R}_I\},\{\vec{\nabla}_I S\}\right)=0 \tag{2.12}$$

with the classical Hamilton function

$$\mathcal{H}\left(\{\vec{R}_I\},\{\vec{P}_I\}\right)=T\left(\{\vec{P}_I\}\right)+V\left(\{\vec{R}_I\}\right) \tag{2.13}$$

where one puts $\vec{P}_K(t)=\vec{\nabla}_K S\left(\{\vec{R}_I\},t\right)$, $\vec{P}_K$ being the conjugated moment of $\vec{R}_K$. Newton's equations of motion $d\vec{P}_K(t)/dt=-\vec{\nabla}_K V\left(\{\vec{R}_I\}\right)$ associated to equation (2.12) are then

$$\frac{d\vec{P}_K(t)}{dt}=M_K\frac{d^2\vec{R}_K(t)}{dt^2}=-\vec{\nabla}_K E_j\left(\{\vec{R}_I\}\right)=-\vec{\nabla}_K V_e^{BO}\left(\{\vec{R}_I\}\right) \tag{2.14}$$

The nuclei move now according to the laws of classical mechanics in an effective potential V_e^{BO} given by the electrons. It results from an averaging over the degrees of freedom of the electrons, weighted by $\mathcal{H}_e$, where the nuclear coordinates are kept constant at their current positions $\{\vec{R}_I\}$.

For the electronic ground state, the Born-Oppenheimer molecular dynamics is given by the equations

$$M_K \frac{d^2\vec{R}_K(t)}{dt^2} = -\vec{\nabla}_K \min_{\Psi_0} \int d\vec{r}\, \Psi_0^*(\{\vec{r}_i\}, \{\vec{R}_I\}) \mathcal{H}_e \Psi_0(\{\vec{r}_i\}, \{\vec{R}_I\}) \tag{2.15}$$

$$\mathcal{H}_e \Psi_0 = E_0 \Psi_0 \tag{2.16}$$

.

In the Born-Oppenheimer method, the computation of the electron structure is reduced to the solution of the stationary Schrödinger equation, which then is used to compute the forces acting at that time on the nuclei so that the nuclei can be moved according to the laws of classical molecular dynamics. The time-dependency of the state of the electrons is here exclusively a consequence of the classical motion of the nuclei. In addition, for the Born-Oppenheimer dynamics, a minimization is needed in every time step according to equation (2.15).

I.2 Equations of motion of nuclei

As it was stated earlier in section I.1, the classical equations of motion are used to describe the trajectories of nuclei in the Born-Oppenheimer approximation. Thus, in order to find the nuclear trajectories, one needs to solve Newton's equations of motion (2.14) which can be reformulated as

$$M_K \frac{d^2\vec{R}_K}{dt^2} = M_K \vec{a}_K = \vec{F}_K(\{\vec{R}_I\}) \tag{2.17}$$

Note that, from equation (2.17), the force $\vec{F}_K$ on nucleus K depends on the position vectors of other nuclei $\left(\vec{R}_1, \vec{R}_2, \dots\right)$. Indeed, the equations of motion of a system of a large number of particles are not too easy to solve because the equation for one particle is coupled to the other equations. These equations of motion cannot be solved exactly for a number of particles larger than 2, but they can be solved numerically without too much difficulty.

I.2.1 Time integration –Velocity Verlet method

The time integration algorithm is the basis of MD simulations, and it is required to integrate the equations of motion of particles and follow their trajectories. In the time integration algorithm, the time is divided into small steps Δt. The time step must be chosen small enough to avoid discretization errors i.e. smaller than the fastest vibrational frequency in the system.

Knowing the positions and their time derivatives for the particles at time t, one can find the same quantities at a later time $t + \Delta t$. By iterating the procedure, the time evolution of the system can be followed for long times.

One popular integration method for MD calculations is the Velocity Verlet algorithm [9]. Usually, for a particle in motion, the position $\vec{R}$ and the velocity $\vec{v}$ are approximated by a Taylor series expansion. At time t, the particle is characterized by $\vec{R}(t)$, $\vec{v}(t)$, and $\vec{a}(t)$. The speed at a mid-interval at $t + \Delta t/2$ can be expressed as

$$\vec{v}(t + \Delta t/2) = \vec{v}(t) + \vec{a}(t)\Delta t/2 \qquad (2.18)$$

From the mid-interval velocity (2.18), one can easily obtain the position at $t + \Delta t$

$$\vec{R}(t + \Delta t) = \vec{R}(t) + \vec{v}(t + \Delta t/2)\Delta t \qquad (2.19)$$

Then, from the calculated position (2.19), one can calculate the acceleration at time $t + \Delta t$.

$$\vec{a}(t+\Delta t) = \vec{F}(\{\vec{r}(t+\Delta t)\})/m \quad (2.20)$$

Usually, the evaluation of forces is the most time-consuming component of an MD calculation. Now, using the results of equations (2.18) and (2.20), the velocity at time $t + \Delta t$ can be calculated as

$$\vec{v}(t+\Delta t) = \vec{v}(t+\Delta t/2) + \vec{a}(t+\Delta t)\Delta t/2 \quad (2.21)$$

Eliminating the half step, the Velocity Verlet algorithm can be shortened to three steps instead of four. Given $\vec{R}(t)$, $\vec{v}(t)$, and $\vec{a}(t)$ at time t, one first calculates $\vec{R}(t+\Delta t)$ from equation (2.22) which results from combining equations (2.18) and (2.19) (Taylor's expansion to the third order).

$$\vec{R}(t+\Delta t) = \vec{R}(t) + \vec{v}(t)\Delta t + \frac{1}{2}\vec{a}(t)(\Delta t)^2 \quad (2.22)$$

Next, $\vec{a}(t+\Delta t)$ can be derived from $\vec{R}(t+\Delta t)$ using equation (2.20). At last, one calculates $\vec{v}(t+\Delta t)$ using equation (2.23) which comes from the combination of equations (2.18) and (2.21).

$$\vec{v}(t+\Delta t) = \vec{v}(t) + \frac{\vec{a}(t) + \vec{a}(t+\Delta t)}{2}\Delta t \quad (2.23)$$

After one iteration, we obtain the position, the velocity and the acceleration of the particle at time $t + \Delta t$. Taking advantage of these quantities at $+\Delta t$, we can easily calculate the same quantities at $t + 2\Delta t$. The same process if continued, allows the evaluation of $\vec{R}$, $\vec{v}$, and $\vec{a}$ at $t + n\Delta t$ where n is an integer. Simulation time can be elongated as much as needed. One advantages of this method is that it conserves the energy of the system; another advantage is that it requires only a small memory since it needs to store only information from one time step.

I.3 Thermostat

To control the temperature in MD simulations, one can use thermostats. In the present work, we have used the Berendsen thermostat [(10)] that is based on the idea of a weak coupling between the system under study and an external heat bath of temperature T_0. In this thermostat, the velocities are scaled at each step and the rate of temperature change is given by

$$\frac{dT}{dt} = \frac{1}{\tau}(T_0 - T) \tag{2.24}$$

where τ is the coupling constant, T is the temperature of the system at time t, and T_0 is the target temperature. Equation (2.24) implies that if $T < T_0$, the temperature will increase, but if $T > T_0$, the heat will be removed. Let the velocities be rescaled as $\vec{v}\,' = \lambda\vec{v}$. Then the change in kinetic energy upon rescaling is

$$\Delta E = \frac{1}{2}\sum_{K}^{N_p} M_K\left(\vec{v}\,'^2_K - \vec{v}^2_K\right) = (\lambda^2 - 1)\frac{1}{2}\sum_{K}^{N_p} M_K\,\vec{v}^2_K = (\lambda^2 - 1)E_{kin} \tag{2.25}$$

According to the equipartition theorem, each independent degree of freedom should possess $k_B T/2$ kinetic energy where k_B is the Boltzmann constant. Thus, the kinetic energy of the system of N_p particles can be expressed as

$$E_{kin} = \frac{3N_p k_B T}{2} \tag{2.26}$$

Inserting (2.26) in (2.25), the change in kinetic energy can be related to the temperature as

$$\Delta E = (\lambda^2 - 1)\frac{3N_p k_B T}{2} \tag{2.27}$$

Equation (2.27) can be converted to express temperature change as

$$\Delta T = (\lambda^2 - 1)T \tag{2.28}$$

Approximating dT/dt with $\Delta T/\Delta t$ in (2.24), and inserting ΔT from (2.28) in equation (2.24), we get

$$\lambda^2 = 1 + \frac{\Delta t}{\tau}\left(\frac{T_0}{T} - 1\right) \tag{2.29}$$

which gives the relation between scaling factor λ, the time step Δt and the coupling constant τ (the time interval between heat exchanges with the bath). The usual compromise value for τ is 0.4 ps, which results in modest temperature fluctuations. The Berendsen thermostat does not strictly fix the temperature, but leads to exponential relaxation of instantaneous temperatures to the target one. Also from physical viewpoint the coupling to heat bath can be viewed as addition of a friction term $-\gamma M\vec{v}$ to the Newton equations of motion, where $\gamma = \frac{1}{\tau}\left(\frac{T_0}{T} - 1\right)$. This results in the modified equation of motion for particle K

$$M_K \frac{d^2\vec{R}_K}{dt^2} = \vec{F}_K(\{\vec{R}_I\}) - \gamma M_K \frac{d\vec{R}_K}{dt} \tag{2.30}$$

Thus, the Berendsen thermostat tries to correct deviations of the actual temperature T form the prescribed one T_0 by multiplying the velocities by a certain factor λ. This method of temperature controlling allows for fluctuations of the temperature, thereby not fixing it to a constant value; however, in each integration step it is insured that the T is corrected to a value more close to T_0.

II Atom-centered density matrix propagation dynamics method ADMP

Unlike Born-Oppenheimer MD, in an extended Lagrangian MD the electronic degrees of freedom are not iterated to converge at each step, but are instead treated as fictitious dynamical variables and propagated along with the nuclear degrees of freedom. The resultant energy surface remains close to a converged adiabatic electronic surface.

Hence, the Lagrangian equations of motion for the nuclei are extended by adding the electronic degrees of freedom and giving them a fictitious mass μ and kinetic energy. With an appropriate choice of fictitious mass, the molecular dynamics can be calculated efficiently and accurately.

The atom-centered density matrix propagation (ADMP [3; 4; 5]) is an extended Lagrangian molecular dynamics method that treats the individual elements of the reduced one-particle density matrix P as dynamic electronic variables, and employs atom-centered Gaussian basis functions which are especially suited to deal effectively with general molecular systems.

II.1 Scalar-mass ADMP

An extended Lagrangian [11] describing the combined nuclear-density matrix system, in an orthonormal basis, can be defined as

$$\mathcal{L} = \frac{1}{2}Tr(V^T MV) + \frac{1}{2}\mu Tr(WW) - E(R,P) - Tr[\Lambda(PP - P)] \tag{2.31}$$

where M, R, and V are the nuclear masses, positions, and velocities respectively. The density matrix, density matrix velocity, and the fictitious mass of the density matrix elements are P, W, and μ, respectively. In equation (2.31), μ is a scalar, and generalizing it to a matrix will be considered forward. The Lagrangian constraint matrix Λ conserves two conditions: (1) the idempotency of the one-particle density matrix ($P^2 = P$), and (2) the electron number ($Tr[P] = N$).

Using the stationary action principle of classical mechanics [12], the Euler-Lagrange equations of motion for the density matrix and the nuclei can be derived from the Lagrangian equation (2.31).

$$\mu \frac{d^2 P}{dt^2} = -\left[\left. \frac{\partial E(R,P)}{\partial P} \right|_R + \Lambda P + P\Lambda - \Lambda \right] \tag{2.32}$$

$$M \frac{d^2 R}{dt^2} = - \left. \frac{\partial E(R,P)}{\partial R} \right|_P \tag{2.33}$$

Equation (2.32) represents the dynamics of the one-electron density matrix, while equation (2.33) represents the dynamics of the nuclei. Thus, these equations are used [13] to propagate the combined nuclear-density matrix system. Using the velocity Verlet algorithm, the propagation of the density matrix at the time step i is given by

$$P_{i+1} = P_i + W_i \Delta t - \frac{\Delta t^2}{2\mu} \left[\left. \frac{\partial E(R_i, P_i)}{\partial P} \right|_R + \Lambda_i P_i + P_i \Lambda_i - \Lambda_i \right] \tag{2.34}$$

$$W_{i+1/2} = W_i - \frac{\Delta t}{2\mu} \left[\left. \frac{\partial E(R_i, P_i)}{\partial P} \right|_R + \Lambda_i P_i + P_i \Lambda_i - \Lambda_i \right] = \frac{P_{i+1} - P_i}{\Delta t} \tag{2.35}$$

$$W_{i+1} = W_{i+1/2} - \frac{\Delta t}{2\mu} \left[\left. \frac{\partial E(R_{i+1}, P_{i+1})}{\partial P} \right|_R + \Lambda_{i+1} P_{i+1} + P_{i+1} \Lambda_{i+1} - \Lambda_{i+1} \right] \tag{2.36}$$

The equations for propagation of the density matrix are simplest in an orthonormal basis. However, for Gaussian basis functions, which are not orthogonal, it is recommended that they are transformed to an orthonormal basis using $P = UP'U^T$ where P is the density matrix in the orthonormal basis, P' is the density matrix in the non-orthogonal Gaussian basis, and U is the transformation matrix. The overlap matrix for the non-orthogonal Gaussian basis S' is given by $S' = U^T U$.

Since Gaussian basis sets are atom-centered, it is important to note that the transformation matrix U is time dependent. The relation between the non-orthogonal and the orthonormal basis is different at each time t.

The non-orthogonal Gaussian basis is used only to calculate the energy $E(R,P)$ and its two derivatives $\partial E(R,P)/\partial P|_R$ and $\partial E/\partial R|_P$ which appear in the equations of motion. For single particle methods (DFT method in our work), the energy $E(R,P)$ is calculated using the McWeeny purification transformation which defines the purified density as $\tilde{P} = 3P^2 - 2P^3$ [14]. Thus, the energy expression is given by

$$E = Tr\left[h'\tilde{P}' + \frac{1}{2}G'_{2e}(\tilde{P}')\tilde{P}'\right] + E_{xc} + V_{NN} = Tr\left[h\tilde{P} + \frac{1}{2}G_{2e}(\tilde{P})\tilde{P}\right] + E_{xc} + V_{NN} \qquad (2.37)$$

Here, h' is the one-electron matrix, and $G'_{2e}(\tilde{P}')$ is the Coulomb potential for DFT calculations, both in the non-orthogonal Gaussian basis. However, h and $G_{2e}(\tilde{P})$ represent, in the orthogonal basis, the one- and two-electron matrices respectively. The relation between h and h' is $h = U^{-T}h'U^{-1}$, and between G_{2e} and G'_{2e} is $G_{2e} = U^{-T}G'_{2e}U^{-1}$. The term E_{xc} is the exchange-correlation functional and V_{NN} is the nuclear repulsion energy.

The derivative of the energy with respect to the density matrix ($\partial E(R,P)/\partial P|_R$) is obtained by using the expression of McWeeny purified density [13] $\tilde{P}$ in equation (2.37).

$$\left.\frac{\partial E(R,P)}{\partial P}\right|_R = 3FP + 3PF - 2FP^2 - 2PFP - 2P^2F \qquad (2.38)$$

$$F = h + G_{2e} + G_{ex} = h + G \; and \; G_{ex} = \frac{\partial E_{xc}}{\partial P} \qquad (2.39)$$

where F is the Kohn-Sham operator for DFT calculations in the orthonormal basis.

The derivative of the energy with respect to the nuclear coordinates ($\partial E/\partial R|_P$) is an important term in ADMP. It is obtained by differentiating equation (2.37) [3].

$$\left.\frac{\partial E(R,P)}{\partial R}\right|_P = Tr\left[\frac{dh'}{dR}\tilde{P}' + \frac{1}{2}\left.\frac{\partial G'_{2e}(\tilde{P}')}{\partial R}\right|_{P'}\tilde{P}' + \left(h' + \frac{1}{2}G'_{2e}(\tilde{P}')\right)\left.\frac{\partial \tilde{P}'}{\partial R}\right|_P\right] + \left.\frac{\partial E_{xc}}{\partial R}\right|_P + \frac{\partial V_{NN}}{\partial R}$$
$$= Tr\left[\frac{dh}{dR}\tilde{P} + \frac{1}{2}\left.\frac{\partial G_{2e}(\tilde{P})}{\partial R}\right|_P\tilde{P}\right] + \left.\frac{\partial E_{xc}}{\partial R}\right|_P + \frac{\partial V_{NN}}{\partial R} \tag{2.40}$$

where $\left.\frac{\partial h}{\partial R}\right|_P = \frac{dh}{dR}$ because h is not a function of P, and similarly for h'. In equation (2.40), the derivatives in the orthonormal basis depend on the derivatives in the non-orthogonal basis in addition to the transformation matrix U.

$$\frac{dh}{dR} = \frac{d(U^{-T}h'U^{-1})}{dR} = U^{-T}\frac{dh'}{dR}U^{-1} + \frac{dU^{-T}}{dR}h'U^{-1} + U^{-T}h'\frac{dU^{-1}}{dR}$$
$$= U^{-T}\frac{dh'}{dR}U^{-1} + \frac{dU^{-T}}{dR}U^{T}h + hU\frac{dU^{-1}}{dR} \tag{2.41}$$
$$= U^{-T}\frac{dh'}{dR}U^{-1} - U^{-T}\frac{dU^{T}}{dR}h - h\frac{dU}{dR}U^{-1}$$

where $U[dU^{-1}/dR] = -[dU/dR]U^{-1}$ is obtained by differentiating $UU^{-1} = 1$.

The derivative of the density matrix in the non-orthogonal basis is given by

$$\left.\frac{\partial \tilde{P}'}{\partial R}\right|_P = \left.\frac{\partial(U^{-1}\tilde{P}U^{-T})}{\partial R}\right|_P = \frac{dU^{-1}}{dR}\tilde{P}U^{-T} + U^{-1}\tilde{P}\frac{dU^{-T}}{dR} = \frac{dU^{-1}}{dR}U\tilde{P}' + \tilde{P}'U^{T}\frac{dU^{-T}}{dR}$$
$$= -U^{-1}\frac{dU^{-1}}{dR}\tilde{P}' - \tilde{P}'\frac{dU^{-T}}{dR}U^{-T} \tag{2.42}$$

where $\partial U/\partial R|_P = dU/dR$, because U is only a function of R and not of P. Now, inserting equation (2.41) and (2.42) into (2.40), the derivative of the energy with respect to the nuclei becomes

$$\left.\frac{\partial E(R,P)}{\partial R}\right|_P = Tr\left[\frac{dh'}{dR}\tilde{P}' + \frac{1}{2}\left.\frac{\partial G'(\tilde{P}')}{\partial R}\right|_{P\prime}\tilde{P}'\right] - Tr\left[F'U^{-1}\frac{dU}{dR}\tilde{P}' + \tilde{P}'\frac{dU^T}{dR}U^{-T}F'\right]$$
$$+\left.\frac{\partial E_{xc}}{\partial R}\right|_P + \frac{\partial V_{NN}}{\partial R}$$
$$= Tr\left[U^{-T}\frac{dh'}{dR}U^{-1}\tilde{P} + \frac{1}{2}U^{-T}\left.\frac{\partial G'}{\partial R}\right|_{P\prime}U^{-1}\tilde{P}\right] \tag{2.43}$$
$$- Tr\left[F\frac{dU}{dR}U^{-1}\tilde{P} + \tilde{P}U^{-T}\frac{dU^T}{dR}F\right] + \left.\frac{\partial E_{xc}}{\partial R}\right|_P + \frac{\partial V_{NN}}{\partial R}$$

Again, the Kohn-Sham operator F' in the non-orthogonal basis set is related to the operator F in the orthonormal basis by $F = U^{-T}F'U^{-1}$.

For an idempotent density matrix, the derivative of the energy with respect to the nuclear coordinates in the non-orthogonal basis simplified to

$$\left.\frac{\partial E}{\partial R}\right|_P = Tr\left[\frac{dh'}{dR}\tilde{P}' + \frac{1}{2}\left.\frac{\partial G'(\tilde{P}')}{\partial R}\right|_{P'}\tilde{P}'\right] - Tr\left[F'\tilde{P}'\frac{dS'}{dR_{ij}}\tilde{P}'\right] + \left.\frac{\partial E_{xc}}{\partial R}\right|_P + \frac{\partial V_{NN}}{\partial R}$$
$$+ Tr\left[[\tilde{P},F]\left(\left(1-\tilde{P}\right)\frac{dU}{dR}U^{-1} - \tilde{P}U^{-T}\frac{dU^T}{dR}\right)\right] \tag{2.44}$$

where $U^{-T}[dU^T/dR] + [dU/dR]U^{-1} = -U^{-T}[dS'/dR]U^{-1}$ which is obtained by differentiating $U^{-T}S'U^{-1} = 1$. For the case where the Kohn-Sham operator and the density matrices commute, the last term on the right hand side of equation (2.44) is zero which yields the Born-Oppenheimer expression of the energy derivative. For converged SCF calculations, it is the Born-Oppenheimer expression that is commonly used.

II.2 Constraints for the scalar-mass ADMP

The Lagrangian constraint matrix for the time step i (Λ_i) is chosen to satisfy the two conditions

$$Tr[P_{i+1}] = N \tag{2.45}$$

$$P_{i+1}{}^2 = P_{i+1} \tag{2.46}$$

While the first constraint conserves the number of electrons, the second constraint represents the idempotency of the density matrix.

For an idempotent density matrix P_{i+1}, $Tr\left[\left(P_{i+1}{}^2 - P_{i+1}\right)^2\right]$ must tend to zero (equation (2.46)). Thus, one can solve for P_{i+1} by a simple iterative procedure that minimizes $Tr\left[\left(P_{i+1}{}^2 - P_{i+1}\right)^2\right]$. Starting with

$$P_{i+1} = P_i + W_i\Delta t - \frac{\Delta t^2}{2\mu}\left[\left.\frac{\partial E(R_i, P_i)}{\partial P}\right|_R\right] \tag{2.47}$$

which is obtained from equation (2.34) by choosing $\Lambda_i = 0$, the idempotency of P_{i+1} is improved iteratively using

$$P_{i+1} \leftarrow P_{i+1} + P_i T P_i + Q_i T Q_i \;\; with \;\; Q_i = 1 - P_i \tag{2.48}$$

$$T = \tilde{P}_{i+1} - P_{i+1} = 3P_i^2 - 2P_i^3 - P_{i+1} \tag{2.49}$$

where the iteration converges rapidly and is stopped when $\left\{Tr\left[\left(P_{i+1}{}^2 - P_{i+1}\right)^2\right]\right\}^{1/2}/N_m < 10^{-12}$; N_m being the size of the involved matrices. Note that the above algorithm comprises only the occupied-occupied and virtual-virtual blocks of P_{i+1} since the occupied-virtual blocks of the constraint term are zero i.e. $P_i[\Lambda_i P_i + P_i\Lambda_i - \Lambda_i]Q_i = Q_i[\Lambda_i P_i + P_i\Lambda_i - \Lambda_i]P_i = 0$ where $Q_i = 1 - P_i$.

To determine the Lagrangian multiplier Λ_{i+1}, not only P_{i+1} is needed to satisfy the idempotency condition, but also W_{i+1}. Thus, one uses the first-order time derivative of the idempotency condition (equation (2.46)) which gives a relation between the final density matrix velocity W_{i+1} and the density matrix P_{i+1}.

$$W_{i+1}P_{i+1} + P_{i+1}W_{i+1} = W_{i+1} \tag{2.50}$$

This can be solved exactly to give Λ_{i+1}

$$\Lambda_{i+1} = [2P_{i+1}W^*{}_{i+1}P_{i+1} - W^*{}_{i+1}](2\mu/\Delta t) \tag{2.51}$$

with

$$W^*{}_{i+1} = W_{i+1/2} - [\partial E(R_{i+1}, P_{i+1})/\partial P|_R](\Delta t/2\mu) \tag{2.52}$$

It must be noted that the iterative scheme corresponds to starting with $\Lambda_i = 0$. However, this is not the only possible choice. A better choice is obtained from the second-order derivative of P_{i+1} for more accuracy.

From the equation of motion (2.32), one can obtain

$$\begin{aligned}\frac{dW_i}{dt} &= -\frac{1}{\mu}\left[\left.\frac{\partial E(R_i, P_i)}{\partial P}\right|_R + \Lambda_i P_i + P_i \Lambda_i - \Lambda_i\right] \\ &= -\frac{1}{\mu}[3F_iP_i + 3P_iF_i - 2F_iP_i^2 - 2P_iF_iP_i - 2P_i^2F_i + \Lambda_iP_i + P_i\Lambda_i \\ &- \Lambda_i]\end{aligned} \tag{2.53}$$

And from the second-order time derivative of the idempotency constraint (equation (2.46)), one finds

$$\frac{dW_i}{dt} = P_i\frac{dW_i}{dt} + 2W_iW_i + \frac{dW_i}{dt}P_i \tag{2.54}$$

Now, with the help of the projection operators P_i and Q_i and their properties ($(P_i)^2 = P_i$, $(Q_i)^2 = Q_i$, and $P_i Q_i = Q_i P_i = 0$), equations (2.53) and (2.54) can be projected to give

$$P_i \frac{dW_i}{dt} P_i = -2P_i[W_i W_i]P_i = -\frac{1}{\mu} P_i \Lambda_i P_i \qquad (2.55)$$

$$Q_i \frac{dW_i}{dt} Q_i = 2Q_i[W_i W_i]Q_i = \frac{1}{\mu} Q_i \Lambda_i Q_i \qquad (2.56)$$

From equations (2.55) and (2.56), one finds

$$\frac{1}{\mu}[\Lambda_i P_i + P_i \Lambda_i - \Lambda_i] = \frac{1}{\mu}[P_i \Lambda_i P_i - Q_i \Lambda_i Q_i] = 2[P_i(W_i W_i)P_i - Q_i(W_i W_i)Q_i] \qquad (2.57)$$

which is an expression for Λ_i, more accurate to start with, and can be used as an initial guess for the iterative scheme.

II.3 Mass-tensor ADMP

Consider a partitioning of the P_{i+1} matrix into the four blocks $[P_i P_{i+1} P_i]$, $[P_i P_{i+1} Q_i]$, $[Q_i P_{i+1} P_i]$, and $[Q_i P_{i+1} Q_i]$. Projecting equation (2.34), we obtain

$$[P_i P_{i+1} P_i] = P_i + \frac{\Delta t^2}{2\mu} P_i \Lambda_i P_i \qquad (2.58)$$

$$[P_i P_{i+1} Q_i] = P_i\{W_i \Delta t\}Q_i - P_i \left\{ \frac{\Delta t^2}{2\mu} \frac{\partial E(R_i, P_i)}{\partial P} \bigg|_R \right\} Q_i \qquad (2.59)$$

$$[Q_i P_{i+1} Q_i] = -\frac{\Delta t^2}{2\mu} Q_i \Lambda_i Q_i \qquad (2.60)$$

where $[Q_i P_{i+1} P_i] = [P_i P_{i+1} Q_i]^T$, by definition, since all matrices are real symmetric. $P_i[\partial E(R_i, P_i)/\partial P|_R]P_i = Q_i[\partial E(R_i, P_i)/\partial P|_R]Q_i = 0$ from equation (2.38) and $P_i W_i P_i = Q_i W_i Q_i = 0$ from equation (2.50).

From equations (2.58) and (2.60), it is seen that the Lagrangian constraint matrix Λ_i affects the occupied-occupied and virtual-virtual blocks of the density matrix, but not the occupied-virtual blocks (equation (2.59)). The occupied-virtual blocks are, however, governed by the fictitious density velocity (which may be arbitrary) and the force on the density matrix. To control this arbitrariness, a mass weighting scheme is introduced by generalizing the fictitious mass μ to a matrix of masses ɥ. Another reason for this generalization is that the density matrix elements for the core orbitals of an atom change more slowly than for the valence orbitals since the core is more tightly bound to the nucleus. Hence, it is useful to have a larger mass for the core orbitals and a smaller mass for the valence orbitals.

If the mass-weighted density velocity is defined as $\left[ɥ^{1/4} W ɥ^{1/4}\right]$, the generalized Lagrangian becomes

$$\mathcal{L} = \frac{1}{2}Tr(V^T M V) + \frac{1}{2}Tr\left(\left[ɥ^{1/4} W ɥ^{1/4}\right]^2\right) - E(R,P) - Tr[\Lambda(PP - P)] \qquad (2.61)$$

And the Lagrange equation for the density matrix is given by

$$ɥ^{1/2}\frac{d^2 P}{dt^2}ɥ^{1/2} = -\left[\frac{\partial E(R,P)}{\partial P}\bigg|_R + \Lambda P + P\Lambda - \Lambda\right] \qquad (2.62)$$

The fictitious mass matrix is assumed to be independent of t; then, equation (2.62) can be integrated to give

$$P_{i+1} = P_i + W_i \Delta t - \frac{\Delta t^2}{2}ɥ^{-1/2}\left[\frac{\partial E(R_i, P_i)}{\partial P}\bigg|_R + \Lambda_i P_i + P_i \Lambda_i - \Lambda_i\right]ɥ^{-1/2} \qquad (2.63)$$

$$W_{i+1/2} = W_i - \frac{\Delta t}{2}ɥ^{-1/2}\left[\frac{\partial E(R_i, P_i)}{\partial P}\bigg|_R + \Lambda_i P_i + P_i \Lambda_i - \Lambda_i\right]ɥ^{-1/2} = \frac{P_{i+1} - P_i}{\Delta t} \qquad (2.64)$$

$$W_{i+1} = W_{i+1/2} - \frac{\Delta t}{2}\mu^{-1/2}\left[\left.\frac{\partial E(R_{i+1}, P_{i+1})}{\partial P}\right|_R + \Lambda_{i+1}P_{i+1} + P_{i+1}\Lambda_{i+1} - \Lambda_{i+1}\right]\mu^{-1/2} \quad (2.65)$$

Unlike the quantity $P_i\left\{\frac{1}{\mu}[\Lambda_i P_i + P_i\Lambda_i - \Lambda_i]\right\}Q_i$ for the scalar mass case, the corresponding quantity for the mass-matrix case is

$$P_i\{\mu^{-1/2}[\Lambda_i P_i + P_i\Lambda_i - \Lambda_i]\mu^{-1/2}\}Q_i \neq 0 \quad (2.66)$$

for $[\mu, P_i] \neq 0$. As a result, mass-weighting allows for the idempotency force $\mu^{-1/2}[\Lambda_i P_i + P_i\Lambda_i - \Lambda_i]\mu^{-1/2}$ to affect the occupied-virtual blocks of the density matrix.

$$[P_i P_{i+1} P_i] = P_i - \frac{\Delta t^2}{2}P_i\left\{\mu^{-1/2}\left[\left.\frac{\partial E(R_i, P_i)}{\partial P}\right|_R + \Lambda_i P_i + P_i\Lambda_i - \Lambda_i\right]\mu^{-1/2}\right\}P_i \quad (2.67)$$

$$[P_i P_{i+1} Q_i] = P_i\{W_i\Delta t\}Q_i - \frac{\Delta t^2}{2}P_i\left\{\mu^{-1/2}\left[\left.\frac{\partial E(R_i, P_i)}{\partial P}\right|_R + \Lambda_i P_i + P_i\Lambda_i - \Lambda_i\right]\mu^{-1/2}\right\}Q_i \quad (2.68)$$

$$[Q_i P_{i+1} Q_i] = -\frac{\Delta t^2}{2}Q_i\left\{\mu^{-1/2}\left[\left.\frac{\partial E(R_i, P_i)}{\partial P}\right|_R + \Lambda_i P_i + P_i\Lambda_i - \Lambda_i\right]\mu^{-1/2}\right\}Q_i \quad (2.69)$$

II.4 Constraints for the mass-matrix ADMP

As in the scalar-mass ADMP, an initial guess for P_{i+1} and W_{i+1} corresponds to choosing $\Lambda_i = 0$. Thus, the equation of motion of P_{i+1} (2.63) becomes

$$P_{i+1} = P_i + W_i\Delta t - \frac{\Delta t^2}{2}\mu^{-1/2}\left[\left.\frac{\partial E(R_i, P_i)}{\partial P}\right|_R\right]\mu^{-1/2} \quad (2.70)$$

From equation (2.63), it is noted that the constraint term has the form $\mathrm{u}^{-1/2}A\mathrm{u}^{-1/2}$, where the matrix A has only occupied-occupied and virtual-virtual blocks. In analogy with the scalar mass case, one may iterate

$$P_{i+1} \leftarrow P_{i+1} + \mathrm{u}^{-1/2}[P_i T P_i + Q_i T Q_i]\mathrm{u}^{-1/2} \qquad (2.71)$$

where $T = \mathrm{u}^{1/2}[\tilde{P}_{i+1} - P_{i+1}]\mathrm{u}^{1/2} = \mathrm{u}^{1/2}[3P_i^2 - 2P_i^3 - P_{i+1}]\mathrm{u}^{1/2}$. As in the scalar mass case, the iterative scheme converges rapidly and it is stopped when $\left\{Tr\left[\left({P_{i+1}}^2 - P_{i+1}\right)^2\right]\right\}^{1/2}/N_m < 10^{-12}$, where N_m is the size of the involved matrices.

To obtain W_{i+1}, it is necessary to satisfy the time derivative of the idempotency condition (equation (2.50)). This is done by solving iteratively using the equation of motion of W_{i+1} that corresponds to choosing $\Lambda_i = 0$.

$$W_{i+1} = W_{i+1/2} - \mathrm{u}^{-1/2}[\partial E(R_{i+1}, P_{i+1})/\partial P|_R]\mathrm{u}^{-1/2}(\Delta t/2) \qquad (2.72)$$

And iterating

$$W_{i+1} \leftarrow W_{i+1} + \mathrm{u}^{-1/2}[P_{i+1}\tilde{T}P_{i+1} + Q_{i+1}\tilde{T}Q_{i+1}]\mathrm{u}^{-1/2} \qquad (2.73)$$

where $\tilde{T} = \mathrm{u}^{1/2}[\widetilde{W}_{i+1} - W_{i+1}^*]\mathrm{u}^{1/2}$ and $\widetilde{W}_{i+1} = \mathrm{d}\,\tilde{P}_{i+1}/dt = P_{i+1}W_{i+1}Q_{i+1} + Q_{i+1}W_{i+1}P_{i+1}$. This iteration converges rapidly and is stopped when $\{Tr[(W_{i+1}P_{i+1} + P_{i+1}W_{i+1} - W_{i+1})^2]\}^{1/2}/N_m < 10^{-12}$.

A higher order, initial guess for an idempotent P_{i+1} may be obtained by using the fact that $W_{i+1}P_{i+1} + P_{i+1}W_{i+1} = W_{i+1}$ is already satisfied by the use of equations (2.72) and (2.73), for the previous time step i. Since a solution to W_{i+1} requires having an approximation to Λ_i see (equation (2.65)), this approximation may be used in generating an initial guess for P_{i+1}. Thus, using equations (2.63), (2.64), and (2.65) one obtains

$$P_{i+1} = P_i + 2W_i\Delta t - W_{i-1/2}\Delta t \qquad (2.74)$$

which is a higher order initial guess for P_{i+1} and may be used in conjunction with the iterative scheme described in equation (2.71).

It must be noted that the ADMP method is already implemented in Gaussian contrary to the perturbative method described in section III. In the present work, we have transformed the perturbative method into a program which was implemented in Gaussian for an easy and quick usage.

III Vibrational corrections to NMR parameters - perturbation theory

Since NMR parameters depend on the molecular geometry, the molecular vibration may result in an important effect on the NMR parameters. The effects of motion of the nuclear framework cannot be ignored when comparing with experimental observations, and vibrational effects must be taken into account in the calculation of NMR parameters. In this section, vibrational effects are calculated using the second-order perturbation theory. We first discuss the calculation of zero-point vibrational effects, and then temperature effects.

III.1 Zero-point vibrational contributions

Molecules are known to move even at 0 K, leading to what is commonly referred to as zero-point vibrational corrections (ZPVC) to molecular properties.

The unperturbed ground-state nuclear Hamiltonian is usually chosen to be the harmonic oscillator Hamiltonian [15]

$$H^{(0)} = \frac{1}{2}\sum_{L}(P_L^2 + \omega_L^2 Q_L^2) \tag{2.75}$$

where Q_L is the normal coordinate L with a harmonic frequency ω_L, and P_L is the momentum operator for the same normal coordinate.

The unperturbed ground-state nuclear wavefunction is given as a product of the harmonic oscillator wavefunctions

$$\varphi^{(0)}(Q) = \prod_L \varphi_L^{(0)}(Q_L) \tag{2.76}$$

where $\varphi_L^{(n)}$ is the nth excited harmonic-oscillator state of the Lth vibrational normal mode.

The unharmonicity of the potential energy surface is treated as perturbations to the harmonic oscillator Hamiltonian. The nth order Hamiltonian in the perturbation expansion is given as

$$H^{(1)} = \sum_L F_L Q_L + \frac{1}{6}\sum_{LMO} F_{LMO} Q_L Q_M Q_O \tag{2.77}$$

$$H^{(n)} = \frac{1}{(n+2)!}\sum_{LMOP\ldots} F_{LMNO\ldots} Q_L Q_M Q_O Q_P \ldots \quad n \geq 2 \tag{2.78}$$

where $F_{LMOP\ldots}$ is the derivative of the electronic energy with respect to the normal coordinates $Q_L Q_M Q_O Q_P \ldots$ at some reference geometry taken usually to be the equilibrium geometry. It must be noted that, F_L is the gradient of the electronic energy with respect to the normal coordinate L ($F_L = 0$ for an equilibrium geometry); F_{LL}, which is the second derivative of the electronic energy, is square the harmonic frequency of the normal mode L since ${\omega_L}^2 = \frac{d^2E}{dQ_L^2}$.

The first-order perturbed wavefunction contains only contributions from single and triple excitations [16; 17]

$$\varphi^{(1)}(Q) = \sum_L [a_L^1 \varphi_L^1(Q) + a_L^3 \varphi_L^3(Q)] + \sum_{L\neq M} b_{LM}^{21} \varphi_{LM}^{21}(Q) + \sum_{L\neq M\neq O} c_{LMO}^{111} \varphi_{LMO}^{111}(Q) \tag{2.79}$$

where $\varphi_{LMO}^{111}(Q)$, for example, has been obtained from $\varphi^{(0)}(Q)$ by exciting the Lth, Mth, and Oth modes to the lth, mth, and oth harmonic oscillator states respectively. The coefficients a_L^1, a_L^3, b_{LM}^{21}, and c_{LMO}^{111} are given by [17]

$$a_L^1 = -\frac{1}{\sqrt{2}\omega_L^{3/2}}\left(F_L + \frac{1}{4}\sum_M \frac{F_{LMM}}{\omega_M}\right) \tag{2.80}$$

$$a_L^3 = -\frac{\sqrt{3}}{36\omega_L^{5/2}} F_{LLL} \tag{2.81}$$

$$b_{LM}^{21} = -\frac{F_{LLM}}{4\omega_L\sqrt{\omega_M}(2\omega_L + \omega_M)} \tag{2.82}$$

$$c_{LMO}^{111} = -\frac{F_{LMO}}{12\sqrt{2\omega_L\omega_M\omega_O}(\omega_L + \omega_M + \omega_O)} \tag{2.83}$$

Let us calculate the zero-point vibrational correction of the chemical shielding σ under consideration in the present work. The chemical shielding can be written as a Taylor series in normal coordinates, in analogy with the vibrational force field, around some reference geometry taken to be the equilibrium geometry

$$\sigma(Q) = \sigma_0 + \sigma_1 + \sigma_2 \ldots = \sigma_0 + \sum_L \frac{d\sigma}{dQ_L} Q_L + \frac{1}{2}\sum_{L\neq M} \frac{d^2\sigma}{dQ_L dQ_M} Q_L Q_M \ldots \tag{2.84}$$

Besides, the averaged value of the nuclear shielding $\langle\sigma\rangle$ can be expanded in a perturbation expansion due to the perturbed nuclear wavefunction φ. We may write

$$\langle\sigma\rangle = \sum_{n=0}^{\infty} \langle\sigma^{(n)}\rangle = \langle\sigma^{(0)}\rangle + \langle\sigma^{(1)}\rangle + \cdots = \langle\varphi^{(0)}|\sigma|\varphi^{(0)}\rangle + 2\langle\varphi^{(0)}|\sigma|\varphi^{(1)}\rangle + \cdots \tag{2.85}$$

where $\langle\sigma^{(n)}\rangle$ is the nth order contribution to the vibrationally averaged shielding tensor. For the unperturbed contribution, the only non-vanishing terms are those of even order [16]

$$\langle\sigma^{(0)}\rangle = \langle\varphi^{(0)}|\sigma_0 + \sigma_2 \dots |\varphi^{(0)}\rangle \tag{2.86}$$

where for the first two contributions

$$\langle\varphi^{(0)}|\sigma_0|\varphi^{(0)}\rangle = \sigma_{eq} \tag{2.87}$$

$$\langle\varphi^{(0)}|\sigma_2|\varphi^{(0)}\rangle = \frac{1}{4}\sum_L \frac{1}{\omega_L}\frac{d^2\sigma}{dQ_L^2}\bigg|_{\sigma_{eq}} \tag{2.88}$$

The contributions to first order $\langle\sigma^{(1)}\rangle$ contain only terms of odd orders [16]

$$\langle\sigma^{(1)}\rangle = 2\langle\varphi^{(0)}|\sigma_1 + \sigma_3 \dots |\varphi^{(1)}\rangle \tag{2.89}$$

where for the first two contributions

$$\langle\varphi^{(0)}|\sigma_1|\varphi^{(1)}\rangle = \sqrt{2}\sum_L \frac{d\sigma}{dQ_L}\frac{a_L^1}{\sqrt{\omega_L}}\bigg|_{\sigma_{eq}} \tag{2.90}$$

$$\begin{aligned}\langle\varphi^{(0)}|\sigma_3|\varphi^{(1)}\rangle = {} & \frac{1}{6}\sqrt{\frac{3}{2}}\sum_L \frac{d^3\sigma}{dQ_L^3}\frac{\sqrt{3}a_L^1 + \sqrt{2}a_L^3}{\omega_L^{3/2}}\bigg|_{\sigma_{eq}} \\ & + \frac{1}{4}\sum_{L\neq M}\frac{d^3\sigma}{dQ_L^2 dQ_M}\left(\frac{\sqrt{2}a_L^1 + 2b_{LM}^{21}}{\omega_L\sqrt{\omega_M}}\right)\bigg|_{\sigma_{eq}} \\ & + \frac{1}{6\sqrt{2}}\sum_{L\neq M\neq O}\frac{d^3\sigma}{dQ_L dQ_M dQ_O}\left(\frac{c_{LMO}^{111}}{\sqrt{\omega_L\omega_M\omega_O}}\right)\bigg|_{\sigma_{eq}}\end{aligned} \tag{2.91}$$

Most calculations include only the three terms $\langle\varphi^{(0)}|\sigma_0|\varphi^{(0)}\rangle$, $\langle\varphi^{(0)}|\sigma_2|\varphi^{(0)}\rangle$, and $\langle\varphi^{(0)}|\sigma_1|\varphi^{(1)}\rangle$ because they were shown to account for more than 90% of the vibrational contribution to the shielding constants in four diatomic molecules [18]. Thus,

$$\langle\sigma\rangle = \langle\varphi^{(0)}|\sigma_0|\varphi^{(0)}\rangle + \langle\varphi^{(0)}|\sigma_2|\varphi^{(0)}\rangle + 2\langle\varphi^{(0)}|\sigma_1|\varphi^{(1)}\rangle \tag{2.92}$$

And then, the expression of the averaged chemical shielding around the equilibrium geometry can be reduced to

$$\langle\sigma\rangle = \sigma_{eq} + \frac{1}{4}\sum_L \frac{1}{\omega_L}\left[\frac{d^2\sigma_{eq}}{dQ_L^2} - \frac{1}{\omega_L}\frac{d\sigma_{eq}}{dQ_L}\sum_M \frac{F_{LMM}^{eq}}{\omega_M}\right] \tag{2.93}$$

Similarly, the ZPVC to spin-spin coupling constants can be calculated using the equation

$$\langle J\rangle = J_{eq} + \frac{1}{4}\sum_L \frac{1}{\omega_L}\left[\frac{d^2J_{eq}}{dQ_L^2} - \frac{1}{\omega_L}\frac{dJ_{eq}}{dQ_L}\sum_M \frac{F_{LMM}^{eq}}{\omega_M}\right] \tag{2.94}$$

III.2 Temperature effects

Temperature has also an effect on the vibrational motion of the nuclear framework, and hence on NMR parameters. The effect of temperature is usually less important than ZPVC; however, it has to be computed for a more complete comparison with experimental results. The observed temperature changes are primarily due to two effects: (1) the populations of higher vibrational states, and (2) centrifugal distortions.

Equation (2.88) and (2.90) for calculating ZPVC to the NMR properties can be extended to the vibrational average of a molecular property in an arbitrary vibrational state described by the vibrational quantum number ν_L [19]

$$\langle\varphi^{(0)}|\sigma_2|\varphi^{(0)}\rangle = \frac{1}{2}\sum_L \frac{\left(\nu_L + \frac{1}{2}\right)}{\omega_L}\frac{d^2\sigma}{dQ_L^2} \tag{2.95}$$

$$\langle\varphi^{(0)}|\sigma_1|\varphi^{(1)}\rangle = 2\sqrt{2}\sum_L \frac{d\sigma}{dQ_L}\frac{a_L^1\left(\nu_L + \frac{1}{2}\right)}{\sqrt{\omega_L}} \tag{2.96}$$

In order to estimate the temperature dependence of the molecular property, we assume that the populations of the excited states are determined by a Boltzmann distribution. By averaging over all possible vibrational states using a Boltzmann weighting of the population of the excited states, the vibrationally averaged molecular properties at thermal equilibrium may be calculated as [19; 20]

$$\langle\varphi^{(0)}|\sigma_2|\varphi^{(0)}\rangle = \frac{1}{4}\sum_L \frac{1}{\omega_L}\frac{d^2\sigma}{dQ_L^2} coth\left(\frac{\omega_L}{2k_BT}\right) \tag{2.97}$$

$$\langle\varphi^{(0)}|\sigma_1|\varphi^{(1)}\rangle = \sqrt{2}\sum_L \frac{d\sigma}{dQ_L}\frac{a_L^1}{\sqrt{\omega_L}} \tag{2.98}$$

where

$$a_L^1 = -\frac{1}{\sqrt{2}\omega_L^{3/2}}\left(F_L + \frac{1}{4}\sum_M \frac{F_{LMM}}{\omega_M} coth\left(\frac{\omega_L}{2k_BT}\right)\right) \tag{2.99}$$

The population of higher rotational states does not in itself change the value of the NMR properties since there is no dependence of the calculated properties on the rotational state. However, the coupling of the rotational and vibrational motion in what is reffered to as centrifugal distortions, that is, the elongation of bonds as the rotational state of the molecule increases, give important contributions to the temperature corrections.

In evaluating the centrifugal distortions, it is customary to assume that the spacings of the rotational energy levels are much smaller than k_BT, allowing for the use of the law of equipartitioning of the energy, leading to the following contribution to the temperature corrections due to centrifugal distortions

$$\langle\varphi^{(0)}|\sigma_1|\varphi^{(1)}\rangle_{centr} = \frac{k_BT}{2}\sum_L \frac{d\sigma}{dQ_L}\frac{1}{\omega_L^2}\sum_\alpha \frac{a_L^{\alpha\alpha}}{I_{\alpha\alpha}} \tag{2.100}$$

where $I_{\alpha\alpha}$ is the moment of inertia tensor at the equilibrium geometry, and $a_L^{\alpha\alpha}$ is the coefficient of expansion of $I_{\alpha\alpha}$ in normal coordinates Q_L.

Thus, the temperature dependent averaged chemical shielding and spin-spin coupling constant around the equilibrium geometry can be expressed as

$$\langle\sigma\rangle = \sigma_{eq} + \frac{1}{4}\sum_{L}\frac{1}{\omega_L} coth\left(\frac{\omega_L}{2k_BT}\right)\left[\frac{d^2\sigma_{eq}}{dQ_L^2} - \frac{1}{\omega_L}\frac{d\sigma_{eq}}{dQ_L}\sum_{M}\frac{F_{LMM}^{eq}}{\omega_M}\right] + \frac{k_BT}{2}\sum_{L}\frac{d\sigma_{eq}}{dQ_L}\frac{1}{\omega_L^2}\sum_{\alpha}\frac{a_L^{\alpha\alpha}}{I_{\alpha\alpha}} \quad (2.101)$$

$$\langle J\rangle = J_{eq} + \frac{1}{4}\sum_{L}\frac{1}{\omega_L} coth\left(\frac{\omega_L}{2k_BT}\right)\left[\frac{d^2J_{eq}}{dQ_L^2} - \frac{1}{\omega_L}\frac{dJ_{eq}}{dQ_L}\sum_{M}\frac{F_{LMM}^{eq}}{\omega_M}\right] + \frac{k_BT}{2}\sum_{L}\frac{dJ_{eq}}{dQ_L}\frac{1}{\omega_L^2}\sum_{\alpha}\frac{a_L^{\alpha\alpha}}{I_{\alpha\alpha}} \quad (2.102)$$

References

1. *Zur Quantentheorie der Molekeln.* **R. Oppenheimer, and M. Born.** 1927, Ann. Phys., Vol. 84, p. 457.

2. *Vibrational corrections to indirect nuclear spin–spin coupling constants calculated by density-functional theory.* **T. A. Ruden, O. B. Lutnaes, T. Helgaker , and K. Ruud.** 2003, J. Chem. Phys., Vol. 118, p. 9572.

3. *Ab initio molecular dynamics: Propagating the density matrix with Gaussian orbitals.* **H. B. Schlegel, J. M. Millam, S. S. Iyengar, G. A. Voth, A. D. Daniels, G. E. Scuseria, and M. J. Frisch.** 2001, J. Chem. Phys., Vol. 114, p. 9758.

4. *Ab initio molecular dynamics: Propagating the density matrix with Gaussian orbitals. II. Generalizations based on mass-weighting, idempotency, energy conservation and choice od initial conditions.* **S. S. Iyengar, H. B. Schlegel, J. M. Millam, G. A. Voth, G. E. Scuseria, and M. J. Frisch.** 2001, J. Chem. Phys., Vol. 115, p. 10291.

5. *Ab initio molecular dynamics: Propagating the density matrix with Gaussian orbitals. III. Comparison with Born-Oppenheimer dynamics.* **H. B. Schlegel, S. S. Iyengar, W. Li, J. M. Millam, G. A. Voth, G. E. Scuseria, and M. J. Frish.** 2002, J. Chem. Phys., Vol. 117, p. 8694.

6. *Calculation of NMR and EPR parameters: Theory and application.* **M. Kaupp, M. Buhl, and V. G. Malkin.** 2004, Wiley-vch.

7. *Gaussian 03, Revision C.02, Gaussian, Inc., Wallingford CT.* **M. J. Frisch, and al.** 2004.

8. *Quantum Physics.* **S.Gasiorowicz.** 1974, John Wiley & Sons, New York.

9. *Computer "Experiments" on Classical Fluids. I. Thermodynamical Properties of Lennard-Jones Molecules.* **L.Verlet.** 1967, Phys. Rev., Vol. 159, p. 98.

10. *Molecular dynamics with coupling to an external bath.* **H. J. C. Berendsen, J. P. M. Postma, W. F. van Gunsteren, A. DiNola, and J. R. Haak.** 1984, J. Chem. Phys., Vol. 81, p. 3684.

11. *Molecular dynamics simulations at constant pressure and/or temperature.* **H.C.Andersen.** 1980, J. Chem. Phys., Vol. 72, p. 2384.

12. *Classical mechanics.* **H.Goldstein.** 1980, Addison-Wesley Press, Cambridge.

13. *Ab initio molecular dynamics: propagating the density matrix with gaussian orbitals.* **H. B. Schlegel, J. M. Millam, S. S. Iyengar, G. A. Voth, A. D. Daniels, G. E. Scuseria, and M. J. Frisch.** 2001, J. Chem. Phys., Vol. 114, p. 9758.

14. **R.McWeeny.** 1960, Rev. Mod. Phys., Vol. 32, p. 335.

15. *Molecular Vibrations.* **E. B. Wilson Jr, J. C. Decius, P. C. Cross.** 1955, MCGraw-Hill, NewYork.

16. *Nuclear Corrections to Electronic Expectation Values: Zero-Point Vibrational Effects in the Water Molecule.* **C. W. Kern, and R. L. Matcha.** 1968, J. Chem. Phys., Vol. 49, p. 2081.

17. *Calculation of the vibrational wave function of polyatomic molecules.* **P. -O. Åstrand, K. Ruud, and P. R. Taylor.** 2000, J. Chem. Phys., Vol. 112, p. 2655.

18. **K. Ruud, P. -O. Astrand, P. R. Taylor.** 2003, Int. J. Comput. Methods. Sci Eng., Vol. 3, p. 7.

19. *Effect of vibration and rotation on the internuclear distance.* **M. Toyama, T. Oka, and Y. Morino.** 1964, Journal of Molecular Spectroscopy, Vol. 13, p. 193.

20. *Temperature dependences of J(C,H) and J(C,D) in 13CH4 and some of its deuterated isotopomers.* **B. Bennett, W. T. Raynes, and C. W. Anderson.** 1989, Spectrochimica Acta Part A: Molecular Spectroscopy, Vol. 45, p. 821.

Chapter 3

Application on Metabolites: Results

This chapter presents our results on the ^{1}H NMR parameters for seven metabolites: involved in prostate (putrescine, spermidine, spermine, and sarcosine), or in brain (acetate, alanine, and serine). It is divided into three parts. In part A, our calculations are illustrated for four metabolites (putrescine, sarcosine, serine, and acetate) chosen as representatives of the seven ones. In part B, the full results are presented in a selection of our published papers. In part C, a synthesis of all the results obtained for metabolites is presented in conclusion.

A: Choice of a Strategy

NMR chemical shifts and spin-spin coupling constants can be obtained from quantum chemical calculations for relatively small molecules. In the present work, we have calculated the proton chemical shifts and the indirect spin-spin coupling constants for seven metabolites: putrescine, spermidine, spermine, acetate, sarcosine, alanine, and serine. With the aim to produce reliable theoretical values of NMR parameters for the analysis of experimental data from magnetic resonance spectroscopy (MRS), three effects on NMR parameters are taken into consideration: solvent, isomers, and vibration.

In this chapter, we determine the different methods to be used in the calculation of NMR parameters. In a first step, we choose the theoretical level of calculation inside the DFT approach (functional and basis set). This type of study is presented here in details for two of the investigated metabolites: putrescine and sarcosine, chosen as examples.

Then, the effects of isomers, taken into account using Boltzmann distribution, are determined through three consecutive steps that will be explained thoroughly for putrescine, taken as an example.

After that, vibrational effects are calculated using different methods (ADMP, quantum mechanics using C_{FOUR} (1), our method) to choose the most suitable one. The effects of vibration on chemical shieldings are studied for sarcosine chosen as an example, while the effects on spin-spin coupling constants are evaluated for serine.

Besides, we describe our attempts to calculate solvent effects using ONIOM method that is compared to the well-known solvent model PCM, for which acetate molecule is taken as an example.

I NMR parameters

In this section, we show the results of calculation of NMR parameters for ground-state putrescine, chosen as an example. The aim of this section is to illustrate the different concepts of NMR parameters and their related numerical values.

To determine the lowest-energy structure of putrescine, we start from its chemical formula ($C_4H_{12}N_2$) from which many arbitrary structures can be proposed. Using molecular dynamics (MD) simulation, many initial geometries can be selected; once they are optimized, one can find the most stable geometry i.e. having the lowest energy, with the condition that the harmonic frequencies of atoms are all real. Molecular dynamics simulation is performed using the graphical interface Gabedit (2) and the semi-empirical method PM6. All calculations are performed using Gaussian03 (3).

I.1 Chemical shifts

For the calculation of the chemical shifts of protons bond to carbons of putrescine, we choose the Tetramethylsilane (TMS) molecule [$(CH_3)_4Si$] as a reference. The chemical shift δ of a certain proton of putrescine is calculated by subtracting its isotropic chemical shielding σ from the isotropic chemical shielding of the protons of TMS (σ_{TMS}).

$$\delta = \sigma_{TMS} - \sigma \tag{3.1}$$

It is important to note that, both putrescine and TMS are optimized and their isotropic chemical shieldings are evaluated, at the same theoretical level. The isotropic chemical shieldings are calculated using the GIAO approach (see chapter 1 – section I.2.1).

Some groups of protons display quite close calculated δ values, indicating similarities in conformation and intermolecular interactions for these protons. Usually, geometrical optimizations are done at 0 K for motionless molecules which results sometimes in different values of δ for protons in the same methylene group. This problem is circumvented by averaging the chemical shifts of protons in the same methylene group because these protons have the same chemical environment as a result of the vibration and rotation of atoms in a molecule. It must be noted that only protons attached to carbon atoms are being studied; the other protons, as well as the other nuclei with $I \neq 0$, are outside the range of study.

The values of σ and δ for ground-state putrescine (figure (3.1)) calculated for its eight protons attached to carbon atoms, at the level B3LYP/6-311+G** are displayed in table (3.1) in units of ppm. σ_{TMS} is calculated at the same theoretical level and found to be 31.982 ppm.

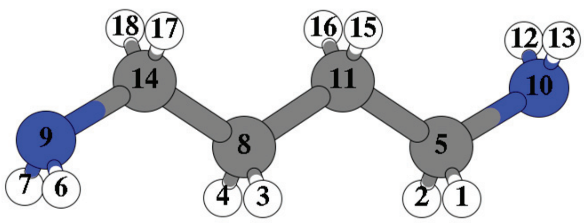

Figure 3.1: ground-state geometry for isolated putrescine, calculated at the B3LYP/6-311+G** level (nitrogen in blue, carbon in grey, and hydrogen in white)

Number of H	*σ (ppm)*	$\delta = \sigma_{TMS} - \sigma$
1	*29.383*	*2.599*
2	*29.383*	*2.599*
15	*30.851*	*1.131*
16	*30.851*	*1.131*
3	*30.851*	*1.131*
4	*30.851*	*1.131*
17	*29.383*	*2.599*
18	*29.383*	*2.599*

Table 3.1: σ and δ results for isolated ground-state putrescine calculated at the level B3LYP/6-311+G**

From table (3.1), one can easily remark that for putrescine there are two values of σ and hence for δ. Then, protons of putrescine can be gathered in two groups; each group has a δ value and it contains protons with similar chemical environment and similar atomic neighbours. We call δ_A the shift corresponding to protons of group A (3, 4, 15, 16) - see figure (3.1) for labelled protons, and δ_B the shift corresponding to protons of group B (1, 2, 17, 18).

The same sort of study is done for the other metabolites, where for spermine there exist four groups of protons, for spermine four groups, for sarcosine two groups, for acetate one group, for alanine two groups, and for serine three groups. A detailed presentation of the chemical shifts of these metabolites will be given in the part B.

I.2 Indirect spin-spin coupling constants

The spin-spin coupling constants J_{ij} (between protons i and j) calculated for the eight protons of ground-state putrescine, at the level B3LYP/ 6-311+G** are given in the table (3.2) in Hz.

H number	*1*	*2*	*15*	*16*	*3*	*4*	*17*	*18*
1	*0.000*							
2	*-12.965*	*0.000*						
15	*3.9530*	*10.332*	*0.000*					
16	*10.332*	*3.953*	*-11.039*	*0.000*				
3	*0.060*	*-0.260*	*3.422*	*11.140*	*0.000*			
4	*-0.260*	*0.060*	*11.140*	*3.423*	*-11.039*	*0.000*		
17	*-0.046*	*0.059*	*0.060*	*-0.260*	*3.953*	*10.332*	*0.000*	
18	*0.059*	*-0.046*	*-0.260*	*0.060*	*10.332*	*3.953*	*-12.965*	*0.000*

Table 3.2: J-couplings for isolated ground-state putrescine at the level B3LYP/6-311+G** before symmetrisation

The interactions between protons belonging to two neighbour methylene groups must give four equal values of spin-spin coupling constants because protons of the same methylene are equivalent. For example, protons 1 and 2 are equivalent and on the other hand protons 15 and 16 are also equivalent; for the interaction between these two couples (1 & 2) and (15 & 16), their spin-spin coupling constants must be equal i.e. $J_{1,15} = J_{1,16} = J_{2,15} = J_{2,16} = J_{(1,2)x(15,16)}$. However, this is not the case for the calculated J-couplings appearing in table (3.2) which is a result of calculations for geometries optimized at 0 K. To solve this problem, we symmetrise the J-values where necessary, in particular, to obtain $J_{3,15} = J_{4,15} = J_{3,16} = J_{4,16} = J_{(3,4)x(15,16)}$ and $J_{3,17} = J_{4,17} = J_{3,18} = J_{4,18} = J_{(3,4)x(17,18)}$ in addition to $J_{(1,2)x(15,16)}$. The symmetrised J-couplings are given in table (3.3).

H number	*1*	*2*	*15*	*16*	*3*	*4*	*17*	*18*
1	*0.000*							
2	*-12.965*	*0.000*						
15	*7.173*	*7.173*	*0.000*					
16	*7.173*	*7.173*	*-11.039*	*0.000*				
3	*0.060*	*-0.260*	*7.281*	*7.281*	*0.0000*			
4	*-0.260*	*0.060*	*7.281*	*7.281*	*-11.039*	*0.0000*		
17	*-0.046*	*0.059*	*0.060*	*-0.260*	*7.143*	*7.143*	*0.0000*	
18	*0.059*	*-0.046*	*-0.260*	*0.060*	*7.143*	*7.143*	*-12.965*	*0.0000*

Table 3.3: J-couplings for isolated ground-state putrescine at the level B3LYP/6-311+G** after symmetrisation

Note that the interactions between protons of neighbour methylene groups, which are the symmetrised spin-spin coupling constants, have large values in comparison with other spin-spin couplings. Moreover, the interactions between the protons of the same methylene group ($J_{1,2}$, $J_{15,16}$, $J_{3,4}$, $J_{17,18}$) have large negative values, but they have no effect on the simulated spectrum (two identical protons with the same chemical shift and a common coupling constant behave as a single proton and absorb energy at a single frequency independent of their spin-spin coupling constant). The other interactions with small values of J_{ij} (< 0.3 Hz) can be neglected.

Hence, the interactions between protons attached to neighbour carbon atoms are the important interactions which play the main role in determining the profile of an NMR spectrum. For putrescine, three main values of spin-spin coupling constants determine its NMR spectrum and they are $J_{(1,2)x(15,16)}$, $J_{(3,4)x(15,16)}$, and $J_{(3,4)x(17,18)}$ which are calculated at the level B3LYP/6-311+G** and found to be 7.173, 7.281, and 7.143 Hz respectively. Due to the symmetrical form of putrescine, we can take $J_{(1,2)x(15,16)} = J_{(3,4)x(17,18)}$ and by that, the number of main spin-spin coupling constants for putrescine decreases from three to two.

The same sort of study is done for the other metabolites, where for spermine there exist five main J-coupling values, for spermine four values, for alanine one value, and for serine three values, while no main J-coupling values exist for sarcosine and acetate. A detailed explanation of the spin-spin coupling constants of these metabolites will be given in the part B.

II Effects of functionals and basis sets - choice of a theoretical level of calculation

The three polyamines putrescine, spermine, and spermidine, are of the same type; i.e. a chain of methyl groups and amines. If a certain theoretical level of calculation is suitable for one of them, it shall be suitable for the two others. It is reasonable to choose putrescine, which has the smallest size, to be the molecule under test in order to investigate various theoretical levels of calculation. This intends to find the best functional and basis set giving the best theoretical results for both types of NMR parameters.

The four metabolites, sarcosine, acetate, alanine, and serine, are of similar types where all of them terminate by a hydroxyl group and are formed of the same type of atoms (H, N, O, C). For this group, we choose sarcosine to be the molecule under study in order to determine the suitable functional and basis set.

II.1 Effects of functionals and basis sets: putrescine, as an example

To study the effects of functionals and basis sets on the calculated NMR parameters of putrescine, we test three functionals B3LYP, PBE, and OPBE in combination with twelve basis sets (6-311+G**,6-311++G**, 6-311++G(2d,2p), 6-311++G(3df,3pd), pc0, pc1, pc2, pc3,pcJ0, pcJ1, pcJ2, pcJ3). The basis sets can be divided into three groups; the first is the Pople's group that includes (6-311+G**,6-311++G**, 6-311++G(2d,2p), 6-311++G(3df,3pd)); the second is the polarisable consistent group that contains (pc0, pc1, pc2, pc3); the third is the polarisable consistent group for J-couplings which includes (pcJ0, pcJ1, pcJ2, pcJ3). It must be noted that in each group the basis sets are arranged according to their size from the smallest to the largest. At each theoretical level of calculation, optimizations for putrescine and TMS molecules are necessary before the calculation of NMR parameters.

Here, we study the effects of functionals and basis sets on the calculated chemical shifts of ground-state putrescine. In tables (3.4) and (3.5), we display, for isolated and solvated putrescine, the calculated chemical shieldings in addition to the chemical shielding of TMS and the resulting chemical shifts. Solvent effects are introduced using the PCM model.

Isolated Putrescine					
B3LYP Functional					
Basis set	σ_{TMS} ***(ppm)***	σ_A ***(ppm)***	σ_B ***(ppm)***	$\delta_A=\sigma_{TMS}-\sigma_A$	$\delta_B=\sigma_{TMS}-\sigma_B$
6-311+G*	*31.982*	*30.851*	*29.339*	*1.131*	*2.599*
6-311++G*	*31.970*	*30.844*	*29.400*	*1.127*	*2.571*
6-311++G(2d,2p)	*31.814*	*30.642*	*29.229*	*1.172*	*2.585*
6-311++G(3df,3 d)	*31.679*	*30.506*	*29.098*	*1.173*	*2.581*
pc0	*32.605*	*31.568*	*29.817*	*1.038*	*2.789*
pc1	*31.519*	*30.250*	*29.127*	*1.268*	*2.392*
pc2	*31.779*	*30.548*	*29.193*	*1.232*	*2.586*
pc3	*32.949*	*30.351*	*29.006*	*2.598*	*3.943*

pcJ0	*32.997*	*31.898*	*30.177*	*1.099*	*2.820*
pcJ1	*31.791*	*30.734*	*29.199*	*1.058*	*2.592*
pcJ2	*31.711*	*30.529*	*29.107*	*1.183*	*2.604*
pcJ3	*31.665*	*30.478*	*29.063*	*1.187*	*2.602*
PBE Functional					
Basis set	σ_{TMS} ***(ppm)***	σ_A ***(ppm)***	σ_B ***(ppm)***	$\delta_A=\sigma_{TMS}-\sigma_A$	$\delta_B=\sigma_{TMS}-\sigma_B$
6-311+G**	*31.771*	*30.363*	*28.875*	*1.408*	*2.897*
6-311++G**	*31.500*	*30.358*	*28.891*	*1.142*	*2.610*
6-311++G(2d,2p)	*31.353*	*30.146*	*28.712*	*1.207*	*2.641*
6-311++G(3df,3 d)	*31.218*	*30.008*	*28.583*	*1.210*	*2.634*
pc0	*32.098*	*31.067*	*29.248*	*1.032*	*2.850*
pc1	*31.123*	*30.169*	*28.612*	*0.954*	*2.511*
pc2	*31.261*	*30.076*	*28.632*	*1.185*	*2.630*
pc3	*31.177*	*29.986*	*28.554*	*1.191*	*2.623*
pcJ0	*32.439*	*31.386*	*29.598*	*1.053*	*2.841*
pcJ1	*31.361*	*30.268*	*28.710*	*1.093*	*2.651*
pcJ2	*31.128*	*30.030*	*28.593*	*1.098*	*2.535*
pcJ3	*31.168*	*29.977*	*28.546*	*1.191*	*2.622*
OPBE Functional					
Basis set	σ_{TMS} ***(ppm)***	σ_A ***(ppm)***	σ_B ***(ppm)***	$\delta_A=\sigma_{TMS}-\sigma_A$	$\delta_B=\sigma_{TMS}-\sigma_B$
6-311+G**	*31.875*	*30.526*	*29.052*	*1.349*	*2.822*
6-311++G**	*31.587*	*30.525*	*29.067*	*1.063*	*2.520*
6-311++G(2d,2p)	*31.470*	*30.320*	*28.896*	*1.150*	*2.574*
6-311++G(3df,3pd)	*31.330*	*30.195*	*28.782*	*1.1350*	*2.548*
pc0	*32.319*	*31.307*	*29.514*	*1.012*	*2.805*
pc1	*31.403*	*30.488*	*28.936*	*0.916*	*2.467*
pc2	*31.379*	*30.233*	*28.814*	*1.147*	*2.565*
pc3	*31.293*	*30.158*	*28.731*	*1.135*	*2.562*

pcJ0	*32.566*	*31.539*	*29.791*	*1.027*	*2.776*
pcJ1	*31.479*	*30.440*	*28.921*	*1.040*	*2.558*
pcJ2	*31.317*	*30.176*	*28.759*	*1.141*	*2.558*
pcJ3	*31.287*	*30.171*	*28.739*	*1.117*	*2.548*

Table 3.4: evolution with the basis set size of isotropic shieldings and chemical shifts for the protons of isolated putrescine for three functionals

Solvated Putrescine					
B3LYP Functional					
Basis set	***σ_{TMS} (ppm)***	***σ_A (ppm)***	***σ_B (ppm)***	***δ_A=σ_{TMS}-σ_A***	***δ_B=σ_{TMS}-σ_B***
6-311+G**	*31.982*	*30.714*	*29.364*	*1.268*	*2.618*
6-311++G**	*31.970*	*30.707*	*29.377*	*1.264*	*2.593*
6-311++G(2d,2p)	*31.81*	*0.531*	*29.212*	*1.283*	*2.602*
6-311++G(3df,3pd)	*31.679*	*30.408*	*29.085*	*1.271*	*2.593*
pc0	*32.605*	*31.492*	*29.882*	*1.113*	*2.723*
pc1	*31.519*	*30.157*	*29.144*	*1.361*	*2.374*
pc2	*31.779*	*30.426*	*29.180*	*1.353*	*2.600*
pc3	*32.949*	*30.255*	*28.993*	*2.694*	*3.956*
pcJ0	*32.997*	*31.824*	*30.241*	*1.173*	*2.756*
pcJ1	*31.791*	*30.608*	*29.208*	*1.183*	*2.583*
pcJ2	*31.711*	*30.410*	*29.091*	*1.302*	*2.620*
pcJ3	*31.665*	*30.373*	*29.048*	*1.292*	*2.617*
PBE Functional					
Basis set	***σ_{TMS} (ppm)***	***σ_A (ppm)***	***σ_B (ppm)***	***δ_A=σ_{TMS}-σ_A***	***δ_B=σ_{TMS}-σ_B***
6-311+G**	*31.771*	*30.222*	*28.850*	*1.549*	*2.921*
6-311++G**	*31.500*	*30.216*	*28.862*	*1.284*	*2.639*
6-311++G(2d,2p)	*31.353*	*30.031*	*28.688*	*1.322*	*2.665*
6-311++G(3df,3pd)	*31.218*	*29.908*	*28.565*	*1.310*	*2.653*

pc0	*32.098*	*30.978*	*29.313*	*1.121*	*2.786*
pc1	*31.123*	*30.049*	*28.622*	*1.074*	*2.501*
pc2	*31.261*	*29.954*	*28.610*	*1.308*	*2.651*
pc3	*31.177*	*29.885*	*28.540*	*1.292*	*2.637*
pcJ0	*32.439*	*31.300*	*29.661*	*1.139*	*2.778*
pcJ1	*31.361*	*30.141*	*28.717*	*1.220*	*2.644*
pcJ2	*31.128*	*29.908*	*28.571*	*1.220*	*2.557*
pcJ3	*31.168*	*29.875*	*28.531*	*1.292*	*2.637*
OPBE Functional					
Basis set	σ_{TMS} ***(ppm)***	σ_A ***(ppm)***	σ_B ***(ppm)***	$\delta_A=\sigma_{TMS}-\sigma_A$	$\delta_B=\sigma_{TMS}-\sigma_B$
6-311+G*	*31.875*	*30.386*	*29.034*	*1.488*	*2.840*
6-311++G*	*31.587*	*30.384*	*29.045*	*1.203*	*2.542*
6-311++G(2d,2p)	*31.470*	*30.207*	*28.877*	*1.263*	*2.593*
6-311++G(3df,3pd)	*31.330*	*30.099*	*28.775*	*1.231*	*2.555*
pc0	*32.319*	*31.200*	*29.574*	*1.120*	*2.745*
pc1	*31.403*	*30.363*	*28.946*	*1.040*	*2.457*
pc2	*31.379*	*30.112*	*28.799*	*1.268*	*2.580*
pc3	*31.293*	*30.057*	*28.722*	*1.236*	*2.570*
pcJ0	*32.566*	*31.437*	*29.851*	*1.129*	*2.715*
pcJ1	*31.479*	*30.314*	*28.934*	*1.165*	*2.545*
pcJ2	*31.317*	*30.075*	*28.756*	*1.242*	*2.561*
pcJ3	*31.287*	*30.067*	*28.730*	*1.220*	*2.557*

Table 3.5: evolution with the basis set size of isotropic shieldings and chemical shifts for the protons of solvated putrescine for three functionals

From the numerical values given in tables (3.4) and (3.5), the evolution of the chemical shifts of putrescine with different theoretical levels of calculation cannot be easily studied and analyzed. We plot for isolated and solvated ground-state putrescine, in figures (3.2) and (3.3), the evolution of the chemical shifts δ_A and δ_B with basis set size for each functional considered.

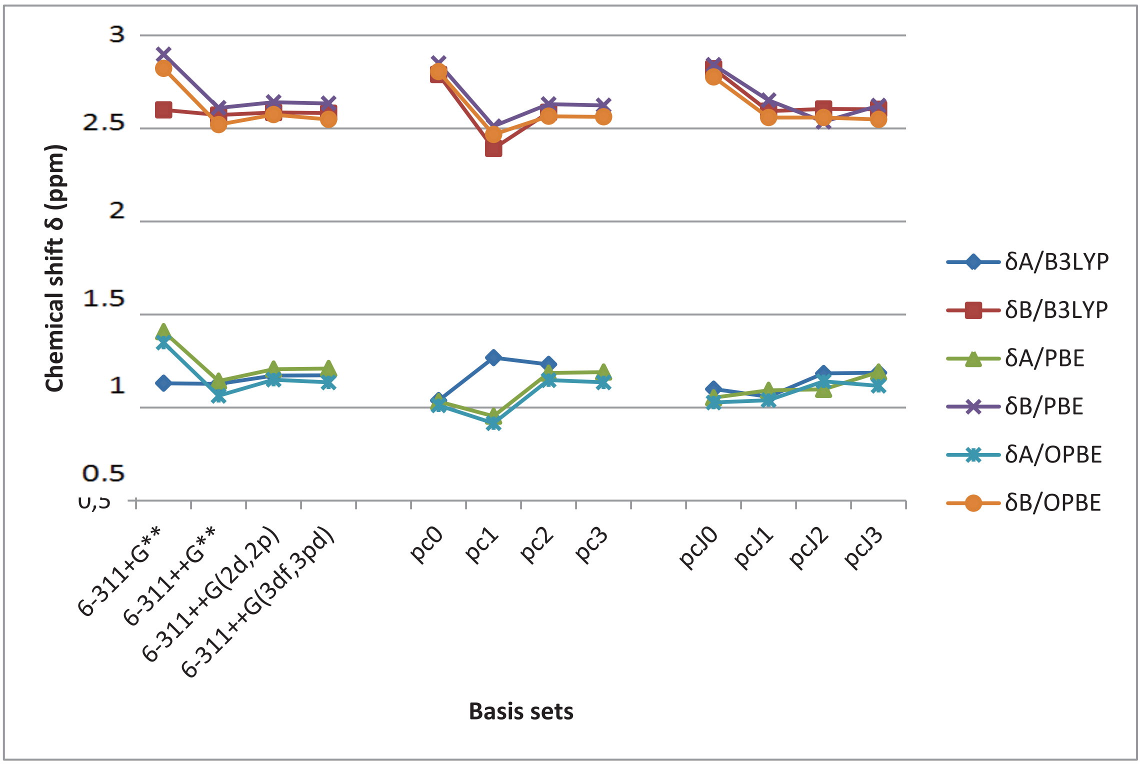

Figure 3.2: variation of calculated chemical shift with basis set size for isolated putrescine, for three functionals

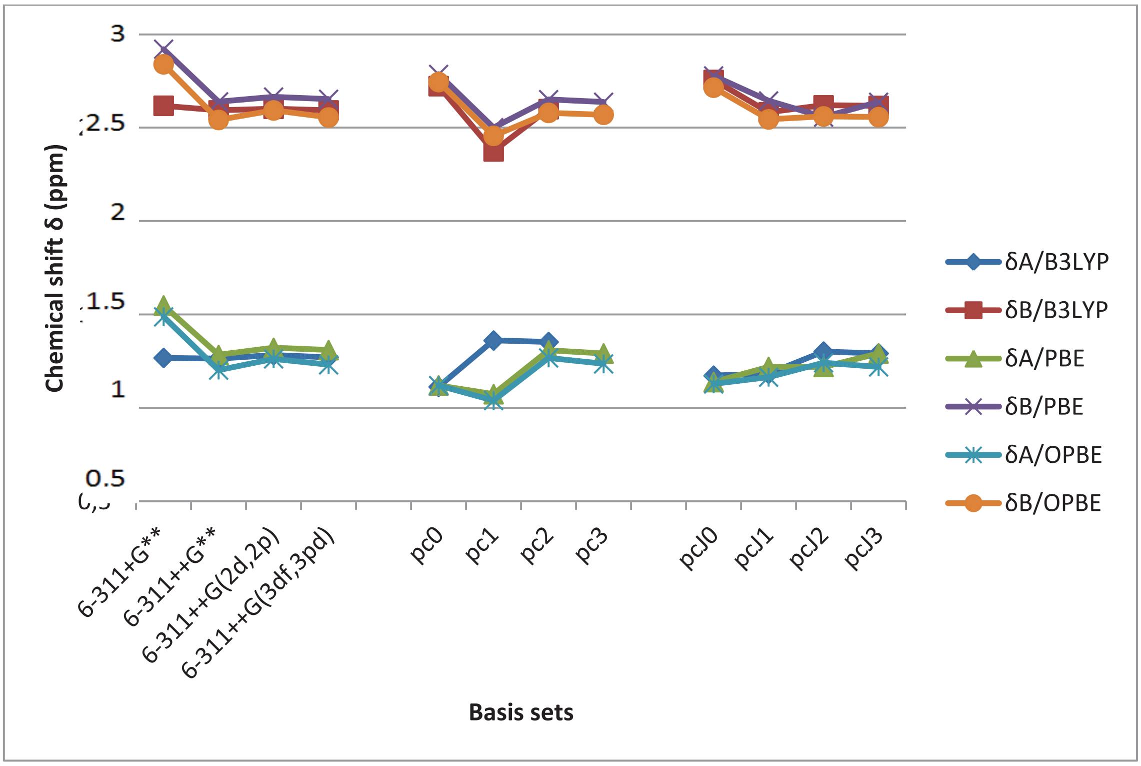

Figure 3.3: variation of calculated chemical shift with basis set size for solvated putrescine, for three functionals

The graphs plotted in figures (3.2) and (3.3) show a similar general evolution of the chemical shifts δ for both isolated and solvated putrescine. We choose to zoom on the variation of the chemical shifts for solvated putrescine, which is of major interest for us, in order to acquire a better understanding of the evolution of these chemical shifts. This is shown in figures (3.4) and (3.5).

As for solvent, it has the same consequence on chemical shifts calculated using different theoretical levels of calculation. The chemical shift δ_A is affected by the solvent more than δ_B where its value increases by ~10% (~ 0.1 ppm) while the latter shows only a change of ~2%.

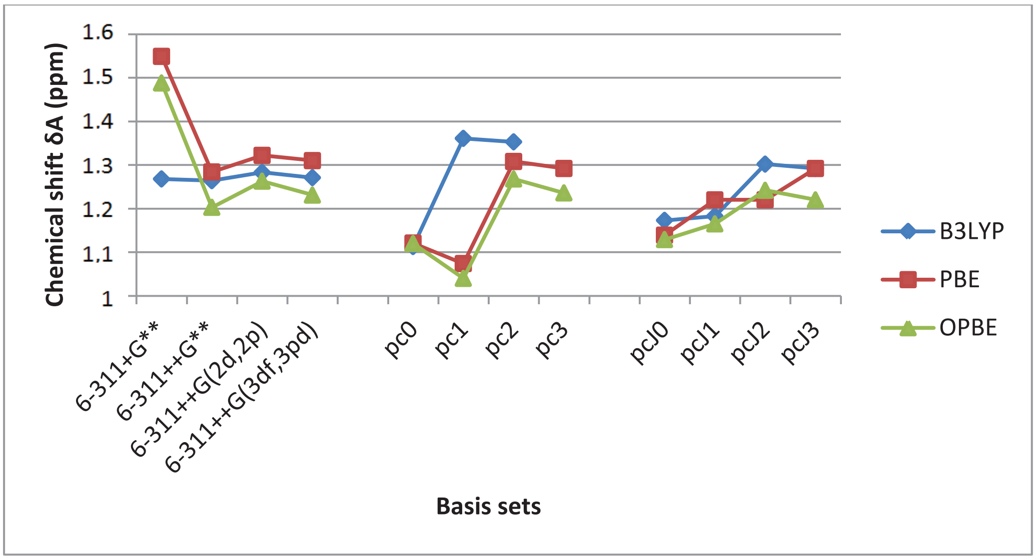

Figure 3.4: variation of the chemical shift δ_A with basis set size for solvated putrescine, and three functionals

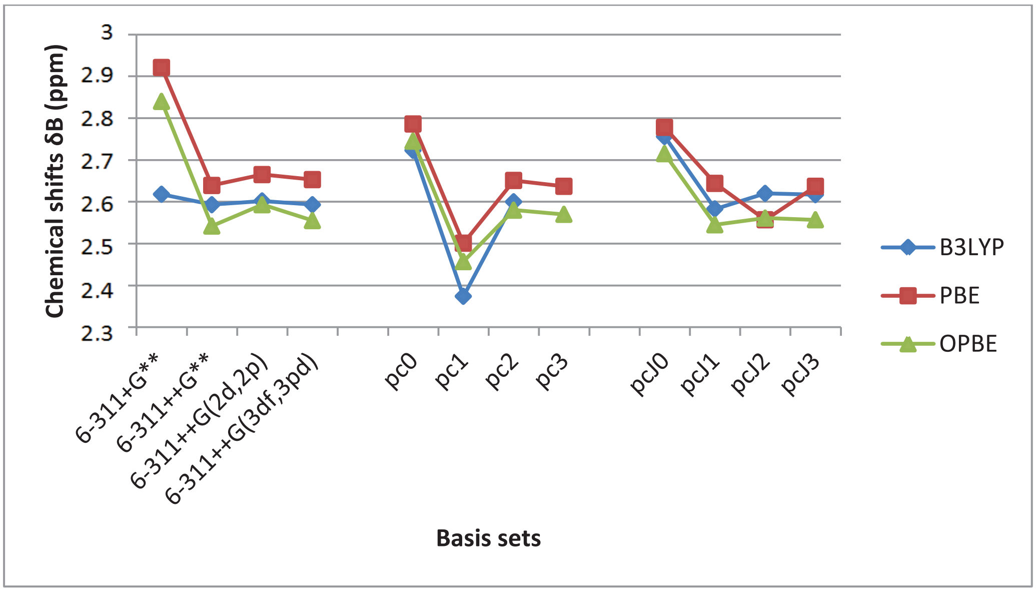

Figure 3.5: variation of the chemical shift δ_B with basis set size for solvated putrescine, and three functionals

From figures (3.4) and (3.5), the Pople's group of basis sets in combination with the B3LYP functional converges rapidly for the two chemical shifts of putrescine δ_A and δ_B where this convergence starts at the basis set 6-311++G**. The Pople's group in combination with the PBE functional shows a better convergence than the OPBE functional where this convergence starts also at the basis set 6-311++G**.

The polarisable consistent group pcn converges starting from the basis set pc2 for the two functionals PBE and OPBE, but it does not converge for B3LYP functional.

The pcJn group of basis sets converges starting from the basis set pcJ2 where this convergence appears to be better for the B3LYP and OPBE functionals than the PBE functional.

It is important to note that the three groups of basis sets converge to close values for each functional; except for the pcn group with the B3LYP functional that does not converge. To clarify, Pople's group and pcJn basis sets with the functional B3LYP converge to close values. Pople's group, pcn, and pcJn basis sets with the functional PBE converge to close values, and similarly for the OPBE functional. This is true for both chemical shifts δ_A and δ_B.

Thus, whatever functional used, we shall arrive always at the same converged values of chemical shifts under the condition that the used basis set is of size equal or larger than the basis set of threshold. For Pople's basis sets, 6-311++G** is the threshold, while for pcn and pcJn basis sets, pc2 and pcJ2 are the thresholds respectively. For putrescine, the contracted basis set sizes for 6-311++G**, pc2, and pcJ2 are 216, 348, and 594 basis functions respectively which shows that the basis set 6-311++G** has the smallest size in addition to being well adapted for the calculation of chemical shifts of putrescine.

A primary choice of a basis set suggests the basis 6-311++G**, while the choice of a functional is not so evident at this point. It shall be discussed later depending on the results of J-couplings. However, the results of the B3LYP functional in combination with Pople's basis sets are attractive where the convergence seems to be fast and quasi-linear.

It is interesting to plot the evolution of the chemical shieldings σ_A and σ_B of putrescine with Pople's basis sets at the level B3LYP in order to understand this convergence. The chemical shielding of TMS is also plotted at the same level of theoretical calculation.

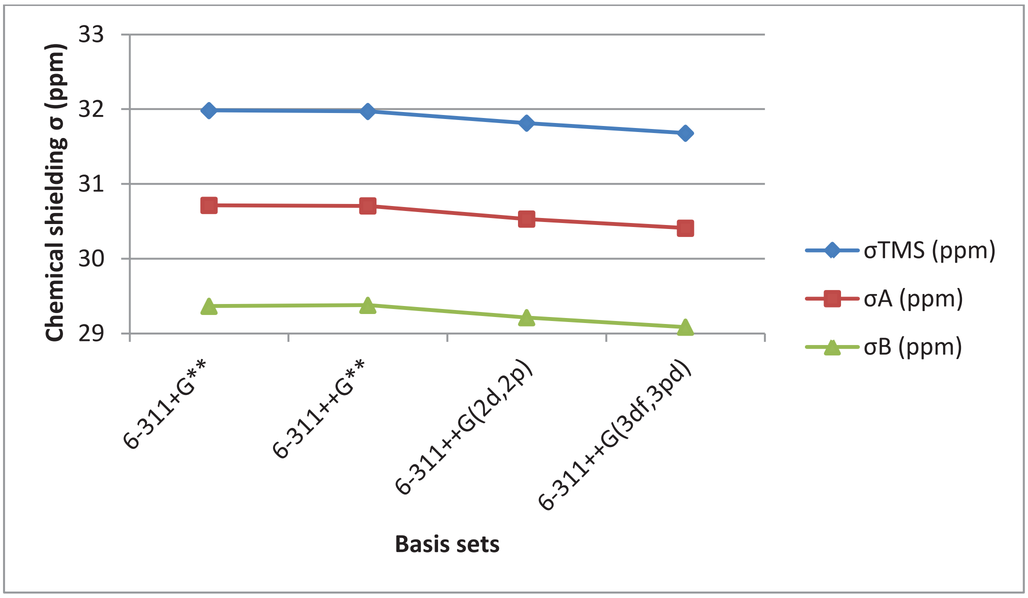

Figure 3.6: variation of σ with basis set size at B3LYP level for TMS and solvated putrescine

From figure 3.6, the chemical shieldings of TMS and putrescine do not converge; passing from one basis set to another basis of larger size, σ_{TMS} decreases by the same amount as σ_A and σ_B The difference between the chemical shielding of TMS (σ_{TMS}) and the chemical shieldings of putrescine (σ_A and σ_B) is almost constant as a function of increasing size of basis sets. This difference represents the chemical shift of putrescine (δ_A or δ_B). Thus, the monotonous behavior of the chemical shieldings (σ_{TMS}, σ_A, and σ_B) is the reason of the quasi-linear convergence of the chemical shifts calculated at the B3LYP level using Pople's basis sets.

To proceed in choosing our theoretical level of calculation, the spin-spin coupling constants of putrescine are calculated using the three functionals (B3LYP, PBE, and OPBE) and the twelve basis sets (6-311+G**,6-311++G**, 6-311++G(2d,2p), 6-311++G(3df,3pd), pc0, pc1, pc2, pc3,pcJ0, pcJ1, pcJ2, pcJ3). We keep in mind that the chosen functional and basis set must be appropriate for the calculation of both NMR parameters (δ and J) at once. For putrescine, we are only interested in two main values of spin-spin coupling constants ($J_{(1,2)x(15,16)}$, and $J_{(3,4)x(15,16)}$); their values are displayed in tables (3.6) and (3.7), calculated for isolated and solvated ground-state putrescine respectively.

Isolated Putrescine		
B3LYP *Functional*		
Basis set	$J_{(1,2)x(15,16)}$	$J_{(3,4)x(15,16)}$
*6-311+G***	*7.14*	*7.28*
*6-311++G***	*7.18*	*7.3*
6-311++G(2d,2p)	*7.48*	*7.56*
6-311++G(3df,3pd)	*7.33*	*7.43*
pc0	*4.35*	*4.56*
pc1	*5.67*	*4.73*
pc2	*9.41*	*8.72*
pc3	*13.34*	*8.71*
pcJ0	*7.69*	*7.95*
pcJ1	*8.82*	*9.02*
pcJ2	*9.14*	*9.27*
pcJ3	*9.25*	*9.38*
PBE *Functional*		
Basis set	$J_{(1,2)x(15,16)}$	$J_{(3,4)x(15,16)}$
*6-311+G***	*6.7*	*6.86*
*6-311++G***	*6.74*	*6.87*
6-311++G(2d,2p)	*7.03*	*7.13*
6-311++G(3df,3pd)	*6.9*	*7.02*
pc0	*3.98*	*4.20*
pc1	*5.57*	*5.68*
pc2	*7.5*	*7.62*
pc3	*8.04*	*8.18*
pcJ0	*6.96*	*7.23*
pcJ1	*8.19*	*8.40*
pcJ2	*8.49*	*8.64*
pcJ3	*8.59*	*8.74*

OPBE *Functional*		
Basis set	$J_{(1,2)x(15,16)}$	$J_{(3,4)x(15,16)}$
*6-311+G*****	*6.42*	*6.11*
*6-311++G*****	*6.45*	*6.62*
6-311++G(2d,2p)	*6.78*	*6.91*
6-311++G(3df,3pd)	*6.56*	*6.71*
pc0	*3.88*	*4.13*
pc1	*5.52*	*5.64*
pc2	*7.15*	*7.31*
pc3	*7.57*	*7.74*
pcJ0	*6.34*	*6.63*
pcJ1	*7.76*	*8.01*
pcJ2	*8.06*	*8.24*
pcJ3	*8.13*	*8.31*

Table 3.6: evolution with the basis set size of spin-spin coupling constants for isolated putrescine for three functionals

Solvated Putrescine		
B3LYP *Functional*		
Basis set	$J_{(1,2)x(15,16)}$	$J_{(3,4)x(15,16)}$
*6-311+G*****	*7.11*	*7.30*
*6-311++G*****	*7.14*	*7.32*
6-311++G(2d,2p)	*7.44*	*7.58*
6-311++G(3df,3pd)	*7.28*	*7.46*
pc0	*4.32*	*4.54*
pc1	*5.52*	*4.68*
pc2	*8.99*	*8.73*
pc3	*8.3*	*9.03*
pcJ0	*7.64*	*7.92*

pcJ1	*8.77*	*9.05*
pcJ2	*9.09*	*9.30*
pcJ3	*9.18*	*9.41*
PBE *Functional*		
Basis set	$J_{(1,2)x(15,16)}$	$J_{(3,4)x(15,16)}$
*6-311+G***	*6.68*	*6.89*
*6-311++G***	*6.71*	*6.90*
6-311++G(2d,2p)	*7.00*	*7.16*
6-311++G(3df,3pd)	*6.86*	*7.05*
pc0	*3.96*	*4.19*
pc1	*5.52*	*5.70*
pc2	*7.47*	*7.65*
pc3	*8.00*	*8.21*
pcJ0	*6.92*	*7.21*
pcJ1	*8.15*	*8.44*
pcJ2	*8.45*	*8.67*
pcJ3	*8.55*	*8.78*
OPBE *Functional*		
Basis set	$J_{(1,2)x(15,16)}$	$J_{(3,4)x(15,16)}$
*6-311+G***	*6.41*	*6.65*
*6-311++G***	*6.43*	*6.65*
6-311++G(2d,2p)	*6.75*	*6.95*
6-311++G(3df,3pd)	*6.53*	*6.76*
pc0	*3.87*	*4.13*
pc1	*5.47*	*5.67*
pc2	*7.13*	*7.35*
pc3	*7.54*	*7.77*
pcJ0	*6.32*	*6.62*

pcJ1	*7.74*	*8.05*
pcJ2	*8.03*	*8.28*
pcJ3	*8.10*	*8.35*

Table 3.7: evolution with the basis set size of spin-spin coupling constants for solvated putrescine for three functionals

Based on tables (3.6) and (3.7), we plotted the evolution of the spin-spin constants $J_{(1,2)x(15,16)}$ and $J_{(3,4)x(15,16)}$ with basis size for isolated and solvated ground-state putrescine in figures (3.7) and (3.8) respectively.

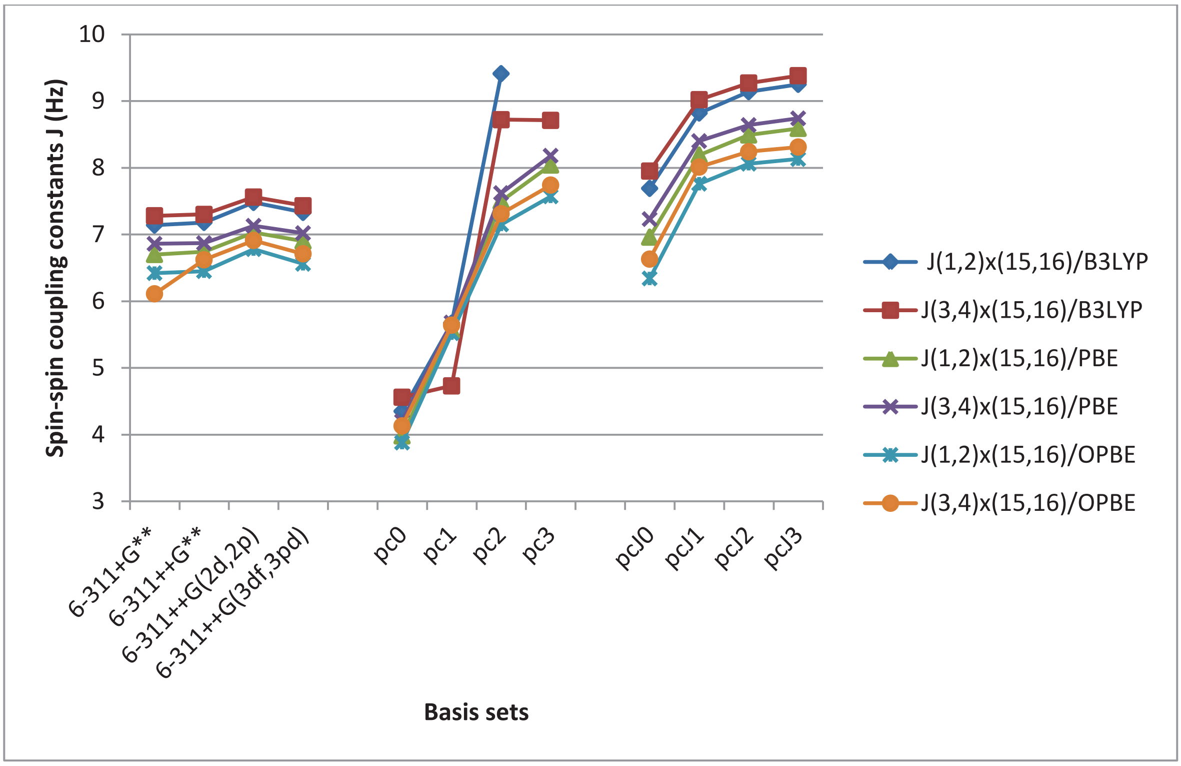

Figure 3.7: evolution of spin-spin coupling constants of isolated putrescine with basis set size using three functionals

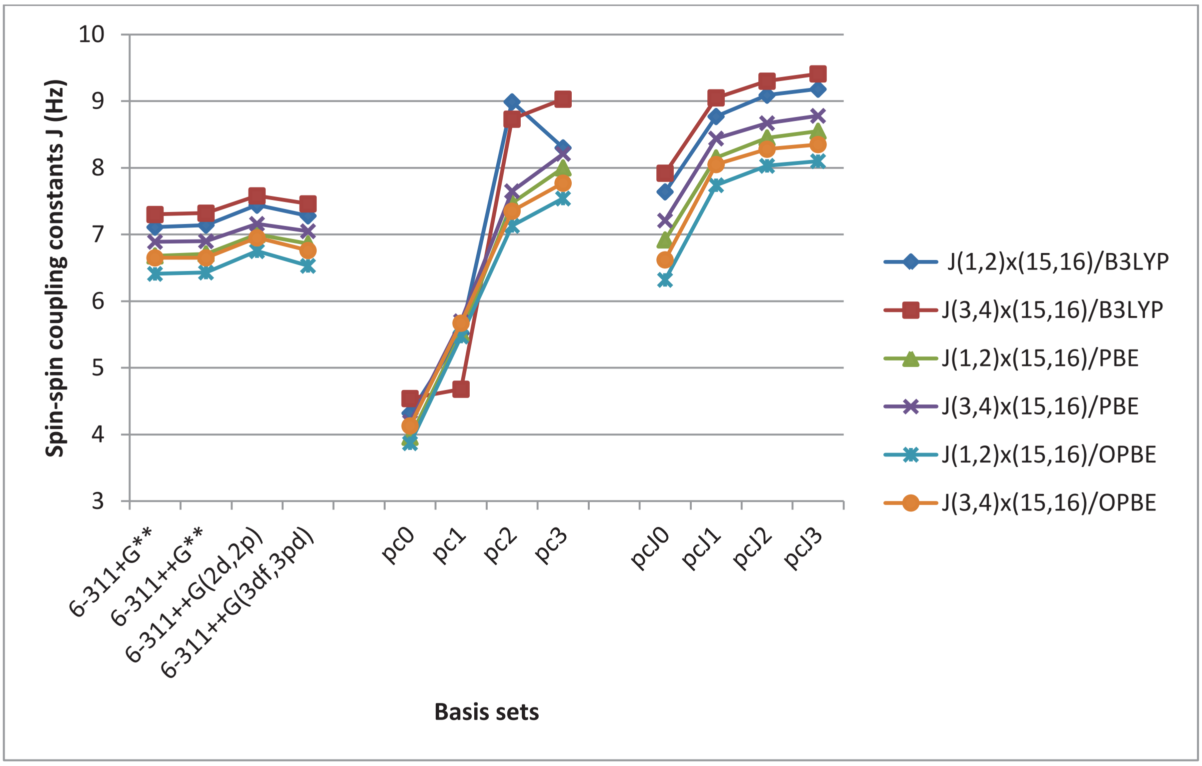

Figure 3.8: evolution of spin-spin coupling constants of solvated putrescine with basis set size using three functionals

Solvent effects on J-couplings of putrescine, introduced through the PCM model, are very small so that they can be neglected (< 1%) (except at the level B3LYP/pc3 where solvent effects are not negligible; however J-couplings calculated at this theoretical level are meaningless since they are away from being converged values). We recall that solvent effects are much important for chemical shifts of putrescine (2% - 10%).

From figures (3.7) and (3.8), the first group of basis sets (6-311+G**, 6-311++G**, 6-311++G(2d,2p), and 6-311++G(3df,3pd)) shows the best convergence of J-couplings where the size of the basis set has a small effect on the calculated spin-spin coupling constants. However, for one functional, the converged spin-spin coupling value is slightly different from another functional. In particular, $J_{(1,2)x(15,16)}$ converges to ~ 7.3, ~ 6.9, ~ 6.5 Hz at the levels B3LYP, PBE, and OPBE respectively, and $J_{(3,4)x(15,16)}$ converges to values ~ 7.4, ~ 7, ~ 6.7 Hz using the functional B3LYP, PBE, and OPBE respectively.

The second group of basis sets (pc0, pc1, pc2, pc3) reveals the same behaviour of J-couplings for the three used functionals. It starts with a relatively small value for the spin-spin coupling constants (~ 4 Hz) using the basis pc0 increasing up to a value of ~ 8 Hz using the basis pc3. The calculated values of spin-spin coupling constants using this group of basis sets do not show a real convergence.

The third group of basis sets (pcJ0, pcJ1, pcJ2, pcJ3) shows the same behaviour of J-couplings using the three different functionals. Spin-spin coupling constants calculated with the group pcJn of basis sets show a better convergence than those calculated with the pcn group. Starting with a value of ~ 6 Hz obtained using the basis pcJ0, spin-spin coupling constants increase up to a value of ~ 9 Hz using the basis pcJ3. Convergence of spin-spin coupling values barely appears using the basis sets pcJ2 or pcJ3 which are, nevertheless, both inappropriate for the calculation of spin-spin constants for molecules larger than putrescine due to their large sizes.

As a conclusion, the Pople's group of basis sets is the most appropriate for the calculation of spin-spin-coupling constants for putrescine. Besides, this group of basis sets is found suitable for the calculation of δ values for putrescine under the condition that the used basis set is of size equal or larger than the threshold (6-311++G**). Thus, we confirm that the basis set 6-311++G**, which has a relatively small size and gives converged values for both δ and J, is appropriate for the calculation of NMR parameters of putrescine.

To choose the functional, we had to simulate the NMR spectrum of solvated putrescine in comparison with the experimental spectrum obtained in D_2O solution.

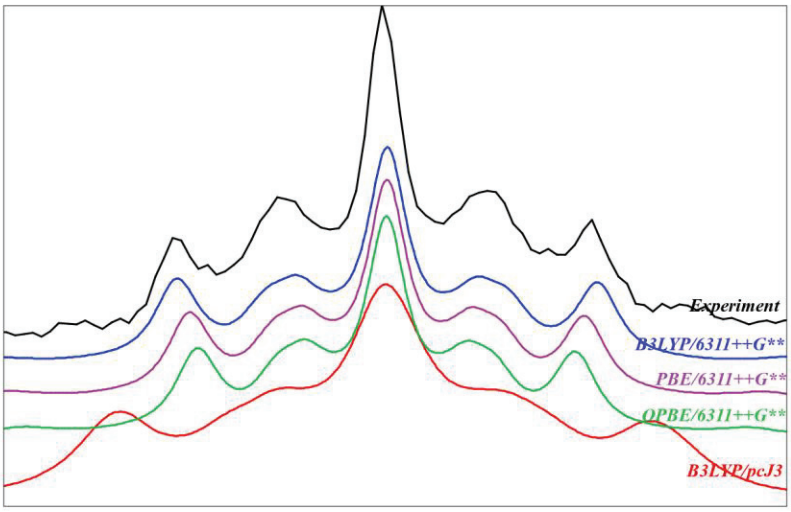

Figure 3.9: comparison between experimental and theoretical multiplet of solvated putrescine

In figure (3.9), we zoom on a particular zone of the spectrum (the NMR spectrum of putrescine is characterized by a triplet and a multiplet - seen later in the part C) where we compare the experimental and theoretical multiplets of putrescine. The theoretical calculations are done for three functionals, B3LYP, PBE, and OPBE, in combination with the chosen basis set 6-311++G**, in comparison with the theoretical level B3LYP/pcJ3.

Figure (3.9) shows that using the basis set 6-311++G**, the functional B3LYP gives a multiplet matching well the experiment, and by that, the calculated spin-spin coupling constants are almost equal to the experimental values (the splitting is controlled by J-couplings). The same result is found for the triplet where the level B3LYP/6-311++G** gives a splitting, matching well the experiment. We conclude that the B3LYP functional is satisfying for the calculation of spin-spin coupling constants of putrescine; not mentioning its efficacy in calculating the chemical shifts, of course, using the 6-311++G** basis set.

Calculations from the B3LYP/6-311++G** level are seen to better reproduce the five peaks of the multiplet than the B3LYP/pcJ3 level which does not give a correct description of the multiplet. We recall that J-couplings of putrescine are ~ 7 Hz when calculated using the 6-311++G** basis set while they reach ~ 9 Hz when calculated using the basis set pcJ3. This comparison between the two basis sets 6-311++G** and pcJ3 shows that pcJ3 (and similarly pcJ2) is less appropriate for the calculation of spin-spin constants of putrescine, not only due to its large size but also for the calculated J-values which are far from the experiment.

As a conclusion, the B3LYP/6-311++G** is a satisfying compromise between accuracy and costs for the calculation of NMR parameters of putrescine. Since the three polyamines, putrescine, spermidine, and spermine, are of the same type, we can conclude that this level of calculation is also suitable for the calculation of NMR parameters of both spermidine and spermine.

II.2 Effects of functionals and basis sets: sarcosine, as an example

The four metabolites, sarcosine, acetate, alanine, and serine, are of similar types where all of them terminate by a hydroxyl group and are formed of the same type of atoms (H, N, O, C). For this group, we choose sarcosine to be the molecule under study in order to determine the suitable functional and basis set. Since the solvated sarcosine is of major interest for us because it allows comparison with experimental spectrum obtained in D_2O, we decide to treat directly the solvated molecule using the well-known PCM model.

To study the effect of functionals and basis sets on solvated sarcosine, we calculate the chemical shifts using four functionals (B3LYP, PBE, OPBE, PBE0) and two basis sets 6-311++G** and pcJ2. The two basis sets 6-311++G** and pcJ2 are chosen because they are expected to be large enough for the calculation of chemical shifts as was found for putrescine (pc2 is ignored and replaced by its recent version, pcJ2). Once the theoretical level, suitable for the calculation of chemical shifts of sarcosine, is determined, the chemical shifts of the other three metabolites can be calculated at the same level.

Despite that sarcosine and acetate have no J-couplings, yet alanine and serine have one and three spin-spin coupling constants respectively. Only acceptable differences between the eight theoretical levels of calculation (combination of four functionals and two basis sets) are expected to exist for the spin-spin coupling constants, as J-couplings of putrescine, calculated using these eight levels, range between (6.5 - 9 Hz). The difference between spin-spin coupling constants calculated using different methods doesn't affect the total profile of the spectrum because it is the chemical shift that determines the position of the main peaks. The difference between the calculated J-couplings is only obvious through a zoom on each peak to point out the splitting. Here, we assume that the theoretical level of calculation suitable for the calculation of chemical shifts is also suitable for the calculation of spin-spin coupling constants.

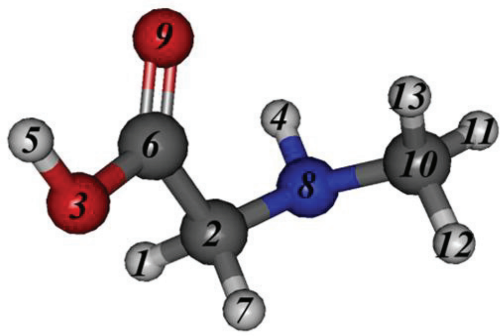

Figure 3.10: ground-state geometry of solvated sarcosine optimized at the B3LYP/6-311++G** level (nitrogen in blue, carbon in grey, oxygen in red, and hydrogen in white)

As usual, we study protons attached to carbon atoms. For sarcosine, we are interested in the two protons (1, 7) of the methylene group and the three protons (11, 12, 13) of the methyl group (see figure 3.10). Equivalent protons belonging to the same group generate a single chemical shift. Let δ_A be the chemical shift corresponding to the methyl protons A (11, 12, 13), while δ_B be the chemical shift corresponding to the methylene protons B (1, 7).

The chemical shieldings of ground-state solvated sarcosine as well as the chemical shielding of TMS are calculated at the eight theoretical levels and are shown in tables (3.8) and (3.9), in addition to the associated chemical shifts. The isotropic chemical shieldings are calculated using the GIAO approach. For each theoretical level, TMS molecule is optimized and the ground-state sarcosine is determined. The ground-state structure of sarcosine is found to be dependent on the used functional.

Functional	σ_{TMS}*(ppm)*	σ_A *(ppm)*	σ_B *(ppm)*	$\delta_A = \sigma_{TMS} - \sigma_A$	$\delta_B = \sigma_{TMS} - \sigma_B$
B3LYP	*31.970*	*29.521*	*28.405*	*2.449*	*3.566*
PBE	*31.500*	*28.991*	*28.223*	*2.510*	*3.277*
OPBE	*31.587*	*29.059*	*28.399*	*2.528*	*3.188*
PBE0	*31.802*	*29.365*	*28.539*	*2.437*	*3.263*

Table 3.8: evolution of σ and δ values of ground-state sarcosine with four functionals and the basis set 6-311++G**

Functional	σ_{TMS}*(ppm)*	σ_A *(ppm)*	σ_B *(ppm)*	$\delta_A = \sigma_{TMS} - \sigma_A$	$\delta_B = \sigma_{TMS} - \sigma_B$
B3LYP	*31.711*	*29.235*	*28.071*	*2.476*	*3.640*
PBE	*31.128*	*28.713*	*27.859*	*2.415*	*3.269*
OPBE	*31.317*	*28.783*	*28.03*	*2.534*	*3.287*
PBE0	*31.560*	*29.090*	*28.185*	*2.470*	*3.375*

Table 3.9: evolution of σ and δ values of ground-state sarcosine with four functionals and the basis set pcJ2

To make numerical data given in tables (3.8) and (3.9) easier to be understood and analyzed, the chemical shifts δ_A and δ_B are plotted in figure (3.11) in comparison with the experimental values. The experimental values of the chemical shifts can be easily acquired from the position of peaks in an NMR spectrum. For sarcosine, the experimental NMR spectrum, acquired in D_2O solution at 300 MHz, shows two peaks from which we can deduce two values of δ - δ_A and δ_B - that are equal to 2.741 and 3.615 ppm respectively. The differences between experimental and calculated results are given in tables (3.10) and (3.11).

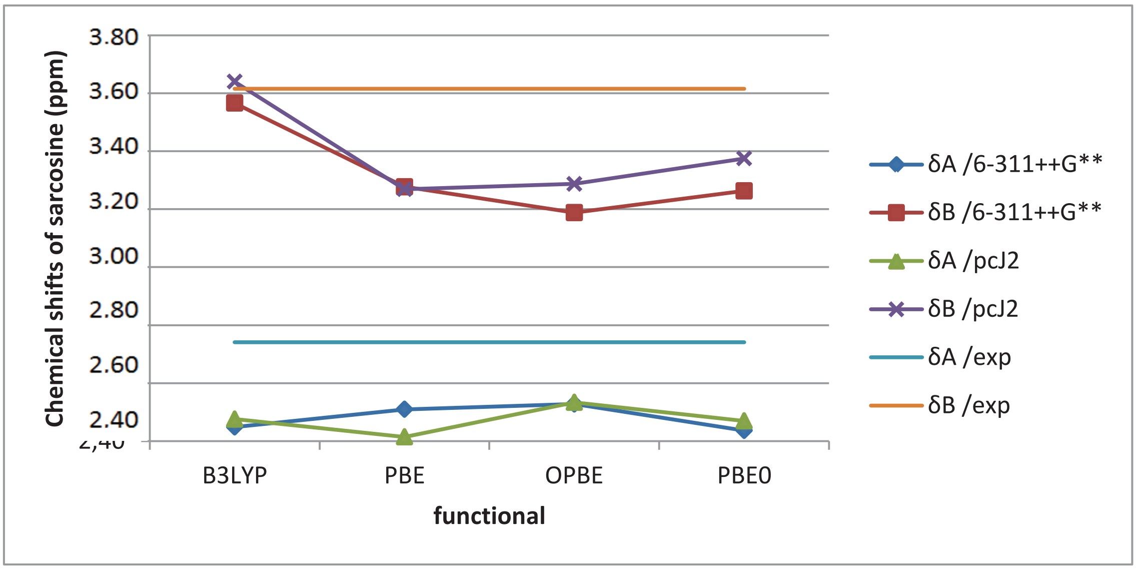

Figure 3.11: calculated δ values of solvated sarcosine with four functionals and two basis sets

Functional	δ_A^{exp} - δ_A	δ_B^{exp} - δ_B
B3LYP	*0.29*	*0.05*
PBE	*0.23*	*0.34*
OPBE	*0.21*	*0.43*
PBE0	*0.30*	*0.35*

Table 3.10: comparison between experimental and theoretical δ values of ground-state sarcosine with four functionals and the basis set 6-311++G**

Functional	δ_A^{exp} - δ_A	δ_B^{exp} - δ_B
B3LYP	*0.26*	*-0.03*
PBE	*0.33*	*0.35*
OPBE	*0.22*	*0.33*
PBE0	*0.27*	*0.24*

Table 3.11: comparison between experimental and theoretical δ values of ground-state sarcosine with four functionals and the basis set pcJ2

Figure (3.11) shows that for each functional, the two basis sets (6-311++G** and pcJ2) give close values of chemical shifts with a maximum difference of 0.1 ppm. The comparison with the experiment shows that the B3LYP functional gives the best values of chemical shifts for both basis sets. Using the basis set 6-311++G**, the functionals PBE, OPBE, and PBE0 give a maximum error of 0.34, 0.43, and 0.35 ppm respectively, in comparison with 0.29 ppm for the B3LYP functional (see table (3.10)). Using the basis set pcJ2, the functionals PBE, OPBE, and PBE0 give a maximum error of 0.35, 0.33, and 0.27 ppm respectively, in comparison with 0.26 ppm for the B3LYP functional (see table (3.11)).

Having determined the most appropriate functional (B3LYP) for the calculation of chemical shifts of ground-state sarcosine, there remains the comparison between the two basis sets 6-311++G** and pcJ2. It is clear that there are no large differences between values calculated using the basis set 6-311++G** and the results of the basis set pcJ2 at the B3LYP level. This means that the two levels of calculation B3LYP/6-311++G** and B3LYP/pcJ2 are approximately of the same quality in calculating δ values for solvated sarcosine. However, 6-311++G** is of smaller size than pcJ2. For sarcosine, the contracted basis set size for 6-311++G** is 181 basis functions in comparison with 474 basis functions for pcJ2. Therefore, it is obvious that the basis set 6-311++G** is more suitable for the calculation of δ values for sarcosine due to its compromise between accuracy and computational needs.

However, one may wonder if the basis set pcJ1, belonging to the same group of pcJ2 but of smaller size, is suitable for the calculation of chemical shifts of sarcosine. To answer this question, we have studied the convergence of the chemical shifts of solvated sarcosine with the four basis sets (pcJ0, pcJ1, pcJ2, pcJ3) at the level B3LYP. Results are given in table (3.12) while data are plotted in figure (3.12).

Basis set	$\boldsymbol{\delta_A}$	$\boldsymbol{\delta_B}$
pcJ0	*2.644*	*3.672*
pcJ1	*2.450*	*3.487*
pcJ2	*2.476*	*3.640*
pcJ3	*2.449*	*3.651*

Table 3.12: δ values of ground-state solvated sarcosine at the B3LYP level

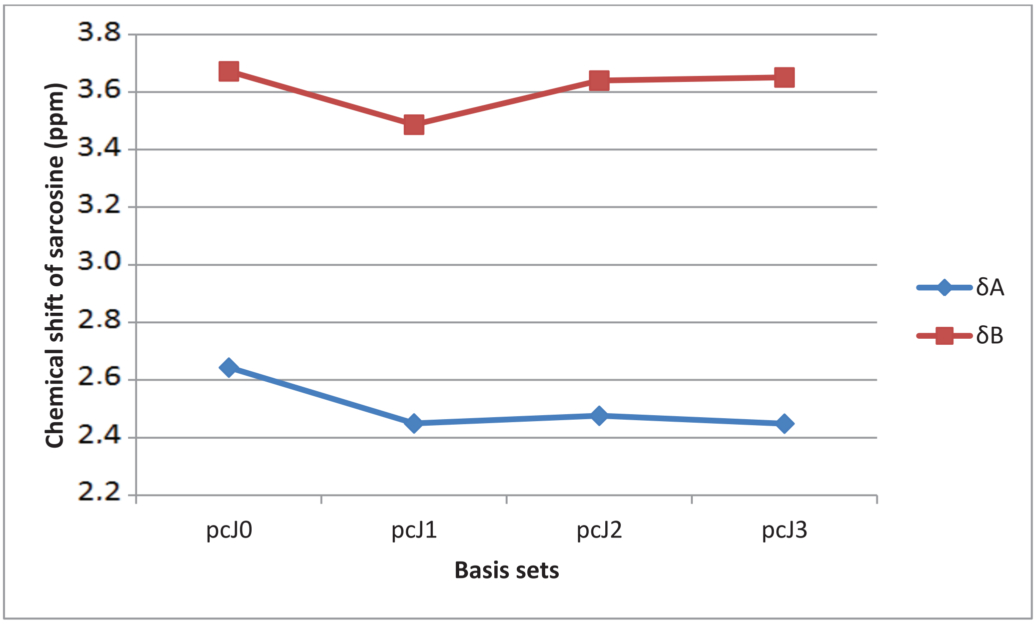

Figure 3.12: evolution of δ values of ground-state solvated sarcosine at the B3LYP level

From figure (3.12), it is clear that the chemical shifts of sarcosine do not converge at the level pcJ1. However, convergence starts to appear at the level pcJ2. In other words, pcJ2 is the basis set of smallest size belonging to the group pcJn and giving converging results of δ.

As a result, the calculation of δ values for ground-state solvated sarcosine is recommended at the level B3LYP/6-311++G** where this theoretical level of calculation can be used also for acetate, alanine, and serine.

III Effects of isomers on NMR parameters

At ambient temperature, not only ground-state structures are present but also excited molecules of higher energy. The presence of spatial isomers affects the experimental NMR spectrum. Thus, isomer effects must be taken into account in the theoretical calculation of NMR parameters to improve our results in comparison with the experiment. In the present work, isomer effects are calculated assuming a Boltzmann distribution. For N stable isomers taken into account, the averaged NMR parameters (δ and J) are calculated using the following equation

$$P_{averaged} = \frac{\sum_i^N P_i e^{-\Delta E_i/kT}}{\sum_i^N e^{-\Delta E_i/kT}} \quad P = \delta, J \tag{3.2}$$

where ΔE_i is the relative energy of the isomer i with respect to the ground-state structure, k is the Boltzmann constant, and T is the temperature taken to be 300 K, close to the ambient temperature of the experiments. The Boltzmann factor $e^{-\Delta E_i/kT}$ usually determines the effect of each isomer on the averaged values; isomers with low relative energies are expected to be very effective. The calculation of averaged NMR parameters seems easy; however, large complexity lies in the determination of isomers whose number is expected to grow with the size of the molecule. Besides, for a large number of determined isomers, the manual calculation of averaged NMR parameters using equation (3.2) costs time and effort.

Our method of calculating isomer effects on NMR parameters is summarized in three steps (see figure (3.13)). In the first step, isomers are selected using the constant energy (NVE) Born Oppenheimer molecular dynamics with the Velocity Verlet algorithm and the semi-empirical method PM6. The simulated time is 15 ps, and the time step is 0.5 ps. A high temperature is chosen (ex: 5000 K for putrescine) in order to ensure a large exploration of the potential surface energy. We select a large number (5000) of geometries during the simulation process. The selected geometries are optimized at the PM6 level and similar geometries are deleted. This step is performed through the graphical interface Gabedit.

In the second step, the geometries obtained from the first step are optimized at the level B3LYP/6-31G* and then filtered using the "Geometry Filtration" program which is a C++ program developed by us. The "Geometry Filtration" program requires two types of data as input: (1) the geometries optimized at the level B3LYP/6-31G*, and (2) a maximum energy value ΔE_{max} chosen large enough so that isomers with an energy higher than the maximum energy are assumed not to affect the averaged NMR parameters. The program omits the similar geometries and the geometries having energies higher than the demanded maximum, arranges the remaining geometries in increasing order according to their energies, and creates for them input Gaussian files ready to be executed. In each input Gaussian file, we demand: (1) optimization at the level B3LYP/6-311++G**, (2) calculation of NMR parameters (chemical shieldings and spin-spin coupling constants), and (3) calculation of harmonic frequencies of atoms at the same theoretical level of calculation.

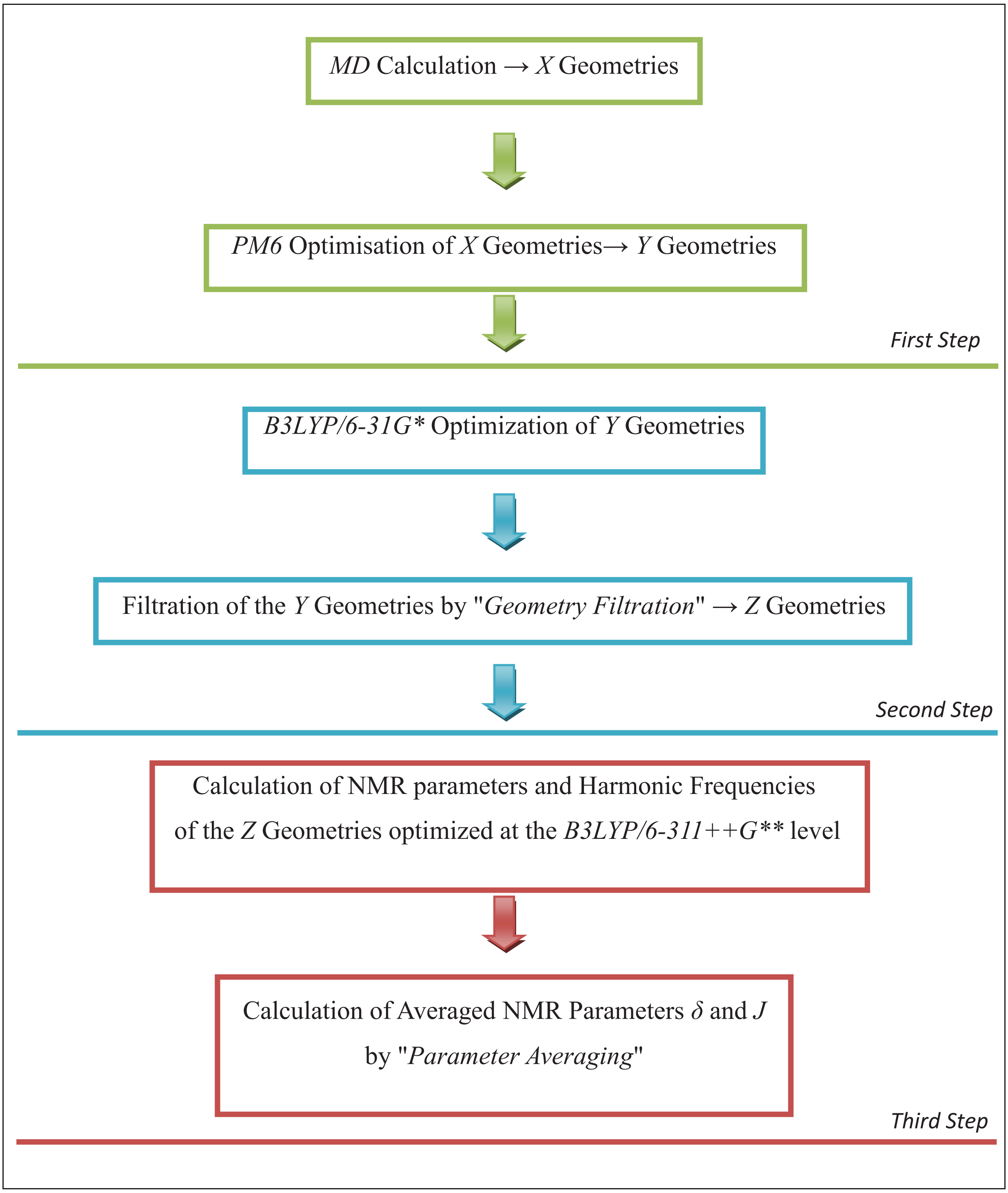

Figure 3.13: scheme showing the three consecutive steps needed to calculate the averaged NMR parameters

In the third step, input Gaussian files obtained from the second step are executed. The averaged NMR parameters are not calculated manually but rather using the program "Parameter Averaging" developed by us. This program requires three types of data as input: (1) the names of the output Gaussian files (which include values of chemical shieldings, spin-spin couplings, energies, and atomic frequencies), (2) the chemical shielding of TMS, and (3) the temperature taken to be 300 K. The program eliminates automatically unstable isomers having at least one negative atomic frequency and calculates, for the remaining isomers, the averaged NMR parameters applying equation (3.2).

It is important to note that in the second step we have used the basis set 6-31G* which is of smaller size than 6-311++G** in order to eliminate the largest possible number of isomers before any calculation using the larger basis set. The choice of the basis set 6-31G* is based on a study that we have done for polyamines, in which we have found that for the two basis sets (6-31G* and 6-311++G**) the arrangement of isomers according to their energies is very close.

In this section, we choose solvated putrescine as an example to explain in details our method of calculation of averaged NMR parameters.

The first step of our method resulted in fifty-five geometries for putrescine. The second step determined forty geometries where the maximum energy was chosen to be ΔE_{max}= 3.5 Kcal/mol. In the third step, these forty geometries were optimized at the level B3LYP/6-311++G** where solvent effects were included at this stage using the PCM model; NMR parameters and atomic frequencies were also calculated for solvated molecule at the same level. For putrescine, no isomer was found unstable.

III.1 Calculation of averaged chemical shifts: putrescine, as an example

The evolution of the averaged chemical shift values of solvated putrescine as a function of relative energy ΔE is given in table (3.13).

Number of geometry	ΔE *(eV)*	δ_A^{av} *(ppm)*	δ_B^{av} *(ppm)*
1	0.000	1.264	2.594
2	0.013	1.289	2.289
3	0.025	1.314	2.692
4	0.026	1.316	2.690
5	0.039	1.322	2.696
6	0.039	1.330	2.704
7	0.040	1.337	2.710
8	0.042	1.343	2.703
9	0.050	1.349	2.705
10	0.051	1.356	2.705
11	0.051	1.358	2.711
12	0.053	1.360	2.714
13	0.056	1.362	2.716
14	0.058	1.367	2.715
15	0.059	1.371	2.718
16	0.061	1.376	2.722
17	0.064	1.377	2.724
18	0.065	1.379	2.723
19	0.066	1.383	2.724
20	0.073	1.386	2.724
21	0.074	1.388	2.726
22	0.079	1.390	2.726
23	0.079	1.391	2.728
24	0.080	1.393	2.728
25	0.081	1.395	2.728
26	0.086	1.397	2.729
27	0.095	1.398	2.730

28	*0.101*	*1.399*	*2.730*
29	*0.104*	*1.400*	*2.731*
30	*0.132*	*1.400*	*2.731*
31	*0.133*	*1.400*	*2.731*
32	*0.133*	*1.401*	*2.731*
33	*0.147*	*1.401*	*2.731*
34	*0.147*	*1.401*	*2.732*
35	*0.156*	*1.401*	*2.732*
36	*0.158*	*1.401*	*2.732*
37	*0.160*	*1.401*	*2.732*
38	*0.163*	*1.401*	*2.732*
39	*0.194*	*1.401*	*2.732*
40	*0.224*	*1.401*	*2.732*
Average		*1.401*	*2.732*

Table 3.13: evolution of the averaged chemical shifts for solvated putrescine with energy

In table (3.13), isomers are arranged according to their energies in an increasing order where the first geometry represents the ground-state structure. The averaged chemical shift value in the row i is defined as the averaged value for the first i isomers. The convergence of the averaged chemical shifts is clear and the averaged values are different from those of the ground-state structure. For solvated putrescine, isomer effects on δ_A and δ_B are found of order 0.14 ppm (10% of δ_A, and 5% of δ_B). Thus, isomer effects on the chemical shifts of solvated putrescine are important and cannot be neglected.

As a further check of our automatized approach, this procedure was repeated again because the molecular dynamics simulations may result in different geometries for different trajectories. Fifty eight geometries were obtained at the first step and forty geometries at the second and the third steps for solvated putrescine. However, a very good matching between the results of the first and the second trial was seen which proves the efficiency of our automatized method.

The maximum energy ΔE_{max} used in the second step was chosen somehow arbitrarily but large enough to ensure convergence of averaged values. To make sure that our choice of the maximum energy was good, we plot in figures (3.14) and (3.15), the averaged chemical shifts for solvated putrescine as a function of the relative energy ΔE.

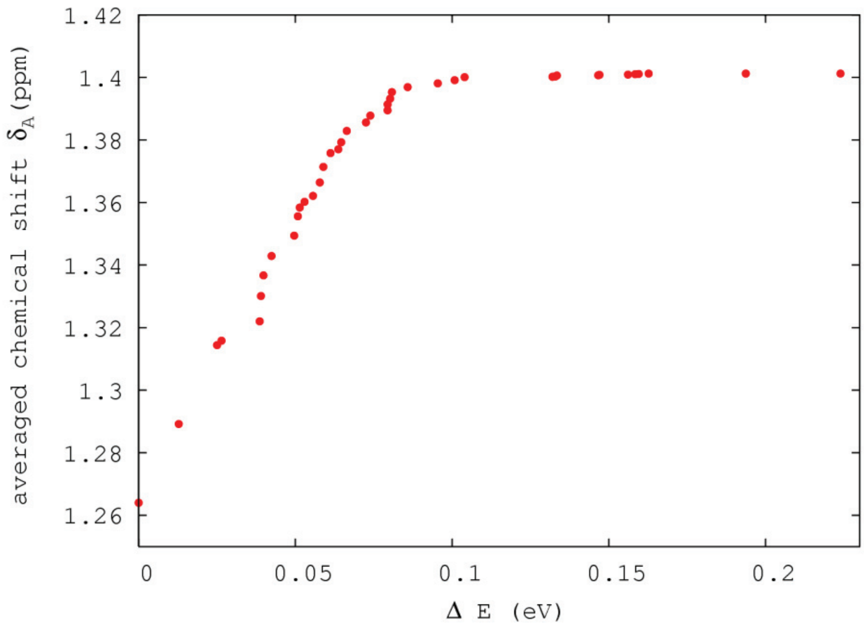

Figure 3.14: evolution of the averaged chemical shift δ_A^{av} for solvated putrescine with relative energy

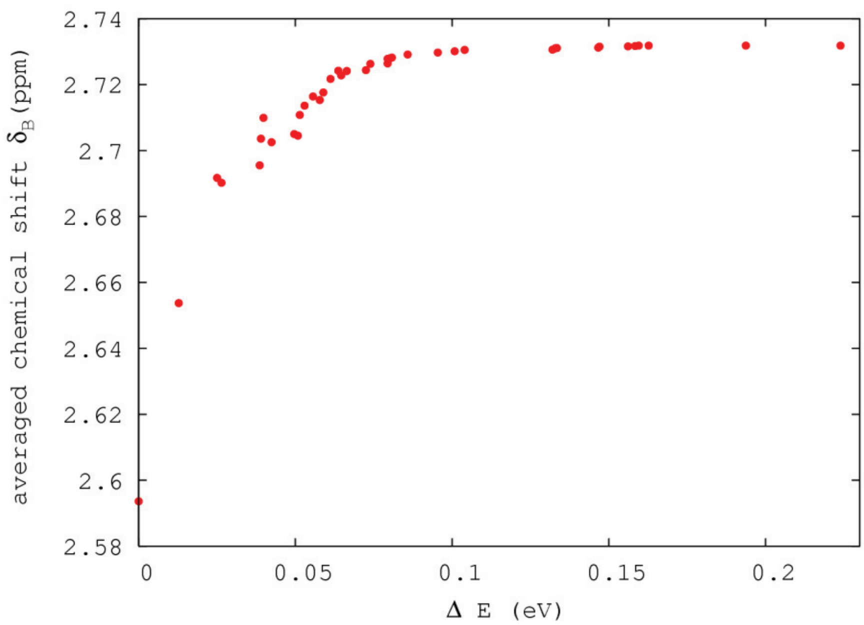

Figure 3.15: evolution of the averaged chemical shift δ_B^{av} for solvated putrescine with relative energy

From figures (3.14) and (3.15), δ_A^{av} and δ_B^{av} converge as ΔE increases, and the convergence starts to appear when reaching $\Delta E \sim 0.1$ eV, which means that the averaged chemical shifts of solvated putrescine are totally determined by the geometries having relative energies smaller than 0.1 eV. We conclude that our choice of the maximum energy for putrescine (in the second step) was large enough to include not only the effective geometries but also a large number of ineffective ones. Moreover, the energy of convergence was found to increase with the size of the molecule (ex: 0.15 eV for spermidine and 0.25 for spermine).

In order to check up if the level B3LYP/6-311++G** is also a good compromise for the calculation of averaged chemical shifts as was found for the chemical shifts of ground-state structure, the averaged chemical shifts of solvated putrescine were calculated using the two functionals PBE and OPBE and the basis 6-311++G**. We recall that the three levels of calculations (B3LYP/6-311++G**, PBE/6-311++G**, and OPBE/6-311++G**) were found to be competitive in the calculation of chemical shifts of ground-state putrescine. Following the same procedure as before, averaged chemical shifts were obtained for solvated putrescine at the levels PBE/6-311++G** and OPBE/6-311++G** where these levels replaced the B3LYP/6-311++G** level in the third step. Results in comparison with experimental values are given in table (3.14).

		6311++G**/B3LYP		
Group	δ^{av}	$\delta^{lowest-energy}$	$\delta^{exp} - \delta^{av}$	$\delta^{exp} - \delta^{lowest-energy}$
A	*1.397*	*1.264*	*0.206*	*0.339*
B	*2.749*	*2.597*	*0.077*	*0.232*
		6311++G**/PBE		
Group	δ^{av}	$\delta^{lowest-energy}$	$\delta^{exp} - \delta^{av}$	$\delta^{exp} - \delta^{lowest-energy}$
A	*1.812*	*1.284*	*-0.209*	*0.319*
B	*3.188*	*2.639*	*-0.362*	*0.187*
		6311++G**/OPBE		
Group	δ^{av}	$\delta^{lowest-energy}$	$\delta^{exp} - \delta^{av}$	$\delta^{exp} - \delta^{lowest-energy}$
A	*1.579*	*1.203*	*0.024*	*0.400*
B	*2.950*	*2.542*	*-0.125*	*0.284*

Table 3.14: comparison between averaged chemical shifts δ^{av}, chemical shifts of lowest-energy solvated putrescine $\delta^{lowest-energy}$, and experimental chemical shifts δ^{exp}

From table (3.14), a comparison between the averaged chemical shifts and the ground-state chemical shifts shows that the two theoretical levels (B3LYP/6-311++G** and OPBE/6-311++G**) improve the chemical shifts when taking isomer effects into account; however, this is not the case when using the level PBE/6-311++G** where averaged chemical shifts are farer from experiment than the ground-state chemical shifts.

Since using the PBE/6-311++G** level for calculating isomer effects is not suitable for solvated putrescine, our choice for an appropriate level of calculation is done through a comparison between the two levels B3LYP/6-311++G** and OPBE/6-311++G**. Despite that the level OPBE/6-311++G** shows a small error for the averaged values in comparison with the experiment (0.13 ppm), yet the level B3LYP/6-311++G** reproduces better the experimental relative position of the two multiplets (δ_A - δ_B); not mentioning its better averaged spin-spin coupling constants which will be discussed later in section III.2.

We choose the B3LYP/6-311++G** for the calculation of isomer effects of putrescine, based on three facts (1) the calculated averaged chemical shifts are closer to the experiment than the lowest-energy chemical shifts, (2) the relative position of multiplets is reproduced well (the relative position is very important in analyzing experimental NMR spectra) and (3) the averaged spin-spin coupling constants (see section III.2) are close to experimental values.

III.2 Calculation of averaged indirect nuclear spin-spin coupling constants: putrescine, as an example

Using our method, we are able to calculate isomer effects on both NMR parameters: chemical shifts and spin-spin coupling constants. Averaged spin-spin coupling constants, as averaged chemical shifts, are calculated automatically in the third step of our automatized method using the equation (3.2).

The evolutions of the averaged spin-spin coupling constants of solvated putrescine ($J_{(1,2)x(15,16)}$ and $J_{(3,4)x(15,16)}$), calculated at the level B3LYP/6-311++G**, are plotted as a function of relative energy ΔE in figures (3.16) and (3.17). Results shown here correspond to the averaged spin-spin coupling constants calculated for the isomers of solvated putrescine whose energies and chemical shifts are previously given in table (3.13).

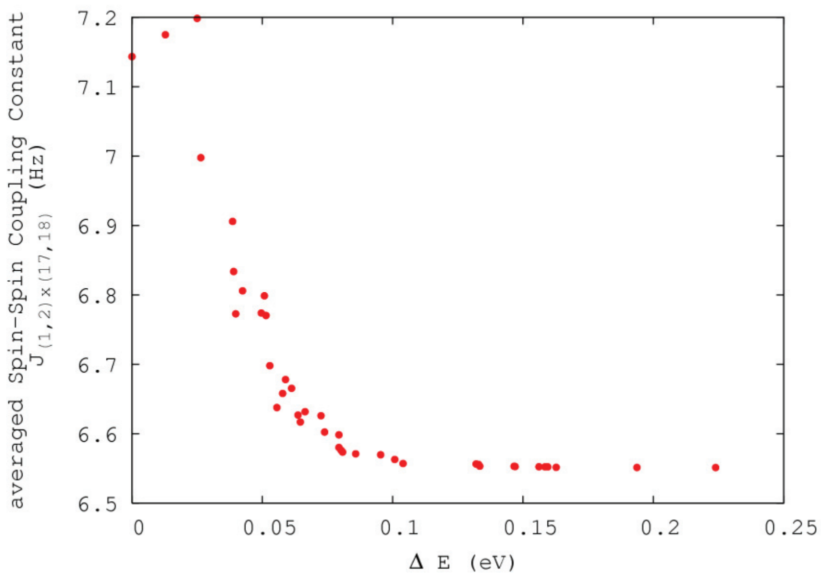

Figure 3.16: evolution of the averaged spin-spin coupling constant $J^{av}_{(1,2)x(15,16)}$ for solvated putrescine with energy

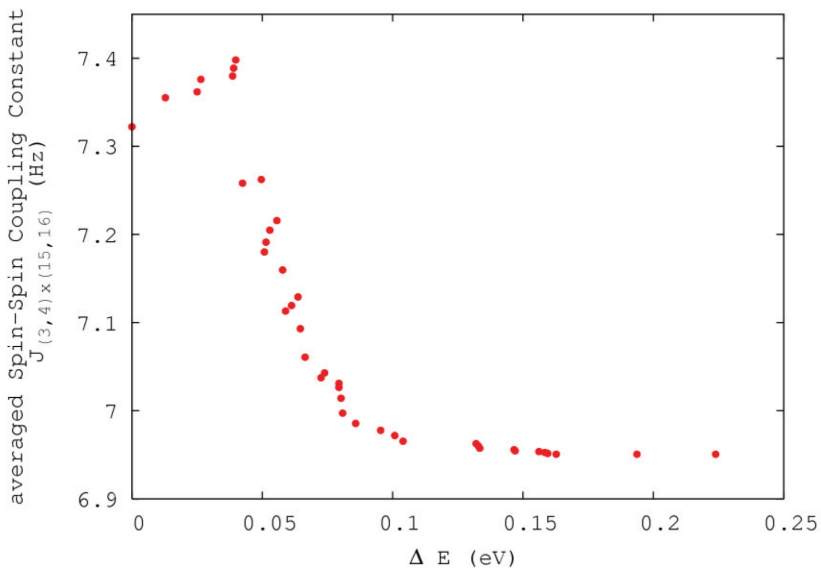

Figure 3.17: evolution of the averaged spin-spin coupling constant $J^{av}_{(3,4)x(15,16)}$ for solvated putrescine with energy

In figures (3.16) and (3.17), the i^{th} point (according to increasing energy scale) represents the averaged spin-spin coupling constant of the first i isomers, for isomers arranged according to their energies. The averaged spin-spin coupling constants $J^{av}_{(1,2)x(15,16)}$ and $J^{av}_{(3,4)x(15,16)}$ converge to 6.55 Hz and 7 Hz respectively, at the B3LYP/6-

311++G** level. The averaged values $J^{av}_{(1,2)x(15,16)}$ and $J^{av}_{(3,4)x(15,16)}$ decrease by 6% and 4% respectively in comparison with J-couplings of the ground-state putrescine. The convergence of the averaged spin-spin coupling constants starts at ΔE ~ 0.1 eV which is the energy of convergence found previously for the averaged chemical shifts of solvated putrescine. This indicates that our choice of isomers of putrescine is sufficient for the calculation of averaged NMR parameters since convergence is attained by averaged chemical shifts and J-couplings.

The procedure of calculating the averaged spin-spin coupling constants using our automatized method was repeated again since molecular dynamics simulations may give different groups of isomers for different trajectories. Despite that, the same results were found for the averaged spin-spin couplings of solvated putrescine. This is a powerful indication that our method is not only good for the calculation of averaged chemical shifts but also for the averaged spin-spin coupling constants.

As was done for the averaged chemical shifts of putrescine, we have tested the two functional PBE and OPBE in combination with the basis set 6-311++G** for the calculation of averaged spin-spin coupling constants for solvated putrescine. Results are then compared with the B3LYP/6-311++G** level which is expected to be the most appropriate. Table (3.15) gives the results of the averaged spin-spin couplings of solvated putrescine for three theoretical levels. The two couplings $J^{av}_{(1,2)x(15,16)}$ and $J^{av}_{(3,4)x(17,18)}$ which are expected to be equal are calculated separately to see if this equality is well valid for averaged values.

Level of Calculation	$J^{av}_{(1,2)x(15,16)}$	$J^{av}_{(3,4)x(15,16)}$	$J^{av}_{(3,4)x(17,18)}$	$J^{av}_{(1,2)x(15,16)} - J^{av}_{(3,4)x(17,18)}$
*B3LYP/6-311++G***	*6.60*	*7*	*6.53*	*0.07*
*PBE/6-311++G***	*6.15*	*6.75*	*5.98*	*0.17*
*OPBE/6-311++G***	*6.20*	*6.61*	*6.04*	*0.16*

Table 3.15: averaged spin-spin coupling constants for solvated putrescine calculated at three different levels

For all calculation levels used, the averaged spin-spin coupling constants are smaller than the spin-spin coupling constants of ground-state putrescine by ~ 0.5 Hz. We have seen earlier that the spin-spin couplings, calculated at the level B3LYP/6-311++G** for ground-state solvated putrescine, reproduce well the experiment. Then, the averaged values of spin-spin coupling constants calculated at the levels PBE and OPBE are relatively small, whereas the values calculated at the level B3LYP are the closest to the experiment. So, as was expected, the best results for the calculation of the averaged spin-spin coupling constants occur at the level B3LYP/6-311++G**. Note that $J^{av}_{(1,2)x(15,16)}$ and $J^{av}_{(3,4)x(17,18)}$ remain approximately equal with a difference going from ~ 1% for B3LYP to ~ 3% for PBE and OPBE.

IV Vibrational effects on NMR parameters

Vibrational effects are to be considered for an accurate calculation of NMR parameters. For vibrational effects on chemical shifts, we have tried two ways (1) classical mechanics through the usage of the ADMP method which is a classical molecular dynamics in the sense that nuclei are moved classically, and (2) quantum mechanics. For this second way, calculations were made through the usage of C_{FOUR} program which allows the calculation of vibrational effects on chemical shifts for a limited number of theoretical levels including HF, and through the usage of our method which calculates vibrational effects semi-numerically; however, it is more general than C_{FOUR} in the sense that it is applicable for all theoretical levels including the DFT one. Vibrational effects on spin-spin coupling constants are calculated via our method.

For vibrational effects on chemical shifts, we give a detailed presentation for sarcosine, and since sarcosine has no J-couplings that affect the NMR spectrum, we choose serine to describe the method for calculating vibrational effects on spin-spin coupling constants.

IV.1 Vibrational effects on chemical shifts: sarcosine, as an example

IV.1.1 Vibrational effects via classical mechanics - ADMP simulations

Using ADMP simulations we have tried to calculate the vibrational effects by two ways (1) at ambient temperature where the molecule is equilibrated at 300 K and then left to propagate without constraints, and (2) giving the molecule an initial energy equal to its vibrational energy $\sum {}^{h\nu}/_{2}$ (the sum is carried over atomic frequencies ν) and then leaving it to propagate without constraints.

While the first way is explained as a classical vibration at ambient temperature, the second way aims to approximate the zero-point vibrational effects which are purely quantum effects, by ADMP simulations. With ADMP simulations, we are not searching for results competitive with quantum mechanics but we are just looking for a correct qualitative trend. As we have said before, ADMP results are shown for sarcosine.

IV.1.1.1 ADMP at ambient temperature

To the ground-state geometry of sarcosine, perturbational calculations are studied using ADMP simulations. Unconstrained ADMP simulations (NVE ensemble), in gas phase, are performed, at the B3LYP/6-311++G** level, starting from the equilibrium geometry optimized at the same level. The fictitious electron mass is fixed to 0.1 amu and a time step of 0.2 fs is used for a global simulation time of 2 ps at temperature 300 K, the first 0.5 ps of which are taken for equilibration. The molecule is equilibrated for 0.5 ps maintaining a temperature of 300 ($\pm$50) K, and then is propagated without constraints for 1.5 ps. Snapshots are taken along the trajectory each 1.6 fs (hence a total of 938 snapshot). Thus, ADMP simulations result in a series of geometries for sarcosine (938); for each geometry obtained at a snapshot, we calculate chemical shieldings at the B3LYP/6-311++G** level, where solvent effects, if needed, are included at this stage using PCM model. Shieldings are computed using the GIAO formalism. All calculations are performed using the Gaussian03 program package and the graphical interface Gabedit.

The vibrational chemical shieldings σ^{vib} of sarcosine are calculated by averaging the chemical shieldings calculated at the snapshots. Although the number of snapshots is quiet large (938), averaged σ values were easily calculated by means of a program, developed by us, that reads the chemical shieldings from output files (938) and calculates their average according to equation (3.3)

$$\sigma^{vib} = \frac{\sum_{i}^{n} \sigma^{i}}{n} \tag{3.3}$$

where i is the snapshot's number running from 1 to n = 938 and σ^{i} is the chemical shift calculated at the snapshot i. Results of σ^{vib} obtained for isolated and solvated sarcosine using ADMP simulations are displayed in table (3.16) in ppm.

	Isolated sarcosine			***Solvated sarcosine***		
Group of Protons	$\boldsymbol{\sigma}$	$\boldsymbol{\sigma^{vib}}$	$\boldsymbol{\Delta\sigma = \sigma^{vib} - \sigma}$	$\boldsymbol{\sigma}$	$\boldsymbol{\sigma^{vib}}$	$\boldsymbol{\Delta\sigma = \sigma^{vib} - \sigma}$
A	*29.525*	*29.178*	*-0.348*	*29.521*	*29.092*	*-0.429*
B	*28.595*	*28.281*	*-0.314*	*28.405*	*28.129*	*-0.276*

Table 3.16: σ^{vib} results for sarcosine at the level ADMP-B3LYP/6-311++G**

The running average of vibrational chemical shifts σ^{vib}, that is, the average up to each point, is found to be well converging so that the time of the simulation is considered as long enough to achieve convergence for this system. Comparing the shielding constants computed at the static level to that obtained when averaging on molecular dynamics snapshots, σ^{vib} values for both groups of protons are found to be deshielded with respect to the equilibrium value (~1 - 1.5%). For isolated sarcosine, both chemical shifts are deshielded by the same amount (~0.3 ppm) which is not the case for solvated sarcosine. This can be explained by the fact that the equilibrium geometries for isolated and solvated sarcosine are different due to solvent effects.

Not only vibrational effects on sarcosine must be taken into account, but also effects on the reference molecule TMS. Once having calculated the vibrational chemical shieldings for our molecule and its reference, vibrational chemical shifts δ^{vib} can be determined. Then after, results can be compared to experimental ones.

Hence, ADMP simulations with the same conditions (equilibration at 300 K, step size, duration ..) are performed for the optimized TMS molecule in the gas phase. Optimization and NMR calculations are done at the B3LYP/6-311++G** level. Results of σ_{TMS}^{vib} at the dynamic level compared to the static level σ_{TMS} are shown in table (3.17).

σ_{TMS}	σ_{TMS}^{vib}	$\Delta\sigma_{TMS} = \sigma_{TMS}^{vib} - \sigma_{TMS}$
31.970	*31.664*	*-0.306*

Table 3.17: σ^{vib} results for sarcosine at the level ADMP-B3LYP/6-311++G**

Comparing σ_{TMS} computed at B3LYP/6-311++G** level to that obtained when averaging on molecular dynamics snapshots, a decrease in σ of order 0.3 ppm is found (~ 1%). Vibration has a deshielding effect on σ of TMS as it was found for sarcosine. It must be noted that only isolated TMS is considered because solvant effects on TMS are assumed to be negligible.

Similar ADMP simulations (equilibration at 300 K, step size = 1.6 fs ..) are performed for both sarcosine and TMS molecules at the HF/6-311++G** level. That means, equilibrium geometries, ADMP simulations, and shielding calculations are all done at the same theoretical level HF/6-311++G**. This calculation allows us to compare the results obtained by two different theoretical levels used for MD simulations. Vibrational shielding values σ^{vib} obtained for isolated sarcosine and TMS at the ADMP-HF/6-311++G** level are displayed in table (3.18).

Molecule	***Group of Protons***	σ	σ^{vib}	$\Delta\sigma = \sigma^{vib} - \sigma$
Sarcosine	*A*	*30.216*	*30.022*	*-0.195*
	B	*29.491*	*29.292*	*-0.199*
TMS	*A*	*32.441*	*32.270*	*-0.171*

Table 3.18: results for sarcosine and TMS at the level HF/6-311++G** using ADMP simulations

The nuclear magnetic shieldings σ computed for the optimized structures (static level) are compared to the average σ^{vib} along ADMP trajectories. The shieldings of sarcosine and TMS molecules are similarly affected by the vibrational effects (deshielded). A decrease in the absolute value of $\Delta\sigma$ is found in comparison with previous results corresponding to the hybrid functional B3LYP ($\Delta\sigma$ ~ -0.3 ppm with B3LYP in comparison with ~ -0.2 ppm with HF).

Having calculated vibrational chemical shieldings σ^{vib} for sarcosine and its reference molecule TMS at the same level of theory, vibrational shifts δ_A^{vib} (or δ_B^{vib}) can be calculated as usual by subtracting σ_A^{vib} (or σ_B^{vib}) from σ_{TMS}^{vib}. Results of δ^{vib} obtained for sarcosine at the dynamic level are displayed in table (3.19). Computed averaged shifts are compared to their equilibrium values.

Molecule	*Calculation level*	*Group*	σ^{vib}	$\Delta\sigma$	$\delta^{vib} = \sigma_{TMS}^{vib} - \sigma^{vib}$	$\Delta\delta = \delta^{vib} - \delta$
Isolated Sarcosine	***B3LYP/6-311++G****	*A*	*29.178*	*-0.348*	*2.486*	*0.042*
		B	*28.281*	*-0.314*	*3.383*	*0.008*
Solvated Sarcosine	***B3LYP/6-311++G****		*29.092*	*-0.429*	*2.573*	*0.123*
		B	*28.129*	*-0.276*	*3.537*	*-0.03*
Isolated Sarcosine	***HF/6-311++G****	*A*	*30.022*	*-0.195*	*2.248*	*0.023*
		B	*29.292*	*-0.199*	*2.978*	*0.027*

Table 3.19: δ^{vib} results for sarcosine using ADMP simulations at 300 K

Vibrational effects show a correction for the calculated ^{1}H chemical shifts of the order of ~0.05 - 0.1 ppm which is in agreement with previous studies [4]. For solvated sarcosine, the solvent plays an important role in modifying the equilibrium geometry leading to a change in vibrational effects in comparison with the isolated molecule where the correction on chemical shifts reaches ~0.12 ppm for the solvated molecule in comparison with ~0.04 ppm for the isolated structure. Besides, although the vibrational effects on chemical shieldings of isolated sarcosine show some difference using the two methods B3LYP and HF, yet the effects on chemical shifts seem more matching.

It must be noted that for the previously done calculations using ADMP simulations, the random number seed N was fixed arbitrarily (IOp(1/44=N)). In fact, when dealing with a random number generator, long runs of numbers can be automatically created with good random properties. Fixing this random number intends to control some initial conditions (particularly the initial velocity) of the classical motion of the molecule under study. The aim of this step is to make the comparison between the two studied functionals more reasonable.

To verify the influence of using different starting points on the molecular dynamics trajectories, two trajectories are chosen arbitrarily just by changing the initial velocity with which the molecule under study is assumed to start its motion. Results of σ^{vib} obtained for isolated sarcosine using different trajectories are shown in table (3.20), and those obtained for TMS using also two trajectories are given in table (3.21).

Trajectory	$\boldsymbol{\sigma_A^{vib}}$	$\boldsymbol{\sigma_B^{vib}}$
1	*29.178*	*28.281*
2	*29.011*	*28.33*
Difference	*0.167*	*-0.049*

Table 3.20: σ^{vib} results for isolated sarcosine at the level B3LYP/6-311++G** with different MD trajectories

Trajectory	$\boldsymbol{\sigma_{TMS}^{vib}}$
1	*31.664*
2	*31.647*
Difference	*-0.017*

Table 3.21: σ^{vib} results for isolated TMS at the level B3LYP/6-311++G** with different MD trajectories

Comparing the trajectories obtained from these MD simulations, we have demonstrated that the starting point does affect the conformational space explored by the studied molecules. Although this effect appears to be weak for TMS which is quite symmetrical, a relatively large correction on σ_A is imposed by the new MD trajectory (~ 0.16 ppm). It is obvious that the ADMP simulations are not very precise in calculating the vibrational effects on molecules especially when considering only a single trajectory. A quick solution of this problem proposes averaging over a large number of trajectories which is quiet impossible in our case due to the large computational costs. However, thermal effects on magnetic shieldings, evaluated from MD, should at least show the correct qualitative trend.

IV.1.1.2 ADMP simulations with an initial energy of $\sum h\nu/2$

Gas phase, unconstrained NVE ADMP simulations were performed starting with the equilibrium geometry of sarcosine and giving it an initial nuclear kinetic energy equal to the zero-point vibrational energy:

$$E_{initial} = \sum \frac{h\nu}{2} \qquad (3.4)$$

where the sum is carried over the normal modes of the structure under study and ν is the frequency characterizing each mode. Of course, a non-linear molecule with A atoms has 3A-6 normal modes (for sarcosine with 13 atoms, there exits 33 normal modes of vibration). These harmonic frequencies are obtained theoretically as analytical second derivatives of energy.

The fictitious electron mass has been fixed to 0.1 amu and a time step of 0.2 fs has been used for a global simulation time of 2 ps. Snapshots were taken along the trajectories each 1.6 fs (hence a total of 1250 snapshot). No previous equilibration of the system was performed; however, it was given an initial kinetic energy and left to propagate without constraints.

Shieldings were computed using the GIAO approach. All calculations were performed using the Gaussian03 program package and the graphical interface Gabedit.

Two calculation levels (B3LYP/6-311++G** and HF/6-311++G**) were used throughout for structural and shielding calculations. At each time, the optimization of the ground-state geometry used as a starting point, ADMP simulations, and shielding calculations are all done at the same theoretical level. By that, we can compare results obtained by the two different methods. These calculations were done not only for sarcosine, but also for the reference molecule TMS. Zero-point vibrational shielding values σ^{vib} obtained for isolated sarcosine and TMS are displayed in tables (3.22) and (3.23) at the levels B3LYP/6-311++G** and HF/6-311++G** respectively.

Molecule	*Group of Protons*	σ	σ^{vib}	$\Delta\sigma = \sigma^{vib} - \sigma$
Isolated Sarcosine	*A*	*29.525*	*28.718*	*-0.807*
	B	*28.595*	*27.943*	*-0.651*
TMS	*A*	*31.970*	*31.340*	*-0.630*

Table 3.22: σ^{vib} results using ADMP simulations with $E_{initial}=\sum h\nu/2$ at the level B3LYP/6-311++G**

Molecule	*Group of Protons*	σ	σ^{vib}	$\Delta\sigma = \sigma^{vib} - \sigma$
Isolated Sarcosine	*A*	*30.216*	*29.526*	*-0.691*
	B	*29.491*	*28.950*	*-0.540*
TMS	*A*	*32.441*	*31.914*	*-0.527*

Table 3.23: σ^{vib} results using ADMP simulations with $E_{initial}$=$\sum h\,\nu/2$ at the level HF/6-311++G**

The magnetic shieldings σ computed for the equilibrium structures are compared to the average σ^{vib} values. All shieldings are deshielded as a result of vibrational effects. This deshielding (~0.6 ppm) is stronger than that obtained for structures equilibrated at 300 K (~0.2 - 0.3 ppm). Of course, this was expected as for light nuclei, zero-point effects are larger than the thermal effects. $\Delta\sigma$ simulated using different functionals remains always in the same order of magnitude.

Having calculated vibrational chemical shieldings σ^{vib} for sarcosine and its reference molecule TMS, vibrational shifts δ_A^{vib} (or δ_B^{vib}) can be calculated. Results of δ^{vib} obtained for sarcosine at the dynamic level are displayed in tables (3.24) and (3.25). Computed averaged shifts are compared to their equilibrium values.

Group of Protons	$\delta^{vib} = \sigma_{TMS}^{vib} - \sigma^{vib}$	$\Delta\delta = \delta^{vib} - \delta$
A	*2.622*	*0.177*
B	*3.39*	*0.021*

Table 3.24: δ^{vib} results for isolated sarcosine using $E_{initial}$=$\sum h\,\nu/2$ at the level ADMP-B3LYP/6-311++G**

Group of Protons	$\delta^{vib} = \sigma_{TMS}^{vib} - \sigma^{vib}$	$\Delta\delta = \delta^{vib} - \delta$
A	*2.388*	*0.163*
B	*2.964*	*0.014*

Table 3.25: δ^{vib} results for isolated sarcosine using $E_{initial}$=$\sum h\,\nu/2$ at the level ADMP-HF/6-311++G**

Vibrational effects show a correction for the calculated ^{1}H chemical shifts of the order of ~0.1 ppm. Although zero-point vibrational corrections for σ ($\Delta\sigma_A^{vib}$, $\Delta\sigma_B^{vib}$, and $\Delta\sigma_{TMS}^{vib}$) are found to be stronger that those simulated at 300 K, the total vibrational effect on chemical shifts remains in the vicinity of 0.1 ppm. In fact, studying a pure quantum property using a classical point of view is not easy. Based on our simulations, we can deduce that zero-point vibrational effects are important to the extent that they can affect the magnetic shieldings of our molecules by an order of ~ 0.6 ppm.

IV.1.2 Vibrational effects via quantum mechanics

Classical ADMP simulations do not include a full perturbative treatment of the ro-vibrational problems; for example, coriolis couplings and the magnitude of the coupling via cubic and quartic terms in the potential which may be eventually important for higher energy modes are not evaluated. However, quantum mechanics can treat correctly the calculation of ZPVC (zero-point vibrational corrections) to nuclear shieldings by approximating solutions to the nuclear Schrodinger equation.

Vibrational effects on the chemical shifts of sarcosine were first estimated quantum mechanically using the C_{FOUR} program package. The optimization of the ground-state geometry used as a starting point for simulations, as well as the perturbational calculations, have been carried out at the HF level using the basis set 6-311++G**. Results of vibrational corrections $\Delta\sigma$ to static chemical shieldings σ of isolated sarcosine are shown in table (3.26).

Molecule	*Group of Protons*	σ	σ^{vib}	$\Delta\sigma = \Delta\sigma^{ZPVC} = \sigma^{vib} - \sigma$
Sarcosine	*A*	*30.216*	*29.518*	*-0.698*
	B	*29.491*	*28.829*	*-0.662*

Table 3.26: σ^{vib} results for sarcosine at the level HF/6-311++G** where σ are the chemical shieldings calculated at the static state

Unfortunately, the C_{FOUR} program is known to be limited to a number of methods; DFT approach, which is our chosen method for metabolites, is not considered in C_{FOUR}. That's why we have limited our calculations to the HF level. Results given in table (3.26) show corrections $\Delta\sigma$ on static shieldings of order ~0.6 ppm which was previously expected when exploiting MD simulations in quantum calculations (comparison with table (3.23)). Alas, we have not been able to calculate the ZPVC on the chemical shielding of the reference TMS through the C_{FOUR} package due to non-converging terms. Without the vibrational shielding of TMS, we cannot calculate the vibrational chemical shifts of sarcosine.

Then, we have developed a specific code, which solves the quantum mechanical correction on the chemical shift $\Delta\sigma$ semi-numerically (see chapter 2, section III). We have implemented the code in version of Gaussian03 at our disposal (which does not allow the evaluation of vibrational effects upon NMR parameters).

$$\Delta\sigma = \frac{1}{4}\sum_{L}\frac{1}{\omega_L}\left[\frac{d^2\sigma_{eq}}{dQ_L^2} - \frac{1}{\omega_L}\frac{d\sigma_{eq}}{dQ_L}\sum_{M}\frac{F_{LMM}^{eq}}{\omega_M}\right] \tag{3.5}$$

The variation of normal coordinates Q_L is discretized into a step of ΔQ_L = 0.03 Å; this allows us to estimate numerically, the first and second derivatives of the chemical shielding ($\frac{d\sigma_{eq}}{dQ_L}$ and $\frac{d^2\sigma_{eq}}{dQ_L^2}$). The numerical calculation of these derivatives requires calculating the chemical shifts for the non-equilibrium geometries resulting from shifting the atomic coordinates by an amount equal to the required step. On the other hand, the frequencies ω_L are calculated analytically, and the third order derivatives of the electronic energy with respect to the normal coordinates (F_{LMM}^{eq}) are performed in Gaussian03.

This program allows not only the implementation of most theoretical methods (in particular the B3LYP functional), but also the treatment of molecules that seemed to be non-converging for C_{FOUR} like TMS. Besides, our program calculates the temperature effects on σ which are known to be very small at the ambient temperature in comparison with ZPVC (see equation (2.101)). Our method has been implemented in the version of Gaussian of our disposal.

Using our method, vibrational shieldings were calculated at the HF and B3LYP levels in combination with the basis set 6-311++G** for isolated ground-state sarcosine and TMS to be compared to previous results. Hereby, the total correction $\Delta\sigma$ is the sum of zero-point vibrational corrections ZPVC ($\Delta\sigma^{ZPVC}$) and temperature corrections TC ($\Delta\sigma^{TC}$). Results of vibrational shieldings are shown in tables (3.27) and (3.28), whereas, effects on shifts are displayed in table (3.29).

Molecule	Group of Protons	σ	σ^{vib}	$\Delta\sigma = \sigma^{vib} - \sigma$	$\Delta\sigma^{ZPVC}$	$\Delta\sigma^{TC}$
Sarcosine	A	29.525	28.736	-0.789	-0.731	-0.058
	B	28.595	27.880	-0.715	-0.701	-0.014
TMS	A	31.970	31.300	-0.670	-0.648	-0.022

Table 3.27: σ^{vib} results for sarcosine at the level B3LYP/6-311++G** using the home-made program

Molecule	Group of Protons	σ	σ^{vib}	$\Delta\sigma = \sigma^{vib} - \sigma$	$\Delta\sigma^{ZPVC}$	$\Delta\sigma^{TC}$
Sarcosine	A	30.216	29.478	-0.738	-0.699	-0.039
	B	29.491	28.821	-0.670	-0.662	-0.008
TMS		31.441	31.794	-0.647	-0.623	-0.024

Table 3.28: σ^{vib} results for sarcosine at the level HF/6-311++G** using the home-made program

Calculation Level	Group of Protons	$\delta^{vib} = \sigma^{vib}_{TMS} - \sigma^{vib}$	$\Delta\delta = \delta^{vib} - \delta$
B3LYP	A	2. 64	0.119
	B	3.420	0.045
HF	A	2.316	0.091
	B	2.973	0.022

Table 3.29: δ^{vib} results using the basis set 6-311++G** and the home-made program

Comparing ZPVC calculated either analytically (using the CFOUR package; see table (3.26)) or semi-numerically (using our program; see table (3.28)) at the HF level shows an excellent accord, which supports the correctness of our program.

A correction of order ~ 0.7 ppm is calculated on static shieldings for both used calculation levels. Temperature corrections are relatively small; yet, they account for ~ 6% of the total correction. Corrections of proton chemical shifts remain always in the vicinity of 0.1 ppm. Regardless of δ^{vib} values, corrections $\Delta\delta$ using the two methods (HF and B3LYP) appear to be harmonic which was also found for isolated sarcosine using (ADMP-300 K) and (ADMP- $E_{initial} = \sum h\nu/2$) simulations.

Since the quantum mechanical methods are the most appropriate in calculating vibrational effects on the chemical shieldings, and since the B3LYP functional was found to be suitable for calculating these magnetic properties, and because our home-made program can perform this job easily, we decided to simulate, at the level B3LYP/6311++G**, the vibrational chemical shieldings of the isomers of sarcosine which were found to be eight (for more details, see the subchapter B). By that, we can join two important factors (isomers and the vibration) affecting the calculated chemical shifts in order to obtain the best agreement with experiment.

The eight isomers of isolated sarcosine were optimized at the level B3LYP/6-311++G** and static chemical shieldings were calculated at the same level of theory. The resulting shieldings were averaged using Boltzmann contribution according to equation (3.2). Results of chemical shieldings of isomers as well as their relative energies ΔE are shown in table (3.30).

Geometry	***ΔE (eV)***	$\boldsymbol{\sigma_A}$	$\boldsymbol{\sigma_B}$
1	*0.000*	*29.525*	*28.595*
2	*0.004*	*29.533*	*28.930*
3	*0.020*	*29.369*	*28.891*
4	*0.024*	*29.422*	*28.555*
5	*0.051*	*29.478*	*28.596*
6	*0.078*	*29.439*	*28.612*
7	*0.096*	*29.377*	*28.476*
8	*0.134*	*29.428*	*28.448*
Boltzmann Average		*29.485*	*28.749*

Table 3.30: static σ and σ^{av} results for isomers of isolated sarcosine at the level B3LYP/6-311++G**

To the optimized structures, vibrational corrections (ZPVC and TC at 300 K) were calculated using our program. Results of vibrational shieldings of isomers as well as their zero-point vibrational relative energies ($\Delta E + \Sigma\, h\upsilon/2$) are shown in table (3.31). ΔE represents the equilibrium energy of an isomer while υ represents the corresponding harmonic frequencies (for sarcosine the sum runs over 33 frequencies).

Geometry	$\Delta E \ + \ \Sigma\, h\upsilon/2$ ***(eV)***	σ_A^{vib}	σ_B^{vib}
1	*0.000*	*28.736*	*27.883*
2	*0.014*	*28.760*	*28.231*
3	*0.015*	*28.701*	*27.790*
4	*0.033*	*28.645*	*28.214*
5	*0.050*	*28.704*	*27.864*
6	*0.088*	*28.655*	*27.762*
7	*0.071*	*28.712*	*27.843*
8	*0.128*	*28.659*	*27.787*
Boltzmann Average		*28.721*	*27.966*

Table 3.31: vibrational σ and σ^{av} results for isomers of isolated sarcosine at the level B3LYP/6-311++G**

Thus, isomer and vibrational effects were combined by calculating the Boltzmann average of vibrational chemical shieldings using equation (3.2). Not only isomer and vibrational effects must be considered, but also solvent effects which play an important role in shift determination. So, we simulated solvent effects $\Delta\sigma^{solv}$ for each isomer through PCM model. For each isomer, optimization and calculation of static shieldings of the isolated structure was done, followed by an optimization and calculation of static shieldings of the solvated structure at the same level of theory (B3LYP/6-311++G**). The difference between solvated and isolated shieldings of an isomer represents the solvent effects $\Delta\sigma^{solv}$ on this isomer and it is displayed in table (3.32).

Geometry	$\Delta\sigma_A^{solv} = \sigma_A^{solv} - \sigma_A^{iso}$	$\Delta\sigma_B^{solv} = \sigma_B^{solv} - \sigma_B^{iso}$
1	*-0.003*	*-0.194*
2	*-0.046*	*-0.297*
3	*0.003*	*-0.192*
4	*-0.037*	*-0.279*
5	*-0.010*	*-0.167*
6	*0.167*	*-0.169*
7	*0.001*	*-0.209*
8	*0.079*	*-0.143*

Table 3.32: solvent effects $\Delta\sigma^{solv}$ on static shieldings of sarcosine calculated at the level B3LYP/6311++G**

In order to group the three important factors (solvent, isomers, and vibration) affecting the calculated shieldings, solvent corrections $\Delta\sigma^{solv}$ were added to vibrational shieldings σ^{vib}, and isomers were taken through Boltzmann contribution for the new values of shieldings ($\Delta\sigma^{solv} + \sigma^{vib}$). Results of vibrational shieldings with solvent effects and the resulting average are shown in table (3.33).

geometry	*Energy ΔE (eV)*	$\sigma_A^{vib} + \Delta\sigma_A^{solv}$	$\sigma_B^{vib} + \Delta\sigma_B^{solv}$
1	*0.000*	*28.733*	*27.689*
2	*0.014*	*28.715*	*27.916*
3	*0.015*	*28.704*	*27.598*
4	*0.033*	*28.608*	*27.935*
5	*0.050*	*28.693*	*27.698*
6	*0.088*	*28.822*	*27.593*
7	*0.071*	*28.713*	*27.634*
8	*0.128*	*28.739*	*2 644*
Boltzmann Average		*28.708*	*27.743*

Table 3.33: vibrational σ^{av} results for sarcosine including solvent effects at the level B3LYP/6-311++G**

Transforming shieldings to shifts allows a better understanding and an easy comparison with experimental results. Table (3.34) shows how different factors affect the simulated chemical shifts through a comparison with experimental values.

Included Effects	$\boldsymbol{\delta_A}$	$\boldsymbol{\delta_B}$	$\boldsymbol{\delta_A^{exp} - \delta_A}$	$\boldsymbol{\delta_B^{exp} - \delta_B}$
Solvent	*2.450*	*3.568*	*0.292*	*0.049*
isomers	*2.486*	*3.221*	*0.255*	*0.394*
vibration	*2.564*	*3.418*	*0.180*	*0.200*
vibration+solvent	*2.567*	*3.611*	*0.174*	*0.004*
vibration+isomer	*2.579*	*3.334*	*0.162*	*0.281*
isomers+solvent	*2.503*	*3.511*	*0.238*	*0.104*
solvent+isomers+vibration	*2.592*	*3.557*	*0.148*	*0.058*

Table 3.34: effect of different factors on calculated chemical shifts of sarcosine

It must be noted that to static shifts, the static TMS shielding was taken as a reference (31.97 ppm) and to vibrational shifts (including vibrational effects), the vibrational TMS shielding was taken as a reference (31.3 ppm).

We conclude that the three factors are important in calculating theoretical shifts. For sarcosine, the solvent has a strong effect on the chemical shift δ_B (~ 0.2 ppm) in comparison with a negligible effect on δ_A. The vibration corrects the shifts by ~ 0.05 ppm for δ_B and ~ 0.1 ppm for δ_A. However, isomers work on ameliorating the difference between the two shifts (~ 0.1 ppm). These three effects joined together give the best agreement between theory and experiment.

IV.2 Vibrational effects on spin-spin coupling constants: serine, as an example

Since sarcosine has no J-couplings that affect the NMR spectrum, we choose serine to illustrate the vibrational effects on spin-spin coupling constants via our method which was found suitable to calculate vibrational chemical shieldings. For serine, we are interested in three main spin-spin coupling constants $J_{13,14}$, $J_{12,13}$, and $J_{12,14}$ (for proton numbers, see figure (3.18)).

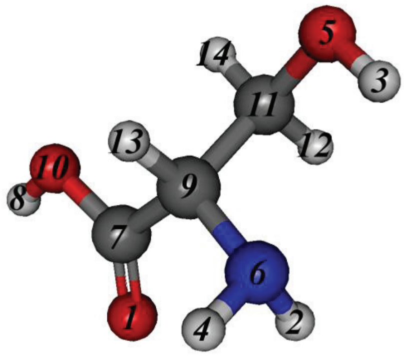

Figure 3.18: Lowest-energy structure of the solvated serine, optimized at the B3LYP/6-311++G** level

Our program calculates the vibrational effects on spin-spin coupling constants for an equilibrium geometry, as it is done for the chemical shieldings, semi-numerically.

$$\Delta J = \frac{1}{4}\sum_{L}\frac{1}{\omega_L}\left[\frac{d^2 J_{eq}}{dQ_L^2} - \frac{1}{\omega_L}\frac{dJ_{eq}}{dQ_L}\sum_{M}\frac{F_{LMM}^{eq}}{\omega_M}\right] \quad (3.6)$$

The calculation of ($\frac{dJ_{eq}}{dQ_L}$ and $\frac{d^2 J_{eq}}{dQ_L^2}$) is done numerically in parallel with the numerical calculation of the derivatives of σ, while F_{LMM}^{eq} and $\omega_L$are calculated by Gaussian03. Besides, our program allows the calculation of the temperature effects on J using equation (2.102).

Using our method, vibrational spin-spin coupling constants were calculated at the B3LYP/6-311++G** level for isolated ground-state serine. Hereby, the total correction ΔJ is the sum of zero-point vibrational corrections ZPVC (ΔJ^{ZPVC}) and temperature corrections TC (ΔJ^{TC}). Results of vibrational spin-spin coupling constants for isolated serine are shown in table (3.35).

Protons of interaction	*J (Hz)*	J^{vib} *(Hz)*	$\Delta J = J^{vib} - J$	ΔJ^{ZPVC} *(Hz)*	ΔJ^{TC} *(Hz)*
13x14	*4.4*	*4.59*	*0.19*	*0.18*	*0.01*
12x13	*8.67*	*9.57*	*0.90*	*1.06*	*-0.16*
12x14	*-9.15*	*-9.74*	*-0.59*	*-0.42*	*-0.17*

Table 3.35: J^{vib} results for isolated ground-state serine at the level B3LYP/6-311++G** using the home-made program

From table (3.35), vibrational corrections on static spin-spin coupling constants of serine vary between 4% and 10%. This means that the inclusion of vibrational effects may change the indirect spin-spin coupling constants significantly. Comparison of the ZPVCs with the temperature effects suggests that changing the temperature from 0 to 300 K causes only a small correction.

We decided to calculate, at the B3LYP/6-311++G** level, the vibrational spin-spin coupling constants for the isomers of serine which were found to be thirty two (for more details, see the subchapter B). By that, we can join two important factors (isomers and the vibration) affecting the calculated spin-spin coupling constants in order to obtain the best accord with experiment.

The thirty-two isomers of isolated serine were optimized at the level B3LYP/6-311++G** and static spin-spin coupling constants were calculated at the same level of theory. The resulting J-couplings were averaged using Boltzmann contribution according to equation (3.2). Results of spin-spin coupling constants of isomers as well as their relative energies ΔE are shown in table (3.36).

Geometry	ΔE *(eV)*	$J_{13,14}$ *(Hz)*	$J_{12,13}$ *(Hz)*	$J_{12,4}$ *(Hz)*
1	*0.000*	*4.40*	*8.67*	*-9.15*
2	*0.002*	*2.76*	*1.59*	*-10.96*
3	*0.111*	*2.17*	*2.72*	*-11.02*
4	*0.037*	*3.62*	*1.14*	*-9.60*
5	*0.066*	*3.85*	*9.55*	*-11.42*
6	*0.143*	*3.59*	*8.36*	*-12.28*

7	*0.068*	*4.12*	*8.67*	*-9.14*
8	*0.147*	*2.99*	*8.98*	*-10.09*
9	*0.181*	*10.05*	*5.28*	*-10.43*
10	*0.141*	*2.88*	*2.30*	*-5.91*
11	*0.185*	*3.68*	*8.43*	*-10.41*
12	*0.207*	*9.34*	*4.71*	*-9.87*
13	*0.189*	*2.51*	*8.29*	*-10.28*
14	*0.196*	*9.80*	*4.85*	*-6.16*
15	*0.094*	*8.59*	*4.37*	*-10.69*
16	*0.126*	*8.14*	*3.85*	*-10.24*
17	*0.192*	*2.77*	*8.92*	*-10.26*
18	*0.065*	*2.28*	*1.94*	*-10.84*
19	*0.015*	*8.66*	*4.39*	*-9.43*
20	*0.226*	*3.53*	*8.49*	*-10.52*
21	*0.176*	*8.73*	*4.49*	*-10.37*
22	*0.172*	*9.94*	*4.73*	*-11.05*
23	*0.138*	*3.31*	*1.25*	*-11.19*
24	*0.135*	*9.44*	*5.22*	*-7.27*
25	*0.112*	*7.61*	*3.78*	*-10.65*
26	*0.118*	*2.89*	*0.99*	*-10.93*
27	*0.199*	*2.26*	*2.24*	*-7.06*
28	*0.161*	*2.19*	*1.06*	*-11.03*
29	*0.322*	*2.79*	*1.29*	*-7.36*
30	*0.368*	*2.47*	*1.01*	*-11.64*
31	*0.331*	*2.59*	*1.66*	*-10.70*
32	*0.394*	*3.75*	*9.92*	*-9.24*
Boltzmann Average		*4.50*	*4.68*	*-9.98*

Table 3.36: static J and J^{av} results for isomers of isolated serine at the level B3LYP/6-311++G**

To the optimized structures, vibrational corrections (ZPVC and TC at 300 K) on spin-spin coupling constants were calculated using our program. Due to the large computational costs of vibrational effects (1 month for an isomer of serine), we have limited our calculations to seventeen isomers having vibrational energies less than 0.16 eV. The remaining fifteen isomers, having relatively large energies, have small weighting factors $e^{-\Delta E/kT}$, so that their effect on the calculated averaged spin-spin coupling constants is expected to be weak.

Results of vibrational spin-spin coupling constants of the seventeen isomers as well as their zero-point vibrational relative energies ($\Delta E + \Sigma\, h\upsilon/2$) are shown in table (3.37). ΔE represents the equilibrium energy of an isomer while υ represents the harmonic frequencies of atoms.

Geometry	$\Delta E + \Sigma\, h\upsilon/2$ *(eV)*	$J^{vib}_{13,14}$ *(Hz)*	$J^{vib}_{12,13}$ *(Hz)*	$J^{vib}_{12,14}$ *(Hz)*
1	*0.000*	*4.59*	*9.57*	*-9.74*
2	*0.009*	*3.08*	*1.72*	*-11.63*
3	*0.099*	*3.23*	*2.42*	*-11.59*
4	*0.035*	*3.57*	*1.39*	*-10.25*
5	*0.074*	*3.92*	*10.31*	*-12.15*
6	*0.139*	*4.04*	*9.56*	*-12.73*
7	*0.068*	*4.64*	*9.79*	*-10.14*
8	*0.133*	*3.07*	*9.72*	*-10.76*
10	*0.128*	*2.87*	*2.38*	*-7.61*
15	*0.093*	*9.68*	*4.84*	*-11.15*
16	*0.113*	*9.13*	*4.15*	*-10.82*
18	*0.071*	*2.54*	*2.00*	*-11.52*
19	*0.032*	*9.67*	*4.62*	*-9.79*
23	*0.138*	*3.89*	*1.44*	*-11.51*
24	*0.132*	*10.76*	*5.66*	*-7.62*
25	*0.108*	*8.88*	*3.97*	*-11.26*
26	*0.120*	*3.20*	*1.10*	*-11.61*
Boltzmann Average		*4.66*	*5.59*	*-10.48*

Table 3.37: vibrational J and J^{av} results for isomers of isolated serine at the level B3LYP/6-311++G**

Isomer and vibrational effects were combined by calculating the Boltzmann average of vibrational spin-spin coupling constants using equation (3.2) where the result of this combination gave 4.66, 5.59, and -10.48 Hz for $J_{13,14}^{vib/av}$, $J_{12,13}^{vib/av}$, and $J_{12,14}^{vib/av}$ respectively.

Not only isomer and vibrational effects must be considered, but also solvent effects. So, we simulated solvent effects ΔJ^{solv} for each isomer through PCM model. For each isomer, optimization and calculation of static spin-spin coupling constants of the isolated structure was done, followed by an optimization and calculation of static spin-spin coupling constants of the solvated structure at the same level of theory (B3LYP/6-311++G**). The difference between solvated and isolated J-couplings of an isomer represents the solvent effects ΔJ^{solv} on this isomer and it is displayed in table (3.38).

Geometry	$\Delta J_{13,14}^{solv} = J_{13,14}^{solv} - J_{13,14}^{iso}$	$\Delta J_{12,13}^{solv} = J_{12,13}^{solv} - J_{12,13}^{iso}$	$\Delta J_{12,14}^{solv} = J_{12,14}^{solv} - J_{12,14}^{iso}$
1	*-1.39*	*-0.28*	*-1.04*
2	*0.89*	*-0.11*	*-0.42*
3	*1.13*	*-0.67*	*0.00*
4	*-1.10*	*0.98*	*-1.21*
5	*-0.16*	*-0.16*	*0.29*
6	*-0.34*	*0.07*	*0.79*
7	*-1.10*	*-0.23*	*-1.05*
8	*-0.01*	*-0.27*	*-0.07*
10	*-0.08*	*0.26*	*-1.50*
15	*1.01*	*0.31*	*0.06*
16	*1.11*	*1.25*	*-0.24*
18	*0.71*	*0.24*	*-0.06*
19	*-0.17*	*-0.49*	*-1.19*
23	*0.53*	*-0.15*	*-0.50*
24	*0.69*	*0.01*	*-0.18*
25	*0.03*	*-0.87*	*-0.37*
26	*0.56*	*-0.15*	*-0.73*

Table 3.38: solvent effects ΔJ^{solv} on static spin-spin coupling constants of serine calculated at the level B3LYP/6-311++G**

In order to group the three important factors (solvent, isomers, and vibration) affecting the calculated spin-spin coupling constants, solvent corrections ΔJ^{solv} were added to vibrational J-couplings, and isomers were taken through Boltzmann contribution for the new values of J ($\Delta J^{solv} + J^{vib}$). Results of vibrational spin-spin coupling constants with solvent effects for serine and the resulting average are shown in table (3.39).

Geometry	$\Delta E + \Sigma h\upsilon/2$ ***(eV)***	$J^{vib}_{13,14} + \Delta J^{solv}_{13,14}$	$J^{vib}_{12,13} + \Delta J^{solv}_{12,13}$	$J^{vib}_{12,14} + \Delta J^{solv}_{12,14}$
1	*0.000*	*3.20*	*9.29*	*-10. 8*
2	*0.009*	*3.97*	*1.61*	*-12.05*
3	*0.099*	*4.36*	*1.75*	*-11.59*
4	*0.035*	*2.47*	*2.37*	*-11.46*
5	*0.074*	*3.76*	*10.15*	*-11.86*
6	*0.139*	*3.70*	*9.64*	*-11.93*
7	*0.068*	*3.54*	*9.56*	*-11.18*
8	*0.133*	*3.06*	*9.45*	*-10.83*
10	*0.128*	*2.79*	*2.63*	*-9.11*
15	*0.093*	*10.70*	*5.15*	*-11.09*
16	*0.113*	*10.24*	*5.39*	*-11.06*
18	*0.071*	*3.25*	*2.23*	*-11.58*
19	*0.032*	*9.49*	*4.14*	*-10.99*
23	*0.138*	*4.42*	*1.29*	*-12.01*
24	*0.132*	*11.45*	*5.67*	*-7.80*
25	*0.108*	*8.91*	*3.10*	*-11.64*
26	*0.120*	*3.75*	*0.95*	*-12.34*
Boltzmann Average		*4.25*	*5.49*	*-11.30*

Table 3.39: vibrational J^{av} results for serine including solvent effects at the level B3LYP/6-311++G**

Comparing our results to the experiment, table (3.40) shows how different factors (isomers, vibration, solvent) affect the simulated spin-spin coupling constants. The experimental values of $J_{13,14}$, $J_{12,13}$, and $J_{12,14}$ were found to be 3.561, 5.959, and -12.254 Hz respectively.

Included Effects	$J_{13,14}$ *(Hz)*	$J_{12,13}$ *(Hz)*	$J_{12,14}$ *(Hz)*	$J^{exp}_{13,14} - J_{13,14}$	$J^{exp}_{12,13} - J_{12,13}$	$J^{exp}_{12,14} - J_{12,14}$
solvent	*3.11*	*8.39*	*-10.2*	*0.54*	*-2.41*	*-2.06*
Isomers	*4.50*	*4.68*	*-9.98*	*-0.94*	*1.30*	*-2.28*
Vibration	*4.59*	*9.57*	*-9.74*	*-1.03*	*-3.59*	*-2.52*
vibration +solvent	*3.20*	*9.29*	*-10.78*	*0.36*	*-3.31*	*-1.47*
vibration +isome	*4.66*	*5.59*	*-10.48*	*-1.10*	*0.39*	*-1.77*
isomers+solvent	*4.03*	*5.55*	*-10.50*	*-0.47*	*0.43*	*-1.75*
solvent+isomer+vibration	*4.25*	*5.50*	*-11.3*	*-0.70*	*0.49*	*-0.96*

Table 3.40: effect of different factors on calculated spin-spin coupling constants of serine

From table (3.40), it is clear that the case where the three effects are taken into account at once gave the best accord with the experiment. We conclude that the three factors are important in calculating theoretical spin-spin coupling constants, as it was found for chemical shifts.

V Solvent effects on NMR parameters via ONIOM method

In vitro experimental spectra are often taken for molecules in solution (D_2O), and then any comparison between experimental and theoretical spectra requires that solvent effects be taken into account in the theoretical study.

In the explicit method of solvation, ONIOM, solvent molecules surrounding the target molecule are taken explicitly into account during calculations. It is well established that water molecules play an important role in the essential functions of systems and that the hydrogen bonding capability of water molecule is crucial in the interactions between solvent water molecules and molecules under study.

Using ONIOM method, the region of the system of interest is treated with an accurate method while the remainder of the system is treated at a lower level. In this section, we examine the efficacity of the ONIOM (DFT:AMBER) approach in calculating the chemical shift of solvated acetate; the acetate molecule is treated quantum mechanically by DFT (in particular by B3LYP/6-311++G**) and water molecules are treated by AMBER molecular mechanics. Acetate molecule was selected because it has the smallest size among our chosen metabolites and it can be easily surrounded by water molecules. Acetate is characterized by a single chemical shift corresponding to the protons (2, 4, and 7) and no J-couplings.

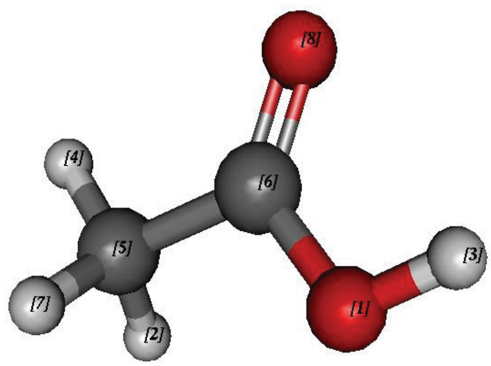

Figure 3.19: lowest-energy acetate optimized at the B3LYP/6-311++G** level (oxygen in red, carbon in grey, and hydrogen in white)

To examine the efficacity of ONIOM method in describing hydrated structures, we hydrated our acetate molecule first by 10 H_2O and then by 120 H_2O molecules and examined the stable structures. In other words, the two sets (10 H_2O + acetate) and (120 H_2O + acetate) were first optimized, and then shielding calculations were done for acetate. Results of chemical shieldings of acetate calculated using ONIOM-GIAO approach in comparison with PCM and experiment are shown in table (3.40).

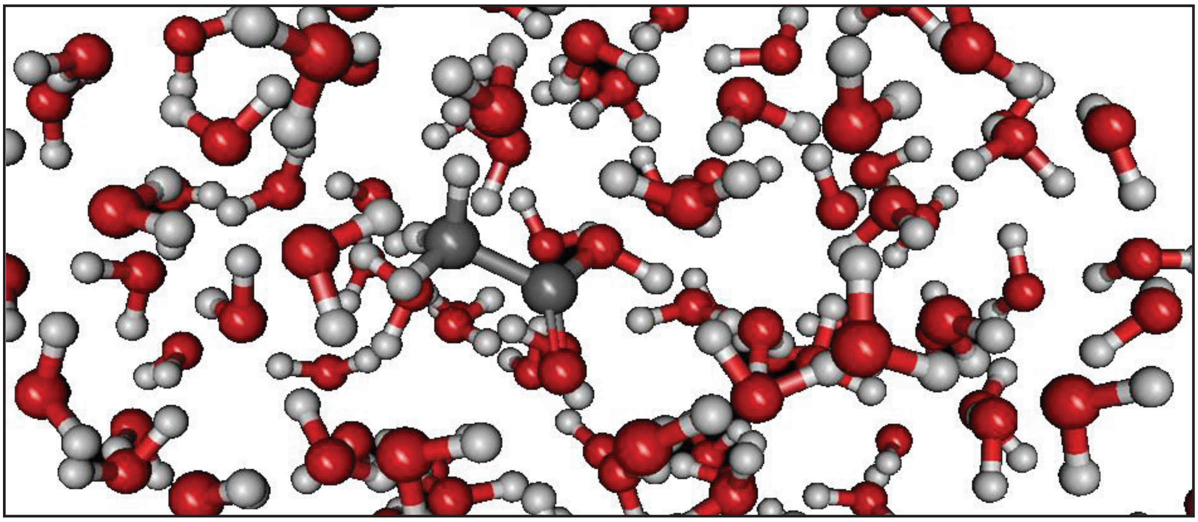

Figure 3.20: acetate molecule surrounded by water molecules

Method	*σ*
ONIOM (num of H_2O=10)	*28.94*
ONIOM (num of H_2O=120)	*29.77*
PCM	*29.86*
Experiment	*30.04*

Table 3.41: comparison of σ results for acetate using two methods: ONIOM and PCM

From table (3.41), it is clear that even 120 water molecules surrounding a small molecule like acetate described through ONIOM model are uncompetitive with PCM model. Of course, different arrangements of H_2O molecules around acetate result in different simulated chemical shieldings even for optimized structures. Therefore, PCM model seems to be more suitable in describing solvent effects for the ^{1}H chemical shieldings though it is modeled as a macroscopic continuum dielectric medium.

Overcoming the problem of different orientations of water molecules spread around acetate, we have used the constant energy (NVE) molecular dynamics calculation and selected 100 geometries during a simulation time of 10 ps where the time step was 1 fs and the temperature was 300 K. MD simulations were carried out starting from the optimized structure (using molecular mechanics). The resulting chemical shielding of acetate was calculated using equation (3.3) (by averaging the chemical shieldings calculated for the 100 snapshots using the level ONIOM-GIAO). This procedure was repeated three times for the acetate molecule surrounded by 180 H_2O where H_2O molecules were rearranged each time in a different manner. Results of chemical shifts of acetate are shown in table (3.42).

Number of trial	***σ***
1	*29.544*
2	*29.386*
3	*29.690*
Average	*29,540*

Table 3.42: σ results for acetate using MD-ONIOM

The averaged value of MD chemical shieldings (29.540 ppm) is comparable to the vibrational chemical shielding calculated using ADMP simulations at 300 K for solvated acetate (29.610 ppm).

We conclude that solvent effects on chemical shieldings of ^{1}H bond to C atoms are better calculated via PCM model than ONIOM method. ONIOM shows many complexes in calculating solvent effects especially for large molecules, not mentioning its computational costs. This justifies our choice of PCM in all our calculations; nevertheless, such a conclusion cannot be transferred without check to other nuclei.

VI studied effects on NMR parameters

In this work, three effects on NMR parameters of metabolites have been studied, which are solvent, isomers, and vibration. The work done is summarized in the scheme of (3.21) which shows the different methods used to investigate each effect.

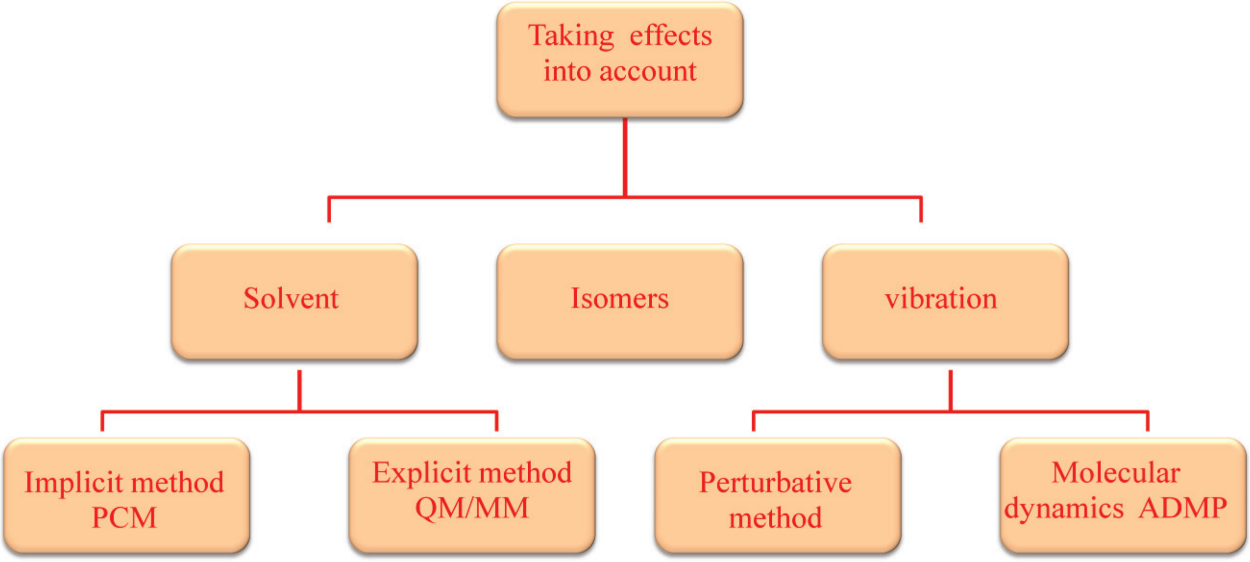

Figure 3.21: different effects studied on NMR parameters of metabolites

References

1. *CFOUR, a quantum chemical program package.* **J.F. Stanton, and al.** see <http://www.cfour.de>.

2. *Gabedit—A graphical user interface for computational chemistry softwares.* **A.R.Allouche.** 2011, A. R. J. Comput. Chem., Vol. 32, p. 174.

3. *Gaussian 03, Revision C.02.* **M. J. Frisch, and al.** 2004, Inc., Wallingford CT.

4. *Calculation of NMR and EPR parameters: Theory and application.* **M. Kaupp, M. Buhl, and V. G. Malkin.** 2004, Wiley-vch.

B: Results in the form of published papers

In part B, the full results are presented in a selection of our published papers. We present here four papers. The first one studies isomers effects on the NMR parameters of the three polyamines putrescine, spermidine, and spermine. The second paper presents the results of the chemical shifts of sarcosine including the three effects: solvent, isomers, and vibration. The third and fourth papers show the results of the three effects (solvent, isomers, and vibration) on both types of NMR parameters (chemical shifts and spin-spin coupling constants) for alanine and serine respectively.

Journal of Molecular Structure: THEOCHEM 945 (2010) 104–109

Contents lists available at ScienceDirect

Journal of Molecular Structure: THEOCHEM

journal homepage: www.elsevier.com/locate/theochem

DFT calculations of isomer effects upon NMR spin-Hamiltonian parameters of prostate polyamines

Z. Atieh, A.R. Allouche *, M. Aubert-Frécon

Université de Lyon, F-69622, Lyon, France
Université Lyon 1, Villeurbanne, France
CNRS, UMR 5579, LASIM, France

ARTICLE INFO

Article history:
Received 8 December 2009
Received in revised form 12 January 2010
Accepted 12 January 2010
Available online 18 January 2010

Keywords:
NMR spin-Hamiltonian parameters
DFT calculations
Isomer effects
Prostate polyamines

ABSTRACT

^{1}H Nuclear Magnetic Resonance (NMR) spin-Hamiltonian parameters: chemical shifts δ and spin–spin coupling constants J have been calculated using density functional theory, for the three polyamines: putrescine, spermidine and spermine present in prostate tissue. The Boltzmann weighted average of the chemical shifts and spin–spin coupling constants over a large number of stable conformers have been evaluated for each molecule. The comparison of such average chemical shifts with experimental values shows a significant improvement from values corresponding to the lowest-energy conformers, with rms errors of 0.15 ppm for putrescine and 0.05 ppm for both spermidine and spermine. From the comparison between spectra simulated from calculated δ and J parameters and experimental ones, the B3LYP/6-311++G** level of theory was seen to be a good compromise between accuracy and computational costs.

1. Introduction

In vivo Magnetic Resonance Spectroscopy (MRS) is a non-invasive powerful technique for detecting and quantifying bio-markers of diseases i.e. metabolites [1]. The analysis of MRS-signals obtained from patients is based on a database of prior knowledge about MRS-signals of metabolites which are simulated quantum–mechanically with the use of the spin-Hamiltonian parameters: chemical shifts δ and indirect spin–spin coupling constants J. Literature values of δ and J are used when available, mainly from experimental determinations [2]. In the present investigation we are interested in the three polyamines: putrescine, spermidine and spermine which are metabolites of prostate tissue. Polyamine concentrations have been shown to decrease in the presence of prostate cancer [3–9]. For these molecules there exist experimental values of ^{1}H chemical shifts in literature [10–12] while we knew no previous values for indirect spin–spin coupling constants. NMR chemical shifts and spin–spin constants can be obtained from quantum chemical methods which are now well established as efficient tools for such predictions (for recent reviews see [13–15] and references therein). With the aim to supply the prior knowledge database for polyamines, we recently performed δ and J calculations for the lowest-energy structure of the three polyamines [16,17] using the Density Functional Theory (DFT) with the hybrid exchange–correlation functional B3LYP [18,19] and the Pople-type [20] basis set 6-311++G**, assumed as a good cost/performance compromise. The main aim of the present paper is to evaluate in a rather systematic way, for each polyamine, the effect upon calculated chemical shifts and spin–spin coupling constants, of isomers higher in energy than the lowest-energy conformer.

The paper is organized in the following way. In Section 2 we outline the computational approaches used. Arguments for our choice of a level of theory (functional/basis set) are presented in Section 3. The contribution of isomers to the calculated NMR parameters is described and discussed in Section 4 while a comparison of our final results with experimental data from ^{1}H NMR spectra is presented in Section 5.

2. Computational approaches

For each polyamine: putrescine, spermidine and spermine, three calculation steps have been carried out (1) the determination of stable geometries of the gas-phase and solvated species in a given range of relative energy above the lowest-energy conformer, (2) the determination of the NMR spin-Hamiltonian parameters: chemical shifts and indirect spin–spin coupling constants for each stable structure previously determined, (3) the simulation of ^{1}H NMR spectra from the calculated NMR spin-Hamiltonian parameters. In the present investigation the three solvated polyamines have been described in the self-consistent reaction field theory

* Corresponding author. Address: Université de Lyon, F-69622, Lyon, France. Tel.: +33 4 72 43 19 29; fax: +33 4 72 43 15 07.
E-mail addresses: zatieh@lasim.univ-lyon1.fr (Z. Atieh), allouche@lasim.univ-lyon1.fr (A.R. Allouche), frecon@lasim.univ-lyon1.fr (M. Aubert-Frécon).

0166-1280/$ - see front matter
doi:10.1016/j.theochem.2010.01.017

based on the Polarisable Continuum Model (SCRF-PCM) [21,22] where water was used as solvent.

To search the stable geometries of a gas-phase or solvated polyamine i.e. the lowest-energy structure as well as the stable isomers lying in a given relative energy range, we have proceeded as follows. First we used the constant energy (NVE) molecular dynamics calculation using the Velocity Verlet algorithm [23] with the semi-empirical PM6 potential [24] to select a reasonably large number of initial geometries. The simulated time was 15 ps, the time step was 0.5 fs and the temperature was 5000 K. This high temperature was chosen in order to provide a large ($\sim$exhaustive) exploration of the potential energy surface. For each polyamine considered we have selected 5000 geometries during the simulation process. Each selected geometry was optimized at the PM6 level and very similar structures were removed. Then the remaining optimized geometries were used as initial geometries in an optimization process using this time the B3LYP method with the small basis set 6-31G$*$ to calculate the potential. Very similar structures were removed. Furthermore only the geometries which lie in a given energy gap ΔE_{max} above the lowest one ($\Delta E_{max} = E_{max} - E_0$ where E_0 is the energy of the lowest-lying structure) were retained. Finally, the remaining structures optimized at the B3LYP/6-31G$*$ level were used as initial geometries in the optimization process where the potential was evaluated this time at the DFT level using various functionals and various basis sets larger than 6-31G$*$. These optimized structures were filtered in order to retain only those which correspond to an energy minimum i.e. with no imaginary calculated frequencies. We have automatized this procedure and adopted it as a good compromise between predictions accuracy and computational costs.

For a given stable geometry, the nuclear magnetic shielding constants σ have been calculated, using the GIAO technique [25] to ensure gauge independence, for each nuclei of each gas-phase and solvated polyamine molecule under investigation as well as for the protons of the tetra methyl silane (TMS) molecule chosen as reference for shielding parameters. Chemical shifts for the protons bound to C atoms in a polyamine, which are data directly comparable to experimental measures, have been obtained from $\delta = \sigma_{TMS} - \sigma$. Indirect spin–spin coupling constants J have also been evaluated for a given stable geometry. To take into account the contribution on the calculated values of the NMR spin-Hamiltonian parameters from the structures higher in energy than the most stable one, we have assumed Boltzmann distributions.

All calculations have been carried out by use of the computational package Gaussian 03 [26] and the graphical interface Gabedit [27]. Using calculated values for the chemical shifts and the indirect spin–spin constants, the NMR spectrum of each polyamine has been simulated through a home-made code developed following the conventional way of solving the spin-Hamiltonian [28] and included in the graphical interface Gabedit.

3. Choice of functional and basis set

In our previous investigations [16,17] of metabolites we assumed, from a limited investigation involving four basis sets of Pople's type, that the B3LYP/6-311++G$**$ level of theory is a good compromise between accuracy and cost. For the completeness of present work, the corresponding calculated lowest-energy structures are reproduced in Fig. 1. The groups of protons having the same calculated chemical shift (noted A, B, C, D) are defined in Table 1 as well as the various spin–spin coupling constants J^a (a = A, B, C, D, E), for the three metabolites: putrescine, spermidine and spermine under investigation. In order to check further the pertinence of our choice functional/basis set we performed calculations with the PBE [29] and OPBE [30] functionals in combination with the eight basis sets: pcn (n = 0.3) [31,32] and pcJn (n = 0.3) [33].

For the gas-phase putrescine, comparing the results obtained with the 6-311++G$**$ basis set (size = 324 primitive Gaussian functions) and with the largest one considered here i.e. the pcJ3 (size = 1374), pointed out only rather small differences. For instance, the difference δ_B–δ_A which determines the calculated relative position of the two multiplets of the NMR spectrum of putrescine, was calculated to be 1.33 ppm at the B3LYP level with both the 6-311++G$**$ and pcJ3 basis sets and 1.34 ppm at both PBE and OPBE levels with the pcJ3 basis set. For spermidine, we compared the δ_a values (a = A, B, C, D) calculated at the level B3LYP/6-311++G$**$ (size = 531) with those obtained from the B3LYP, PBE and OPBE functionals using the pcJ2 basis set (size = 1261) which is the largest one for which calculations were performed for the isolated molecule. The δ_a results were seen to lie inside the disper-

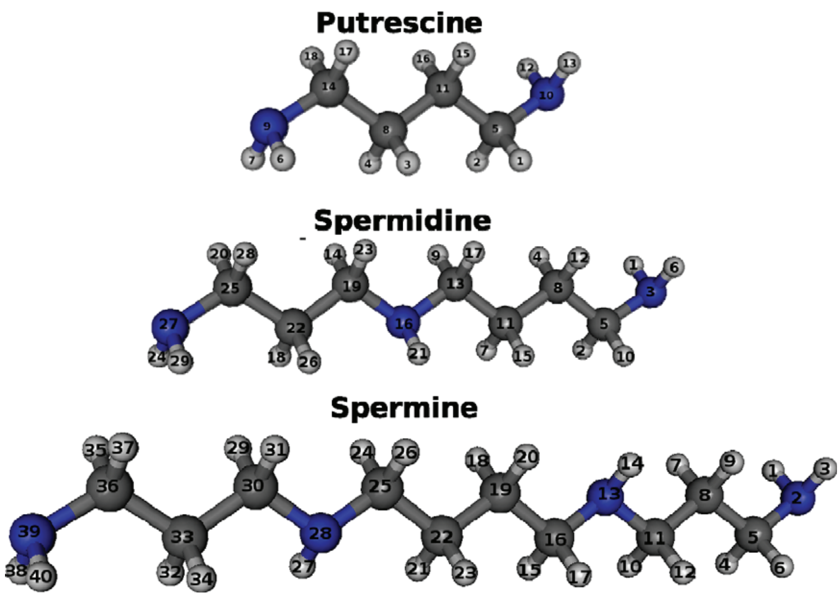

Fig. 1. Lowest-energy structure for the solvated putrescine, spermidine and spermine molecules, determined at the B3LYP/6-311++G$**$ level of theory. N atoms in blue, C atoms in black, H atoms in grey. (For interpretation of the references to color in this figure legend, the reader is referred to the web version of this paper.)

Table 1
Groups of protons (labelled a = A, B, C, D) having the same chemical shifts and definition of the various J^a (a = A, B, C, D, E) spin–spin coupling constants for the three molecules: putrescine, spermidine and spermine.

Group	Putrescine Proton labels[a]	Spermidine Proton labels[a]	Spermine Proton labels[a]
Chemical shifts			
A	3, 4, 15, 16	4, 7, 12, 15	18, 20, 21, 23
B	1, 2, 17, 18	18, 26	7, 9, 32, 34
C		9, 14, 17, 23	10, 12, 15, 17, 24, 26, 29, 31
D		2, 10, 20, 28	4, 6, 35, 37
J spin–spin coupling constants			
J^A	$J_{(1,2)\times(15,16)} \equiv J_{(3,4)\times(17,18)}$[a]	$J_{(2,10)\times(4,12)}$	$J_{(4,6)\times(7,9)} \equiv J_{(32,34)\times(35,37)}$
J^B	$J_{(3,4)\times(15,16)}$	$J_{(4,12)\times(7,15)}$	$J_{(7,9)\times(10,12)} \equiv J_{(29,31)\times(32,34)}$
J^C		$J_{(7,15)\times(9,17)}$	$J_{(15,17)\times(18,20)} \equiv J_{(21,23)\times(24,26)}$
J^D		$J_{(14,23)\times(18,26)}$	$J_{(18,20)\times(21,23)}$
J^E		$J_{(18,26)\times(20,28)}$	

[a] The shortened notation $J_{(i,k)\times(j,l)}$ stands for $J_{i,j} = J_{i,l} = J_{k,j} = J_{k,l}$. See Fig. 1 for the proton labels of the three polyamines, respectively.

sion range of the results obtained at the B3LYP or PBE or OPBE/pcJ2 levels of theory. A similar result was obtained for the isolated spermine when comparing the δ_a (a = A, B, C, D) results obtained at the B3LYP/6-311++G** level of theory with those obtained from the three functionals B3LYP, PBE and OPBE using the pc2 basis set (size = 1280) which is the largest one for which calculations were performed for this molecule.

Contrarily to what was observed for the δ calculations where the B3LYP/6-311++G** results were seen to be quite close to those involving the largest basis set considered, J results were seen to be significantly different. For putrescine, the $J^{A,B}$ values are $\sim$7 Hz when calculated using the 6-311++G** basis set while they reach $\sim$9 Hz when calculated using the pcJ3 basis set, and this for any of the three functionals considered in the present study. Similar results were obtained for the five J^a (a = A, B, C, D, E) numerical values for spermidine and the four J^a (a = A, B, C, D) numerical values for spermine (see Table 1 for the definition of A, B, C, D, E). At this step of our theoretical investigation, we have no criterion to select the correct values of J and then the correct level of theory. Nevertheless the comparison with experiment (see Section 5) will demonstrate that J values $\sim$7 Hz better reproduce experimental structures in NMR spectra.

In conclusion, our choice of the B3LYP/6-311++G** level of theory appears as a reasonable compromise between accuracy and cost for the further calculations of the NMR spin-Hamiltonian parameters for a large number of isomers of the three polyamines.

4. Contribution of isomers in the calculation of NMR spin-Hamiltonian parameters

Up to now we have considered only the lowest-energy geometry of each of the polyamines when calculating the δ and J NMR parameters. In fact during the search procedure described in Section 2, we found many isomer structures at DFT/6-31G* level lying in a given energy gap ΔE_{max} above the lowest one, that may affect the results. The number of isomers to be taken into account grows with the size of the molecule, as expected.

For each polyamine, we first chose a value for ΔE_{max} from which we filtered the isomer structures obtained at the DFT/6-31G* level i.e. only isomer structures with a relative energy $<\Delta E_{max}$ were selected. All these structures were re-optimized at the DFT/6-311++G** level. Then we arranged these isomers following increasing relative energies. For each retained geometry (having a relative energy ΔE_i, i = 0, 1, ..., N) we calculated the chemical shifts and the spin–spin coupling constants. The contribution from the ith conformer to the averaged values of δ and J is evaluated under the assumption of Boltzmann distribution:

$$P^{(i)}_{\text{averaged}} = \frac{\sum_{j=0,i} P_j e^{-\Delta E_j/kT}}{\sum_{j=0,i} e^{-\Delta E_j/kT}}, \quad i = 0,\ 1,\ \ldots\ N \tag{1}$$

where N is the number of stable structures to be taken into account and P stands for δ or J. ΔE_j is the relative energy of the isomer j, k is the Boltzmann constant and T is the temperature. In present work we chose T = 300 K, close to the ambient temperature of experiments. Proceeding in that way allows us to point out the convergence of the results.

For putrescine we chose ΔE_{max} = 3.5 kcal/mol and then 44 isomers are to be taken into account. Averaged chemical shifts δ^{av}_A and δ^{av}_B were seen to converge for ΔE_{conv} = ~2.3 kcal/mol. For spermidine we chose ΔE_{max} = 5 kcal/mol and then 230 isomers are to be taken into account. Averaged chemical shifts δ^{av}_A, δ^{av}_B, δ^{av}_X and δ^{av}_D were seen to converge for $\Delta E = \Delta E_{conv}$ = ~3.5 kcal/mol. For spermine we chose ΔE_{max} = 6.5 kcal/mol and then 300 isomers are to be taken into account. Averaged chemical shifts δ^{av}_A, δ^{av}_B, δ^{av}_X and δ^{av}_D were seen to converge for $\Delta E = \Delta E_{conv}$ = ~5.8 kcal/mol. The evolution of the averaged chemical shifts versus the relative energy, using the 6-311++G** basis set are drawn in Fig. 2 for the spermidine chosen as example, the same evolution trends being observed for the solvated putrescine and spermine. Chemical shift results evaluated at the B3LYP/6-311++G** level of theory, including the averaged values as well as the values for the lowest-energy structure (quoted as δ^0) are gathered in Table 2 for the three solvated polyamines. The contributions from isomers, evaluated through the root mean square deviations rms = $\sqrt{\sum_{i=1}^{M} \frac{(\delta^0_i - \delta^{av}_i)^2}{M}}$ where M is the number of δ values (M = 2 for putrescine, M = 4 for spermidine and spermine), are seen to be larger for putrescine (rms = 0.14 ppm) and spermidine (rms = 0.09 ppm) than for spermine (rms = 0.02 ppm). This is consistent with the fact that the energy difference between the first isomer and the lowest-energy conformer is ~0.013 eV for both putrescine and spermidine while it is ~0.1 eV for spermine.

The convergence of the J constants with the increasing values of the relative energy was also evidenced for the solvated putrescine, spermidine and spermine molecules. It is illustrated in Fig. 3 for the spermidine chosen as example. Convergence is reached for the same value of the relative energy ΔE_{conv} than for chemical shifts. Once more, contributions from isomers to the averaged values of J are larger for putrescine and spermidine with rms deviations of 0.58 Hz than for spermine with rms = 0.23 Hz. Spin–spin coupling constants evaluated at the B3LYP/6-311++G** level of theory, including the averaged values (quoted as J_{av}) as well as the values for the lowest-energy structure (quoted as J_0) are gathered in Table 3 for the three solvated polyamines.

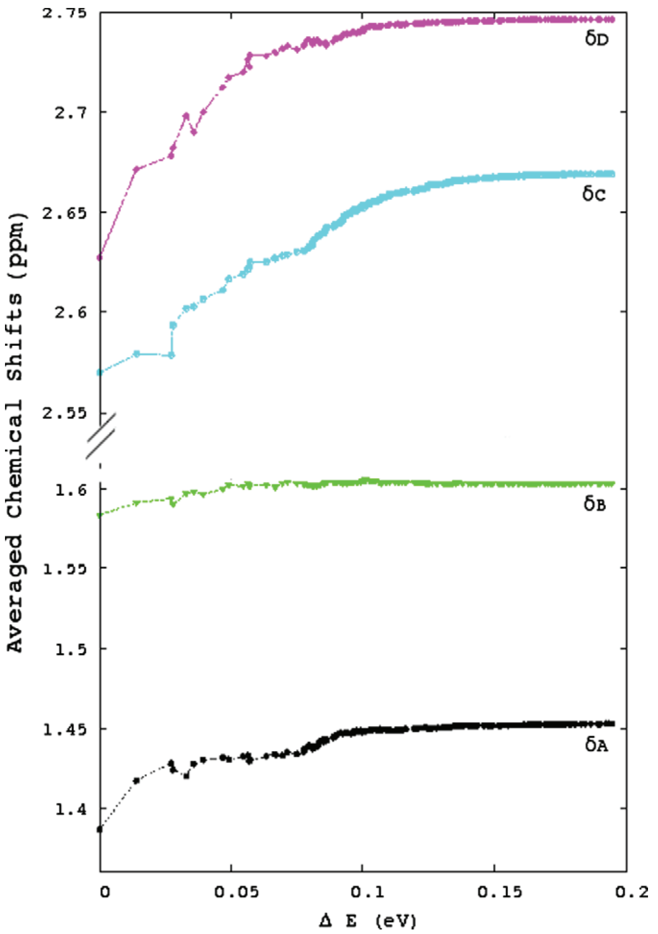

Fig. 2. Evolution versus the relative energy of isomers of the calculated δ_A^{av}, δ_B^{av}, δ_C^{av}, δ_D^{av} Boltzmann weighted average chemical shift values of the solvated spermidine evaluated at the B3LYP/6-311++G** level of theory.

Table 2
Calculated chemical shifts at the B3LYP/6-311++G** level of theory within the SCRF-PCM model, for the three solvated polyamines: δ_a^{av} averaged values and δ_a^0 values for the lowest-energy geometry together with δ_a^{exp} experimental values (see text for the definition of the various a = A,B,C,D ^{1}H groups). All δ values in ppm. The number N of isomers taken into account as well as the relative energy for which convergence is reached ΔE_{conv} are quoted.

	Putrescine	Spermidine	Spermine
N	44	230	300
ΔE_{conv} (kcal/mol)	2.3	3.5	5.8
δ_A^{av}	1.410	1.453	1.529
δ_B^{av}	2.734	1.604	1.600
δ_C^{av}	–	2.669	2.619
δ_D^{av}	–	2.746	2.663
δ_A^0	1.264[a]	1.387	1.509
δ_B^0	2.594	1.584	1.594
δ_C^0	–	2.570	2.590
δ_D^0	–	2.627	2.634
δ_A^{exp}	1.603	1.519	1.540
δ_B^{exp}	2.826	1.664	1.681
δ_C^{exp}	–	2.634	2.652
δ_D^{exp}	–	2.686	2.705

[a] Previous results [16] for the δ_A^0 and δ_A^0 of putrescine were obtained within the C-PCM [35] model.

5. Comparison with experiment and discussion

Experimental ^{1}H NMR spectra were acquired at 400 MHz for the three molecules in solution in D_2O [16,17]. The ^{1}H NMR experimental spectrum of solvated putrescine displays two structures, one triplet and one multiplet. Four structures are present for both the solvated spermidine and spermine with two overlapping multiplets on the left part of the experimental spectra. The number of observed multiplets is in agreement with the number of calculated chemical shifts. From experimental spectra, experimental values for the various chemical shifts have been extracted and the values are recalled in Table 2 for the three polyamines. For the two δ_A and δ_B values of putrescine the errors (defined as the difference between experimental and calculated values) are 0.34 and 0.23 ppm, respectively for the calculations with the lowest-energy geometry alone with a root mean square error rms = 0.29 ppm, while these errors are significantly reduced (0.19, 0.09 ppm) with rms = 0.15 ppm by taking into account averaged contributions from isomers. This agreement with experiment is quite satisfying. For the four values δ_A, δ_B, δ_C and δ_D of spermidine the errors are smaller than for putrescine. They range from 0.06 to 0.13 ppm (rms = 0.09 ppm) for the lowest-energy structure and are reduced to 0.04–0.06 ppm (rms = 0.05 ppm) by taking into account the contributions from isomers providing a good agreement with experiment. A good agreement with experimental values is also obtained for the four values δ_A, δ_B, δ_C and δ_D of solvated spermine with rms = 0.07 ppm for the lowest-energy structure and rms = 0.05 ppm when taking into account the averaged contribution from the isomers. For the 10 δ values of the three polyamines,

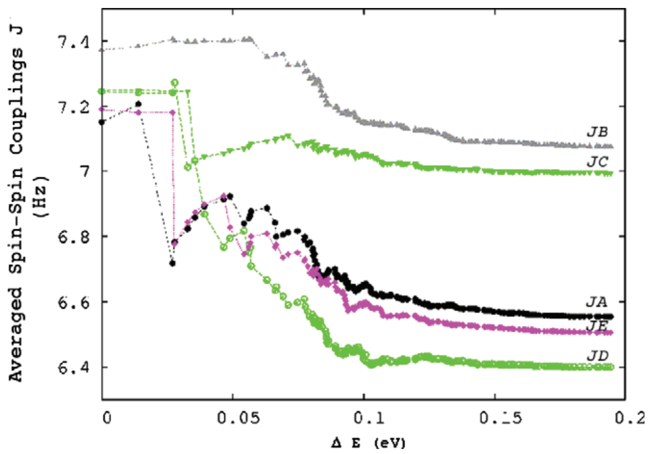

Fig. 3. Evolution versus the relative energy of isomers of the Boltzmann weighted average spin–spin coupling constant values of the solvated spermidine evaluated at the B3LYP/6-311++G** level of theory.

Table 3
Calculated indirect spin–spin coupling constants at the B3LYP/6-311++G** level of theory within the SCRF-PCM model, for the three solvated polyamines: J_{av}^Z averaged values and J_0^Z values for the lowest-energy geometry (see text for the definition of the various Z = A, B, C, D, E ^{1}H groups). All J values in Hz.

	Putrescine	Spermidine	Spermine
J_{av}^A	6.43	6.55	7.07
J_{av}^B	6.94	7.08	7.14
J_{av}^C	–	6.99	6.86
J_{av}^D	–	6.40	7.27
J_{av}^E	–	6.51	–
J_0^A	7.14[a]	7.15	7.19
J_0^B	7.32	7.37	7.24
J_0^C	–	7.25	7.25
J_0^D	–	7.24	7.43
J_0^E	–	7.19	–

[a] Previous results [16] for the J_0^A and J_0^B of putrescine were obtained within the C-PCM [35] model.

the rms error is 0.15 ppm for the lowest-energy structures and 0.08 ppm when taking into account the isomer effects.

In order to evidence the correlation between experimental and calculated results, we used, as often done, a linear scaling procedure [34] in which $\delta_{calc} = a + b\ \delta_{exp}$, taking into account the 10 δ values for the three polyamines treated together. For the solvated polyamines we obtained $\delta_{calc} = -0.170 + 1.025\ \delta_{exp}$ with a regression coefficient $R = 0.988$ for the lowest-energy structures and $\delta_{calc} = -0.163 + 1.054\ \delta_{exp}$ with $R = 0.995$ when contribution from isomers are included. From these linear scalings, the rms deviations reduce from 0.15 ppm (no scaling) to 0.08 ppm for the lowest-energy structures and from 0.08 ppm to 0.06 ppm when isomers are taken into account.

For the solvated putrescine for which the less satisfying chemical shift results have been obtained we have performed two more calculations taking into account the averaged contribution from isomers using the PBE and OPBE functionals with the 6-311++G** basis set. Results are presented in Table 4 together with the results previously obtained for the lowest-energy structure. When comparing with the δ_A and δ_B experimental data, the best results when considering only the lowest-energy structure are obtained with the PBE functional with a rms error of 0.26 ppm, to be compared to rms = 0.34 ppm for B3LYP and rms = 0.33 for OPBE. When considering the weighted contribution from the isomers, the best results are obtained for the OPBE functional with rms = 0.09 ppm to be compared to rms = 0.15 ppm for B3LYP and rms = 0.30 for PBE. Nevertheless the experimental relative position of the two multiplets $\Delta\delta = \delta_B - \delta_A = 1.22$ ppm, is somewhat better reproduced by B3LYP calculations ($\Delta\delta^{av} = 1.32$ ppm) than PBE ($\Delta\delta^{av} = 1.38$ ppm) or OPBE ($\Delta\delta^{av} = 1.37$ ppm) ones.

We have not been able to extract experimental values for the spin–spin coupling constants from our *in vitro* ^{1}H NMR spectra of the polyamines in solution in D_2O, due to their complexity. To compare these data with experiment we have simulated the ^{1}H NMR spectra and compare the simulated and experimental multiplet structures so obtained. Comparative results are presented in Fig. 4 for the multiplet of the solvated putrescine at $\delta = 2.826$ ppm, calculated using the J^A_{av} and J^B_{av} values of the spin–spin coupling constants reported in Table 4. Calculations from the B3LYP/6-311++G** level are seen to better reproduce the five peaks of the multiplets than the PBE and OPBE ones. The multiplet structure calculated with the *J* values from B3LYP/pcj3 level of theory which were seen to be ~9 Hz, is also drawn in Fig. 4. It is clear that these values do not allow a correct description of the multiplet. Similar comparisons were performed for each multiplet of each molecule, leading to similar results as those illustrated for the putrescine multiplet.

Table 4
Chemical shifts (ppm) for the solvated putrescine calculated at various level of theory within the SCRF-PCM model.

Level of theory	δ_A^{exp}	δ_A^0	δ_A^{av}	δ_B^{exp}	δ_B^0	δ_B^{av}
	1.603			2.826		
B3LYP/6-311++G**		1.264	1.410		2.594	2.734
PBE/6-311++G**		1.284	1.812		2.639	3.188
OPBE/6-311++G**		1.203	1.579		2.572	2.950

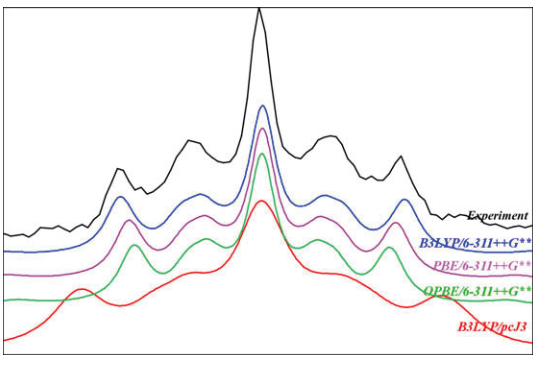

Fig. 4. Comparison with experiment of the structure of the multiplet of the solvated putrescine (situated at $\delta = 2.826$ ppm), calculated at different levels of theory.

6. Conclusion

A theoretical investigation, based on density functional methods, of the δ and *J* NMR spin-Hamiltonian parameters have been performed for the protons attached to the carbon atoms of the three polyamines: putrescine, spermidine and spermine involved in prostate tissue. From the trends of the calculated results completed by the comparison with the ^{1}H NMR experimental spectra of these molecules, we conclude that δ and *J* values calculated at the B3LYP/6-311++G** level of theory reproduce quite well the corresponding experimental data. Results are excellent for the four chemical shifts of spermidine and spermine with rms errors of 0.05 ppm when comparing with experiment. Taking into account the Boltzmann weighted contributions from conformers reduces the rms errors by ~40% for the spermidine and by ~30% for the spermine. For the two chemical shifts of putrescine the agreement remains satisfying with a rms error of 0.15 ppm, reduced by ~50% by converged isomer contributions.

Acknowledgments

This work was supported by the E.U. Marie Curie Research Network MRTNCT-2006-035801, 2006–2010. The authors thank the “Pôle Scientifique de Modélisation Numérique (PSMN)” at Lyon, France, for generous computational facilities.

References

[1] J.F. Jansen, W.H. Backes, K. Nicolay, M.E. Kooi, Radiology 240 (2006) 318.
[2] V. Govindaraju, K. Young, A.A. Maudsley, NMR Biomed. 13 (2000) 129.
[3] M.A. Thomas, T. Lange, S.S. Velan, R. Nagarajan, S. Roman, A. Gomez, D. Margolis, S. Swart, R.R. Raylman, R.F. Schulte, P. Boesiger, Magn. Reson. Mater. Phys. 21 (2008) 443.
[4] Y. Mazaheri, A. Shukla-Dave, A. Muellner, H. Hricak, Magn. Reson. Mater. Phys. 21 (2008) 379.
[5] P. Swindle, S. Ramadan, P. Stanwell, S. McCredie, P. Russell, C. Mountford, Magn. Reson. Mater. Phys. 21 (2008) 423.
[6] T. Lange, R.F. Schulte, P. Boesiger, Magn. Reson. Med. 59 (2008) 966.
[7] P. Younès, N. Chemla, B. Hamzé, J. Mani, J.-F. Naouri, Ann. Urol. 41 (2007) 145.
[8] A. Shukla-Dave, H. Hricak, C. Moskowitz, N. Ishill, O. Akin, K. Kuroiwa, J. Spector, M. Kumar, V.E. Reuter, J.A. Koutcher, K.L. Zakian, Radiology 245 (2007) 499.
[9] M.G. Swanson, D. Vigneron, Z.L. Tabatabai, R.G. Males, L. Schmitt, P.R. Carroll, J.K. James, R.E. Hurd, J. Kurhanewicz, Magn. Reson. Med. 50 (2003) 944.
[10] E.M. Lenz, B.F. Hägele, I.D. Wilson, S.J. Simpson, Insect Biochem. Mol. Biol. 32 (2001) 51.
[11] C.D. Meo, D. Capitani, L. Mannina, E. Brancaleoni, D. Galesso, G.D. Luca, V. Crescenzi, Biomacromoles 7 (2006) 1253.
[12] W. Willker, U. Flögel, D. Leibfritz, NMR Biomed. 11 (1998) 47.
[13] H. Fukui, Nucl. Magn. Reson. 38 (2009) 166.
[14] L.B. Casabianca, A.C. de Dios, J. Chem. Phys. 128 (2008) 052201.
[15] T. Helgaker, M. Jaszunski, M. Pecul, Prog. Nucl. Magn. Reson. Spectrosc. 53 (2008) 249.
[16] A.R. Allouche, D. Graveron-Demilly, F. Fauvelle, M. Aubert-Frécon, Chem. Phys. Lett. 466 (2008) 219.
[17] Z. Atieh, A.R. Allouche, F. Fauvelle, D. Graveron, M. Aubert-Frécon, Meas. Sci. Technol. 20 (2009) 104024.
[18] A.D. Becke, J. Chem. Phys. 98 (1993) 5648.
[19] C. Lee, W. Yang, R.G. Parr, Phys. Rev. B 37 (1988) 785.
[20] R. Krishnan, J.S. Binkley, R. Seeger, J.A. Pople, J. Chem. Phys. 72 (1980) 650.
[21] S. Miertus, E. Scrocco, J. Tomasi, Chem. Phys. 55 (1981) 117.
[22] V. Barone, M. Cossi, J. Tomasi, J. Chem. Phys. 107 (1997) 3210.
[23] W.C. Swope, H.C. Andersen, P.H. Berens, K.R. Wilson, J. Chem. Phys. 76 (1982) 637.

[24] J.J.P. Stewart, J. Mol. Model. 13 (2007) 1173.
[25] J.R. Cheeseman, G.W. Trucks, T.A. Keith, M.J. Frisch, J. Chem. Phys. 104 (1996) 5497.
[26] M.J. Frisch et al., Gaussian 03, Revision C.02, Gaussian, Inc., Wallingford, CT, 2004.
[27] A.R. Allouche, Gabedit is a graphical user interface for various computational chemistry packages. Available from: <http://gabedit.sf.net>.
[28] J.D. Roberts, An Introduction to the Analysis of Spin–Spin Splitting in High-Resolution Nuclear Magnetic Resonance Spectra, W.A. Benjamin, Inc., New York, 1961.
[29] J.P. Perdew, K. Burke, M. Ernzerhof, Phys. Rev. Lett. 77 (1996) 3865.
[30] N.C. Handy, A.J. Cohen, Mol. Phys. 99 (2001) 403.
[31] F. Jensen, J. Chem. Phys. 115 (2001) 9113. erratum J. Chem. Phys. 116 (2002) 3502.
[32] F. Jensen, J. Chem. Phys. 116 (2002) 7372.
[33] F. Jensen, J. Chem. Theory Comput. 2 (2006) 1360.
[34] D.B. Chesnut, Rev. Comput. Chem. 8 (1996) 245.
[35] M. Cossi, N. Rega, G. Scalmani, V. Barone, J. Comput Chem. 24 (2003) 669.

Chemical Physics Letters 492 (2010) 297–301

Contents lists available at ScienceDirect

Chemical Physics Letters

journal homepage: www.elsevier.com/locate/cplett

DFT calculations of ^{1}H chemical shifts, simulated and experimental NMR spectra for sarcosine

Z. Atieh [a], A.R. Allouche [a,*], A. Lazariev [b], D. Van Ormondt [c], D. Graveron-Demilly [b], M. Aubert-Frécon [a]

[a] Université de Lyon, F-69622 Lyon, France; Université Lyon 1, Villeurbanne; CNRS, UMR 5579, LASIM, France
[b] Université de Lyon, F-69622 Lyon, France; Université Lyon 1, Villeurbanne; CNRS, UMR 5220, INSERM U630, CREATIS-LRMN, France
[c] Applied Physics Department, Delft University of Technology, Delft, The Netherlands

ARTICLE INFO

Article history:
Received 24 February 2010
In final form 20 April 2010
Available online 24 April 2010

ABSTRACT

Chemical shifts δ have been calculated for the ^{1}H attached to carbon atoms of sarcosine. Eight levels of theory within the DFT approach were used, mixing the four functionals B3LYP, PBE, OPBE, PBE0 and the two basis sets 6-311++G** and pcJ2. Boltzmann weighted isomer effects have been evaluated. By comparison of the ^{1}H NMR spectrum simulated from the calculated δ and the experimental one that we acquired at 300 MHz, the B3LYP/6-311++G** calculation was seen to be a good compromise between accuracy and cost. Zero-point vibrational corrections, estimated using a second-order perturbation approach, increase the agreement with experiment.

1. Introduction

Sarcosine is the *N*-methyl derivative of glycine. It is a natural amino-acid found in muscles and other body tissues. Very recently [1], sarcosine was identified as a differential metabolite that was highly increased during prostate cancer progression to metastasis. Sarcosine levels seemed to control the invasiveness of the cancer. This metabolite can be detected non-invasively in urine and may distinguish between slow-growing and aggressive prostate cancers. Changes in concentration of metabolites in body tissues could be detected by *in vivo* Magnetic Resonance Spectroscopy (MRS) [2], a non-invasive powerful technique for detecting and quantifying bio-markers of diseases. The analysis of MRS-signals obtained from patients is based on a database of prior knowledge about MRS-signals of metabolites which are simulated quantum–mechanically with the use of the spin Hamiltonian parameters: chemical shifts δ and indirect spin–spin coupling constants J. Literature values of δ and J are used, when available, mainly from experimental determination.

Being currently involved in calculations of NMR spin Hamiltonian parameters for metabolites [3–5], in order to produce reliable values of these parameters from which NMR spectra could be simulated and used further in quantitation procedures, we investigated sarcosine in the present study.

2. Computational approaches

For the sarcosine molecule ($C_3H_7NO_2$) in gas phase and in water solution, four calculation steps have been carried out: (1) the determination of stable geometries lying in a given range of relative energy above the lowest one, (2) the determination of the chemical shifts for the protons attached to carbon atoms, (3) the estimation of zero-point vibrational corrections on these chemical shifts, and (4) the simulation of the ^{1}H NMR spectrum of the sarcosine from the calculated ^{1}H chemical shifts. The solvated sarcosine has been described by the self-consistent reaction field theory (SCRF) based on the Polarisable Continuum Model (PCM) [6,7]. All calculations have been carried out by use of the computational package Gaussian03 [8] and the graphical interface Gabedit [9].

2.1. Conformational search

To search the lowest-energy structure of the sarcosine as well as the stable isomers lying in a given relative energy range above the lowest one, we performed first a molecular dynamics calculation for the gas-phase molecule (constant energy NVE, velocity Verlet algorithm [10]) with the semi-empirical PM6 potential [11], in order to select initial geometries. The simulated time was 10 ps, the time step was 1.0 fs and the temperature was 5000 K in order to provide a large exploration of the potential energy surface. We have selected 5000 geometries during the simulation process. Each selected geometry was further optimized at the PM6 level and very similar structures were removed. Twenty-two geometries were obtained in that way, each of them was further used as initial geometry in an energy minimization procedure

* Corresponding author. Fax: +33 4 72 43 15 07.
E-mail address: allouche@lasim.univ-lyon1.fr (A.R. Allouche).

0009-2614/$ - see front matter © 2010 Elsevier B.V. All rights reserved.
doi:10.1016/j.cplett.2010.04.054

performed at the B3LYP/6-31G* level, for the solvated molecule. Very similar structures were removed and only the stable geometries (i.e. with no imaginary calculated frequencies) which lie in a given energy gap of 3.5 kcal/mol above the lowest one were retained. At the end of the process eight geometries were obtained. Finally, these eight structures were used as initial geometries in DFT optimization calculations. Eight different levels of theory were considered, using the four functionals: B3LYP [12,13], PBE [14], OPBE [15], PBE0 [16] with the two basis sets: 6-311++G** [17] and pcJ2 [18]. Note that for sarcosine the 6-311++G** basis set contains 181 functions while the pcJ2 basis set contains 474 functions. As an example, the lowest-energy structure of the solvated sarcosine determined at the B3LYP/6-311++G** level of theory is displayed in Fig. 1.

2.2. Chemical shifts calculation

For the most stable geometry of solvated sarcosine, the isotropic nuclear magnetic shielding constants σ have been calculated at each level of theory considered, using the GIAO technique [19] to ensure gauge independence, for the protons attached to carbon atoms, i.e. the two protons (labelled 1, 7 in Fig. 1) of the methylene group and the three protons (labelled 11–13 in Fig. 1) of the methyl group. A similar calculation was performed at the same level of theory for the protons of the tetra methyl silane (TMS) molecule, chosen as reference for the shielding parameters, in order to obtain the chemical shifts for the protons under consideration through $\delta = \sigma_{TMS} - \sigma$. It should be noted that, having performed calculations for a motionless molecule, the numerical σ values obtained were not exactly identical for the two ^1H of the methylene group as well as for the three ^1H of the methyl group, contrarily to what should have been expected. This was bypassed by averaging the σ values for the ^1H of CH_2 and the ^1H of CH_3, respectively, so that only two different values: δ_A {11, 12, 13} and δ_B {1, 7} were obtained.

To take into account the contribution on the calculated values of the ^1H chemical shifts under consideration, from the seven structures higher in energy than the most stable conformer, the chemical shifts $\delta^i_{A,B}$ were evaluated for all the isomers i. Then, the Boltzmann weighted average $\delta^{av}_{A,B}$ over the stable conformers were evaluated through:

$$\delta^{av}_{A,B} = \frac{\sum_{i=1}^{8} \delta^i_{A,B}\, e^{-\Delta E_i/kT}}{\sum_{i=1}^{8} e^{-\Delta E_i/kT}} \tag{1}$$

where ΔE_i is the relative electronic energy of the isomer i, k is the Boltzmann constant and T is the temperature. In the present work we chose $T = 300$ K, close to the ambient temperature of the experiments. These calculations were performed for each of the eight levels of theory considered.

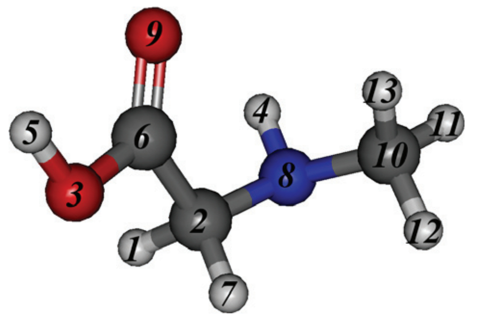

Fig. 1. Lowest-energy structure of the solvated sarcosine, calculated at the B3LYP/6-311++G** level of theory. The numbering of atoms is quoted. C atoms in black, N in blue, O in red and H in grey. (For interpretation of the references in color in this figure legend, the reader is referred to the web version of this article.)

Note that the calculated indirect spin–spin coupling constant J are $\sim$0 (<0.02 Hz), apart from large negative values for the protons of the same group.

2.3. Estimation of vibrational effects

In order to account for the correction to the nuclear magnetic shielding due to the zero-point vibrational motion we used second-order perturbation theory with the sarcosine in its equilibrium geometry as the unperturbed system. Following [20], the zero-point vibration correction (ZPVc) to the nuclear magnetic shielding of a given nucleus is calculated through:

$$\sigma_{ZPVc} = \frac{1}{4}\sum_K \frac{1}{\omega_K}\frac{d^2\sigma}{dQ_K^2} - \frac{1}{4}\sum_K \frac{1}{\omega_K^2}\frac{d\sigma}{dQ_K}\sum_L \frac{F_{KLL}}{\omega_L} \tag{2}$$

Q_K is the normal coordinate K with an harmonic frequency ω_K, and the cubic force constant F_{KLL} is defined as the third derivative of the electronic energy E with respect to the normal coordinates $Q_K,\ Q_L,\ Q_L$. The sums over K and L run over all the normal vibrational modes of the sarcosine, i.e. 33 terms are involved. The vibrational average of σ is given by: $\sigma_{vib} = \sigma + \sigma_{ZPVc}$, where σ is the isotropic shielding for the non-vibrating equilibrium geometry evaluated in previous Section 2.2.

We had first to develop a specific code for the evaluation of σ_{ZVPc} through Eq. (2), that we have implemented in the version of Gaussian03 at our disposal (which does not allow the evaluation of vibrational effects upon NMR parameters). Harmonic frequencies and cubic force constants are evaluated through Gaussian03 at the equilibrium geometry. The first- and second-order derivatives of the nuclear shielding with respect to the normal coordinates are evaluated numerically with a step of 0.03 Å. In order to check our code we have calculated $\sigma_{vib,A(B)}$ for the two groups of protons under investigation for the isolated sarcosine at the HF/6-311++G** level of theory. The values obtained were found to be identical to those provided by the C_{FOUR} package [21] at the same level of theory.

Within the B3LYP/6-311++G** level of theory, selected as a good choice, $\sigma^{isol}_{vib,A(B)}$ vibrational averages have been calculated for the A and B group of protons of the isolated sarcosine. In order to calculate the $\delta_{vib,A(B)}$ vibrational average of the chemical shifts, the $\sigma_{vib,TMS}$ vibrational average was also calculated for the protons of the TMS. For the isolated sarcosine, calculations were performed for $\sigma^{i,isol}_{vib,A(B)}$ for each of the eight isomers previously determined. Boltzmann averaged values $\sigma^{av,isol}_{vib,A(B)}$ were then evaluated through a formula similar to Eq. (1) (with σ replacing δ) in which the energies E_i to be considered are the sum of the electronic energy determined in Section 2.1 plus the vibrational part evaluated as $\sum_K \frac{\hbar\omega_K}{2}$.

Solvent effects upon vibrational average of chemical shielding were approximated from the values for the isolated molecule corrected by adding for each isomer i the difference between the chemical shielding evaluated for the solvated $\sigma^i_{solv,A(B)}$ and for the isolated $\sigma^i_{isol,A(B)}$ non-vibrating molecule

$$\sigma^{i,solv}_{vib,A(B)} = \sigma^{i,isol}_{vib,A(B)} + \Delta\sigma^i_{solv,A(B)}$$

with $\Delta\sigma^i_{solv,A(B)} = \sigma^i_{solv,A(B)} - \sigma^i_{isol,A(B)}$.

Boltzmann averaged values $\sigma^{av,solv}_{vib,A(B)}$ were then obtained in the same way as for the isolated molecule.

3. Results

3.1. Nuclear magnetic shieldings and chemical shifts for non-vibrating molecules

Results for σ_{TMS}, σ_A, σ_B as well as δ_A and δ_B calculated for the four functionals and the two basis sets considered are displayed in Table 1 for the lowest-energy structure together with the δ_A^{av} and δ_B^{av} values including isomer effects. To compare the various results to each other we chose as criteria the root mean square deviation (rmsd) between two sets of results. First, we considered the basis set effect on the σ_{TMS}, σ_A and σ_B nuclear shielding values, for the lowest-energy structure of the solvated sarcosine. It is seen to be quite small for each of the four functionals considered. Using pcJ2 instead of 6-311++G** basis set results in systematically smaller values of σ either for TMS or for solvated sarcosine. The largest rmsd value for σ (rmsd $= \sqrt{(\sigma_{6\text{-}311{+}{+}G^{**}} - \sigma_{pcJ2})^2}$ for a given functional) is ~0.37 ppm. The largest rmsd value for δ (rmsd $= \sqrt{(\delta_{6\text{-}311{+}{+}G^{**}} - \delta_{pcJ2})^2}$ for a given functional) is ~0.13 ppm. Then, we considered the functional effect on the various δ values for the lowest-energy structure as well as when taking the isomers into account. The rmsd (rmsd $= \sqrt{\frac{\sum_{i=A,B}(\delta_i^{F1}-\delta_i^{F2})^2}{2}}$ where $F1$ and $F2$ stand for two different functionals among the four considered) are generally smaller for results including the eight isomers (rmsd < 0.18 ppm) than for the lowest-energy structure alone (rmsd < 0.27 ppm). The largest rmsd are observed for the PBE, OPBE and PBE0 compared to B3LYP, they reach 0.27 ppm. When comparing the results for the PBE, OPBE and PBE0 to each other, the rmsd are quite small with the largest one ~0.10 ppm.

3.2. Vibrational corrections to nuclear magnetic shieldings and chemical shifts

Zero-point vibrational corrections σ_{ZPVc} have been calculated at the B3LYP/6-311++G** level of theory for the ^{1}H of sarcosine and TMS, from which are deduced chemical shifts for the A and B group of protons of sarcosine. Values are gathered in Table 2 together with the values for the non-vibrating molecules and the Boltzmann averaged values taking into account isomer effects. For both molecules in their lowest-energy geometry, zero-point vibrational corrections decrease the ^{1}H nuclear magnetic shieldings by amounts ~0.7 ppm while the subsequent corrections on chemical shifts are 0.08 ppm for the ^{1}H of the methyl group (A) and 0.05 ppm for the ^{1}H of the methylene group (B). Taking into account isomer effects for the vibrating gas-phase molecule increases δ_A by 0.05 ppm and decreases δ_B by 0.08 ppm. Solvent effects are seen to be nearly negligible for δ_A (+0.02 ppm) while they are quite larger for δ_B (+0.23 ppm).

4. Comparison with experiment and discussion

We have acquired the ^{1}H NMR spectrum for sarcosine in solution in pure D_2O with TMS for chemical shift reference (0 ppm) on a 300 MHz avance 300DRX Bruker spectrometer (7 Tesla). From this spectrum, which displays two singlets (consistent with indirect spin–spin coupling constants J calculated to be zero), we measured the two chemical shifts $\delta_A^{exp} = 2.73$ ppm and $\delta_B^{exp} = 3.61$ ppm, in very good agreement with literature experimental results [22]. We compare calculated values for each level of theory with the corresponding experimental ones. Calculated rmsd $= \sqrt{\frac{\sum_{i=A,B}\left(\delta_i^F-\delta_i^{exp}\right)^2}{2}}$, where F is one of the functionals {B3LYP, PBE, OPBE, PBE0}, are recorded in Table 3 for the two basis sets. The agreement with experiment is better when taking into account isomers effects than when considering the equilibrium geometry alone at any of the levels of theory considered. The rmsd corresponding to calculations performed with the three functionals PBE, OPBE and PBE0 for any of the two basis sets are larger than those corresponding to the B3LYP calculations. They range from 0.18 ppm (isomers/PBE0/pcJ2) to 0.33 ppm (equilibrium geometry/OPBE/6-311++G** and equilibrium geometry/PBE/pcJ2) while for the B3LYP calculations the rmsd are in the range 0.14 ppm (isomers/B3LYP/pcJ2)–0.20 ppm (equilibrium geometry/B3LYP/6-311++G**). The best agreement with experiment, i.e. the smallest rmsd (0.14 ppm)

Table 1
Calculated nuclear magnetic shieldings and ^{1}H $\delta_{A,B}^j$ chemical shifts (in ppm) (j = 0: lowest-structure alone; j = av: isomer effects included) for the solvated sarcosine.

Calculation	σ_{TMS}	σ_A	σ_B	δ_A^0	δ_B^0	δ_A^{av}	δ_B^{av}
B3LYP	31.97[a]	29.52	28.41	2.45	3.57	2.50	3.51
	31.71[b]	29.24	28.07	2.48	3.64	2.54	3.59
PBE	31.50[a]	28.99	28.22	2.51	3.28	2.54	3.37
	31.13[b]	28.71	27.86	2.42	3.27	2.42	3.37
OPBE	31.59[a]	29.06	28.40	2.53	3.19	2.50	3.31
	31.32[b]	28.78	28.03	2.53	3.29	2.52	3.38
PBE0	31.80[a]	29.37	28.54	2.44	3.26	2.45	3.40
	31.56[b]	29.09	28.19	2.47	3.38	2.51	3.48
MP2	31.90[a]	29.46	28.41	2.44	3.49	2.46	3.45

[a] 6-311++G** basis set.
[b] pcJ2 basis set.

Table 3
Root mean square deviations (rmsd) from experimental values for the ^{1}H chemical shifts of solvated sarcosine evaluated at eight DFT levels of theory: functional/basis set. Results of a MP2/6-311++G** check calculation are also quoted. All values in ppm.

Calculation	Basis set	rmsd(δ^0)[a]	rmsd(δ^{av})[b]
B3LYP	6-311++G**	0.20	0.18
	pcJ2	0.18	0.14
PBE	6-311++G**	0.28	0.22
	pcJ2	0.33	0.28
OPBE	6-311++G**	0.33	0.27
	pcJ2	0.27	0.22
PBE0	6-311++G**	0.32	0.24
	pcJ2	0.25	0.18
MP2	6-311++G**	0.22	0.20

[a] The index 0 stands for the equilibrium geometry alone.
[b] The index ^{av} stands for isomers.

Table 2
Vibrational average of nuclear magnetic shieldings (and chemical shifts) for the sarcosine and TMS molecules, evaluated at the B3LYP/6-311++G** level of theory. All values in ppm.

Molecule	Isolated molecule, lowest-energy structure					Isomer and solvent effects		Experiment
	σ^0	σ^0_{ZVPc}	σ^0_{vib}	δ^0	δ^0_{vib}	$\delta^{av,isol}_{vib}$	$\delta^{av,solv}_{vib}$	δ^{exp}
TMS	31.97	−0.65	31.32					
Sarcosine A[a]	29.53	−0.73	28.80	2.44	2.52	2.57	2.59	2.73
Sarcosine B	28.60	−0.70	27.90	3.37	3.42	3.34	3.57	3.61

The index 0 stands for the lowest-energy geometry alone.
[a] Group A: {11, 12, 13}; group B: {1, 7}; see Fig. 1 for the ^{1}H labelling in brackets.

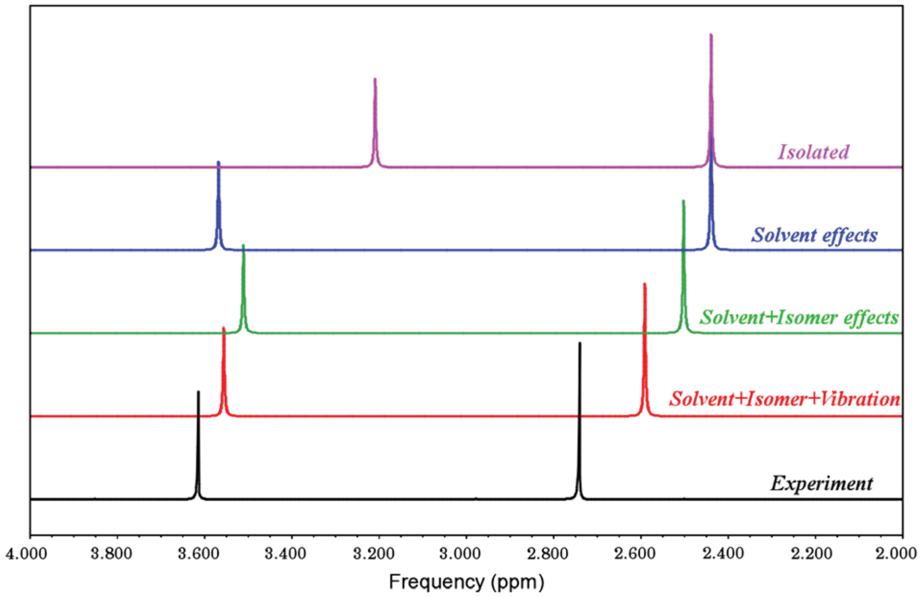

Fig. 2. Experimental and simulated ^1H NMR spectra of sarcosine under various assumptions, within the B3LYP/6-311++G** level of theory.

corresponds to the (isomers/B3LYP/pcJ2) calculation. Nevertheless the rmsd (0.18 ppm) for the (isomers/B3LYP/6-311++G**) calculation is also quite small. Then, taking into account the larger size of the pcJ2 basis set for sarcosine (474 functions) as compared to the 6-311++G** one (181 functions) the B3LYP/6-311++G** level of theory appears as the best compromise between cost and accuracy, among the eight type of calculations performed in the present study.

It should be noted that, sarcosine being a rather small molecule, we performed some restricted *ab initio* MP2 calculations using the 6-311++G** basis set in order to compare with the present B3LYP calculations. For the eight conformers previously considered, geometrical structures were optimized at the MP2/6-311++G** level of theory using as initial geometries those already determined at the B3LYP/6-311++G** one. Isotropic nuclear magnetic shieldings were calculated for the eight isomers of sarcosine as well as for TMS. MP2 calculations were performed using the computational package Gaussian09 [23]. Results are quoted in Table 1 for the solvated sarcosine. They are seen to be quite close to the B3LYP/6-311++G** corresponding ones. The root mean square deviations from experimental chemical shift values (quoted in Table 3) are only marginally larger than those corresponding to the B3LYP/6-311++G** calculations.

For the solvated sarcosine at the B3LYP/6-311++G** level of theory, taking into account vibrational effects improves significantly the agreement with experimental data as displayed in Table 2. The rmsd decreases from 0.18 ppm (isomers/non-vibrating molecule) to 0.10 ppm (isomers/vibrational average) which represents the best agreement achieved by present calculations.

We have simulated the ^1H NMR spectrum of sarcosine for calculated values of the chemical shifts for the proton groups A and B, evaluated under various assumptions:

- isolated non-vibrating molecule in its lowest-energy structure;
- solvated non-vibrating molecule in its lowest-energy structure;
- Boltzmann weighted isomer effects for the solvated non-vibrating molecule;
- Boltzmann weighted isomer effects for the solvated vibrating molecule.

These simulated spectra are compared to the experimental one in Fig. 2. Solvent effects for the non-vibrating molecule are seen to be larger for the ^1H of the methylene group than for the ^1H of the methyl group. Including isomer effects for the non-vibrating solvated molecule correct the two group of protons by similar but opposite amounts. Vibrational corrections are larger for the group A than for the group B and provide the best agreement with experiment.

5. Conclusion

A theoretical investigation, based on density functional methods, of the chemical shifts δ have been performed for the protons attached to the carbon atoms of the sarcosine. Four functionals and two basis sets were used in combination. By comparison with the experimental spectra, the best result was obtained at the B3LYP/pcJ2 level of theory. Nevertheless the B3LYP/6-311++G** was seen to be the best compromise between accuracy and cost. Zero-point vibrational corrections upon nuclear magnetic shieldings and chemical shifts have been evaluated through a second-order perturbational approach at the B3LYP/6-311++G** level of theory via a home-made code that we have implemented in the version of Gaussian03 at our disposal. These corrections were seen to increase the agreement between simulated and experimental NMR spectra of sarcosine.

References

[1] A. Sreekumar et al., Nature 457 (2009) 910.
[2] J.F. Jansen, W.H. Backes, K. Nicolay, M.E. Kooi, Radiology 240 (2006) 318.
[3] A.R. Allouche, M. Aubert-Frécon, D. Graveron-Demilly, PCCP 9 (2007) 3098.
[4] A.R. Allouche, D. Graveron-Demilly, F. Fauvelle, M. Aubert-Frécon, Chem. Phys. Lett. 466 (2008) 219.
[5] Z. Atieh, A.R. Allouche, F. Fauvelle, D. Graveron, M. Aubert-Frécon, Measur. Sci. Technol. 20 (2009) 104024.
[6] S. Miertus, E. Scrocco, J. Tomasi, Chem. Phys. 55 (1981) 117.
[7] V. Barone, M. Cossi, J. Tomasi, J. Chem. Phys. 107 (1997) 3210.
[8] M.J. Frisch et al., Gaussian03, Revision C.02, Gaussian Inc., Wallingford, CT, 2004.
[9] A.R. Allouche, Gabedit is a Graphical User Interface for Various Computational Chemistry Packages. <http://www.gabedit.sf.net>.
[10] W.C. Swope, H.C. Andersen, P.H. Berens, K.R. Wilson, J. Chem. Phys. 76 (1982) 637.
[11] J.J.P. Stewart, J. Mol. Model. 13 (2007) 1173.
[12] A.D. Becke, J. Chem. Phys. 98 (1993) 5648.
[13] C. Lee, W. Yang, R.G. Parr, Phys. Rev. B 37 (1988) 785.
[14] J.P. Perdew, K. Burke, M. Ernzerhof, Phys. Rev. Lett. 77 (1996) 3865.
[15] N.C. Handy, A.J. Cohen, Mol. Phys. 99 (2001) 403.
[16] C. Adamo, V. Barone, J. Chem. Phys. 110 (1999) 6158.

[17] R. Krishnan, J.S. Binkley, R. Seeger, J.A. Pople, J. Chem. Phys. 72 (1980) 650.
[18] F. Jensen, J. Chem. Theor. Comput. 2 (2006) 1360.
[19] J.R. Cheeseman, G.W. Trucks, T.A. Keith, M.J. Frisch, J. Chem. Phys. 104 (1996) 5497.
[20] M. Kaupp, M. Buhl, V.G. Malkin, Calculation of NMR and EPR Parameters, Wiley–VCH, 2004.
[21] J.F. Stanton et al., C_{FOUR}, A Quantum Chemical Program Package. <http://www.cfour.de>.
[22] <http://www.hmdb.ca/labm/servlet/labm.mlims.showFile?tbl=tbl_hnmrw&id=121821893165250904>.
[23] M.J. Frisch et al., GAUSSIAN09, Revision A.02, Gaussian Inc., Wallingford, CT, 2009.

Solvent, isomers and vibrational effects in DFT calculations for the NMR spin-Hamiltonian parameters of alanine

Calculated NMR parameters of alanine

Zeinab Atieh, Abdul-Rahman Allouche, Monique Aubert-Frécon
Université de Lyon,
Université Lyon 1, CNRS, UMR5579, LASIM
Villeurbanne, France

zatieh@lasim.univ-lyon1.fr; allouche@lasim.univ-lyon1.fr; frecon@lasim.univ-lyon1.fr

Danielle Graveron
Université de Lyon
Université Lyon1, CNRS, UMR5220, INSERM U630, CREATIS-LRMN
Danielle.Graveron@univ-lyon1.fr

Abstract—**DFT calculations of the ^{1}H chemical shifts and spin-spin coupling constant have been performed for the brain metabolite alanine. Contributions from solvent, isomers and zero-point vibrational corrections have been evaluated. Comparison with experiment demonstrate that all these effects are necessary to improve the agreement between calculated and experimental data.**

Keywords: ^{1}H spin Hamiltonian parameters; DFT/B3LYP calculations ; alanine.

I. Introduction

Hydrogen ^{1}H magnetic resonance spectroscopy (MRS) enables noninvasive in vivo quantification of brain metabolites [1]. The analysis of MRS-signals obtained from patients may be performed via methods which incorporate prior knowledge, including chemical shifts, spin-spin coupling constants …, about the metabolites that contribute to the ^{1}H NMR spectroscopic signals, recorded in a metabolite basis set. The knowledge of spin Hamiltonian parameters enables to build such a database. They may be obtained from measurements, as done for 35 brain metabolites [2], or from first principles by using quantum chemistry methods. Some years ago we undertook to calculate chemical shifts and coupling constants for metabolites. We have already investigated a brain metabolite: GABA [3] as well as prostate metabolites: polyamines [4-6] and sarcosine [7], using density functional theory (DFT) with the exchange-correlation B3LYP functional [8, 9]. In the present work, we calculate ^{1}H spin Hamiltonian parameters for the brain metabolite alanine, including solvent, isomers and vibrational effects.

II. Methodology

A. Conformational search

In our previous work on prostate polyamines [6] we have designed an automatic process by which to obtain the stable geometrical structures for the isomers of a given molecule. This is achieved in three steps: 1) a very large number of initial geometries are selected from a molecular dynamics (MD) calculation (constant energy NVE , Verlet velocity algorithm [10], semi-empirical PM6 potential [11]), 2) each selected geometry is optimized at the PM6 level and very similar structures are removed, 3) the remaining geometries are further optimized at the DFT/B3LYP/6-31G* level and very similar geometries are removed. The remaining structures at the end of step 3 are the isomer structures under search. For the present study of alanine, the parameters of the MD calculation were the following: a simulated time of 10 ps, a time step of 1.0 fs, a temperature of 3000K and 5000 geometries were selected at this step. At the end of the search process six isomers were obtained for both isolated and solvated alanine which were then used as initial geometries in B3LYP/6-311++G** optimization calculations. This level of theory was chosen as a good compromise between accuracy and cost from our previous studies of NMR spin-Hamiltonian parameters of metabolites [5, 6]. All these calculations were performed for the gas-phase (isolated) alanine as well as for the alanine in water solution. Solvent effects were taken into account through the self-consistent reaction field theory (SCRF) based on the Polarisable Continuum Model (PCM) [12, 13]. In this approach the alanine molecule is treated quantum mechanically, while the solvent is modeled as a macroscopic continuum dielectric medium.

B. *Chemical shifts and indirect spin-spin coupling constant calculation*

For each of the six isomers previously determined for both the isolated and the solvated alanine molecule, the isotropic nuclear magnetic shielding constants σ have been calculated, at the B3LYP/6-311++G** level of theory, using the GIAO technique [14] to ensure gauge independence. Similar calculations were performed for the protons of the tetra methyl silane (TMS) molecule chosen as reference for shielding parameters. Chemical shifts for the protons bound to C atoms in alanine, which are data directly comparable to experimental measures, have been obtained from $\delta=\sigma_{TMS}-\sigma$. Indirect spin-spin coupling constants J have also been evaluated.

To take into account the contribution on the calculated values of the NMR spin-Hamiltonian parameters from the structures higher in energy than the most stable one, we have assumed Boltzmann distributions so that averaged values of the parameters P ($P=\delta$ or J) could be evaluated through:

$$P_{average} = \frac{\sum_i P_i e^{-\Delta E_i/kT}}{\sum_i e^{-\Delta E_i/kT}} \qquad (1)$$

where ΔE_i is the relative energy of the isomer *i*, k is the Boltzmann constant and T is the temperature. In present work we chose T=300 K, close to the ambient temperature of experiments.

All calculations have been carried out by use of the computational package Gaussian09 [15] and the graphical interface Gabedit [16].

C. *Vibrational corrections*

In order to account for the correction to the NMR parameters due to the zero-point vibrational (ZPV) motion we used second-order perturbation theory [17] with the alanine in its equilibrium geometry as unperturbed system. We have developed a specific code for the evaluation of these ZPV corrections, both for nuclear magnetic shieldings and J coupling constants. This code was validated in our previous study of sarcosine [7].

III. Results

The lowest-energy structure determined for the solvated alanine, chosen as example, is displayed in Fig 1 in which are quoted the label of the various ^{1}H under investigation.

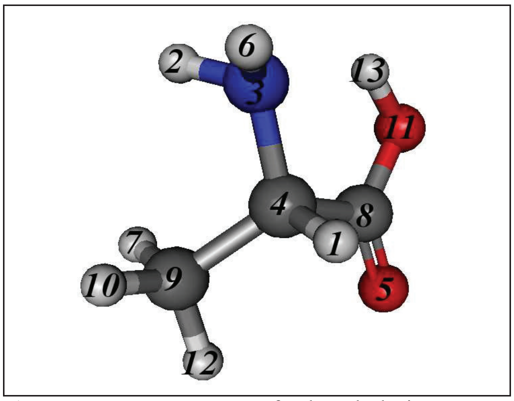

Figure 1. Lowest-energy structure of solvated alanine. N atom in blue, C atoms in black, O atoms in red and H atoms in grey.

A *Chemical shifts and indirect spin-spin coupling constant for non-vibrating alanine*

The protons under investigation are those attached to C atoms, they are gathered in two groups: group A [7,10,12] and group B [1] (for the ^{1}H labels see Fig 1). The isotropic nuclear magnetic shielding σ have been calculated for the TMS as well as for the six isomers of both the isolated and the solvated alanine and the chemical shifts $\delta_{A,B}$ have been evaluated. For each isomer the indirect spin-spin coupling constants J have been evaluated. The Boltzmann averaged values δ_B^{av} and J^{av} have then been obtained using Eq (1). Results are compiled in Table I.

TABLE I. CALCULATED CHEMICAL SHIFTS (IN PPM) AND J COUPLING CONSTANT (IN HZ) FOR NON-VIBRATING ALANINE

Isomer i	ΔE(eV)	δ_A^i	δ_B^i	J^i
Isolated 1	0.000	1.34	3.45	6.54
2	0.001	1.43	3.23	6.36
3	0.046	1.33	3.36	6.35
4	0.057	1.28	3.76	6.11
5	0.098	1.30	3.50	5.97
6	0.248	1.23	3.02	6.52
Boltzmann-averaged values		1.37	3.37	6.42
Solvated 2	0.000	1.44	3.50	6.51
1	0.124	1.37	3.60	6.58
3	0.161	1.36	3.44	6.42
4	0.162	1.40	3.77	6.17
5	0.194	1.41	3.53	6.04
6	0.236	1.31	3.40	6.47
Boltzmann-averaged values		1.44	3.51	6.51

B Vibrational corrections for chemical shifts and indirect spin-spin coupling constant

Within the B3LYP/6-311++G** level of theory, the ZPV corrections have been calculated for the A and B group of protons of the isolated alanine as well as for the TMS, in order to deduce the ZPV corrections of the chemical shifts. ZVP corrections were also evaluated for the J constant. Calculations were performed for each of the six isomers previously determined. For a given isomer i, the corrected NMR parameters are given through: $P^{i,vib}=P^i+P^i_{ZVP}$ with $P=\delta$ or J. Boltzmann averaged values of δ^{vib} and J^{vib} were then evaluated through a formula similar to Eq.(1) in which the energies E_i to be considered this time are the sum of the electronic energy plus the vibrational part evaluated as $\sum_K \frac{\hbar\omega_K}{2}$ where the ω_K are harmonic frequencies evaluated for each normal vibrational mode K (for alanine there are 33 such modes). Results are gathered in Table II.

TABLE II. CALCULATED CHEMICAL SHIFTS (IN PPM) AND J COUPLING CONSTANT (IN HZ) INCLUDING VIBRATIONAL CORRECTIONS FOR ISOLATED ALANINE

Isomer	i	ΔE(eV)	$\delta^{i,vib}_A$	$\delta^{i,vib}_B$	$J^{i,vib}$
Isolated	1	0.000	1.39	3.55	6.87
	2	0.015	1.43	3.37	7.13
	3	0.046	1.36	3.53	6.89
	4	0.054	1.36	3.85	6.63
	5	0.095	1.37	3.65	6.50
	6	0.237	1.32	3.24	6.87
Boltzmann-averaged values			1.40	3.52	6.93

Solvent effects upon vibrational average of nuclear magnetic shieldings and coupling constant were approximated from the corresponding values $\sigma^{i,vib}$ and $J^{i,vib}$ for the isolated molecule. In fact a correction equal to the difference between the value evaluated for the solvated and for the isolated non-vibrating molecule was added for each isomer. For the solvated alanine this results in: $\delta^{vib}_A=1.44$ ppm, $\delta^{vib}_B=3.64$ ppm, $J^{vib}=7.28$ Hz for the ground-state structure alone and in the following Boltzmann-averaged NMR parameters: $\delta^{av,vib}_A=1.43$ ppm, $\delta^{av,vib}_B=3.68$ ppm, $J^{av,vib}=7.01$ Hz when considering the six isomers.

C Comparison with experiment

Measurements of proton NMR chemical shifts and J coupling constant of brain metabolites among which alanine, were obtained using high-field NMR spectra in solution [2]. Experimental values are the following: $\delta^{exp}_A=1.4667$ ppm, $\delta^{exp}_B=3.7746$ ppm, $J^{exp}=7.2340$ Hz, to which to compare present calculated values. To quantify the differences between calculated and experimental chemical shift values, we have evaluated the root mean square (rms) deviation for the three values: $\delta_{A,B}$ and $\Delta(\delta_A-\delta_B)$ which measures the relative position of the two structures. Values are gathered in Table III together with the error $\Delta(J)$ for the J coupling constant.

TABLE III. Comparison with experiment

Model	rms(δ) (ppm)	Δ(J) (Hz)
Lowest-energy, isolated	0.25	0.69
+ ZPV correction	0.17	0.36
Lowest-energy, solvated	0.19	0.73
+ ZPV correction	0.10	-0.05
Six isomers, isolated	0.30	0.81
+ ZPV correction	0.19	0.31
Six isomers, solvated	0.19	0.72
+ ZPV correction	0.07	0.22

Taking into account solvent effects reduce rms(δ) from 0.25 ppm to 0.19 ppm for the lowest-energy structure alone and from 0.30 ppm to 0.19 ppm when including the six isomers. Zero-point vibrational corrections reduce rms(δ) from 0.25 ppm to 0.17 ppm for the lowest-energy structure alone and from 0.30 ppm to 0.19 ppm when including the six isomers. The best agreement with experiment for the [1]H chemical shift of the two groups A and B and their relative position corresponds to the calculations including solvent and vibrational effects besides contributions from the six isomers. Contrarily to what is observed for δ values, both solvent and isomer effects upon Δ(J) are seen to be small (≈0.06 Hz) while ZPV corrections are the larger ones. For non-vibrating alanine, ΔJ values are in the range 0.63-0.81 Hz, reduced to 0.05-0.31 with ZPVc.

These results are illustrated in Fig 2 where are drawn the [1]H NMR spectra of alanine, simulated using Gabedit from the experimental and from the various calculated values of δ and J. The right part shows the relative position of the two structures: a doublet at 1.4667 ppm and a quartet at 3.7746 ppm. These two structures are enhanced in the left part.

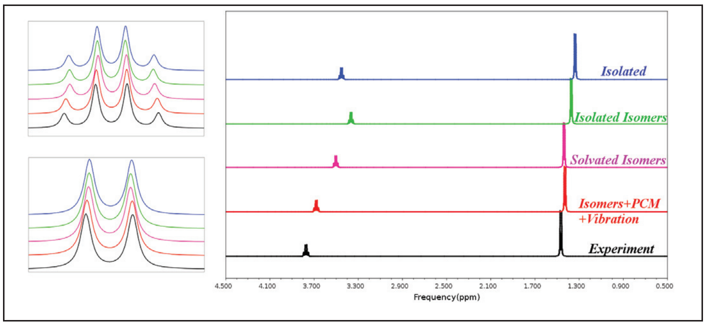

Figure 2. [1]H NMR spectra of alanine, simulated from experimental (in black) and calculated NMR parameters.

Taking into account both criteria: the position of the peaks and their pattern, the best agreement with experiment is obtained when solvent, isomers and vibrational effects are taken into account.

IV. CONCLUSION

The chemical shift for the two groups of protons attached to carbon atoms as well as the indirect spin-spin coupling constant have been calculated for the alanine molecule at the DFT/B3LYP/6-311++G** level of theory. Solvent and isomers effects were seen to be important contributions to improve the results for the chemical shifts. These contributions are quite negligible for the coupling constant for which vibrational corrections were seen to be significant.

ACKNOWLEDGMENT

This work was supported by the EU Marie Curie Research Network MRTNCT-2006-035801, 2006-2010. The authors thank the "Pôle Scientifique de Modélisation Numérique (PSMN)" at Lyon, France, for generous computational facilities.

REFERENCES

[1] F. A. Jansen, W. H. Backes, K. Nicolay, and M. Eline Kooi, "1H MR spectroscopy of the brain: absolute quantification of metabolites," Radiology, vol. 240, pp. 240-332, 2005.

[2] V. Govindaraju, K. Young, and A. A. Maudsley, "Proton NMR chemical shifts and coupling constants for brain metabolites," NMR Biomed., vol. 13, pp. 129-153, 2000.

[3] A. R. Allouche, M. Aubert-Frécon, and D. Graveron-Demilly, "Quantum chemistry based NMR spin Hamiltonian parameters of GABA for quantitation in magnetic resonance spectroscopy," PCCP, vol. 9, pp. 3098-3103, 2007.

[4] A. R. Allouche, D. Graveron-Demilly, F. Fauvelle, and M. Aubert-Frécon, "Theoretical and experimental investigation of the 1H NMR spectrum of putrescine," Chem. Phys. Lett., vol. 466, pp. 219-222, 2008.

[5] Z. Atieh, A. R. Allouche, D. Graveron-Demilly, F. Fauvelle, and M. Aubert-Frécon, "Density functional theory calculations of the nuclear magnetic resonance spin-Hamiltonian parameters for two polyamines of prostate tissue : spermidine and spermine," Measurement Science and Technology, vol. 20, 104024, 2009.

[6] Z. Atieh, A. R. Allouche, and M. Aubert-Frécon, "DFT calculations of isomer effects upon NMR spin-Hamiltonian parameters," J. Mol. Struc. THEOCHEM, vol. 945, pp. 104-109, 2010.

[7] Z. Atieh, A. R. Allouche, A. Lazariev, D. Van Ormondt, D. Graveron-Demilly, and M. Aubert-Frécon, "DFT calculations of 1H chemical shifts, simulated and experimental NMR spectra for sarcosine," unpublished.

[8] A. D. Becke, "Density-functional thermochemistry III.The role of exact exchange," J. Chem. Phys. Vol. 98, pp. 5648-5652, 1993.

[9] C. Lee, W. Yang, and R. G. Parr, "Development of the Colle-Salvetti correlation-energy formula into a functional of the electron density," Phys. Rev. B., vol. 37, pp. 785-789, 1988.

[10] W. C. Swope, H. C. Andersen, P. H. Berens, and K. R. Wilson, "A computer simulation method for the calculation of equilibrium constants for the formation of physical clusters of molecules: application to small water clusters," J. Chem. Phys., vol. 76, pp. 637-649, 1982.

[11] J. J. P. Stewart, "Optimization of parameters for semi-empirical methods V: modification of NDDO approximations and application to 70 elements," J. Mol. Modeling, vol. 13, pp. 1173-1213, 2007.

[12] S. Miertus, E. Scrocco, and J. Tomasi, "Electrostatic interaction of a solute with a continuum. A direct utilization of ab initio molecular potentials for the prevision of solvent effects," Chem. Phys., vol. 55, pp. 117-129, 1981.

[13] V. Barone, M. Cossi, and J. Tomasi, "A new definition of cavities for the computation of solvation free energies by the polarisable continuum model," J. Chem. Phys., vol. 107, pp. 3210-3221, 1997.

[14] J. R. Cheeseman, G. W. Trucks, T. A. Keith, and M. J. Frisch, "A comparison of models for calculating nuclear magnetic resonance shielding tensors," J. Chem. Phys., vol. 104, pp. 5497-5509, 1996.

[15] M. J. Frisch et al. Gaussian 09, Revision A.2, Gaussian, Inc., Wallingford CT, 2009.

[16] A. R. Allouche, Gabedit is a graphical user interface for various computational chemistry packages. It is freely available from http://gabedit.sf.net

[17] M. Kaupp, M. Buhl, and G. Malkin, Calculation of NMR and EPR parameters, Wiley-VCH, pp. 153-159, 2004.

IOP Publishing Measurement Science and Technology

Meas. Sci. Technol. 22 (2011) 114015 (5pp) doi:10.1088/0957-0233/22/11/114015

Density functional theory (DFT) calculations of the proton nuclear magnetic resonance (NMR) spin-Hamiltonian parameters for serine

Z Atieh[1], A R Allouche[1], D Graveron-Demilly[2] and M Aubert-Frécon[1]

[1] CNRS, UMR 5579, LASIM, Université Lyon l, F-69622 Villeurbanne, France
[2] CNRS, UMR 5220, INSERM U630, CREATIS-LRMN, Université Lyon l, F-69622 Villeurbanne, France

E-mail: zatieh@lasim.univ-lyon1.fr, allouche@lasim.univ-lyon1.fr, danielle.graveron@univ-lyon1.fr and frecon@lasim.univ-lyon1.fr

Received 7 December 2010, in final form 22 August 2011
Published 14 October 2011
Online at stacks.iop.org/MST/22/114015

Abstract

^{1}H nuclear magnetic resonance spin-Hamiltonian parameters: chemical shifts δ and indirect spin–spin coupling constants J, have been calculated for serine, a brain metabolite. Serine molecules in the gas-phase as well as in solution in water have been investigated using density functional theory. Solvent and conformer effects as well as zero-point vibrational corrections have been taken into account. For the non-vibrating molecule, the best agreement is obtained when solvent and conformer effects are included. Zero-point vibrational corrections improve the agreement with experimental values, leading to a root mean square deviation of 0.05 ppm for chemical shifts and 0.7 Hz for spin–spin coupling constants.

Keywords: serine, NMR parameters, DFT/B3LYP calculations, simulated NMR spectra

(Some figures in this article are in colour only in the electronic version)

1. Introduction

In vivo magnetic resonance spectroscopy (MRS) is a non-invasive powerful technique for detecting and quantifying metabolites which are bio-markers of diseases (for a recent review see [1]). In MRS, quantitation based on a metabolite basis set is nowadays very popular. In this approach, MRS signals obtained from patients are expanded as a linear combination of the MRS signals—either quantum mechanically simulated or *in vitro* measured—of the metabolite basis set. Simulations of the basis set signals, based on quantum chemistry, need prior knowledge of the nuclear magnetic resonance (NMR) spin-Hamiltonian parameters: chemical shifts δ and indirect spin–spin coupling constants J. Literature values of δ and J are used when available, mainly from experimental determinations. For instance, estimated values from experiments of proton NMR parameters δ and J are tabulated in [2] for 35 low molecular weight brain metabolites, among which is serine.

Another way of producing the necessary input data for computer simulations is to perform quantum chemistry calculations of δ and J, which are feasible for these not too large molecules. NMR chemical shifts and spin–spin coupling constants can be obtained from quantum chemical methods which are now well established as efficient tools for such predictions (for recent reviews see [3–5] and references therein). Despite its potential usefulness, it appears that this possibility had not been considered for metabolites previously to our early investigations of the γ-amino butyric acid (GABA) [6].

With the aim of producing reliable theoretical values of proton NMR parameters for the metabolite basis set, we have calculated to date the proton chemical shifts and the indirect spin–spin coupling constants and we have simulated the ^{1}H MR spectra of six metabolites: GABA [6], putrescine (put) [7–9], spermidine (spd) [8, 9], spermine (sp) [8, 9], sarcosine (sar) [10] and alanine (ala) [11]. A similar investigation of the amino-acid serine (ser), a brain metabolite, is presented here together with a synthesis of our work on the seven metabolites already considered.

2. Summary of the computational approach

Serine has been investigated following the computational approach used in our previous studies of metabolites. Only the main features are reported here for completeness. Two distinct parts have to be carried out. The first part of the computational approach concerns the determination of all (at least expected) the stable structures (i.e. corresponding to an energy minimum) lying inside a given energy gap above the lowest-energy conformer, for the serine molecule in both the gas-phase and in water solution. Our aim being to provide useful NMR data for further use in analysis of *in vivo* MRS spectra, it is necessary to take solvent effects into account. Here water is used to simulate the physiological media. Furthermore, experimental spectra are obtained at room temperature so that they may correspond not only to the most stable conformer but rather to an average of different conformers.

In the course of our previous investigation of the prostate metabolites [7–10] as well as of alanine [11], we have designed a procedure summarized in the following, to best achieve this aim. It is based on a molecular dynamics (MD) selection of 5000 initial geometries, using a temperature of 5000 K in order to provide a large (∼exhaustive) exploration of the potential energy surface. These initial geometries are selected, in a first step, from the constant energy (NVE) MD calculation using the Velocity Verlet algorithm [12] with the semi-empirical PM6 potential [13]. The simulated time is 15 ps, and the time step is 0.5 fs. In a second step, each selected geometry is optimized at the PM6 level, using the eigenvector following routine [14] and very similar structures are removed. In a third step, the remaining optimized geometries are used as initial geometries in an optimization process using this time the density functional theory (DFT) approach with the hybrid exchange-correlation B3LYP functional [15, 16] with the rather small basis set of Pople's type [17] 6-31G* to calculate the energy. The B3LYP functional involves the Becke's three-parameter exchange functional [15] together with the LYP's correlation functional [16]. Very similar structures are removed, and only the conformers which lie in a given energy gap above the lowest one are retained. In a fourth step, each of these conformers is further optimized at the B3LYP/6-311++G** level of theory, selected as a good compromise between accuracy and cost from our previous investigations. At the end of the procedure, these optimized structures are filtered in order to retain only those which correspond to an energy minimum, i.e. with no imaginary calculated frequencies.

This general conformational search procedure is available for both the gas-phase and the solvated species described in the self-consistent reaction field theory based on the polarizable continuum model (SCRF-PCM) [18, 19] where water was used as solvent. In this model, the solute is placed in a cavity created by a set of overlapping spheres, surrounded by a polarizable continuum medium representing the solvent and characterized by an effective dielectric constant.

The second part of the computational approach concerns the calculation of the proton nuclear magnetic shieldings σ, performed via the gauge-including atomic orbital (GIAO) method [20] ensuring gauge invariance, for both the metabolite under consideration and the tetra-methyl silane (TMS) molecule chosen as reference. The chemical shifts δ for the ^{1}H bound to the C atoms are obtained from $\delta = \sigma(^1\mathrm{H})_{\mathrm{TMS}} - \sigma(^1\mathrm{H})_{\mathrm{metabolite}}$. Indirect spin–spin coupling constants J are also calculated. The calculations of the various σ and J are performed for each stable conformer determined in the first part of the computational approach.

It should be noted that, up to now in the present calculations, each stable structure has been treated as motionless. This is a crude assumption that can be corrected partly by taking into account effects due to the vibration of the molecule. Zero-point vibrational (ZPV) corrections to NMR parameters have been taken into account. They have been evaluated for each conformer in a second-order perturbational approach as described in [21] and were used previously for sarcosine [10] and alanine [11].

The effects of the various conformers upon the NMR parameters and their ZPV corrections are averaged under a Boltzmann distribution assumption.

Energy calculations as well as nuclear magnetic shieldings and indirect spin–spin coupling constants have been calculated using the package Gaussian03 [22] via the easy-to-use graphical interface Gabedit [23]. ZPV corrections to NMR parameters within the DFT approach have been calculated through a home-made code that we have implemented in the version of Gaussian03 at our disposal. Using the chemical shifts and indirect spin–spin coupling constants, NMR spectra have been simulated via Gabedit from a home-made code developed following the conventional way of solving the time-independent Schrödinger equation with the spin-Hamiltonian [24].

3. Results

For the serine molecule in water solution the lowest-energy structure optimized at the B3LYP/6-311++G** level of theory is displayed in figure 1 showing the numbering of the protons under investigation. Three distinct chemical shift values were obtained for the three protons attached to the carbon atoms, labeled 12 and 14 ($\in CH_2$) and 13 ($\in$CH) in figure 1. Three distinct values of the indirect spin–spin coupling constants between these three protons were obtained. They are labeled $J_{13,14}$, $J_{12,13}$ and $J_{12,14}$. Numerous stable conformers were determined above the lowest-energy one for both the gas-phase and the solvated molecule. For each conformer, the values of the three chemical shifts and spin–spin coupling constants have been calculated. Then, contributions to the averaged values of δ and J through the Boltzmann distribution assumption have been taken into account for conformers with

Table 1. Serine MR parameters calculated at the B3LYP/6-311++G** level of theory, for various models. Rms deviations from experimental values are also quoted.

Model	Chemical shifts (ppm)				Spin–spin coupling constants (Hz)			
	δ_{13}[a]	δ_{14}	δ_{12}	rms(δ)	$J_{13,14}$	$J_{12,13}$	$J_{12,14}$	rms(J)
Exp[b]	*3.835*	*3.938*	*3.976*		*3.561*	*5.979*	*−12.254*	
Gas-phase, equilibrium	3.48	3.84	3.16	0.52	4.40	8.67	−9.15	2.4
Solvated, equilibrium	3.88	3.91	3.52	0.26	3.11	8.39	−10.2	1.8
Gas-phase, conformers	3.32	3.62	3.84	0.36	3.75	9.92	−9.24	2.8
Solvated, conformers	3.86	3.94	3.89	0.05	2.54	8.40	−10.7	1.8
Gas-phase, equilibrium + ZPV corrections	3.54	3.96	3.29	0.43	4.59	9.57	−9.74	2.6
Solvated, equilibrium + ZPV corrections	3.94	4.03	3.65	0.20	3.20	9.29	−10.8	2.1
Gas-phase, conformers + ZPV corrections	3.42	3.77	3.82	0.27	4.66	5.59	−10.5	1.2
Solvated, conformers + ZPV corrections	3.91	3.97	4.01	0.05	4.25	5.50	−11.3	0.7

[a] For the ^{1}H numbering see figure 1.
[b] From [2].

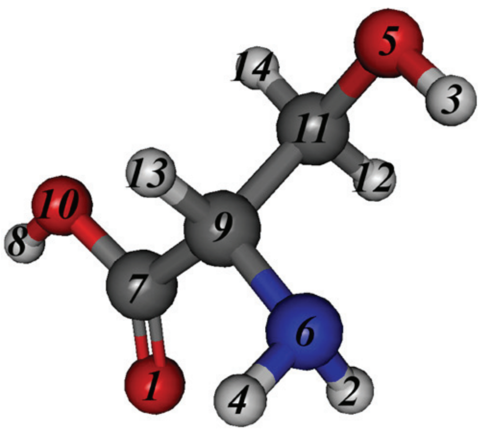

Figure 1. Lowest-energy structure of solvated serine, optimized at the B3LYP/6-311++G** level of theory. The numbering of atoms is quoted.

increasing energies included one by one until convergence was reached. Proceeding in that way, we noticed that 22 conformers (lying in an energy gap of 2.3 kcal mol^{-1} above the lowest-energy one) had to be taken into account to ensure convergence. Corrections due to the 23rd conformer were seen to be $\lesssim$ 0.001 ppm for chemical shifts and $\lesssim$ 0.02 Hz for spin–spin couplings. ZPV corrections have been evaluated for each conformer of the gas-phase molecule, and Boltzmann averaged values of the corrected NMR parameters, over the 22 conformers retained, have been obtained. For the solvated molecule, ZVP corrections have been approximated from the corresponding values for the gas-phase molecule as previously done for sarcosine [10] and alanine [11].

Eight distinct models have then been considered for the serine molecule, taking or not into account solvent, conformer and vibrational effects. The three calculated values of the chemical shifts and the spin–spin coupling constants are displayed in table 1 for each model together with the experimental values. Measurements of proton NMR chemical shifts and coupling constants of brain metabolites, among which is serine, were obtained using high-field NMR spectra in solution [2].

To quantify the influence of the different effects taken into account, solvent, conformer and/or vibration, as well as to measure the accuracy of the various predictions, the root mean square (rms) deviations between experimental and calculated values have been calculated for $P = \delta$ or J: $\mathrm{rms}(P) = \sqrt{\frac{\sum_{k=1}^{N}(P_{\mathrm{exp}}^{(k)} - P_{\mathrm{calc}}^{(k)})^2}{N}}$ where N is the number of data. These rms values are displayed in table 1.

For the chemical shifts of the non-vibrating molecule, the solvent effects are seen to be important, reducing the rms from 0.52 to 0.26 ppm for the equilibrium structure and from 0.36 to 0.05 ppm when conformers are taken into account too. They are more important than the conformer effects which nevertheless are quite significant, reducing the rms from 0.52 to 0.36 ppm for the gas-phase molecule and from 0.26 to 0.05 ppm for the solvated molecule. ZPV corrections are smaller than solvent and conformer effects; nevertheless added to these effects they lead to a good value of the rms(δ) (0.05 ppm), furthermore reproducing correctly the near relative values of δ_{12}, δ_{13} and δ_{14}. For the spin–spin coupling constants of the non-vibrating molecule, solvent effects reduce the rms(J) for both the equilibrium structure (from 2.4 to 1.8 Hz) and when conformers are included too (from 2.8 to 1.8 Hz) while conformer effects are seen to be small. Including ZPV corrections does not improve the predictions for the equilibrium structure, both in gas-phase or in solution, while these corrections are seen to be important when conformers are taken into account. As for chemical shifts, the best predictions for the spin–spin coupling constants of serine correspond to the model where solvent, conformer and ZPV effects are included, leading to a good rms(J) value (0.7 Hz).

For both ^{1}H chemical shifts and spin–spin coupling constants for serine, solvent effects are seen to be large, larger than conformer effects and ZPV corrections. It should be noted that these effects have been estimated in the present investigation from the implicit PCM model. It may be expected that such estimations should be improved by using a more sophisticated approach such as treating water molecules explicitly. This has not been considered in this work.

From the experimental and calculated chemical shifts and spin–spin coupling constants, NMR spectra have been

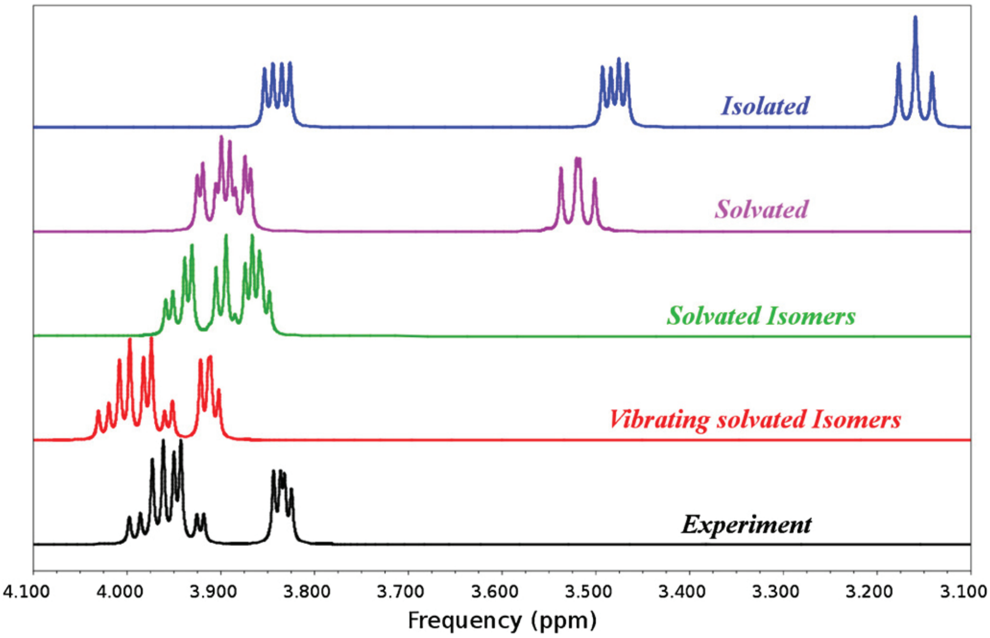

Figure 2. NMR spectra of serine simulated from experimental as well as from calculated values of the NMR parameters at the B3LYP/6-311++G** level of theory, for various models.

Table 2. Comparison between experimental and calculated (B3LYP/6-311++G**) MR parameters (δ in ppm, J in Hz) for the seven metabolites investigated.

Model	Metabolite	N_δ	rms(δ)	Metabolite	N_J	rms(J)
Gas-phase, equilibrium structure	Gaba, put, spd, sp, sar, ala, ser	20	0.29	ala, ser	4	2.1
				gaba, ala, ser	8	1.2
Solvated, equilibrium structure	Gaba, put, spd, sp, sar, ala, ser	20	0.18	ala, ser	4	1.6
Gas-phase, conformers	put, sar, ala, ser	9	0.30	ala, ser	4	2.5
Solvated, conformers	put, spd, sp, sar, ala, ser	17	0.11	ala, ser	4	1.6
Gas-phase, equilibrium structure + ZVP corrections	sar, ala, ser	7	0.31	ala, ser	4	2.3
Solvated, equilibrium structure + ZVP corrections	sar, ala, ser	7	0.16	ala, ser	4	1.8
Gas-phase, conformers + ZVP corrections	sar, ala, ser	7	0.24	ala, ser	4	1.0
Solvated, conformers + ZVP corrections	sar, ala, ser	7	0.07	ala, ser	4	0.6

simulated using Gabedit [23]. Some are drawn in figure 2. It is clear that considering only the equilibrium geometry of the serine molecule, evenly in water solution, does not lead to a realistic description of the NMR spectrum simulated from the experimental values for the δ and J parameters. Adding the effects of solvated conformers greatly improves the agreement, the best one being displayed when ZPV corrections are added too.

4. Comparison with experimental data for seven metabolites

Up to now we have calculated the NMR parameters of the GABA [6], alanine [11], serine, putrescine [7–9], spermidine [8, 9], spermine [8, 9] and sarcosine [10] molecules in various more or less sophisticated models. A synthesis of all the data is presented in table 2. We knew experimental chemical shifts for each molecule while, to the best of our knowledge, experimental spin–spin coupling constants are available only for the three brain metabolites: GABA, alanine and serine [2].

In order to compare the experimental and calculated NMR parameters, the rms(δ) and rms(J) have been calculated and their values are recorded in table 2 together with the number N of data and the list of metabolites considered.

Taking into account solvent effects greatly improves the agreement between calculated and experimental δ values; the rms values are significantly reduced for the equilibrium geometry (from 0.29 to 0.18 ppm) as well as for conformers (from 0.30 to 0.11 ppm). The ZPV corrections are small for gas-phase as well as solvated molecules in their equilibrium geometry. In contrast they improve the accuracy of calculated results when conformer effects are included, reducing the rms from 0.30 to 0.24 ppm for the gas-phase molecules and from 0.11 to 0.07 ppm for the solvated molecules. For chemical shifts our best result is obtained when solvent, conformer and vibrational effects are taken into account, with a good value for the corresponding rms (0.07 ppm). Solvent effects are also important for the J constants, reducing the rms from 2.1 to 1.6 Hz for molecules in their equilibrium structure and from 2.5 to 1.6 Hz when conformer effects are included. Taking into account vibrational effects improves the accuracy when conformer effects are included too, reducing the rms from 2.5 to 1.0 Hz for gas-phase molecules and from 1.6 to 0.6 Hz for solvated molecules. Once more our best result for J values is obtained when solvent, conformer and vibrational effects are taken into account, with a good value for the corresponding rms (0.6 Hz).

5. Conclusion

The ^{1}H NMR spin-Hamiltonian parameters have been calculated at the B3LYP/6-311++G**/GIAO level of theory for the serine molecule under eight various assumptions: taking or not into account solvent, conformer and vibrational effects. From the comparison between these predicted values and the known experimental ones, it is demonstrated that the best agreement is obtained when solvent, conformer and vibrational corrections are taken into account, leading to good values for the rms deviations for both the chemical shifts and the spin–spin coupling constants. The same conclusion is pointed out from similar comparisons involving the seven metabolites investigated to date.

Our best calculated values for the various δ and J parameters will be implemented as data in the jMRUI software package [25], a popular standard for quantitation of MRS signals.

Acknowledgments

This work is supported by the EU Marie Curie Research Network MRTNCT-2006-035801, 2006–2010. The authors thank the 'Pôle Scientifique de Modélisation Numérique (PSMN)' at Lyon, France, for generous computational facilities. This work was granted access to the HPC resources of [CCRT/CINES/IDRIS] under the allocation 20XX-c2010086341 made by GENCI (Grand Equipement National de Calcul Intensif).

References

[1] Van der Graaf M 2010 *In vivo* magnetic resonance spectroscopy: basic methodology and clinical applications *Eur. Biophys. J.* **39** 527–40

[2] Govindaraju V, Young K and Maudsley A A 2000 Proton NMR chemical shifts and coupling constants for brain metabolites *NMR Biomed.* **13** 129–53

[3] Fukui H 2009 Theoretical aspects of spin–spin couplings *Nucl. Mag. Reson.* **38** 166–93

[4] Casabianca L B and de Dios A C 2008 *Ab initio* calculations of NMR chemical shifts *J. Chem. Phys.* **128** 052201

[5] Helgaker T, Jaszunski M and Pecul M 2008 The quantum chemical calculation of NMR indirect spin–spin coupling constants *Prog. Nucl. Magn. Reson. Spectrosc.* **53** 249–68

[6] Allouche A R, Aubert-Frecon M and Graveron-Demilly D 2007 Quantum chemistry-based NMR spin Hamiltonian parameters of GABA for quantitation in magnetic resonance spectroscopy *Phys. Chem. Chem. Phys.* **9** 3098–103

[7] Allouche A R, Graveron-Demilly D, Fauvelle F and Aubert-Frecon M 2008 Theoretical and experimental investigation of the ^{1}H NMR spectra of putrescine *Chem. Phys. Lett.* **466** 219–22

[8] Atieh Z, Allouche A R, Fauvelle F, Graveron D and Aubert-Frécon M 2009 Density functional theory (DFT) calculations of the (NMR) nuclear magnetic resonance spin-Hamiltonian parameters for two polyamines of prostate tissue: spermidine and spermine *Meas. Sci. Technol.* **20** 104024

[9] Atieh Z, Allouche A R and Aubert-Frécon M 2010 DFT calculations of isomer effects upon NMR spin-Hamiltonian parameters of prostate polyamines *J. Mol. Struct. THEOCHEM* **945** 104–9

[10] Atieh Z, Allouche A R, Lazariev A, van Ormondt D, Graveron-Demilly D and Aubert-Frécon M 2010 DFT calculations of ^{1}H chemical shifts, simulated and experimental NMR spectra for sarcosine *Chem. Phys. Lett.* **492** 297–301

[11] Atieh Z, Allouche A R, Graveron-Demilly D and Aubert-Frécon M 2010 Solvent, isomers and vibrational effects in DFT calculations for the NMR spin-Hamiltonian parameters of alanine *Proc. 2010 IEEE Int. Workshop on Imaging Systems and Techniques (IST)* pp 369–72

[12] Swope W C, Andersen H C, Berens P H and Wilson K R 1982 A computer simulation method for the calculation of equilibrium constants for the formation of physical clusters of molecules: application to small water clusters *J. Chem. Phys.* **76** 637–49

[13] Stewart J J P 2007 Optimization of parameters for semi-empirical methods V: modification of NDDO approximations and application to 70 elements *J. Mol. Model.* **13** 1173–213

[14] Baker J 1986 An algorithm for the location of transition states *J. Comp. Chem.* **7** 385–95

[15] Becke A D 1993 Density-functional thermochemistry: III. The role of exact exchange *J. Chem. Phys.* **98** 5648–52

[16] Lee C, Yang W and Parr R G 1988 Development of the Colle–Salvetti correlation-energy formula into a functional of the electron density *Phys. Rev.* B **37** 785–9

[17] Krishnan R, Binkley J S, Seeger R and Pople J A 1980 Self-consistent molecular orbital methods: XX. A basis set for correlated wavefunctions *J. Chem. Phys.* **72** 650–4

[18] Miertus S, Scrocco E and Tomasi J 1981 Electrostatic interaction of a solute with a continuum. A direct utilization of *ab initio* molecular potentials for the prevision of solvent effects *Chem. Phys.* **55** 117–29

[19] Barone V, Cossi M and Tomasi J 1997 A new definition of cavities for the computation of solvation free energies by the polarisable continuum model *J. Chem. Phys.* **107** 3210–21

[20] Cheeseman J R, Trucks G W, Keith T A and Frisch M J 1996 A comparison of models for calculating nuclear magnetic resonance shielding tensors *J. Chem. Phys.* **104** 5497–509

[21] Kaupp M, Buhl M and Malkin V G 2004 *Calculation of NMR and EPR Parameters* (New York: Wiley)

[22] Frisch M J *et al* 2004 Gaussian 03, Revision D.02, Gaussian, Inc., Wallingford, CT

[23] Allouche A R 2011 Gabedit. A graphical user interface for computational chemistry softwares *J. Comp. Chem.* **32** 174–82

[24] Roberts J D 1961 *An Introduction to the Analysis of Spin–Spin Splitting in High-Resolution Nuclear Magnetic Resonance Spectra* (New York: Benjamin)

[25] Stefan D *et al* 2009 Quantitation of magnetic resonance spectroscopy signals: the jMRUI software package *Meas. Sci. Technol.* **20** 104035

C: Synthesis of results

In the present work, we have designed, for the calculations of the ^1H NMR parameters (δ and J) of metabolites, many computational methods that allows (1) the determination of all the stable isomers of a metabolite in a given energy range above the lowest one, (2) the calculation of the chemical shifts δ and the spin-spin coupling constants J for the protons of each isomer and averaging the values following a Boltzmann distribution, (3) the calculation of zero-point vibrational corrections for these NMR parameters for the protons of each isomer and averaging the corrected values following a Boltzmann distribution, (4) the simulation of the corresponding MR spectrum. These computational methods are based on the DFT/B3LYP method with the 6-311++G** basis set.

In this part C, a synthesis of the results using these computational methods is presented for seven metabolites (Gaba [(1)], putrescine (put) [(2; 3)], spermidine (spd) [(4; 3)], spermine (sp) [(4; 3)], sarcosine (sar) [(5)], alanine (ala) [(6)] and serine (ser) [(7)]), one of which (Gaba) was studied within the group.

For each molecule, we knew experimental chemical shifts while, to the best of our knowledge, experimental spin-spin coupling constants are available for only the three brain metabolites: GABA, alanine and serine [(8)].

In order to compare the experimental and calculated NMR parameters, the root mean square (rms) deviations have been calculated for the chemical shifts and spin-spin coupling constants using equation (3.7)

$$rms\ (P) = \sqrt{\frac{\sum_k^N \left(P_k^{exp} - P_k^{calc}\right)^2}{N}} \quad P = \delta \ or \ J \tag{3.7}$$

where N is the number of data. rms values for different models of calculation are displayed in table (3.43).

Eight models of calculation were done : 1: gas phase + equilibrium structure, 2: solvated, equilibrium structure, 3 : gas phase + isomers, 4 : solvated + isomers, 5 : 1 + vibration ; 6 : 2 + vibration ; 7 : 3 + vibration, 8 : 4 + vibration.

Results of table (3.43) are plotted in figures (3.21) and (3.22) for rms of chemical shifts and spin-spin coupling constants respectively.

Model	***Metabolite***	N_δ	***Rms (δ)***	***Metabolite***	N_J	***rms (J)***
Gas-phase, equilibrium struc ure	*Gaba, put, spd, sp, sar, ala, ser*	*20*	*0.29*	*ala, ser*	*4*	*2.1*
				gaba, ala, ser	*8*	*1.2*
Solvated, equilibrium structure	*Gaba, put, spd, sp, sar, ala, ser*	*20*	*0.18*	*ala, ser*	*4*	*1.6*
Gas-phase, isomers	*put, sar, ala, ser*	*9*	*0.3*	*ala, ser*	*4*	*2.5*
Solvated, isomers	*put, spd, sp, sar, ala, ser*	*17*	*0.11*	*ala, ser*	*4*	*1.6*
Gas-phase, equilibrium structure + ZVP corrections	*sar, ala, ser*	*7*	*0.31*	*ala, ser*	*4*	*2.3*
Solvated, equilibrium structure + ZVP corrections	*sar, ala, ser*	*7*	*0.16*	*ala, ser*	*4*	*1.8*
Gas-phase, isomers + ZVP corrections	*sar, ala, ser*	*7*	*0.24*	*ala, ser*	*4*	*1.0*
Solvated, isomers + ZVP corrections	*sar, ala, ser*	*7*	*0.07*	*ala, ser*	*4*	*0.6*

Table 3.43: σ results for acetate using MD-ONIOM

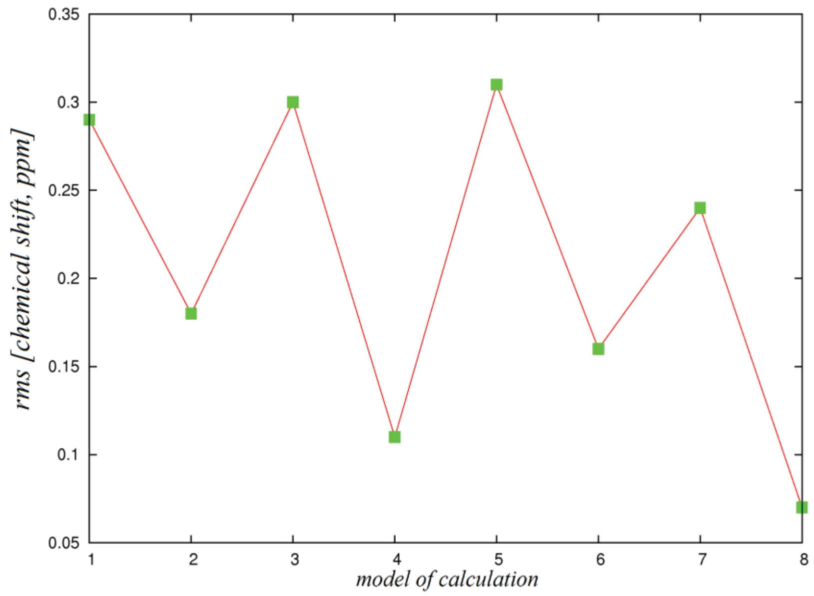

Figure 3.21: rms of the chemical shifts

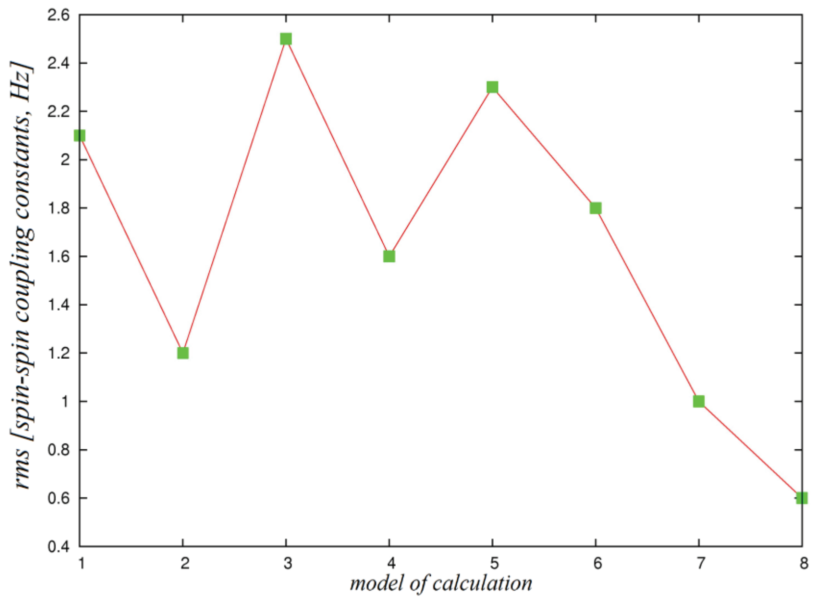

Figure 3.22: rms of the spin-spin coupling constants

From table (3.42) and figure (3.21), we can note that taking into account solvent effects greatly improves the agreement between calculated and experimental δ values, as could be expected, the rms values are significantly reduced for the equilibrium geometry (from 0.29 ppm to 0.18 ppm) as well as for isomers (from 0.30 ppm to 0.11 ppm). The zero-point vibrational corrections are small for gas-phase as well as solvated molecules in their equilibrium geometry. On the contrary they improve the accuracy of calculated results when isomers effects are included, reducing the rms from 0.30 ppm to 0.24 ppm for the gas-phase molecules and from 0.11 ppm to 0.07 ppm for the solvated molecules. For chemical shifts our best result is obtained when solvent, isomers and vibrational effects are taken into account, with a good value for the corresponding rms (0.07 ppm).

Solvent effects are also important for the *J* constants, reducing the rms from 2.1 Hz to 1.6 Hz for molecules in their equilibrium structure and from 2.5 Hz to 1.6 Hz when isomers effects are included. Taking into account vibrational effects improves the accuracy when isomers effects are included too, reducing the rms from 2.5 Hz to 1.0 Hz for gas-phase molecules and from 1.6 Hz to 0.6 Hz for solvated molecules. Once more our best result for *J* values is obtained when solvent, isomers and vibrational effects are taken into account, with a good value for the corresponding rms (0.6 Hz).

As a conclusion, from the comparisons with experiments for the 7 metabolites under investigation, the best agreement for the chemical shifts of the non-vibrating metabolites (with a rms of 0.1 ppm) is obtained when taking into account the isomers effects for the solvated species. Zero-point vibrational corrections improve this agreement, reducing the rms from 0.1 ppm to 0.07 ppm. The best agreement for the spin-spin coupling constants of the non-vibrating metabolites (with a rms of 1.6 Hz) is obtained when taking into account the isomers effects for the solvated species. Zero-point vibrational corrections improve this agreement, reducing the rms from 1.6 Hz to 0.6 Hz.

These results demonstrate that the DFT/B3LYP/6-311++G** level of theory is able to provide accurate values of ^{1}H NMR parameters. It may be inferred that they are reliable enough to serve as good starting values for the simulation of basis-set signals for further quantitation methods for metabolites.

References

1. *Quantum chemistry-based NMR spin Hamiltonian parameters of GABA for quantitation in magnetic resonance spectroscopy.* **A. R. Allouche, M. Aubert-Frécon, and D. Graveron-Demilly.** 2007, Phys. Chem. Chem. Phys., Vol. 9, p. 3098.

2. *Theoretical and experimental investigation of the 1H NMR spectrum of putrescine.* **A. R. Allouche, D. Graveron-Demilly, F. Fauvelle, and M. Aubert-Frécon.** 2008, Chem. Phys. Lett., Vol. 466, p. 219.

3. *DFT calculations of isomer effects upon NMR spin-Hamiltonian parameters of prostate polyamines.* **Z. Atieh, A. R. Allouche, and M. Aubert-Frécon.** 2010, J. Mol. Structur. THEOCHEM, Vol. 945, p. 104.

4. *Density functional theory calculations of the nuclear magnetic resonance spin-Hamiltonian parameters for two polyamines of prostate tissue: spermidine and spermine .* **Z. Atieh, A. R. Allouche, F. Fauvelle, D. Graveron, and M. Aubert-Frécon.** 2009, Measurement Science & Technology, Vol. 20, p. 104024.

5. *DFT calculations of 1H chemical shifts, simulated and experimental NMR spectra for sarcosine.* **Z. Atieh, A. R. Allouche, A. Lazariev, D. Van Ormondt, D. Graveron-Demilly, and M. Aubert-Frécon.** 2010, Chem. Phys. Lett., Vol. 492, p. 297.

6. *Solvent, isomers and vibrational effects in DFT calculations for the NMR spin-Hamiltonian parameters of alanine.* **Z. Atieh, AR. Allouche, D. Graveron-Demilly, and M. Aubert-Frécon.** 2010, Proceedings of the 2010 IEEE International Workshop on Imaging Systems and Technics (IST), p. 369.

7. *Density Functional Theory (DFT) calculations of the (NMR) nuclear magnetic resonance spin-Hamiltonian parameters for serine.* **Z. Atieh, A. R. Allouche, D. Graveron-Demilly, and M. Aubert-Frécon.** Measurement Science & Technology.

8. *Proton NMR chemical shifts and coupling constants for brain metabolites.* **V. Govindaraju, K. Young, and A. A. Maudsley.** 2000, NMR Biomed., Vol. 13, p. 129.

Chapter 4

Model to Predict NMR chemical shifts for biological molecules

The NMR chemical shifts, measurable under very general conditions and with a good accuracy are sensitive probes of chemical environment of atoms. They are particularly suited for characterizing the structure of biological molecules. One major obstacle, however, has been the difficulty to understand in details the complicated conformational dependencies of the chemical shifts.

Several approaches are now available for the increasingly quantitative prediction of chemical shifts from a 3D protein structure. SHIFTX [(1)] is a widely used program, which uses chemical shift hypersurfaces to describe the structural effects such as torsion angles, and classical equations to calculate physical effects. Quite a similar approach is adopted in the PRSI program [(2)]. In the SPARTA program [(3)] a combination of local sequence homology is combined with dihedral angle effects. ^{1}H chemical shifts are modeled with density functional calculations in the SHIFTS [(4)] approach, and PROSHIFT [(5)] uses artificial neural networks to predict the chemical shifts from empirical structural information. Recently, in the recent CamShift [(6)] program, the chemical shifts in proteins are calculated from inter-atomic distances. All these approaches have been developed specifically for proteins. Abraham [(7)] and his collaborators have developed a model, based on effective charges for predicting the proton chemical shifts for organic molecules.

An alternative method of determining NMR chemical shifts is by using the ab initio gauge-invariant atomic orbital (GIAO) method, together with the DFT method or with any method based on wave-function (like MP2 [(8)], CCSD [(9)], …) in which the nuclear shielding tensor is calculated. Since the protons are located on the periphery of the molecule their chemical shifts will be more sensitive to intermolecular interactions. So the solvent effects cannot be neglected. The experiments are usually performed at 300 K. It is therefore likely that the measured spectrum is that of several isomers of the molecule. A conformational search is then often necessary [10]. It was also shown that the zero-point vibrational correction is not negligible [11]. Taking into account of all these corrections makes the calculations very expansive for molecules of medium size and unfordable for proteins. Several recent studies have shown that the chemical shifts calculated by averaging the values along a trajectory of molecular dynamics can improve the quality of the predicted values [12; 13; 14]. Having a simple, fast and accurate model to predict chemical shifts for a given geometry is very important to achieve this type of study.

In this chapter, we present a new model, BioShift, that can be used to predict chemical shifts for biological molecules (proteins, DNA, RNA, polyamines ...). It is simple, fast and involves a limited number of parameters. It is particularly adapted to be used in molecular dynamics studies with a molecular mechanics potential. We test the model for polyamines which are rather small molecules as well as for proteins for which a lot of NMR chemical shifts are available. The tests show that our simple and fast model is competitive, by his accuracy, with sophisticated models specifically developed for proteins. It was seen to be also successful for polyamines.

I Description of the model

In the BioShift method, the chemical shift of an atom A is approximated formally as a sum of: (1) a term depending on the atom-type of A (we have used Amber [15] types in our study), (2) bond terms, (3) angle terms, (4) dihedral terms, and (5) non-bonded terms. The chemical shift of a given atom A, of type TA is then modeled by:

$$\begin{aligned}\delta_A = \delta_{TA} &+ \sum_{(bonds:B)} f_b(TA, TB, r_{AB}) + \sum_{(angles:B,C)} f_a(TA, TB, TC, r_{AC}) \\ &+ \sum_{(dihedrals:B,C,D)} f_d(TA, TB, TC, TD, r_{AD}) \\ &+ \sum_{(non-bonded:B)} f_{nb}(TA, TB, r_{AB})\end{aligned} \tag{4.1}$$

where TB, TC, TD are the Amber types of atoms B, C and D respectively. The bond term $\left[\sum_{(bonds:B)} f_b(TA, TB, r_{AB})\right]$ includes the effect of all atoms B making a chemical bond with the atom A. The bond term depends on the types of atoms A and B as well as the distance between them.

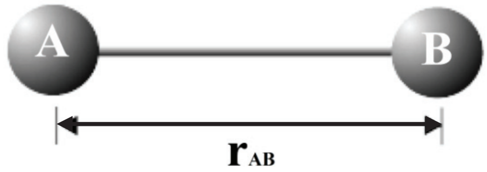

Figure (4.1): atoms A and B related by a chemical bond

The angle term $\left[\sum_{(angles:B,C)} f_a(TA, TB, TC, r_{AC})\right]$ includes the effects of all atoms C separated from the atom A by two chemical bonds where B is the intermediate atom. The angle term depends on the types of atoms A, B, and C, as well as the distance between atoms A and C.

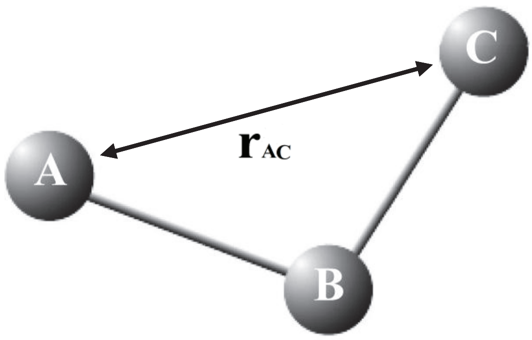

Figure (4.2): atoms A and C related through an angle

The dihedral term $\left[\sum_{(dihedrals:B,C,D)} f_d(TA, TB, TC, TD, r_{AD})\right]$ includes the effects of all atoms D separated from the atom A by three chemical bonds where atoms B and C are the intermediate atoms. The dihedral term depends on the types of atoms A, B, C, and D, as well as the distance between the atoms A and D.

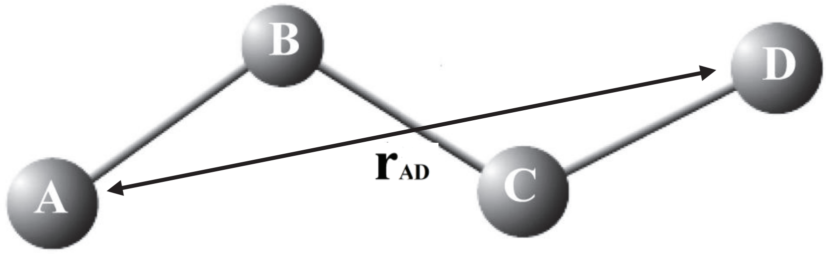

Figure (4.3): atoms *A* and *D* related through a dihedral angle

The non-bonded term $\left[\sum_{(non-bonded:B)} f_{nb}(TA, TB, r_{AB})\right]$ includes the effects of all atoms B non-bonded to the atom A. The non-bonded term depends on the types of atoms A and B, as well as the distance between them.

We have chosen a simple generic model form for the four functions f_u, where u is equal to b (bond), a (angle), d (dihedral), or nb (non-bonded), and taken into account the contribution to the chemical shift of atom A from one atom X bonded to A ($X = B, u = b$) or connected to A through an angle ($X = C, u = a$) or through a dihedral ($X = D, u = d$) or non-bonded to A ($X = B, u = nb$)

$$f_u = \sum_{i=1}^{N_u} \alpha_i^u r_{AX}^{\beta_i^u} \tag{4.2}$$

where r_{AX} is the distance between atoms A and X. The parameters α_i^u depend on the types of atoms A and X as well as on the connection-types (b, a, d, nb). The number of terms N_u is generally chosen to be equal to 1 or 2. For the parameters β_i^u, the values +1, -3, -6 or -8 may be used, following the connection-type (b, a, d, nb) as well as the atom-type.

It must be noted that, we have tried to replace the function f_u which depends on the distance, by other functions that depend on the angle for angle terms or on the dihedral angle for dihedral terms; however, the function depending on the distance showed a better stability and performance in predicting chemical shifts.

The α_i^u and δ_{TA} parameters are to be fitted by maximizing the agreement between predicted and experimental chemical shifts for a set of biological molecules for which both structures and chemical shifts are known experimentally. Using these fitted parameters, chemical shifts can be predicted for other biological molecules.

II Illustrative results and discussion

Since NMR chemical shifts are available for a vast number of proteins, we have tested our model for this type of molecules. For fitting the α_i^u and δ_{TA} parameters and choosing the more appropriate values of β_i^u, we used the RefDB17 database of chemical shifts and the corresponding Protein Data Bank (PDB) structures, and we extracted the chemical shifts of *HA, HN, CA, CB, CO,* and *N* nuclei for ten proteins (1IAR, 1BDO, 1MMS, 2IHB, 1KQR, 1QOG, 2RN2, 1MXE, 1CWC, 2J1K). We used the known chemical shifts for the first five proteins of the precedent list to fit the parameters of our model. The other five proteins were used for testing the accuracy of the prediction obtained from our fitted parameters.

The PDB structures do not contain the positions of the hydrogen atoms, these were added. The positions of H atoms were optimized using the Amber force-field potential implemented in Gabedit.

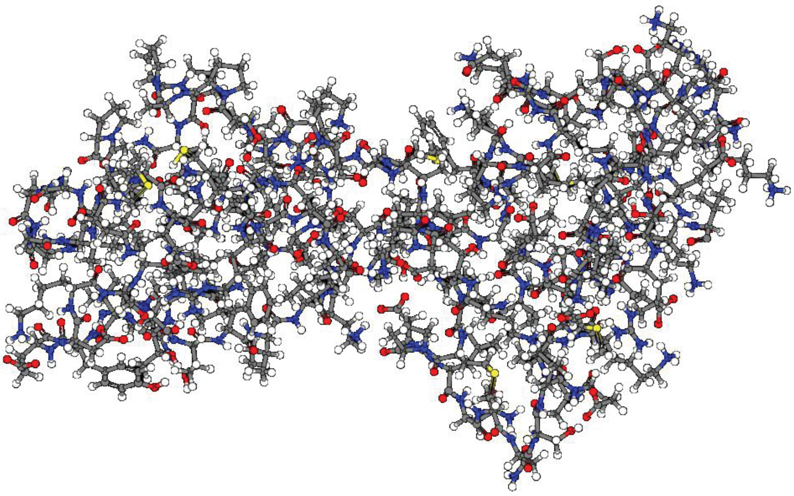

Figure (4.4): protein 1MMS after the addition of H atoms and optimizing their positions

Here, we present our results for the smallest number of parameters allowing a good accuracy together with a comparison with the results we obtained via SHIFTX and those published from CamShift which are two of the state-of-the-art chemical shift predictors. For the six nuclei (HA, HN, CA, CB, CO, and N) the root mean squares deviations (rmsd) between experimental and fitted chemical shift values are displayed in tables (4.1) while rmsd values between experimental and predicted chemical shifts are displayed in table (4.2). The correlation coefficient R, reflecting the quality of the agreement between a certain model and experimental data, is also quoted for the set of the 5 proteins included in the fitting process.

Nuclei	***HA*** ***P**=20/1310/300* [a]		***HN*** ***P**=15/608/235*		***CA*** ***P**=35/1539/349*	
Fitted proteins	N_δ	***rmsd***	N_δ	***rmsd***	N_δ	***rmsd***
1IAR	*129*	*0.26/0.23/0.21* [b]	*1 5*	*0.43/0.44/0.39*	*129*	*1.76/1/1.01*
1BDO	*86*	*0.31/0.28/0.24*	*75*	*0.46/0.55/0.45*	*79*	*1.71/1.01/1.31*
1MMS	*136*	*0.33/0.34/0.30*	*123*	*0.53/0.6/0.64*	*126*	*2.14/2.3/1.46*
2IHB	*113*	*0.35/0.24/0.21*	*108*	*0.57/0.54/0.49*	*111*	*1.91/1.22/1.19*
1KQR	*165*	*0.44/0.39/0.32*	*149*	*0.59/0.59/0.70*	*159*	*1.83/1.15/1.18*
The set of 5 proteins	*629*	*0.35/0.31/0.27* *R=0.76/0.84* [c]	*580*	*0.53/0.55/0.56* *R=0.63/0.64*	*604*	*1.88/1.44/1.23* *R=0.91/0.95*
Nuclei	***CB*** ***P**=40*		***CO*** ***P**=22*		***N*** ***P**=35/1168/271*	
Fitted proteins	N_δ	***Rmsd***	N_δ	***rmsd***	N_δ	***rmsd***
1IAR	*124*	*1.36/1.25/1.11*	*128*	*1.06/1.08/0.87*	*120*	*2.91/2.79/2.40*
1BDO	*71*	*1.94/1.49/1.30*	-	-	*75*	*3.48/1.97/2.49*
1MMS	*116*	*2.2/3.37/1.26*	*126*	*1.78/2.29/1.18*	*123*	*3.24/3.17/3.13*
2IHB	*107*	*2.39/0.93/0.81*	*111*	*1.38/1.27/1.10*	*06*	*2.46/2.1/2.28*
1KQR	*149*	*1.96/1.38/1.28*	*156*	*1.26/1.15/1.10*	*148*	*3.47/2.93/3.23*
The set of 5 proteins	*567*	*1.99/1.56/1.15* *R=0.99/0.99*	*521*	*1.39/1.51/1.07* *R=0.78/0.78*	*572*	*3.14/2.72/2.79* *R=0.80/0.86*

Table (4.1): root mean square deviation (rmsd, in ppm) between chemical shift values from models and experimental ones. The number of adjustable parameters (P) in each model as well as the number of chemical shifts (N_δ) is quoted. The sign '-' means lack of experimental data for the concerned nucleus.

[a] the first entry corresponds to number of adjustable parameters in our model, the second one to the number of parameters of hypersurfaces used in SHIFTX, the third one to the adjustable parameters in CamShift.

[b] the first entry corresponds to present results, the second one to the results we obtained using SHIFTX, the third one to literature results from CamShift

[c] the first entry corresponds to present results, the second one to the results we obtained using SHIFTX

nuclei	***HA***		***HN***		***CA***	
Predicted proteins	N_δ	***rmsd***	N_δ	***rmsd***	N_δ	***rmsd***
1QOG	*89*	*0.38 /0.37*[a]	*76*	*0.49/0.48*	*84*	*2.33/1.29*
2RN2	*169*	*0.37/0.30*	*148*	*0.56/0.52*	*122*	*1.87/0.82*
1MXE	*155*	*0.25/0.20*	*142*	*0.47/0.38*	*144*	*2.13/0.87*
1CWC	*167*	*0.35/0.36*	*156*	*0.73/0.65*	*159*	*2.09/1.21*
2J1K	*122*	*0.36/0.40*	*108*	*0. /0.47*	*106*	*1.61/1.17*
The 10 proteins set	*1331*	*0.35 /0.32*	*1210*	*0.55 /0.53*	*1219*	*1.95/1.27*
nuclei		***CB***		***CO***		***N***
Predicted proteins	N_δ	***rmsd***	N_δ	***rmsd***	N_δ	***rmsd***
1QOG	*80*	*2.04/1.11*	*45*	*1.63/1.87*	*76*	*4.2/2.43*
2RN2	-	-	-	-	*148*	*3.95/2.46*
1MXE	-	-	*144*	*1.28/0.78*	*144*	*2.52/2.09*
1CWC	-	-	*148*	*1.46/1.26*	*148*	*3.98/2.68*
2J1K	*93*	*2.16/1.62*	*91*	*1.25/1.12*	*92*	*3.10/3.00*
The 10 proteins set	*740*	*2.02/1.53*	*949*	*1.38/1.37*	*1180*	*3.37/2.60*

Table (4.2): root mean square deviation (rmsd, in ppm) between chemical shift values from models and experimental ones. The number of predicted chemical shifts (N_δ) is quoted.

[a] the first entry corresponds to present results, the second one to the results we obtained using SHIFTX

Chemical shift values obtained from models (BioShift and SHIFTX) are plotted against their experimental values in figures (4.5), (4.6), (4.7), (4.8), (4.9), and (4.10) for the six nuclei HA, HN, CA, CB, CO and N respectively, for the five proteins: 1IAR, 1BDO, 1MMS, 2IHB, 1KQR.

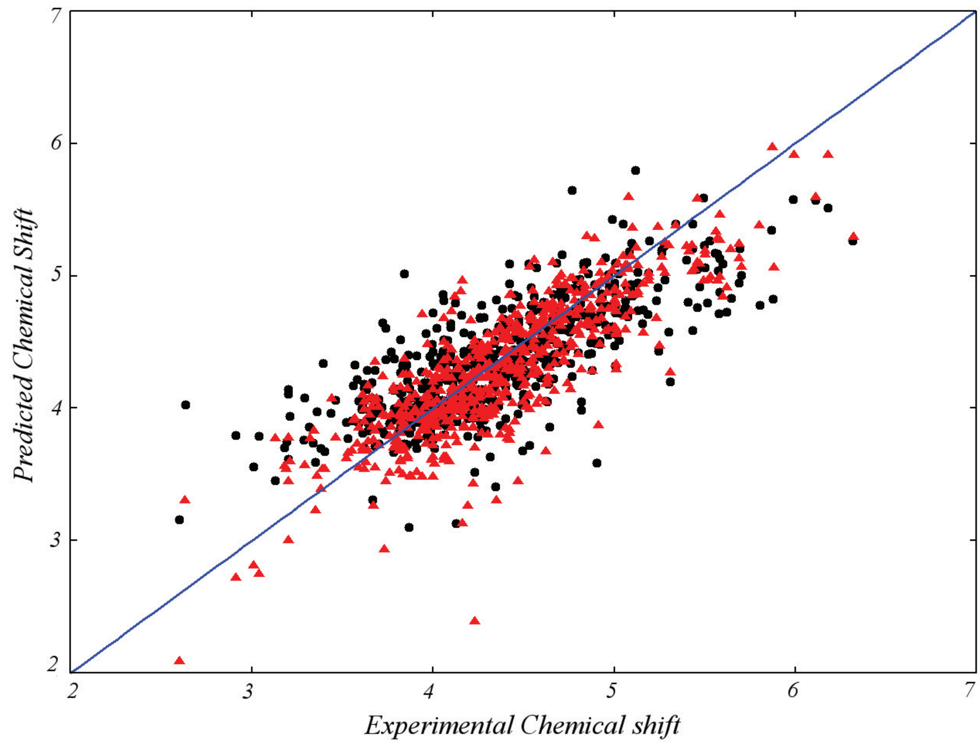

Figure (4.5): scatter plots for the chemical shifts (in ppm) of the HA atoms of the set of 5 proteins: 1IAR, 1BDO, 1MMS, 2IHB, 1KQR. (Black) points ● for present data (correlation coefficient R=0.76), (red) points Δ for SHIFTX data (R=0.84).

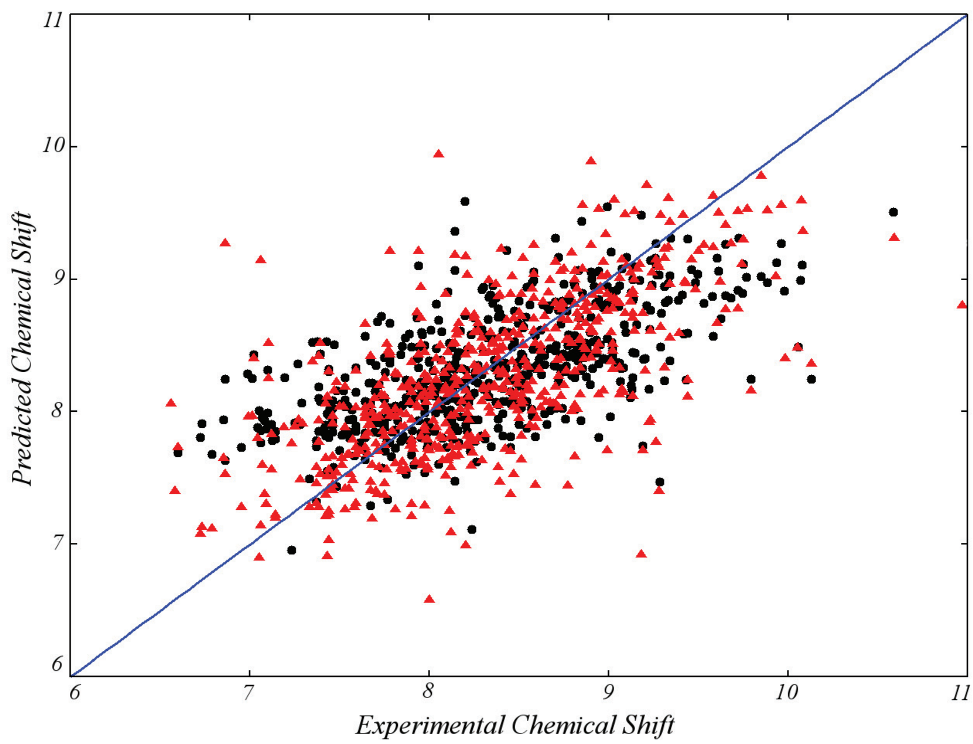

Figure (4.6): scatter plots for the chemical shifts (in ppm) of the HN atoms of the set of 5 proteins: 1IAR, 1BDO, 1MMS, 2IHB, 1KQR. (Black) points ● for present data (R=0.63), (red) points Δ for SHIFTX data (R=0.64).

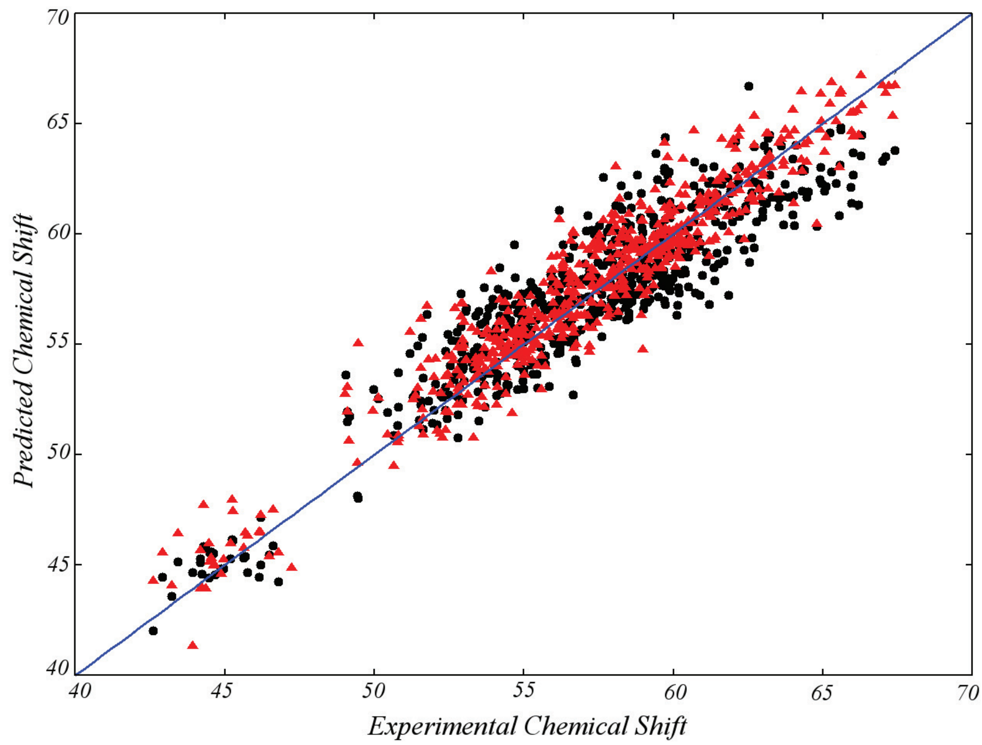

Figure (4.7): scatter plots for the chemical shifts (in ppm) of the CA atoms of the set of 5 proteins: 1IAR, 1BDO, 1MMS, 2IHB, 1KQR. (Black) points ● for present data (R=0.91), (red) points Δ for SHIFTX data (R=0.95).

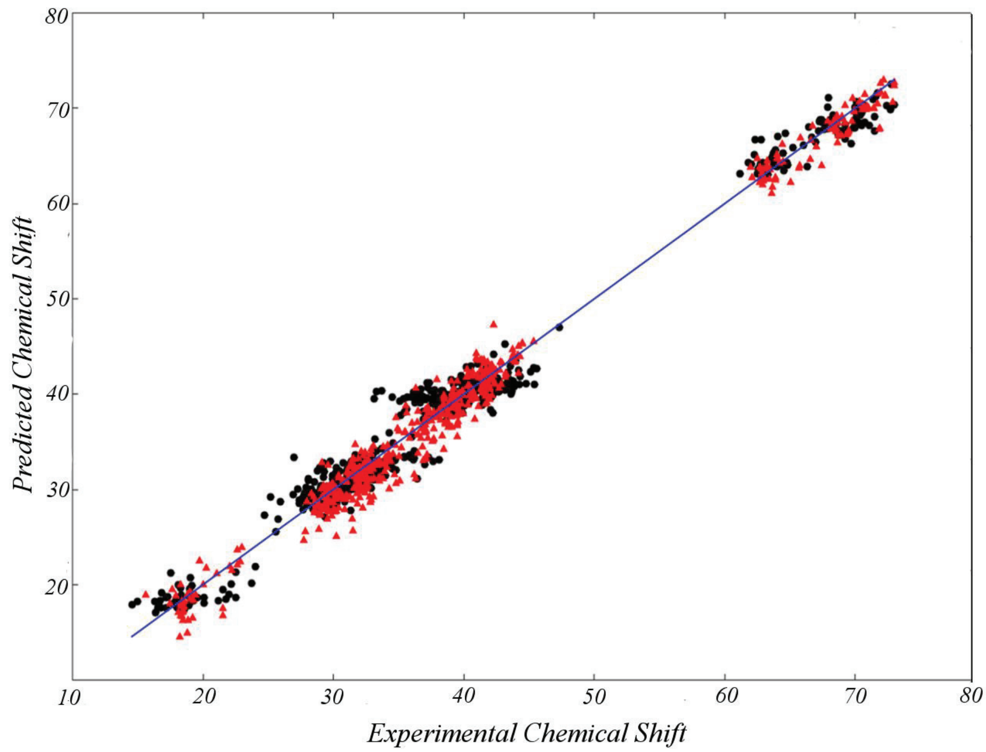

Figure (4.8): scatter plots for the chemical shifts (in ppm) of the CB atoms of the set of 5 proteins: 1IAR, 1BDO, 1MMS, 2IHB, 1KQR. (Black) points ● for present data (R=0.99), (red) points Δ for SHIFTX data (R=???).

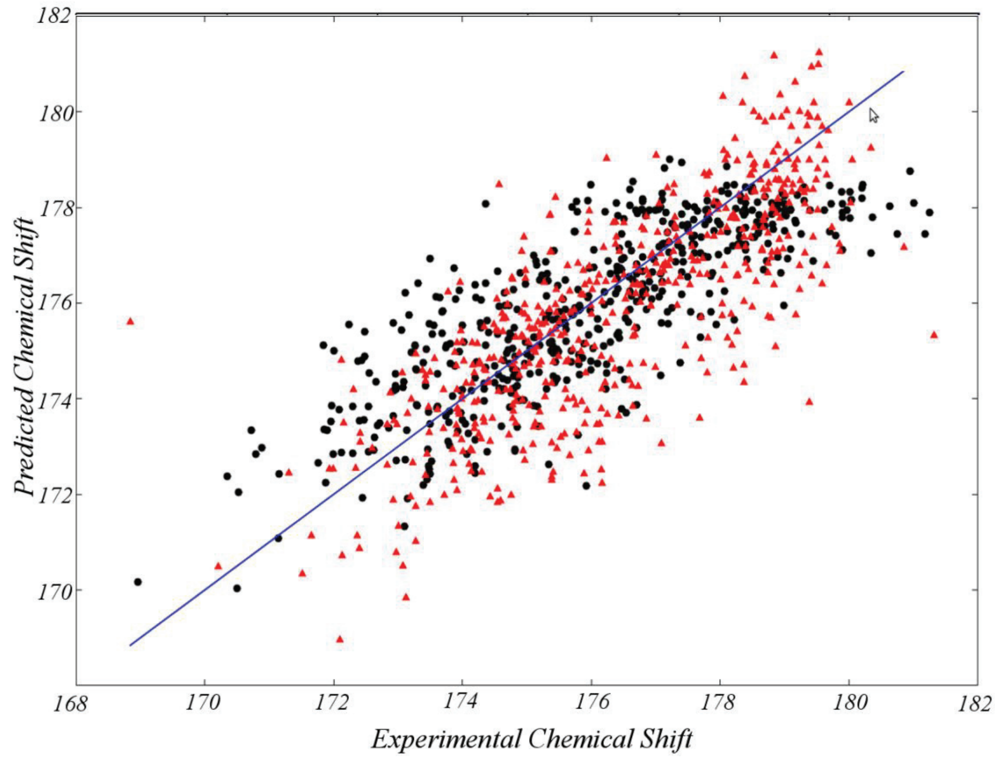

Figure (4.9): scatter plots for the chemical shifts (in ppm) of the CO atoms of the set of 4 proteins: 1IAR, 1MMS, 2IHB, 1KQR. (Black) points ● for present data (R=0.78), (red) points Δ for SHIFTX data (R=????)

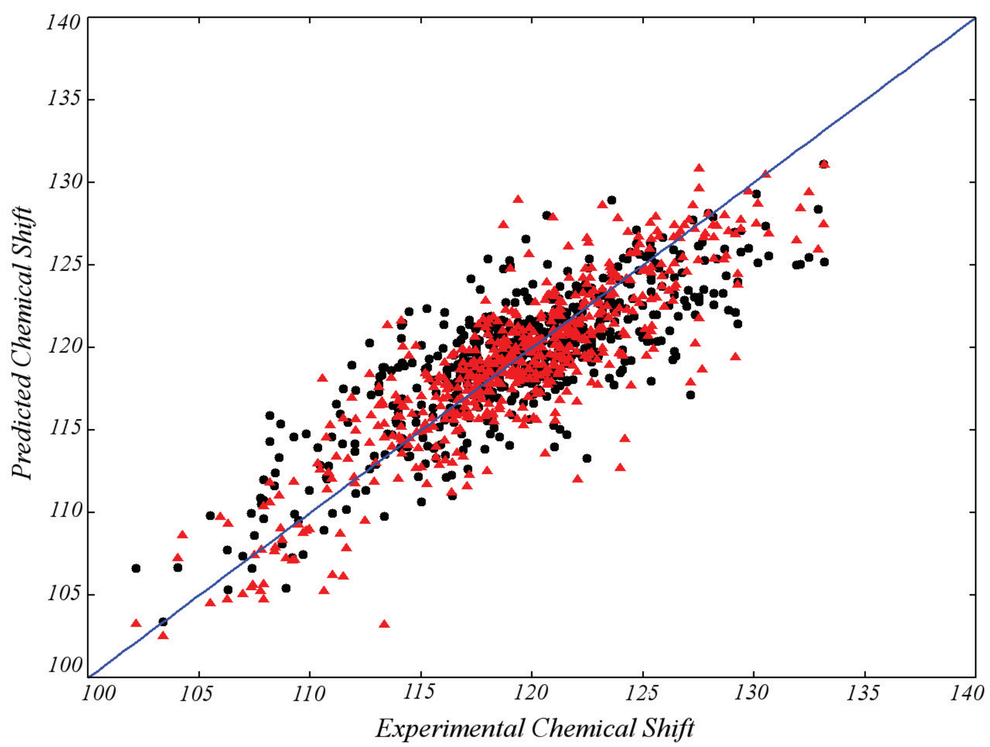

Figure (4.10): scatter plots for the chemical shifts (in ppm) of the N atoms of the set of 5 proteins: 1IAR, 1BDO, 1MMS, 2IHB, 1KQR. (Black) points ●for present data (R=0.80), (red) points Δ for SHIFTX data (R=0.86).

The full list of the parameters used in our model (BioShift) and their numerical values are displayed in appendix B.

The results of table (4.1) show that, BioShift with a limited number of parameters provide an overall similar accuracy in comparison with SHIFTX for HN and HA protons, sligthly poorer than the results from CamShift for HA. With only 15 parameters (to compare to 608 parameters in SHIFTX and 235 parameters in CamShift), BioShift reproduces the chemical shifts for 580 HN protons with a root mean square deviation rmsd = 0.53 ppm (the correlation between the experimental chemical shifts and BioShift's predictions R=0.63), to be compared to rmsd = 0.55 ppm (R=0.64) obtained from the SHIFTX program. A similar accuracy was obtained for 629 HA protons using 20 parameters (to compare to 1310 parameters in SHIFTX and 300 parameters in CamShift).

For the CA, CB, and N nuclei, the fits are quite good with values of R larger than 0.8 similar to the values obtained from SHIFTX, while the rmsd are somewhat larger than both results from SHIFTX and CamShift. The increase of the number of non-bonded parameters (and consequently the computational time) was seen to slightly improve the predictions. For CA, the rmsd was 1.73 ppm instead of 1.88 ppm for the 604 CA of the 5 proteins included in the fitting process. For CB, the rmsd was 1.56 ppm instead of 1.99 ppm for the 567 CB nuclei while for N the rmsd was 2.92 ppm instead of 3.14 ppm for the 572 N nuclei. The discrepancies with the results from SHIFTX are lowered but remain larger than for the protons. According to our tests, it seems that taking a function that depends on the dihedral angle in place of a function that depends upon the distance between atoms connected through a dihedral does not improve the accuracy of the prediction. Note that in our model, we have used the same parameters for an atom-type in any amino acid, whereas in the model implemented in the SHIFTX program as well as in other models such as CamShift, different parameters are used for a given atom-type for each amino acid. Besides, it has been shown that taking into account the fluctuation of the chemical shift of C nuclei over time improves (about 1 ppm more accuracy) the quality of the prediction [(16)]. A time averaging on the chemical shift values, computed by our model, over conformations obtained by molecular dynamics simulations should improve the accuracy of the present predictions.

For CO, the fits are good with a value of R = 0.78 similar to the value obtained from SHIFTX. The rmsd for the fitted proteins is in between the rmsd values obtained from SHIFTX and CamShift. The rmsd values are 1.39, 1.51, and 1.07 ppm using the present model, SHIFTX, and CamShift for the 521 CO nuclei of the proteins included in the fitting process.

From table (4.2), present results show also that the parameters fitted to reproduce at the best the experimental values for the five proteins: 1IAR, 1BDO, 1MMS, 2IHB, 1KQR, can predict with as good accuracy, the chemical shifts for the five other proteins considered: 1QOG, 2RN2, 1MXE, 1CWC, 2J1K.

As a further test of the present model, we used it to obtain the chemical shifts of the H1 protons of the four polyamines: putrescine, spermidine, spermine, and cadaverine (a fourth polyamine) that we have investigated from DFT calculations. Using parameters previously fitted for proteins together with two more parameters specific to polyamines (angle term: H1 CT NT, α=35.457501, β=1; dihedral term: H1 CT NT H, α=-14.143552, β=1) the experimental values of the chemical shifts for the 16 H1 were reproduced with a rmsd of 0.03 ppm and R=0.86, showing that the model works also for this type of molecules.

Besides, using the parameters previously fitted for proteins, we tested our model in the prediction of H1 chemical shifts for 20 amino acids. The rmsd between predicted and experimental values was found to be 0.3 ppm. This precision of prediction is usually expected, and of course, better precisions can only be obtained by quantum chemistry calculation in which the inclusion of different corrections is sometimes needed (solvent, vibration, temperature …).

As a conclusion, we proposed the BioShift method to predict chemical shifts for biomolecules and we applied it successfully to rather small ones (polyamines) and to proteins. The functional form and the number of parameters of our model make the BioShift predictions very rapid and suitable to compute chemical shift in molecular dynamics simulations for macromolecules like proteins, DNA and RNA. This model should be particularly useful for certification of molecular dynamics trajectories with NMR chemical shifts using a molecular mechanic potential.

References

1. *Rapid and accurate calculation of protein 1H, 13C and 15N chemical shifts.* **S. Neal, A. M. Nip, H. Y. Zhang, and D. S. Wishart.** 2003, J. Biomol. NMR, Vol. 26, p. 215.

2. *Predicting 15N chemical shifts in proteins using the preceding residue-specific individual shielding surfaces from φ, ψi−1, and χ1torsion angles.* **Y. J. Wang, and O. Jardetzky.** 2004, J. Biomol. NMR, Vol. 28, p. 327.

3. *Protein backbone chemical shifts predicted from searching a database for torsion angle and sequence homology.* **Y. Shen, and A. Bax.** 2007, J. Biomol. NMR, Vol. 38, p. 289.

4. *A new model for chemical shifts of amide hydrogens in proteins.* **S. Moon, and D. A. Case.** 2007, J. Biomol. NMR, Vol. 38, p. 139.

5. *PROSHIFT: Protein chemical shift prediction using artificial neural networks.* **J.Meiler.** 2003, J. Biomol. NMR, Vol. 26, p. 25.

6. *Fast and Accurate Predictions of Protein NMR Chemical Shifts from Interatomic Distances.* **K. J. Kohlhoff, P. Robustelli,A. Cavalli, X. Salvatella, and M. Vendruscolo.** 2009, J. Am. Chem. Soc., Vol. 131, p. 13894.

7. *1H chemical shifts in NMR: Part 23, the effect of dimethyl sulphoxide versus chloroform solvent on 1H chemical shifts.* **R. J. Abraham, J. J. Byrne, L. Griffiths, and M. Perez.** 2006, Mag. Res.Chem., Vol. 44, p. 491.

8. *MP2 energy evaluation by direct methods.* **M. Head-Gordon, J. A. Pople, and M. J. Frisch.** 1988, Chem. Phys. Lett., Vol. 153, p. 503 .

9. *A full coupled-cluster singles and doubles model: The inclusion of disconnected triples.* **G. D. P., and R. J. Bartlett.** 1982, J. Chem. Phys., Vol. 76, p. 1910.

10. *DFT calculations of isomer effects upon NMR spin-Hamiltonian parameters of prostate polyamines.* **Z. Atieh, A. R. Allouche, and M. Aubert-Frecon.** 2010, J. Mol. Struct.-THEOCHEM, Vol. 945, p. 104.

11. *DFT calculations of 1H chemical shifts, simulated and experimental NMR spectra for sarcosine.* **Z. Atieh, A. R. Allouche, A. Lazariev, D. Van Ormondt ,D. Graveron-Demilly, and M. Aubert-Frecon.** 2010, Chem. Phys. Lett., Vol. 492, p. 297.

12. *Certification of Molecular Dynamics Trajectories with NMR Chemical Shifts.* **D. Li, and R. Brueschweiler.** 2010, J. Phys. Chem. Lett., Vol. 1, p. 246.

13. *Time Averaging of NMR Chemical Shifts in the MLF Peptide in the Solid State.* **I. De Gortari, G. Portella, X. Salvatella, V. S. Bajaj, P. C. A. van der Wel, J. R. Yates, M. D. Segall, C. J. Pickard, M. C. Payne, and M. Vendruscolo.** 2010, J. Am. Chem. Soc., Vol. 132, p. 5993.

14. *4D prediction of protein 1H chemical shifts.* **J. Lehtivarjo, T. Hassinen, S. Korhonen, M. Perakyla, and R. Laatikainen.** 2009, J. Biomol. NMR, Vol. 45, p. 413.

15. *A Second Generation Force Field for the Simulation of Proteins, Nucleic Acids, and Organic Molecules.* **W. D. Cornell, P. Cieplak, C. I. Bayly, I. R. Gould, K. M. Merz, D. M. Ferguson, D. C. Spellmeyer, T. Fox, J. W. Caldwell, and P. A. Kollman.** 1995, J. Am. Chem. Soc., Vol. 117, p. 5179.

16. *Time Averaging of NMR Chemical Shifts in the MLF Peptide in the Solid State.* **I. De Gortari, G. Portella, X. Salvatella, V. S. Bajaj, P. C. A. van der Wel, J. R. Yates, M. D. Segall, C. J. Pickard, M. C. Payne, and M. Vendruscolo.** 2010, J. Am. Chem. Soc., Vol. 132, p. 5993.

Conclusion and perspectives

In the first part of the present work, ^{1}H Nuclear Magnetic Resonance (NMR) spin-Hamiltonian parameters: chemical shifts δ and spin–spin coupling constants J have been calculated using the density functional theory for seven metabolites: four involved in prostate diseases (putrescine, spermidine, spermine, and sarcosine) and three involved in brain diseases (acetate, serine, and alanine). A theoretical investigation of the NMR parameters has been performed for the protons attached to carbon atoms for these metabolites. Several levels of theory within the DFT approach were used, mixing four functionals B3LYP, PBE, OPBE, PBE0 and twelve basis sets belonging to three groups: (1) Pople's basis sets (6-311+G**, 6-311++G**, 6-311++G(2d,2p), 6-311++G(3df,3pd)), (2) polarisable consistent basis sets designed for the calculation of chemical shifts (pc0, pc1, pc2, pc3), and (3) the polarisable consistent basis sets designed for the calculation of spin-spin coupling constants (pcJ0, pcJ1, pcJ2, pcJ3). By comparison with the experiment, we have demonstrated that the DFT/B3LYP/6-311++G** level of theory is able to provide accurate values of ^{1}H NMR spin-Hamiltonian parameters. Using this level of theory, we have studied three effects on the NMR parameters of metabolites: (1) isomers (2) vibration, and (3) solvent.

The effects on calculated chemical shifts and spin-spin coupling constants, of isomers higher in energy than the lowest-energy conformer were taken into account. To search the stable geometries lying in a relative energy range, we have put forward an automatized method that can be summarized in three consecutive steps: (1) molecular dynamics calculation using the semi-empirical PM6 potential followed by optimization at the same level and filtration of similar geometries, (2) optimization of the remaining geometries at the level B3LYP/6-31G* followed by filtration of similar geometries in addition to geometries having energies higher than a chosen maximum, and (3) optimization of geometries remaining from step two at the level B3LYP/6-311++G** followed by calculation of NMR parameters of each isomers at the same level. The effects of isomers were taken into account through the calculation of the averaged NMR parameter (δ or J) as an average of the NMR parameter of the various isomers weighted by Boltzmann factor. For all studied metabolites, isomer effects were seen to reduce the differences between experimental and simulated spectra.

The second type of studied effects has been the molecular vibration. To calculate vibrational corrections on chemical shifts and spin-spin coupling constants, we have used several methods like the ADMP of Gaussian and the C_{FOUR} package; however, zero-point vibrational corrections were better evaluated through the second order perturbational approach at the B3LYP/6-311++G** level of theory via a home-made code that we have implemented in the version of Gaussian03 at our disposal. The corrections due to vibration were seen to increase the agreement between simulated and experimental NMR spectra.

For the reliable calculation of NMR parameters, the effects of a solvent, particularly water, were studied using two approaches based on different methodologies of the solvent model: (1) PCM method which treats the solvent as a continuum having an effective dielectric constant, and (2) ONIOM method with which explicit solvent molecules can be considered during calculation. The PCM model was found to be better than ONIOM in calculating chemical shifts of protons attached to carbon atoms for the metabolites considered in the present work.

For the calculations of the NMR parameters of metabolites, the three effects: isomers, vibration, and solvent, were grouped together in the following way: (1) determination of all the stable isomers of a metabolite in a given energy range above the lowest one, (2) calculation of the chemical shifts and the spin-spin coupling constants for the protons of each isomer, (2) calculation of the zero-point vibrational corrections for these NMR parameters of each isomer via our method, (3) calculation of solvent corrections of each isomer as a difference between isolated and solvated isomers, (4) averaging the corrected values of the NMR parameters following a Boltzmann distribution. For all studied metabolites, the three effects grouped together were seen to give the best accord with experiment. The root mean square deviation of δ between calculated and experimental values decreases from 0.29 ppm for gas-phase molecules to 0.07 ppm when the three effects are taken into account. The root mean square deviation of J decreases from 2.1 Hz for gas-phase molecules to 0.6 Hz when the three effects are taken into account.

Despite the potential usefulness of quantum chemistry calculations, it appears that this possibility had not been considered for determining the NMR parameters of metabolites previously to our early investigations.

The second part of the present work was devoted to put forward a method that allows the prediction of chemical shifts for biological molecules. We proposed the BioShift method which is based on the distance between atoms as well as their Amber types. As a test, we have chosen 5 proteins to fit the parameters of our method and 5 other proteins for the prediction of chemical shifts. Bioshift was seen to be competitive with well-known methods for chemical shift prediction of proteins such as SHIFTX. For the set of 10 proteins, the root mean square deviations between chemical shifts from BioShift and experiment were found to be 0.32, 0.55, 1.95, 2.02, 1.38, 3.37 ppm for HA (20 parameters), HN (15 parameters), CA (35 parameters), CB (40 parameters), CO (22 parameters), and N (35 parameters) respectively.

BioShift was found to be successful when applied to large molecules (proteins) as well as small ones (polyamines). It is able to predict the chemical shifts of different types of nuclei (hydrogen, carbon, nitrogen). The functional form and the small number of parameters of our model make the BioShift predictions very rapid and suitable to compute chemical shifts for macromolecules (proteins, DNA and RNA).

The present work opens the door to new domains of research. Reliable NMR parameters calculated theoretically within the DFT approach can be obtained for various metabolites of interest, in particular, metabolites related to cancers and illnesses. The calculated NMR parameters would form a good basis for the analysis of in vivo NMR spectra, which allows the identification of health problems and prescribing the correct treatment.

It is well known that the extraction of spin-spin coupling constants from experimental NMR spectra is very hard and sometimes impossible in the case of complex multiplets. Thus, developing a model that allows the prediction of spin-spin coupling constants would be very useful not only for small molecules, but also for large ones where quantum chemistry calculations require lot of time and effort.

APPENDIX A

Proteins are biochemical compounds consisting of one or more polypeptides typically folded into a globular or fibrous form, facilitating a biological function. A polypeptide is a single linear polymer chain of amino acids bonded together by peptide bonds between the carboxyl and amino groups of adjacent amino acid residues.

Amino acids are molecules containing an amine group (- NH2), a carboxylic acid group (- COOH) and a side-chain (- R) that varies between different amino acids. The key elements of an amino acid are carbon, hydrogen, oxygen, and nitrogen.

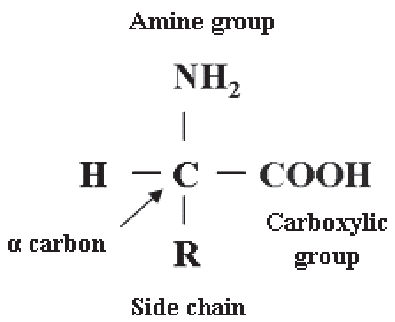

Amino acid structure in its unionized form

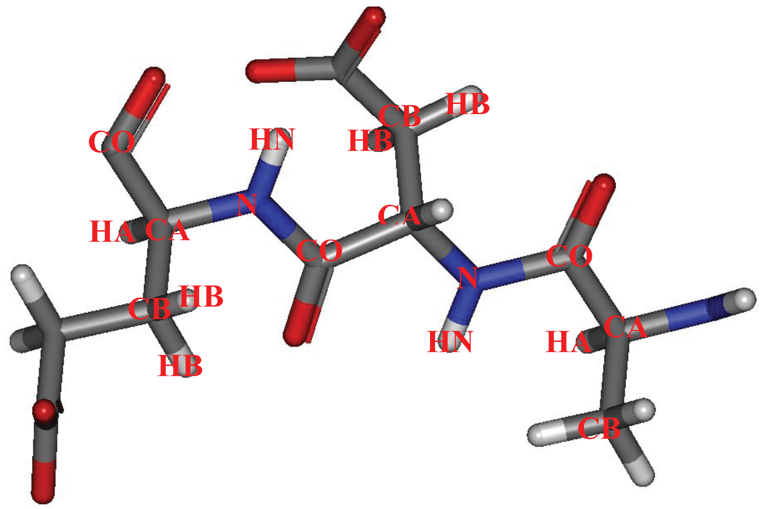

PDB types of atoms in a polypeptide (chain of amino acids); red sticks correspond to oxygen, white ones to hydrogen, grey ones to carbon, and blue ones to nitrogen

The alpha carbon (Cα or CA) in an amino acid refers to the first carbon that attaches to the carboxylic group and amine group. By extension, the second carbon (belonging to the chain - R) is the beta carbon (Hβ or HB). This nomenclature is also applied to the hydrogen atoms attached to the carbons. A hydrogen attached to an alpha carbon is called an alpha-hydrogen (Hα or HA); a hydrogen on the beta-carbon is a beta-hydrogen (Hβ or HB). Besides, the nomination CO denotes the carbon of the hydroxyl group and HN corresponds to the hydrogen atom of the amine.

These atom types, often called PDB (Protein Data Bank) types, are used in the PBD files to give a 3-D structural data for proteins.

In addition to PDB types, there appears in the text the usage of amber types of atoms which are more general than PDB types. The definitions of amber types for atoms used in the text are given in the table below.

C	sp2 C carbonyl group
CA	sp2 C pure aromatic (benzene)
CB	sp2 aromatic C, 5&6 membered ring junction
CC	sp2 aromatic C, 5 membered ring HIS
CT	sp3 aliphatic C
CW	sp2 aromatic 5 membered ring w/1 N-H and 1 H (HIS)
H	H bonded to nitrogen atoms
HC	H aliphatic bonded to C without electron withdrawing group
H1	H aliphatic bonded to C with one electron withdrawing group
HA	H aromatic bonded to C without electron withdrawing groups
H4	H aromatic bonded to C with one electron withdrawing group
HO	hydroxyl group
HS	hydrogen bonded to sulphur
N	sp2 nitrogen in amide groups
NA	sp2 N in 5 membered.ring w/H atom (HIS)
O	carbonyl group oxygen
OH	oxygen in hydroxyl group
O2	carboxyl and phosphate group oxygen
S	sulphur in disulfide linkage
SH	sulphur in cystine

APPENDIX B

The full list of the parameters used in our model (BioShift) and their numerical values are displayed in the following table.

Nuclei	*Connection-type*	*atom-type*				*α*	*B*
HA	***angle***	*H1*	*CT*	*H1*		*-0.001252*	*1*
δ_{HA}*=4.360674*		*H1*	*CT*	*CT*		*0.178129*	*1*
						1.081202	*1*
						-1.068982	*1*
	dihedral	*H1*	*CT*	*CT*	*H1*	*0.002180*	*1*
		H1	*CT*	*CT*	*HC*	*0.001545*	*1*
		H1	*CT*	*CT*	*CA*	*0.095887*	*1*
		H1	*CT*	*C*	*N*	*-0.228869*	*1*
		H1	*CT*	*C*	*O2*	*-0.107976*	*1*
		H1	*CT*	*CT*	*C*	*-0.060482*	*1*
		H1	*CT*	*CT*	*CT*	*-0.015104*	*1*
	non-bonded	*H1*	*HC*			*-27.848934*	*-6*
		H1	*H4*			*-34.669321*	*-6*
		H1	*HO*			*-24.785825*	*-6*
		H1	*O*			*106.188718*	*-6*

		H1	*O2*			*90.742822*	*-6*
		H1	*CT*			*69.095932*	*-6*
		H1	*C*			*-118.150118*	*-6*
		H1	*CA*			*-114.834903*	*-6*
HN	***angle***	*H*	*N*	*C*		*-3.99023*	*1*
δ_{HN}=*8.31992*		*H*	*N*	*CT*		*1.67604*	*1*
	dihedral	*H*	*N*	*C*	*O*	*2.28325*	*1*
		H	*N*	*C*	*CT*	*038737*	*1*
		H	*N*	*CT*	*CT*	*-0.48176*	*1*
		H	*N*	*CT*	*C*	*-0.30465*	*1*
		H	*N*	*CT*	*H1*	*-0.52654*	*1*
	non-bonded	*H*	*H1*			*25.37866*	*-6*
		H	*HC*			*0.06955*	*-6*
		H	*CT*			*-17.87494*	*-6*
		H	*C*			*-51.49065*	*-6*
		H	*O*			*24.64331*	*-6*
		H	*O2*			*40.67695*	*-6*
		H	*N*			*-65.27136*	*-6*
CA	***bond***	*CT*	*CT*			*-7.5010*	*1*
δ_{CA}=*57.1789*		*CT*	*H1*			*-29.7513*	*1*

		CT	C			26.3300	1
		CT	N			-10.4114	1
		CT	CT	HC		-2.1773	1
		CT	CT	H1		-1.8889	1
		CT	N	C		3.3544	1
		CT	N	H		17.1286	1
		CT	CT	CA		0.4589	1
		CT	C	N		0.3922	1
		CT	C	O		-4.3712	1
		CT	CT	CT		-0.0808	1
		CT	CT	C		15.9541	1
		CT	CT	OH		-0.0824	1
		CT	CT	SH		0.0767	1
		CT	CT	CC		-0.3221	1
		CT	CT	C*		0.6442	1
		CT	C	O2		-1.7196	1
		CT	N	CT		-0.5063	1
	dihedral	CT	N	C	CT	-1.9012	1
		CT	C	N	CT	-0.3581	1
		CT	CT	CT	C	-0.0488	1
		CT	CT	CT	CT	-0.2458	1
		CT	CT	CT	S	-0.1936	1

		CT	*CT*	*C*	*N*	*-6.8084*	*1*
		CT	*CT*	*C*	*O*	*-6.6614*	*1*
		CT	*CT*	*SH*	*SH*	*-0.4644*	*1*
		CT	*N*	*CT*	*CT*	*18.6519*	*1*
		CT	*CT*	*C*	*O2*	*-6.7330*	*1*
	non-bonded	*CT*	*H1*			*-598.2073*	*-6*
		CT	*CT*			*71.8596*	*-6*
		CT	*C*			*3901.1357*	*-6*
		CT	*O*			*-1518.9212*	*-6*
		CT	*N*			*3582.3359*	*-6*
CB δ_{CB}*=38.96958*	***bond***	*CT*	*CT*			*6.394357*	*1*
		CT	*H1*			*-16.281169*	*1*
		CT	*C*			*48.611209*	*1*
		CT	*HC*			*-19.145002*	*1*
		CT	*CC*			*-169.12476*	*1*
		CT	*C**			*-54.578441*	*1*
		CT	*SH*			*89.661579*	*1*
		CT	*CA*			*5.387395*	*1*
		CT	*OH*			*23.775073*	*1*
		CT	*CT*	*HC*		*-3.757956*	*1*
		CT	*CT*	*H1*		*10.260945*	*1*

		CT	*C*	*N*		*-16.054964*	*1*
		CT	*C*	*O*		*-9.913498*	*1*
		CT	*CT*	*C*		*-2.989766*	*1*
		CT	*C*	*O2*		*-15.224503*	*1*
		CT	*CT*	*N*		*-0.300033*	*1*
		CT	*OH*	*HO*		*-7.628854*	*1*
		CT	*C**	*CB*		*39.503018*	*1*
		CT	*CC*	*CW*		*194.525548*	*1*
		CT	*SH*	*HS*		*-76.576509*	*1*
		CT	*CA*	*CA*		*21.008331*	*1*
		CT	*CT*	*S*		*-21.094927*	*1*
		CT	*SH*	*SH*		*5.585565*	*1*
		CT	*CC*	*NA*		*-103.774854*	*1*
		CT	*C**	*CW*		*-11.992778*	*1*
	dihedral	*CT*	*CT*	*CT*	*CT*	*-0.565275*	*1*
		CT	*CT*	*CT*	*H1*	*-0.513591*	*1*
		CT	*CT*	*C*	*O*	*1.224747*	*1*
		CT	*CT*	*C*	*O2*	*0.645703*	*1*
		CT	*CT*	*N*	*H*	*5.59301*	*1*
		CT	*C*	*N*	*H*	*-2.052032*	*1*
		CT	*CA*	*CA*	*CA*	*-11.139753*	*1*
		CT	*CA*	*CA*	*HA*	*-5.472510*	*1*
		CT	*CT*	*CT*	*N*	*11.316408*	*1*

		CT	*SH*	*SH*	*CT*	*0.835525*	*1*
		CT	*CT*	*N*	*CT*	*-4.351534*	*1*
		CT	*CT*	*S*	*CT*	*-0.539585*	*1*
	non-Bonded	*CT*	*C*			*3621.223558*	*-6*
		CT	*O*			*-1411.054849*	*-6*
CO δ_{CO}*=175.90247*	***bond***	*C*	*CT*			*8.432198*	*1*
		C	*O*			*-5.462836*	*1*
		C	*O2*			*-1.539415*	*1*
		C	*N*			*-14.437318*	*1*
	angle	*C*	*CT*	*H1*		*-1.083785*	*1*
		C	*CT*	*CT*		*0.248137*	*1*
		C	*CT*	*N*		*-6.819603*	*1*
		C	*N*	*H*		*6.073799*	*1*
	dihedral	*C*	*CT*	*CT*	*CT*	*0.000012*	*1*
		C	*CT*	*CT*	*H1*	*-0.410838*	*1*
		C	*CT*	*N*	*C*	*0.396539*	*1*
		C	*CT*	*N*	*H*	*4.117023*	*1*
		C	*CT*	*N*	*CT*	*3.583480*	*1*
		C	*N*	*CT*	*CT*	*1.03740*	*1*

		C	*N*	*CT*	*H1*	*1.09002*	*1*
		C	*N*	*CT*	*C*	*-0.153706*	*1*
		C	*CT*	*CT*	*C*	*-0.303321*	*1*
	non-bonded	*C*	*H1*			*-318.273833*	*-6*
		C	*HC*			*-222.85729*	*-6*
		C	*CT*			*305.315903*	*-6*
		C	*N*			*693.117868*	*-6*
N	***bond***	*N*	*H*			*4.00616*	*1*
δ_N*=119.34712*		*N*	*CT*			*13.15210*	*1*
		N	*C*			*59.68094*	*1*
	angle	*N*	*C*	*O*		*-12.86645*	*1*
		N	*C*	*CT*		*-18.75183*	*1*
		N	*CT*	*CT*		*7.78220*	*1*
		N	*CT*	*H1*		*3.49654*	*1*
		N	*CT*	*C*		*-21.59006*	*1*
	dihedral	*N*	*C*	*CT*	*N*	*-15.76468*	*-3*
		N	*C*	*CT*	*N*	*-1908.1756*	*-6*
		N	*CT*	*CT*	*CT*	*-9.04791*	*-3*
		N	*CT*	*CT*	*CT*	*857.69117*	*-6*
		N	*C*	*CT*	*CT*	*163.06129*	*-3*

		N	*C*	*CT*	*CT*	*-5407.3957*	*-6*
		N	*CT*	*C*	*O*	*322.99561*	*-3*
		N	*CT*	*C*	*O*	*-6019.8547*	*-6*
		N	*CT*	*C*	*N*	*131.01339*	*-3*
		N	*CT*	*C*	*N*	*-3500.1412*	*-6*
		N	*CT*	*CT*	*CA*	*89.35759*	*-3*
		N	*CT*	*CT*	*CA*	*-4687.6471*	*-6*
		N	*CT*	*CT*	*SH*	*7.51588*	*-3*
		N	*CT*	*CT*	*SH*	*-3704.6268*	*-6*
		N	*CT*	*CT*	*OH*	*-458.45137*	*-3*
		N	*CT*	*CT*	*OH*	*7634.98493*	*-6*
		N	*CT*	*CT*	*C*	*-164.25794*	*-3*
		N	*CT*	*CT*	*C*	*2274.69501*	*-6*
		N	*CT*	*C*	*O2*	*690.17839*	*-3*
		N	*CT*	*C*	*O2*	*-14986.972*	*-6*
	non-bonded	*N*	*H1*			*-558.31208*	*-6*
		N	*HC*			*-734.66475*	*-6*
		N	*CT*			*3407.37310*	*-6*
		N	*C*			*-719.16881*	*-6*
		N	*O*			*356.88755*	*-6*
		N	*O2*			*774.41414*	*-6*

Model parameters for the six nuclei of amber types: HA, HN, CA, CB, CO and N, where N_u = 1 ∀ u, except for dihedral terms for the N nuclei for which N_d= 2

Title: Theoretical Determination of NMR Parameters of Metabolites and Proteins

---

Abstract: The present work presents a theoretical study of the NMR spectra of biological molecules. In the first part, DFT calculations of the spin-Hamiltonian NMR parameters (chemical shifts and spin-spin coupling constants) for protons attached to carbon atoms have been performed for four prostate metabolites: putrescine, spermidine, spermine, and sarcosine, and three brain metabolites: acetate, alanine, and serine. A theoretical investigation, within the DFT approach, of the NMR parameters of metabolites has shown that the B3LYP/6-311++G** level of calculation is a good compromise between accuracy and costs. Contributions from solvent were evaluated using the PCM model, Boltzmann weighted isomer effects were calculated, and zero-point vibrational corrections were estimated using a second order perturbation approach. Comparison with experiment has demonstrated that all these effects are necessary to improve the agreement between calculated and experimental data. In the second part, we have presented a new model, BioShift, that allows the prediction of chemical shifts of different nuclei (H, N, C…) for biological molecules (proteins, DNA, RNA, polyamine …). It is simple, fast, and involves a limited number of parameters. Comparison with well-known sophisticated models designed especially for the prediction of chemical shifts of proteins showed that Bioshift is competitive with such models.

Keywords: DFT calculations, B3LYP/6-311++G**, NMR, chemical shifts, spin-spin couplings, metabolites, conformers, molecular vibration, prediction of chemical shifts of proteins

---

Titre: Détermination Théorique des Paramètres RMN de Métabolites et Protéines

---

Résumé: Ce travail présente une étude théorique des spectres RMN de molécules biologiques. Dans la première partie, les calculs DFT des paramètres RMN (déplacements chimiques et constantes de couplage spin-spin) pour les protons liés à des atomes de carbone ont été réalisés pour quatre métabolites de la prostate: la putrescine, la spermidine, la spermine, et la sarcosine, et trois métabolites du cerveau: l'acétate, l'alanine et la sérine. Une étude théorique systématique, dans l'approche DFT, des paramètres de RMN des métabolites a montré que la méthode B3LYP/6-311++G** est un bon compromis entre la précision et les coûts. Les contributions du solvant ont été évaluées en utilisant le modèle PCM, les effets des isomères, pondérés dans l'approximation de Boltzmann, ont été pris en compte, et les corrections de vibration de point zéro ont été estimées en utilisant une approche perturbative au second ordre. La comparaison avec l'expérience a démontré que tous ces effets sont nécessaires pour améliorer l'accord entre les données calculées et expérimentales, aboutissant à des résultats de grande précision. Dans la deuxième partie, nous avons développé un nouveau modèle, BioShift, qui permet la prédiction des déplacements chimiques des différents noyaux (H, N, C ...) pour des molécules biologiques (protéines, ADN, ARN, polyamine ...). Il est simple, rapide, et comporte un nombre limité de paramètres. La comparaison avec des modèles sophistiqués conçus spécialement pour la prédiction des déplacements chimiques des protéines a montré que Bioshift est concurrentiel avec de tels modèles.

Mots-clefs: calculs DFT, B3LYP/6-311++G**, RMN, déplacement chimique, couplage spin-spin, métabolites, conformères, vibration moléculaire, prédiction des déplacements chimique de protéines

---

Adresse du Laboratoire: Laboratoire de Spectrométrie Ionique et Moléculaire UMR 5579 Université Claude Bernard Lyon 1, Bâtiment Kastler, 43 Bd du 11 Novembre 1918
69622 Villeurbanne Cedex France